

Novel Electrochemiluminescent Interfaces for Chemical Sensing Applications.

Submitted by David James Eastman Piper

Bachelor of Science with Honours

La Trobe University

**A thesis submitted in total fulfilment
of the requirements for the degree of
Doctor of Philosophy**

**Department of Physics
Faculty of Science, Technology and Engineering**

**La Trobe University
Bundoora, Victoria 3086
Australia**

March 2011

Dedicated to the memory of Bruce David James

(1942 – 2009)

A great friend and the world's best lecturer



'Life is a thesis, this is only part of it.'

Abstract

Electrogenerated Chemiluminescence otherwise known as Electrochemiluminescence (ECL) is an effective analytical tool for many organic compounds of clinical and environmental importance. The technique can allow for the regeneration of the luminescent reagent during the course of analysis making it well suited to the development of solid state sensing platforms. In addition, immobilisation of the luminescent reagent can provide opportunities for improved sensitivity and reproducibility compared to solution phase ECL systems. The overall aim of this thesis is to further the development of sensitive and stable ECL-based detection platforms.

The thesis focuses on two distinct methods for the immobilisation of the luminescent reagent, tris(2,2'-bipyridyl) ruthenium(II). The first modification method involves the use of a composite polymer based on the perfluorinated ionomer, Nafion and the conducting polymer polypyrrole. The presence of polypyrrole results in improved layer stability when compared to Nafion-based layers. The improvement in layer stability comes at the cost of sensitivity, with detection limits for the model analytes oxalate and tripropylamine being 10 μM and 100 nM, respectively; an order of magnitude decrease in sensitivity compared with Nafion-based layers.

The second electrode modification method investigates the use of aryl diazoniums to form thin films of luminescent reagent at the electrode surface. Diazoniums were used to form ECL active films via both the attachment of a ligand and subsequent complexation at the surface and the attachment of the luminescent complex directly at the electrode surface. Attachment of the luminescent complex was achieved via both electroreduction of the diazonium from aqueous solution and the spontaneous deposition of the film with the

resulting films characterised using CV, XPS, TOF-SIMS and AFM. The films were found to be stable over a period of several hours while remaining sensitive to low concentrations (10 nM) of model analytes such as 2-(dibutylamino)ethanol.

Statement of Authorship

Except where reference is made in the text of the thesis, this thesis contains no material published elsewhere or extracted in whole or in part from a thesis submitted for the award of any another degree or diploma.

No other person's work has been used without due acknowledgement in the main text of the thesis.

The thesis has not been submitted for the award of any degree or diploma in any other tertiary institution.

David J.E. Piper

March 2011

Acknowledgements

I would like to thank **ALL** the people who have assisted me in the researching and writing of this Thesis, it has been a long and sometimes arduous time but I have got there. My most sincere and heartfelt thanks to you all.

In particular I would like to thank the following people for their direct contribution to this body of work.

Firstly, a big thank you to my supervisors, **Paul Pigram, Conor Hogan, and Narrelle Brack**. At times it has been a challenge but I could not have done this without you. Your patience has been appreciated.

I would like to acknowledge the support of the people who have directly assisted in my research. The following people have helped immensely with the surface analysis of my samples in particular the XPS and ToF-SIMS components - **Penny Hale, Grant van Riessen, Rob Jones, Peter Kappen and Anton Tadich**.

I would also like to explicitly thank **Gregory Barbante** for without his synthesis skills, lively discussions and ideas much of this document may not exist.

In addition, thank you to Tim, (**Walaipron Prissanaroon**), you have provided a path for me to follow.

To my proof readers, **Russell Bowen, Morgan Langdon, Eli Hazel** – your help has been invaluable and this document is much better for your efforts. At this point a special mention must go to **Meg Rosse** from Academic Skills, thank you.

My appreciation goes out to the administrative and technical staff that have assisted me, in particular, **Margarita Bakalova, Brad East, Robert Polglase** and **Eric Huwald**.

Thanks must also go to the friends who have shared an office, a laboratory and ideas with me over my time here. In Chemistry - **Egan Doeven, Ellen Reid, David Bower, Jacqui Delaney, Peitro Barilla** and **Reshmi Kiran**. In Physics - the old boys - **Petar Stojanov, Michael Gilbert, Alexander Fink, Robert Greenwood, Kevin Hannah** and the new – **Kevin Rietwyk, Daniel Langley, Tom Payten, Yaou Smets, Mark Edmonds, Jeff, Paris, Heidi, and Amanda**. I especially extend my appreciation to the man who sat beside me, **Barry Halstead**, your support and ideas throughout the years has been strong and constant. I am ever grateful, thanks Baz.

Of course an acknowledgements section would not be complete without the express thanking of family and friends, they have carried the torch when I dropped it. My parents – **Jim & Alison**, siblings **Glen** and **Karen**, grandparents **Russell, Audrey, Dulcie** and **George** and aunt **Robyn**. Thank you. (And **Lisa**, you deserve a mention, I don't know where you fit, never have, but thank you in my own special way) Also, my friends who have not yet been mentioned but deserve explicit thanks, **Laura James, Meredith Jay, Hamish Duckmanton, David Wyndham** and especially **Dale Ross-Soden** – you have a patience and maturity that is worth bottling (then served in a Pint glass at 12 °C).

Finally I would like to thank the man who this document is dedicated to, **Dr Bruce James**. I finally got there. No matter how slowly...

Author's Publications:

1. **D. Piper**, G. Barbante, N. Brack, C. Hogan, P. Pigram; An electrochemiluminescent film via the electrografting of a diazonium salt derivative in acidic media. *Langmuir* **2011** 27(1) pp 474-480
2. **D. Piper**, N. Brack, C. Hogan, P. Pigram; Characterisation of Ru(bpy)₃²⁺ loaded Nafion/polypyrrole composites for electrochemiluminescent detection. *In Preparation*.

Table of Contents

Abstract	iv
Statement of Authorship	vi
Acknowledgements	vii
Authors Publications:	ix
Table of Contents	x
List of Abbreviations used in this Thesis	xiii
Chapter 1: Introduction	1
References	5
Chapter 2: Background and Literature Review	6
2.1. Introduction to Electrochemical Sensing	6
2.2. Modified Electrodes	7
2.2.1. Polymer Modified Electrodes	8
2.2.1.1. Pre-formed Redox Polymers	9
2.2.1.2. Conducting Polymers	9
2.2.1.3. Ionomers and Composites	14
2.2.1.4. Ionomer/Conducting Polymer Composites	15
2.2.2. Monolayer Modified Electrodes	17
2.2.2.1. Alkanethiol Monolayers	18
2.2.2.2. Organosilane Monolayers	21
2.2.3. Diazonium Modified Electrodes	22
2.3. Electrogenerated Chemiluminescence	29
2.4. ECL for Chemical Sensing	35
2.4.1. Solution Phase ECL	35
2.5. Immobilisation Methods for ECL Active Compounds	37
2.5.1. Polymer Modified Electrodes	38
2.5.2. Monolayer Modified Electrodes	41
2.6. References	45
Chapter 3: Experimental Methods and Characterisation	61
3.1. Fabrication and Synthesis Methods	61
3.1.1. Fabrication of Nafion/Polypyrrole Films	62
3.1.2. Electrodeposition of Ruthenium Based Layers using Diazonium Chemistry..	62
3.1.2.1. Two-step Synthesis of Ru(bpy) ₂ (dpb) ²⁺ Films	63
3.1.2.2. Direct Electrodeposition of Ru(bpy) ₂ (apb) ²⁺ Films	64
3.1.3. Spontaneous Deposition of Ru(bpy) ₂ (apb) ²⁺ Films	65
3.2. Characterisation Methods	66
3.2.1. X-ray Photoelectron Spectroscopy	67
3.2.1.1. Basic Concepts	67
3.2.1.2. Instrumentation	71
3.2.1.3. Experimental	73
3.2.2. Time-of-Flight Secondary Ion Mass Spectrometry	75
3.2.2.1. Basic Concepts	75
3.2.2.2. Instrumentation	77
3.2.2.3. Experimental	79
3.2.3. Atomic Force Microscopy	80
3.2.3.1. Basic Concepts	80
3.2.3.2. Experimental	82
3.2.4. Cyclic Voltammetry	84

3.2.4.1. Basic Concepts:.....	84
3.2.4.2. Instrumentation	87
3.2.4.3. Experimental	88
3.2.5. Electrochemical Quartz Crystal Microbalance	90
3.2.5.1. Basic Concepts.....	90
3.2.5.2. Experimental	90
3.3. References.....	92
Chapter 4: Nafion/Polypyrrole composites for ECL sensing.....	95
4.1. Introduction.....	95
4.2. Results and Discussion	96
4.2.1. Layer Thickness	96
4.2.2. Ruthenium Absorption and Polypyrrole Deposition.....	97
4.2.3. Electrochemical Characterisation of Films	98
4.2.4. Surface Characterisation of Films.....	102
4.2.5. ECL Response.....	111
4.2.6. Layer Stability.....	114
4.3. Conclusions.....	117
4.4. References.....	118
Chapter 5: Covalently bound ECL active films - a two-step approach	121
5.1. Introduction.....	121
5.2. Results and Discussion	121
5.2.1. Phenyl-bipyridine Layer Deposition.....	122
5.2.1.1. AFM of dpb Layers.....	126
5.2.2. dpb Layer Characterisation	129
5.2.2.1. Electrochemical Characterisation of dpb Layers	129
5.2.2.2. XPS Analysis of dpb Layers	131
5.2.2.3. ToF-SIMS Analysis of dpb Layers	136
5.2.3. Attachment of Ru(bpy) ₂ Cl ₂ to dpb Films and Subsequent Characterisation.	143
5.2.3.1. Electrochemistry of Ru (bpy) ₂ (dpb) ²⁺ Films.....	143
5.2.3.2. XPS Characterization of Ru (bpy) ₂ (dpb) ²⁺ Films	144
5.2.3.3. ToF-SIMS of the Complexed Layer	147
5.2.3.4. Electrochemiluminescence.....	150
5.3. Conclusions.....	152
5.4. References.....	154
Chapter 6: The Electrodeposition of Ru(bpy)₂(apb)²⁺ films.	157
6.1. Introduction.....	157
6.2. Results and Discussion	157
6.2.1. Layer Deposition.....	158
6.2.2. Layer Characterisation	159
6.2.2.1. Electrochemical Characterisation	159
6.2.2.2. Surface Analysis	160
6.2.3. Electrochemiluminescence.....	165
6.2.4. Stability	168
6.3. Conclusions.....	172
6.4. References.....	173

Chapter 7: The Spontaneous Deposition of Ru(bpy)₂(apb)²⁺ Films	175
7.1. Introduction.....	175
7.2. Spontaneous Deposition of Ru(bpy) ₂ (apb) ²⁺ onto Glassy Carbon.....	176
7.2.1. Surface Analysis	178
7.2.2. ECL Response.....	183
7.2.3. Stability	185
7.3. Spontaneous Deposition of Ru(bpy) ₂ (apb) ²⁺ onto Diamond Like Carbon	186
7.4. Conclusions.....	189
7.5. References.....	191

Chapter 8: Conclusions and Future work	193
8.1. Concluding Remarks.....	193
8.1.1. Nafion/Polypyrrole composites.....	193
8.1.2. Phenyl-bipyridine attachment and complexation.....	194
8.1.3. Electrodeposition of Ru(bpy) ₂ (apb) ²⁺ films.	195
8.1.4. The spontaneous deposition of Ru(bpy) ₂ (apb) ²⁺ films	196
8.2. Future Work	197
8.3. References.....	200

Appendix I: Supporting Information	201
---	------------

Appendix II: Reprints

1. An electrochemiluminescent film via the electrografting of a diazonium salt....205
derivative in acidic media.; **D. Piper**, G. Barbante, N. Brack, C. Hogan,
P. Pigram; Langmuir, 27(1) **2011** pp 474-480

List of Abbreviations used in this Thesis

AFM	Atomic Force Microscopy
apb	para-amino-4'-phenyl-2,2'-bipyridine
bpy	2,2'-bipyridine
CV	Cyclic Voltammetry
DBAE	2-(dibutylamino)ethanol
DBSA	dodecylbenzenesulfonic acid
dpb	para-diazonium-4'-phenyl-2,2'-bipyridine
EQCM	Electrochemical Quartz Crystal Microbalance
GC	Glassy Carbon
PPy	polypyrrole
Ru(bpy)₃²⁺	tris(2,2'-bipyridyl) ruthenium(II)
Ru(bpy)₂(apb)²⁺	bis(2,2'-bipyridyl)(4'-(4-aminophenyl)-2,2'-bipyridyl) ruthenium(II)
Ru(bpy)₂Cl₂	bis(2,2'-bipyridyl)dichloro ruthenium(II)
ToF-SIMS	Time of Flight Secondary Ion Mass Spectrometry
TPA	tripropylamine
XPS	X-Ray Photoelectron Spectroscopy

Chapter 1: Introduction

Electrochemical-based sensing methods are well established analytical techniques for the detection of a diverse range of compounds that have led to the development of numerous commercial sensing devices. Electrochemical systems form the basis of small, simple, inexpensive sensors that provide rapid response times. In contrast, chemiluminescence sensing offers excellent sensitivity, selectivity and high linear range. The combination of these two methods in the form of electrochemiluminescence (ECL) can create a sensing platform that offers the best aspects of both forms of chemical analysis.¹ Traditionally, ECL-based sensing systems have required that the luminescent reagents are present in solution. However, this requirement can be circumvented if the active form of the luminescent reagent is regenerated during the course of the reaction. In this situation the luminescent reagent can be bound to or otherwise immobilised at the surface of the electrode. A number of possible benefits can be gained by modifying the electrode with the ECL active agent, such as simplified sensor design and ease of miniaturisation, improved detection limits and reduced sensor costs. These enhancements have the capacity to provide low-cost, reliable ECL-based sensors as well as simplified detection systems for a range of devices including high performance liquid chromatography and lab-on-a-chip.

Many methods have been used to immobilise luminescent reagents at electrode surfaces. For example, the luminescent moiety may be bound to a polymer chain which is then coated on the electrode in the form of a thin film² or the luminophore may be polymerised directly onto the surface by electrochemical methods or other means.³ Electrostatic attachment within sol-gels^{4,5} and ion-exchange polymers^{3,6} has also been popular and formation of luminescent monolayer films by self assembly or covalent bonding has been

demonstrated.⁷⁻¹¹ However, these immobilisation methods have shown varying success in the fabrication of effective ECL-based sensors, with many methods suffering from poor stability, sensitivity, and reproducibility.¹

This thesis investigates the synthesis and surface chemistry of two distinct approaches to electrode modification for the creation of high performance ECL active layers. The first modified electrode is a composite polymer system based on the perfluorinated ionomer, Nafion^a and polypyrrole. The second system centres on the creation of a thin covalently-bound film formed via the electrodeposition of diazonium compounds. In both systems the surface chemistry of the layer is central to its effectiveness in producing a sensitive and stable ECL sensor. Parameters such as reagent concentration and availability, and charge and mass transport within the layer are significant in determining the sensitivity of the film. The stability of the film is affected by the bonding arrangement between the luminophore and the surface and the luminophore polarity.

The aim of this thesis is to develop and understand alternative immobilisation methods for ECL-based sensors that provide improvements to device stability, sensitivity and reproducibility. The relationship between the structure of the immobilised films and the factors limiting device performance will be investigated. There is a particular focus on understanding the long term stability of the modified electrodes and the associated degradation pathways.

Chapter 2 presents the rationale of the thesis and a review of the background literature relevant to this work. It focuses on the various electrode modification techniques used for electrochemical sensing, such as polymer-based and diazonium modification methods,

^a Nafion is a registered trademark of DuPont

and provides a framework for understanding the phenomenon of ECL and its application to electrochemical sensing.

Chapter 3 introduces the experimental techniques used for the fabrication and analysis of the modified electrodes. Surface analysis techniques such as X-ray Photoelectron Spectroscopy (XPS) and Time-of-Flight Secondary Ion Mass Spectrometry (ToF-SIMS) have been extensively used in the characterisation of the modified electrodes. By investigating the surface chemistry (XPS and ToF-SIMS), the electrochemistry (via Cyclic Voltammetry, (CV) and Electrochemical Quartz Crystal Microbalance (EQCM)) and the morphology of the layers (Atomic Force Microscopy (AFM)), a more complete understanding of the structure and behaviour of the modified electrode can be determined. Chapter 3 discusses the implementation of these analytical techniques and the specific instrumentation employed in this thesis.

Chapter 4 presents a polymer composite used to produce stable modified electrodes for potential use in ECL-based sensing applications. The chapter discusses the incorporation of tris(bipyridyl) ruthenium(II), $\text{Ru}(\text{bpy})_3^{2+}$, and polypyrrole into a Nafion layer and its subsequent characterisation via electrochemical (CV) and surface analysis methods (XPS, ToF-SIMS, AFM). It assesses the resulting film suitability as an ECL-based sensor by investigating its response to the model analytes tripropylamine and the oxalate anion. The Nafion/polypyrrole composite is compared with a Nafion film and a model is developed for the improved performance of the composite layers over the Nafion-based layer.

Chapters 5 and 6 discuss methods for creating modified electrodes via the grafting of diazotised ligands and complexes to a metal or carbon surface. Chapter 5 details a method to create a covalently attached ECL active layer on the surface of gold and glassy carbon electrodes via the electrodeposition of the diazotised ligand, 4-(4-diazoniumphenyl)-2,2'-

bipyridine tetrafluoroborate, followed by a reaction with bis(2,2'-bipyridyl)dichlororuthenium(II). The deposited layer is characterised using CV, EQCM, XPS, ToF-SIMS and AFM at all stages of synthesis to determine the performance in ECL sensing.

Chapter 6 explores an alternate approach to the two step method described in Chapter 5 by diazotising the ECL active compound, bis(2,2'-bipyridyl)(4'-amino-4-phenyl-2,2'-bipyridyl) ruthenium(II), $\text{Ru}(\text{bpy})_2(\text{apb})^{2+}$, and then reducing the diazotised complex *in-situ* to bind it to the electrode in a single pot reaction. As with Chapter 5, the layer is characterised via electrochemical (CV) and surface analytical methods (XPS, ToF-SIMS, AFM). The resulting layer is assessed for its suitability as an ECL sensor with particular focus on film stability. In addition, a layer degradation mechanism is proposed.

Chapter 7 expands on the work presented in Chapter 6 by investigating the spontaneous deposition of the diazotised $\text{Ru}(\text{bpy})_2(\text{apb})^{2+}$. The deposition of $\text{Ru}(\text{bpy})_2(\text{apb})^{2+}$ onto a glassy carbon electrode is monitored via open circuit potential measurement and the resulting electrode is characterised by CV, XPS and ToF-SIMS prior to being assessed for its suitability as an ECL sensor. In addition, the suitability of this deposition for micro array electrodes is demonstrated through selective deposition of $\text{Ru}(\text{bpy})_2(\text{apb})^{2+}$ onto a micropatterned surface of silicon nitride.

Finally Chapter 8 presents the general conclusions of the thesis and outlines possible future research activities emerging from this thesis.

References

- (1) Gorman, B. A.; Francis, P. S.; Barnett, N. W. *The Analyst* **2006**, *131*, 1-24.
- (2) Dennany, L.; Hogan, C. F.; Keyes, T. E.; Forster, R. J. *Anal. Chem.* **2006**, *78*, 1412-1417.
- (3) Rubinstein, I.; Bard, A. J. *J. Am. Chem. Soc.* **1980**, *102*, 6641-6642.
- (4) Dvorak, O.; De Armond, M. K. *J. Phys. Chem.* **1993**, *97*, 2646-2648.
- (5) Choi, H. N.; Cho, S.-H.; Park, Y.-J.; Lee, D. W.; Lee, W.-Y. *Anal. Chim. Acta.* **2005**, *541*, 47-54.
- (6) Downey, T. M.; Nieman, T. A. *Anal. Chem.* **1992**, *64*, 261-268.
- (7) Xu, X.-H.; Bard, A. J. *Langmuir* **1994**, *10*, 2409-2414.
- (8) Obeng, Y. S.; Bard, A. J. *Langmuir* **1991**, *7*, 195-201.
- (9) Bertocello, P.; Kefalas, E. T.; Pikramenou, Z.; Unwin, P. R.; Forster, R. J. *J. Phys. Chem. B* **2006**, *110*, 10063-10069.
- (10) D'Aleo, A.; Williams, R. M.; Chriqui, Y.; Iryer, V. M.; Belser, P.; Vergeer, F.; Ruiz, V.; Unwin, P. R.; De Cola, L. *The Open Journal of Inorganic Chemistry* **2007**, *1*, 26-36.
- (11) Dennany, L.; O'Reilly, E. J.; Keyes, T. E.; Forster, R. J. *Electrochem. Commun.* **2006**, *8*, 1588-1598.

Chapter 2: Background and Literature Review

2.1. Introduction to Electrochemical Sensing

Electrochemical methods have been used extensively by chemists for the detection of almost every class of compound, providing in many cases, very sensitive quantitative information while maintaining good chemical selectivity. Like all sensing techniques, electrochemical sensors require at least two steps for the detection and quantification of the analyte to take place. The initial step of any sensing design is analyte recognition, where the desired analyte selectively interacts with the sensor to provide a detectable event. In electrochemical systems, this recognition step could range from a selective redox reaction to the more complex binding of an antigen to an antibody. Once the analyte recognition event occurs, it is then translated into a useable electrical signal such as a change in current, potential or capacitance. Optical transduction pathways can also be used in spectroscopic and luminescence-based experiments. Once an electrical signal is produced by the transducer (usually an electrode), signal processing can then be undertaken *in-silico* to complete the detection and quantitation of the target analyte.

All electroanalytical methods require an electrochemical cell comprising at least two electrodes. Amperometric and voltammetric methods where current is measured as a function of the driven potential of the cell require a minimum of a working electrode and a counter electrode. The working electrode is typically the electrode where the electrochemistry of interest occurs, while the counter electrode completes the circuit. Usually, a third electrode is used as a reference providing a stable and known electrochemical reaction to measure cell potential against (Section 3.2.4.2). In contrast potentiometric methods where the open circuit potential of the cell is measured require an indicator electrode (equivalent of a working electrode) and a reference electrode. In both

cases the electrochemical cell must contain a conductive fluid which is in electrical contact with the electrodes. Typically this contacting solution also contains the analyte(s) of interest.¹

The interactions between the working electrode and contacting solution are critical to the response of the system. By intentionally modifying the electrode or the solution (such as a change in electrolyte species or concentration or the addition of a catalyst or redox mediator), a change in the system response can be effected, providing improved sensitivity or selectivity for the analyte. As the contacting solution contains the analyte(s) of interest, the ability to modify the contacting solution can be limited and often time consuming. The addition of reagents to the solution for pretreatment prior to analysis, such as analyte derivatisation or tagging, pH buffering and removal of interferences can be difficult, time consuming and prone to user error. To avoid these issues, the electrode may be modified prior to analysis, creating a range of opportunities for more facile electrochemical detection of analytes.

2.2. Modified Electrodes

The direct chemical modification of a surface provides an excellent opportunity to customise electrode properties via the immobilisation of one or more chemical species to the surface. The modified electrode should then demonstrate characteristics of the immobilised species, allowing for the enhanced electrode to be tuned to a specific application or purpose. For example, the attachment of luminescent compounds allows for the incorporation of an optical transduction pathway, while the immobilisation of a redox active moiety can be used for electrocatalytic sensing. Additionally, the attachment of biomolecules such as DNA, antibodies or enzymes can provide a high level of analyte selectivity.

Extensive research into electrode modification for chemical sensing has been undertaken with the literature demonstrating a wide range of modification strategies applicable to chemical sensing.²⁻⁶ By modifying the surface of the electrode, improvements can be incorporated into the sensing method when compared to the use of an unmodified electrode. These improvements include but are not limited to decreased limits of detection, increased dynamic range, improved selectivity, extended sensor lifetime through the prevention of electrode fouling, enhanced reaction kinetics and the enabling of reactions at the surface that otherwise would not be thermodynamically possible.⁷

Numerous approaches to the attachment of compounds for electrode modification exist, including the use of simple physisorbed and chemisorbed layers, such as Langmuir-Blodgett films, electrostatically or hydrophobically bound polymers, and a wide range of covalently attached systems.⁷⁻⁹ These attachment procedures have proven useful for a variety of sensing applications and the area has been extensively reviewed.^{1,6-8}

2.2.1. Polymer Modified Electrodes

Polymer coatings represent the most prevalent form of electrode modification. Polymer modified electrodes (PME) have the advantages of ease of construction, large synthetic variability and a large analyte interaction zone when compared to monolayer-based systems (Section 2.2.2).

The use of polymer films typically involves the deposition of many monolayer equivalents onto the electrode. Depending on the application, films can range from sub-nanometre to several microns in thickness, and when a porous morphology is also employed, the resulting increase in surface area provides a large increase in the number of active sites present when compared to a monolayer system. A polymer film can be attached to the electrode via a number of interactions, typically with a combination of

physisorption and low solubility in the contacting solution, although some films are functionalised so that they form covalent bonds with the surface of the electrode.⁷

A PME can be formed by either the casting of the pre-formed polymer onto the electrode from solution, typically via drop or spin coating, or through the direct polymerisation at the electrode as with electrodeposition techniques. Three broad polymeric classes are often used in the construction of a PME: pre-formed redox polymers, conducting polymers and ion-exchange polymers otherwise known as ionomers.⁵

2.2.1.1. Pre-formed Redox Polymers

Pre-formed redox polymers typically involve the synthesis of an electroinactive polymer backbone prior to modification with a redox active moiety and subsequent deposition onto the electrode via drop or spin coating from a solvent. A range of polymers are used as the basic starting polymer, with polyvinylpyridine and poly(N-vinylimidazole) being commonly used examples.⁴ Often metal complexes, for example complexes of Fe,¹⁰ Ru, Os, and Ir,¹¹⁻¹⁴ are attached to the polymer forming a metallopolymer. However, non-metallic redox active materials such as fullerenes,¹⁵ or TCNQ¹⁶ may also be used.

Pre-formed redox polymer materials have primarily been investigated for use for catalysis and sensing applications. However, the use of these materials can be limited, with this limitation due to both slow charge transport through the material¹² and the layers suffering from short lifetimes resulting from leaching, dissolution, and photo-degradation of the layer.¹³

2.2.1.2. Conducting Polymers

Conducting polymers are organic polymeric materials which possess intrinsic electrical conductivity. This unique class of polymers affords outstanding electron transport

resulting from a highly π -conjugated polymer backbone. The conjugation of the polymer results in a band structure similar to that observed in inorganic semiconductors. By changing the oxidation state of the polymer, electronic charges can be introduced into the polymer forming intermediate states in the band gap, allowing for the thermal excitation of electrons into the conduction band and facilitating charge transport as demonstrated in Figure 2-1.¹⁷ On oxidation, or reduction counter ions, commonly referred to as dopants, enter into the polymer structure to maintain charge neutrality. Conducting polymers include polypyrrole (PPy), polyaniline, and polyacetylene. Typically, conducting polymer films are formed by oxidation of the desired monomers either via chemical or electrochemical methods,¹⁷ however reductive pathways are also possible.¹⁸ The electrochemical oxidation of pyrrole is provided as an example in Scheme 2-1.

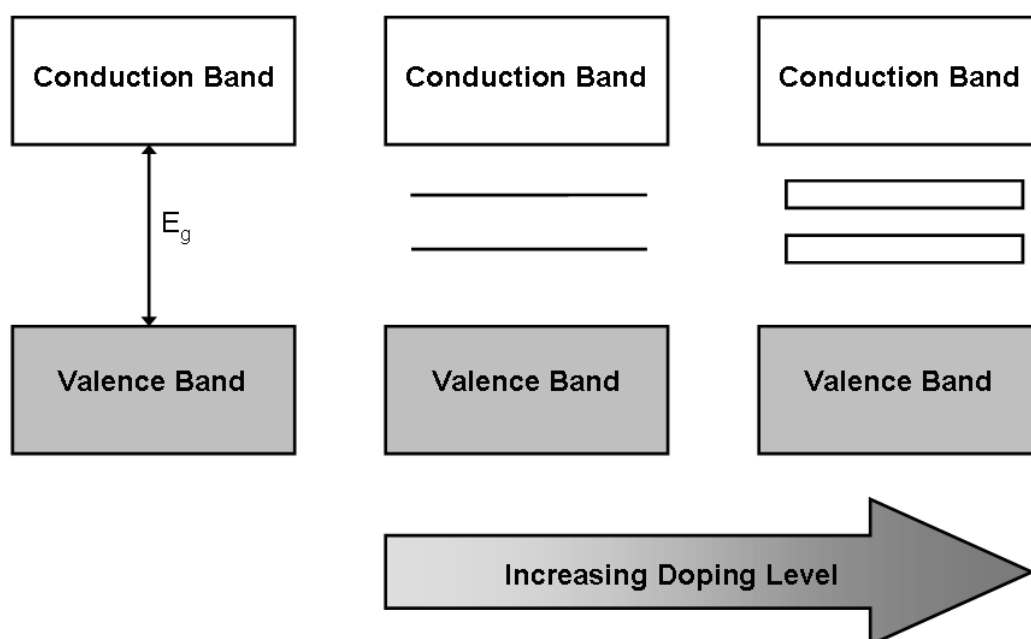
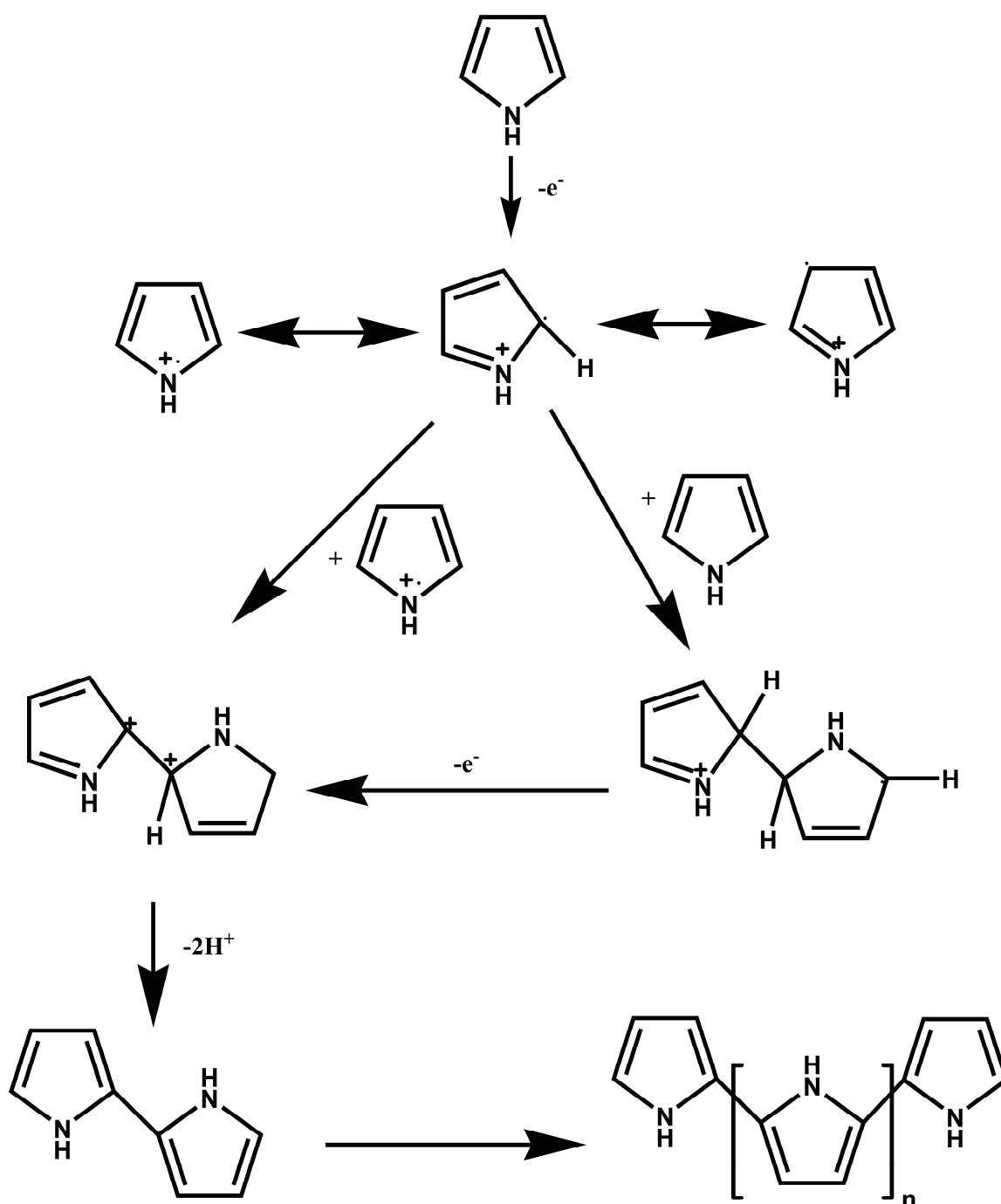


Figure 2-1: The formation of intermediate states in the band gap due to the increasing doping of the polymer. Redrawn from Ref [19].



Scheme 2-1: The electro-polymerisation mechanism of PPy. Redrawn from Ref [20].

Electrodes modified with conducting polymers have found a number of applications in the field of electrochemical sensing,^{21,22} with an extensive range of analytes being detected using this type of PME. Due to their redox-active nature, conducting polymers can often function as a complete sensor without the need for further modification, as they perform both a molecular recognition (via oxidation and reduction) and signal transduction role (due to their conductivity). This is the case in many conducting

polymer-based potentiometric sensors used for pH, gas or ion sensing. In these sensors, ion selectivity can be designed into the conducting polymer film through the control of both the growth conditions and dopants used. Such conducting polymer films have demonstrated selectivity for amines,²³⁻²⁵ halogens,²² surfactants²⁶ and various cations.²²

With the addition of separate compounds for molecular recognition, conducting polymers can provide numerous options for specific sensors. These compounds can be included in the polymer film using a variety of methods, including physical and electrostatic entrapment or covalent attachment through direct functionalisation or subsequent grafting onto the polymer.²⁷

The physical entrapment method is the most straightforward of the immobilisation methods. The desired compound is included in the polymerisation solution, and is incorporated into the film by being encased by the polymer during deposition. This physical entrapment design has been successfully used to immobilise a range of biological compounds in PPy in order to endow it with sensing capabilities.²⁸ Enzymes such as horseradish peroxidase and glucose oxidase, various antibodies and even complete cells have been incorporated using this configuration.²⁸ By controlling the composition of the deposition solution and the charge passed through the electrode, the electrodeposition method can allow for exacting control over the quantity and location of the deposited polymer. This control can also be used to locate the detection elements between multiple polymer layers coated onto the electrode. The layered approach has been used to prevent enzyme folding, improve adhesion of the recognition moiety²⁹ and include multiple enzymes in a sensor.³⁰

The electrostatic incorporation of the recognition compound into the conducting polymer matrix is often achieved via the control of the dopant or counterion used with the polymer. If the recognition moiety is natively an ionisable compound, such as an acid, then it is possible to incorporate the compound into the film directly during polymerisation or via ion-exchange after the formation of the film. Control of the dopant provides control of the mass and charge transport properties of the film and is often used in the creation of gas and ion sensors.^{22,24} Both direct incorporation and ion-exchange methods have been used to bind tris(4,7-diphenyl-1,10-phenanthroline)disulfonic acid) ruthenium(II) into a derivatised PPy film.³¹⁻³³ These films have been used to detect oxalate ions and amines via electrochemiluminescence.³¹⁻³³

The covalent attachment of the recognition moiety to the polymer film can be achieved by two pathways. Firstly, the recognition element or other moiety can be modified to include a polymerisable functional group, often with the incorporation of an alkane spacer,^{28,34} allowing for electrode modification to be undertaken in a single step. Alternatively a multi-step grafting procedure can allow for the incorporation of the moiety into the film after polymer deposition at the electrode.³⁴ Both methods have proven useful for the attachment of a number of compounds into the film.^{28,34-36} The functionalisation of pyrrole prior to electropolymerisation has resulted in the creation of glucose sensors via the inclusion of modified glucose oxidase³⁴ as well as DNA sensitive films via the incorporation of pyrrole functionalised single stranded DNA.^{35,36} The use of the PPy-DNA film for the detection of DNA hybridisation has been demonstrated through both microgravimetric and fluorescence measurements.

Electrodeposition of a conducting polymer can sometimes expose the detection elements to harsh polymerisation conditions. By utilising a multi-step grafting procedure, the

recognition moiety can be protected from degradation. This multi-step method is favourable for biosensing designs using enzymes and proteins where tertiary structure is important.²⁸ Depending on the sensor design, a number of manufacturing methods can be used. A common pathway for this sensor design is the use of a biotin-avidin bridge where both the recognition element and the underlying polymer are functionalised with biotin.³⁷⁻³⁹ The biotinylated-polymer is then exposed to the protein avidin which binds to the layer through its interaction with the biotin. As avidin has a number of binding sites, the functionalised recognition element can then be subsequently attached to the film. The method is illustrated in Figure 2-2, and has been used with the creation of an enzymatic based sensor for glucose and catechol,³⁷ as well as DNA.³⁸

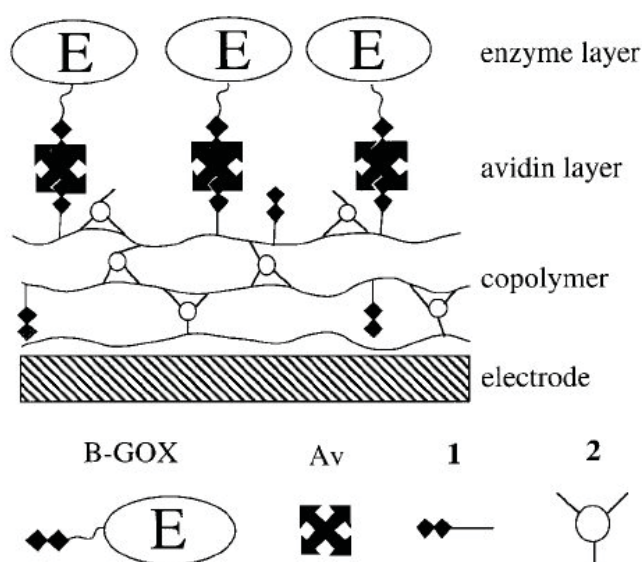


Figure 2-2: A PPy based glucose sensor where B-GOX is biotin bound to glucose oxidase, Av is the protein avidin, 1 is the pyrrole based biotin derivative and 2 is a pyrrole based tris(2,2'-bipyridyl)ruthenium(II) derivative. Redrawn from Ref [40].

2.2.1.3. Ionomers and Composites

Ionomeric polymers or ionomers, are branched polymers possessing ion exchange functionality through the incorporation of functional groups such as sulfonic acids (for example, Nafion (Figure 2-3) and polystyrene sulfonate), carboxylic acids, amines and other nitrogen-containing groups (for example, polyvinylpyridine, PVP). The use of this

class of polymer provides a range of electrode modification opportunities. In their native form, ionomers may act as a membrane barrier or be used for their ion exchange abilities. In acting as a membrane barrier, the ionomer film can be used to reduce interferences and improve analyte selectivity via the restriction of the flow of counterions through the film. For example, Nafion films have been successfully used to minimise ascorbic acid interferences during the detection of neurotransmitters.⁴¹ Similarly through cation exchange, Nafion can also assist in the preconcentration of cationic analytes.⁴²

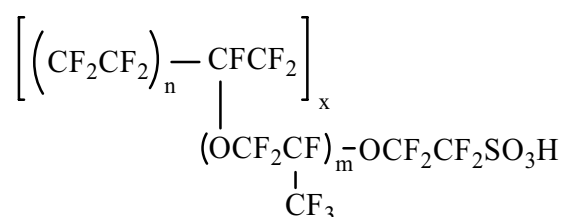


Figure 2-3: The chemical structure of Nafion.

It is also possible to modify the ionomer through the electrostatic attachment of charged compounds to the ion exchange sites. A range of compounds have been immobilised via ion exchange for use in sensing. There have been a number of papers on the electrostatic immobilisation of the electrochemiluminescent complex, tris(2,2'-bipyridyl) ruthenium(II) ($\text{Ru}(\text{bpy})_3^{2+}$) in Nafion and related polymers (Section 2.5.1.). Alternative metal complexes such as those of osmium, iron, and cobalt have also been immobilised in Nafion,⁴³⁻⁴⁵ with anionic metal complexes, such as IrCl_6^{3-} , $\text{W}(\text{CN})_8^{3-}$ and $\text{Fe}(\text{CN})_6^{3-}$ immobilised in PVP.^{46,47} In addition, Nafion and the related ionomer Eastman AQ, have been employed for the formation of enzyme-based sensors, with enzymes such as glucose and choline oxidase being electrostatically incorporated into the films.⁴¹

2.2.1.4. Ionomer/Conducting Polymer Composites

Commonly, conducting polymers require use of an ionic dopant to be conductive. The dopant used can have a significant effect on the properties of the conducting polymer

film. For example, the physical size of the dopant may provide control over the mechanical and morphological characteristics of the film, with smaller ions providing a more porous and less mechanically stable material than larger ions.⁴⁸ Dopant size also affects the ion exchange properties of the film. Small, mobile dopants enable anion exchange while large, sterically immobilised dopants are favourable for cation exchange.⁴⁹ In addition, the polymer conductivity can be modified by varying the pK_a of the dopant, with resistivity varying proportionally to pK_a .⁵⁰

The use of an ionomer such as Nafion as a dopant allows for the formation of films that are both mechanically sound and highly conductive, potentially providing an excellent platform for a range of PME-based sensors.⁵¹ Two manufacturing methods exist for the construction of ionomer/conducting polymer composites. The most common method is a two-step procedure involving the coating of the electrode with the ionomer prior to the deposition of the conducting polymer into the deposited ionomer. The alternative method is a one-step procedure where the ionomer is present in the electrodeposition solution. However, this method suffers from poor reproducibility caused by competition between the ionomer and the electrolyte in the doping of the conducting polymer.⁵¹ As reproducibility is a requirement of any sensor design, the two step production method is the logical choice and thus will be discussed in detail below.

A range of glucose sensors based on Nafion/PPy composites have been developed using a two-step synthesis.^{52,53} It was reported that these sensors provide improved enzyme entrapment when compared to using Nafion alone and reduce interferences from compounds such as urate and ascorbate.⁵³ Metallised Nafion/PPy composites have also been used as the basis for an electrochemical H_2 gas sensor.⁵⁴ In this case, the addition of PPy to the Nafion membrane significantly increased the lifetime of the sensor.⁵⁴

A common use for ionomer/conducting polymer composites, in particular Nafion/PPy composites, has been for membranes in direct methanol fuel cells and electro dialysis.⁵⁵ This type of composite has been shown to improve cell efficiency and lifetime by reducing methanol crossover in the fuel cell by up to 80%.⁵⁶ The reduction in methanol crossover is attributed to diminished permeability of the membrane caused by the presence of the PPy.⁵⁷ It has been suggested that the PPy restricts the molecular mobility of methanol through the film by obstructing the reversed micellar structure of the Nafion.⁵⁷

2.2.2. Monolayer Modified Electrodes

Modification of a surface by the covalent deposition or adsorption of monolayers is an accepted method of creating electrodes for a variety of sensing applications.^{7,9} In comparison with polymer-based designs, monolayer construction can provide a sensing system that is easy to construct, often by spontaneous self-assembly, while typically providing a highly ordered layer that allows for the construction of more complex sensing systems, such as protein-based biosensors.⁹ Many monolayer attachment chemistries have been used for electrochemical sensing applications. Arguably the two most important categories are: self assembled systems (otherwise known as self-assembled monolayers or SAMs) and electrografted layers. Self-assembled systems include chemistries such as alkanethiols on coinage metals^{9,58,59} and silanes on oxide surfaces.^{7,58} Whereas electrografting layers rely on the formation of radicals by either oxidation (as in the case for amines,⁶⁰⁻⁶² carboxylates,⁶⁰⁻⁶² alcohols⁶² and Grignard reagents⁶³) or reduction (as in the case of alkenes^{58,61,64} and diazoniums^{58,60,61,65}) of the attachment moiety. Currently alkanethiol and diazonium chemistries have found the most widespread use in electrochemical sensing applications, with the other attachment chemistries mentioned often proving unsuitable. For example, organosilanes require the presence of an oxide layer thus producing an insulating layer that can limit electron transfer rates making them

unsuitable for signal transduction to the electrode; alkene-based chemistries often require *in-vacuo* preparation of substrates,⁶⁴ and carboxylate chemistries often have low yields.⁷

2.2.2.1. Alkanethiol Monolayers

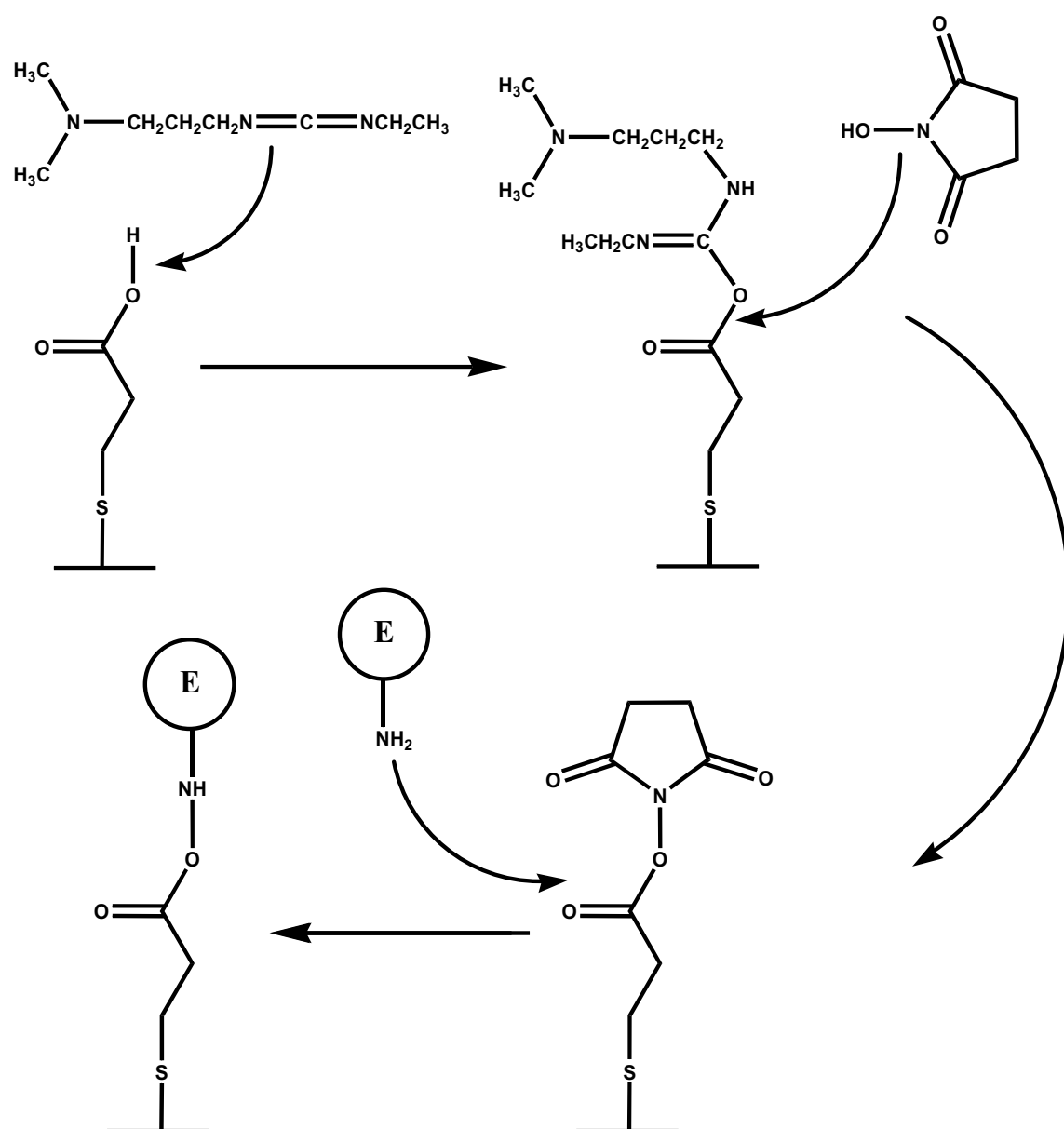
Historically, alkanethiol monolayers have been used extensively for sensing applications due to their ability to form stable, well ordered, densely packed monolayers on a range of metallic surfaces.^{58,59} Alkanethiols have been shown to chemisorb spontaneously to the surfaces of coinage metals such as gold, silver, platinum and copper via the formation of a metal-thiol bond.⁶⁶ Gold is the most common substrate used, due to its lack of stable oxide under ambient conditions.

Alkanethiol-based monolayers provide an easy to synthesise layer with the initial deposition undertaken via immersion in a dilute (~1 mM) solution of the thiol for a short period of time (~1 hr). Initially, the thiol is deposited randomly across the surface. The thiol is, however, partially mobile and can reorder over time to form a well-defined layer with alkyl chains angled at 20-30° from the surface normal.⁵⁸

The use of a large alkane group can insulate the electrode from the contacting solution, thereby limiting their usefulness for electrochemical applications. However, short-chained alkanethiol SAMs (such as 3-mercaptopropionic acid) are suited to electrochemical sensing applications as they form relatively disordered monolayers⁶⁷ while providing a low electron tunnelling barrier, allowing sufficient electron transport from the sensing moiety to the electrode. The use of conjugated,^{68,69} DNA⁷⁰ and nanotube based^{71,72} alkanethiol SAMs have also been shown to provide alternative electron transfer pathways making them suitable for use in most sensing applications.

Alkanethiols can have large electrochemical potential windows making them suitable for a wide range of sensing applications. Long chain alkanethiols can be electrochemically stable between potentials of about -1 and +1 V vs Ag/AgCl in some aqueous media.^{58,73,74} However, this potential window is reduced rapidly with decreasing chain length, as demonstrated with the 3-mercaptopropionic acid window of -0.4 to 0.6 V.^{75,76} The monolayer is oxidised to sulfinates ($-\text{SO}_2^-$) and sulfonates ($-\text{SO}_3^-$)^{76,77} at more anodic potentials and as a consequence, long term storage of the monolayer is difficult. To prevent oxidation of the monolayer, alkanethiol-based sensors are often stored in silver packaging to limit the effects of light and oxygen.⁵⁸

Despite the limitations of alkanethiol-based SAMs, a large number of electrochemical sensors have been developed using this attachment chemistry.⁶⁶ Two methods are employed. In the first method, the desired compound used for analyte recognition is synthesised with a thiol functionality present prior to deposition. The second approach builds the sensor via the sequential reaction of the layer with the desired chemistry, adding and removing functionality until the sensor is complete.⁹ Scheme 2-2 provides an example of the multi-step method for the construction of an enzyme-based sensor, with 3-mercaptopropionic acid used as the base thiol.



Scheme 2-2: A typical multi-step reaction scheme used for the construction of an enzyme based sensor using an alkanethiol SAM for grafting to the surface. Redrawn from Ref [9].

A number of steric issues can arise from the use of bulky detection moieties in sensor construction. This may result in the creation of pinholes and other surface defects leading to possible non-specific binding of compounds at the electrode, often resulting in poor sensor performance. To overcome this issue, a mixture of thiols can be used in the layer formation, providing more space between recognition sites while inhibiting non-specific binding to the electrode. An example of the use of this dilution method is found in the production of a DNA sensor shown in Figure 2-4. In this example, thiolated single-

stranded DNA is diluted by a short chained thiol preventing the direct absorption of the DNA to the electrode, ensuring it protrudes into the solvent phase allowing for better hybridisation of the DNA.⁷⁸

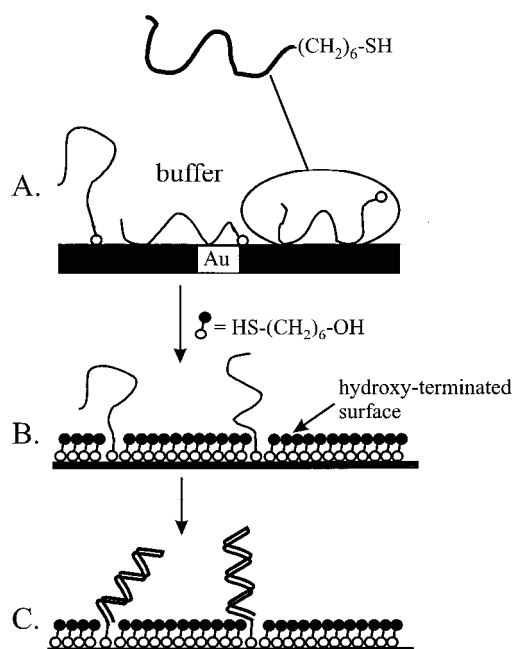


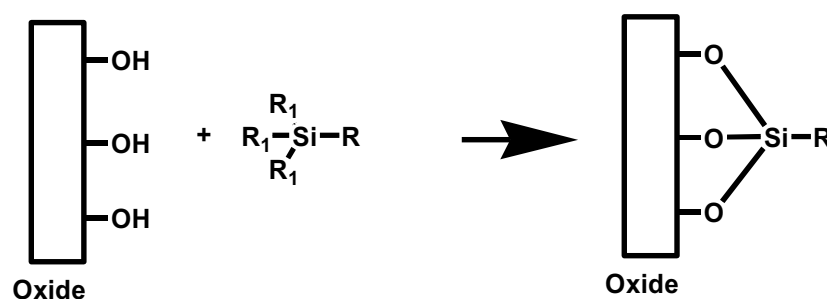
Figure 2-4: The formation of a DNA probe through multiple applications of alkane thiols. In (A) Single-stranded DNA (ssDNA) is adsorbed to the gold substrate through the thiol group as well as through backbone/substrate contacts. (B) After immersion in mercaptohexanol, the ssDNA is left attached by the thiol. (C) The end-tethered DNA can then successfully hybridise with ssDNA to form complementary oligonucleotides. Redrawn from Ref [78].

These construction methods have led to effective sensors being developed for the monitoring of pH,⁷⁹⁻⁸² inorganic,^{75,83-88} organic⁸⁹⁻⁹¹ and biochemical species^{78,92-96} using a range of chemical and biochemical-based sensing moieties. The majority of these sensors are based on either the detection of redox chemistry from the selected analyte or the blocking of access to the modified electrode surface to a mediator such as $\text{Fe}(\text{CN})_6^{3-}$, caused by the binding of the analyte to the surface.⁶⁶

2.2.2.2. Organosilane Monolayers

Organosilane monolayers provide an alternative attachment mechanism to the alkanethiol chemistry. This method allows for a different class of substrates to be used. Organosilanes spontaneously bind to a range of hydrogenated oxide surfaces forming $-\text{O}-\text{Si}-$ bonds, as

described in Scheme 2-3. The silane can then undergo further modification to provide the desired surface functionality. An oxide layer at the surface is required for the use of organosilanes. Use in an electrochemical sensor is limited, as many oxide materials introduce an insulating layer which can limit signal transduction. However, some conducting oxide materials exist, enabling electrochemically active organosilane-based layers to be constructed.^{7,97,98} Current literature suggests that very few of these monolayers have been developed into useful electrochemical sensing devices.

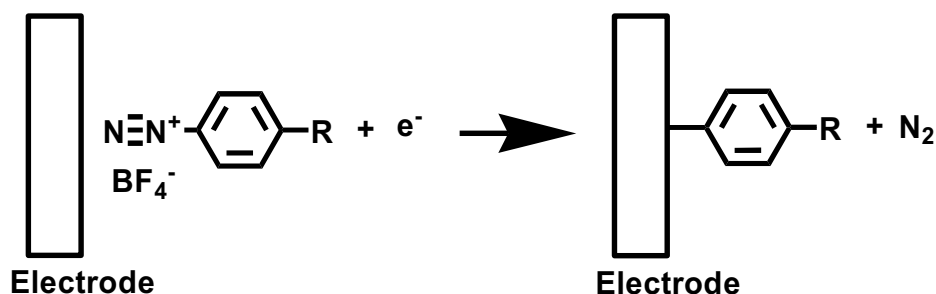


Scheme 2-3: Organosilane monolayer formation. The layer can be formed on any oxide surface. R_1 is typically either a halogen, or a methoxy group.

2.2.3. Diazonium Modified Electrodes

The use of diazonium chemistry to modify electrode surfaces provides an excellent opportunity to overcome many of the limitations of alkanethiol and organosilane-based systems. The grafting of aryl diazonium salts was first described by Pinson and co-workers⁹⁹ in 1992 and is achieved via a one-electron reduction and subsequent radical formation at the electrode surface as demonstrated in Scheme 2-4. The reductive deposition of the diazonium occurs at very low electrochemical potentials near 0 V,⁵⁸ and can be controlled by either CV¹⁰⁰ or potentiostatic deposition¹⁰¹ from an aprotic solvent such as acetonitrile, or acidic aqueous media (e.g. 0.1 M H₂SO₄).^{61,101} Diazonium systems have also been reported to chemisorb spontaneously^{102,103} without the use of an applied potential.¹⁰⁴⁻¹⁰⁷ This spontaneous deposition is thought to proceed through a similar mechanism to the electrochemical reduction with surface and solution impurities acting as

an electron source.¹⁰⁵ Diazoniums are known to be highly reactive; therefore low temperatures ($\sim 0\text{ }^{\circ}\text{C}$) are required for their storage and use. Due to the difficulty in storage, the diazonium is often created *in-situ* using the aryl amine and nitrous acid (HNO_2) in acidic media just prior to its deposition.¹⁰⁸



Scheme 2-4: Electrochemical deposition of aryl diazoniums.

Aryl diazonium salts are known to form stable bonds with a range of conductive materials including carbon (glassy carbon,¹⁰⁹⁻¹¹¹ graphite,^{101,112} nanotubes¹¹³⁻¹¹⁷ and doped diamond¹¹⁸⁻¹²⁰), polymers,¹²¹ metals,^{61,122-128} and semiconductors such as indium tin oxide,¹²⁹ gallium arsenide¹⁰³ and silicon.¹³⁰⁻¹³² As expected, the nature of the bonding with carbon materials is covalent while metals show the existence of a metal carbide bond.^{109,123,124,133,134} The bonding orientation of the diazonium on the surface has also been calculated using DFT calculations which demonstrate that in the case of the metallic substrates, binding can occur either as a σ -bond orientated normal to the surface or favouring π -bonding with the aryl group lying parallel to the surface.¹³⁴ When bonding to a graphitic surface, the binding exists normal to the surface irrespective of basal or edge planes.¹³⁵

The bond formed during the diazonium grafting can be stronger than most other attachment chemistries (c.f. 21 to 200 kJ mol^{-1} for Au-S^{59,61,136-139} to $\sim 265\text{ kJ mol}^{-1}$ for edge plane C-C¹³⁵). As a consequence the resulting layer is typically more stable. Diazonium modified electrodes have shown long term stability when stored in air and

also withstand sonication in a range of organic solvents.^{99,111,140} Additionally, the layers have been demonstrated to withstand temperatures of up to 700 K¹¹¹ and resist electrochemical degradation over a range of 5.6 V depending on the diazonium used.¹⁴¹

The stability of 4-nitrobenzenediazonium modified gold surfaces has been directly compared to the equivalent thiol (4-nitrobenzenethiol) modified surface¹⁴² and provides direct evidence for the enhanced stability of diazonium layers over thiols. It was found that while a higher portion of the thiol film survived sonication and refluxing, the thiol layer was completely removed after displacement with octadecanethiol while 25 % of the diazonium film remained, suggesting that the diazonium film is more strongly bound.

This excellent stability over a wide potential range and flexibility in terms of electrode substrates make diazonium modified electrodes highly suitable for electrochemical sensing applications, including ECL-based sensing.¹⁴³ While diazonium-based layers can provide excellent stability and wide potential range, the formation of these layers at the electrode surface is less controlled than that of alkanethiol or silane-based chemistry. Diazonium deposition is often controlled by varying the applied potential and deposition time. By assessing the charge passed through the electrode, surface coverage and layer thickness can be ascertained.^{61,144} However, this calculated surface coverage tends to be an upper limit of the amount of material deposited onto the surface. This overestimation of surface coverage is due to two factors. Firstly, not all free radicals generated are captured by the electrode. It has been reported that between 56 % (for Highly Orientated Pyrolytic Graphite, HOPG) and 84 % (for glassy carbon) of the radicals generated form bonds to carbon substrates.¹¹¹ On gold substrates, electrochemical quartz-crystal microbalance data indicates that the number of free radicals captured can be as low as

14 %.¹²⁴ Secondly, in addition to the reaction described in Scheme 2-4, a number of side reactions are also known to occur.

The two most important side reactions are the attack of an aryl group already bound to the surface at the meta position relative to the diazonium functionality¹⁰⁰ (and also the para position in the case of the R group in Scheme 2-4 being hydrogen) forming a multilayered system, and bonding to the surface without the loss of the diazonium creating an azo bond (-N=N-).^{145,146} The nature of these reactions is dependent on both the diazonium and substrate used.⁶⁵

It is commonly accepted that the attack of the aryl groups present at the surface allows for the possibility of multilayer formation in most aryl-diazonium based systems.^{100,124} Atomic Force Microscopy (AFM) and Scanning Electron Microscopy (SEM) show that the resulting layer can range from a well ordered monolayer to a loosely structured porous multilayered system in excess of 2 μm thick,^{100,144,147,148} (Figure 2-5) dependent on the deposition conditions and substrate used. It has been suggested that the morphology of the layer is dependent on the relative rates of reaction of the electrogenerated phenyl radical with the substrate and the already bound aryl groups.⁶⁰ If the reaction with the surface is faster, it is more likely that a monolayer will form before a second layer is established. However, if the reaction with the bound aryl groups is faster then bonding will occur at nucleation sites on the surface resulting in a more porous structure.¹¹² As a result, aryl layers on gold tend to be more porous than the equivalent carbon-based system.⁵⁸

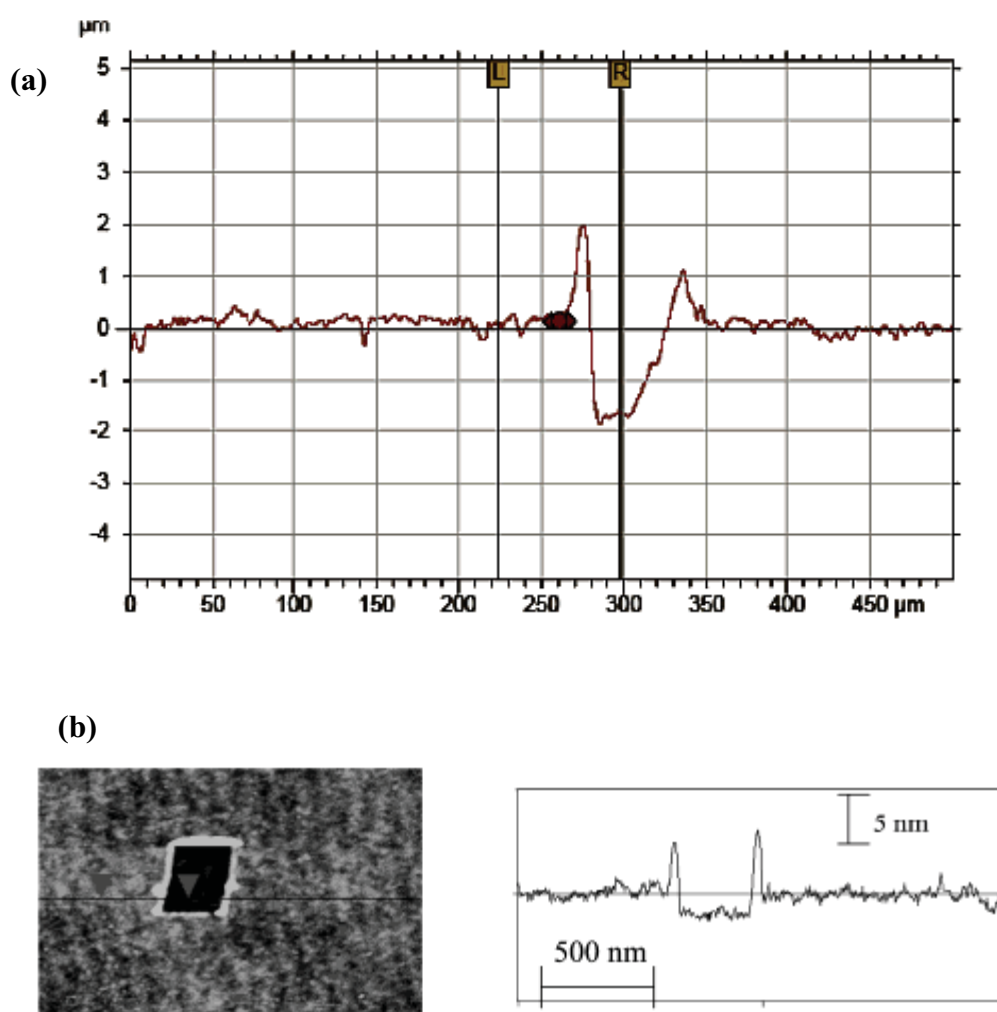


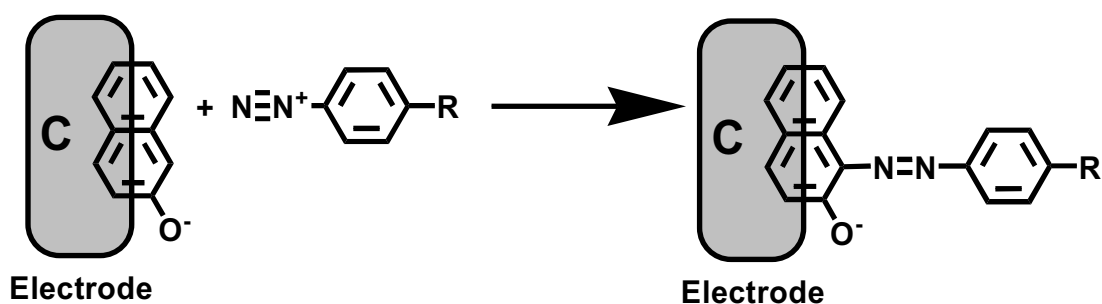
Figure 2-5: Profilometry of thick (a) and thin (b) films deposited from the diazonium precursor. Presented in (a) is a line scan of a scratched 2 μm thick polyphenylene film on an iron substrate (Redrawn from Ref [148]). In (b) below a line scan of a terphenyl monolayer 1.5 nm thick is shown (Redrawn from Ref [100]).

Layer morphology is not only influenced by reaction rate but also by the shape of the diazonium. It has been shown that the thickness of the layer can be controlled by altering the substituent at the ortho and meta positions relative to the diazonium group.⁶⁵ It has been further demonstrated that ortho-substituted diazoniums do not participate in grafting and the more bulky meta substituted diazoniums such as 3,5,-bis-*tert*-butyl benzenediazonium result in thinner more monolayer-like films than their less sterically-hindered counterparts.

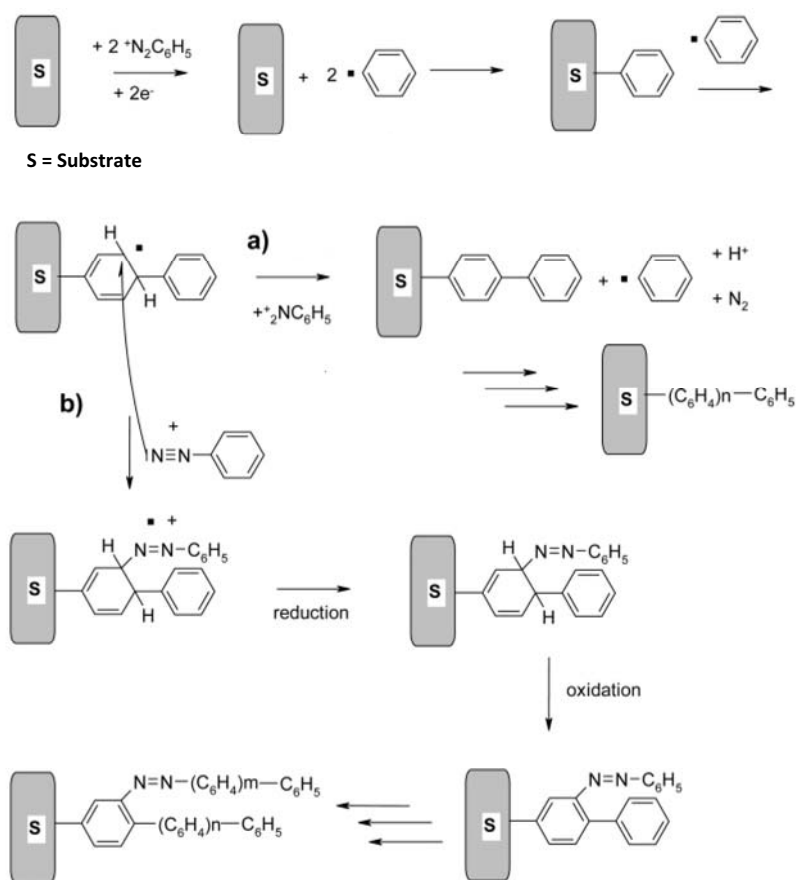
From an electrochemical sensing view, the formation of multilayers, porous or otherwise, is not necessarily detrimental. As the aryl diazonium layers will often allow charge transport through the conjugated sp^2 structure,^{100,149,150} transduction of an analyte recognition event can readily be achieved. In addition, a porous structure allows for an increase in the active analysis area when compared to a two dimensional monolayer. Currently, only a few sensing applications require a well defined layer, with only some biochemical-based sensors, such as those used for DNA detection, explicitly benefiting from highly ordered surfaces.^{76,151-154}

The other important side reaction is the formation of azo functionalities throughout the layer. This type of reaction can be problematic for the creation of sensing devices. The binding of the diazonium through the azo group could possibly provide a less stable bond which is susceptible to oxidation.^{155,156} The XPS spectra of diazonium films can reveal a peak at about 400 eV in the N 1s region.¹²⁴ This peak has often been discounted as a contaminant or unwanted by-product of the surface modification. Studies by Bélanger¹⁴⁵ were first to suggest that this peak was due to the azo functionality and suggested the mechanism of formation (Scheme 2-5). The formation mechanism is proposed to be similar to the solution phase reactions observed with diazoniums and phenol or naphthol, and results from the use of partially oxidised carbon substrates. Further, Time-of-Flight Secondary Ion Mass Spectrometry (ToF-SIMS) studies of diazonium derived phenylene layers by Pinson¹⁴⁶ are supportive of the formation mechanism proposed in Scheme 2-5. In a multilayered system azo functionalised binding between layers is also thought to exist.^{125,146} Pinson¹⁴⁶ also presents ToF-SIMS evidence for the alternative formation mechanisms described in Scheme 2-6. This scheme presents two possibilities; in the ideal case (path a) a linear chain is formed with the diazonium constantly reacting in the para position, resulting in perfect molecular chains originating from the electrode surface.

However, it is thought that the second pathway (path b) also occurs, with the diazonium reacting at the ortho position without the loss of nitrogen forming the azo linkage. This pathway can be considered sterically more favourable in some cases than other multilayer mechanisms previously proposed that suggest the complete loss of N_2 .⁶¹



Scheme 2-5: The proposed formation of azo bonds at the surface Redrawn from Ref [146].



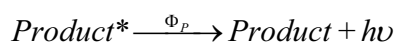
Scheme 2-6: Proposed mechanisms for polyphenylene multilayer synthesis, via the use of a phenyl diazonium salt. Path (a), is the ideal situation without azo formation, and path (b) the suspected mechanism for the formation of azo groups within such a layer. Redrawn from Ref [146].

Some studies have suggested that up to 75 % of the aryl groups in the layer are bound by -N=N- bonds.^{145,157} This high percentage of azo bonding may present a problem for some sensing applications due to the possibility of oxidative cleavage of the bond,^{155,156} which would adversely affect device lifetimes.

Irrespective of the issues discussed above, a number of electrochemical sensors have been successfully developed with the use of diazonium-based surface modification. These sensors have been created using both multi-step and single step methods, and as with alkanethiols, they cover the full spectrum of analytical chemistry, with the development of pH,¹⁵⁸ gas,^{159,160} biochemical,^{108,161-169} inorganic¹⁷⁰ and organic^{120,171,172} sensors.

2.3. Electrogenated Chemiluminescence

Electrogenated chemiluminescence, otherwise known as electrochemiluminescence or ECL, is the light emission that arises from the high energy electron transfer between electrochemically generated species. An ECL reaction can be considered a subset of a broader class of charge transfer chemiluminescence (CL) reactions that adhere to the general reaction:



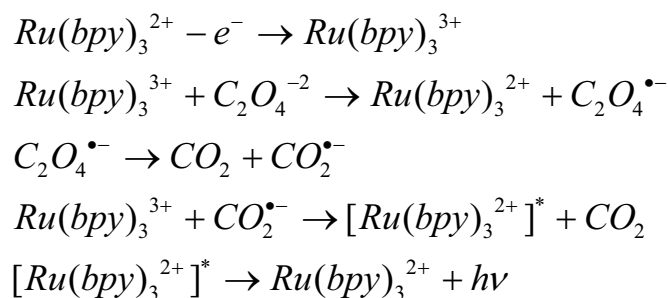
Where A and B are the reactants that form a product in an electronically excited state with an efficiency of Φ_{ES} that subsequently relaxes with the emission of a photon with an efficiency of Φ_P .¹⁷³ In ECL, one or more of the reactants are electrochemically generated, resulting in the creation of highly oxidising or reducing intermediates suitable for a CL

reaction. Electrochemical initiation provides a number of benefits over alternate chemically initiated pathways: giving greater control over the reaction, minimising side reactions, as well as providing precise control over the temporal and spatial location of the reaction. ECL may be produced by reactions involving organic species such as polyaromatic hydrocarbons, like anthracene or luminol. However, more commonly studied is the ECL arising from luminescent metal complexes such as the prototypical ECL luminophore, $\text{Ru}(\text{bpy})_3^{2+}$.¹⁷⁴

The emission of light upon electrolysis can form the basis of a detection scheme for a range of analytes and hence is of much interest to the analytical chemist. A number of reaction pathways result in light emission. Initially it was thought that ECL was only possible through the annihilation pathway where the oxidised and reduced forms of the luminophore, e.g. $\text{Ru}(\text{bpy})_3^{3+}$ and $\text{Ru}(\text{bpy})_3^+$, comproportionate to form the excited luminophore, $\text{Ru}(\text{bpy})_2^{2+*}$.¹⁷⁵ This pathway is often not useful from an analytical view point, due to the wide potential window required for the formation of the reduced species. This makes the annihilation pathway unsuitable for use in aqueous media, and therefore unsuitable for most analytical applications.

In 1977 Bard demonstrated an alternate ECL mechanism involving the use of a co-reactant, where only a single potential step is needed,^{176,177} reducing the potential window required and allowing the reaction to proceed in aqueous media often without deoxygenation.¹⁷⁸ Typically, this mechanism involves the oxidation of the co-reactant to form a strong reducing agent (replacing $\text{Ru}(\text{bpy})_3^+$) which then proceeds to reduce $\text{Ru}(\text{bpy})_3^{3+}$ to $\text{Ru}(\text{bpy})_2^{2+*}$. As expected, the converse with $\text{Ru}(\text{bpy})_3^+$ being oxidised to $\text{Ru}(\text{bpy})_2^{2+*}$ is also possible with the appropriate co-reactant.¹⁷⁹ An example of the co-reactant mechanism involving the oxalate anion is shown in Scheme 2-7 below. Here the

$Ru(bpy)_3^{3+}$ acts to oxidize the co-reactant, however this function can also be performed by the electrode, particularly in the case of co-reactants containing amine moieties.



Scheme 2-7: ECL reaction of $Ru(bpy)_3^{2+}$ with the oxalate anion.

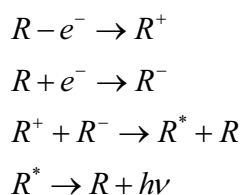
Many compounds have been demonstrated to act as a co-reactant in mechanisms similar to Scheme 2-7, with compounds containing organic acids and amines, in particular tertiary amines, being shown to be most suitable for the oxidative pathway, and peroxydisulfate ($S_2O_8^{2-}$) and similar compounds being suitable for the reductive pathway.¹⁷⁹

Reactions involving a co-reactant are desirable in analytical applications as the ECL intensity is usually proportional to the concentrations of the co-reactant and the luminescent species. Thus, depending on the concentration of either reagent, ECL can be used in the detection and quantification of a co-reactant, the luminescent reagent itself or compounds labelled with either reagent, such as detection of $Ru(bpy)_3^{2+}$ tagged DNA^{174,180-183} In the case of CL, this co-reactant pathway requires the use of a strong oxidant such as lead dioxide or cerium(IV) sulfate.¹⁷⁴

The formation of the excited state and the resultant light emission are not unit efficiency processes and a system can suffer from low photon yields reducing suitability for analytical applications. The efficiency in producing a photon from a given redox event (Φ_{ECL}) can be considered a product of two factors: the efficiency of production of the

excited state (Φ_{ES}) and the efficiency of light emission from the excited state (Φ_p). The ECL efficiency can vary significantly between compounds. The most investigated compound, $\text{Ru}(\text{bpy})_3^{2+}$, is accepted to have an efficiency of 5% (via annihilation) under ideal conditions, however, values of up to 33 % for tris(4,7-diphenyl-1,10-phenanthroline) ruthenium(II) have been reported.¹⁸⁴ The variation in Φ_{ECL} is due to variations in both Φ_{ES} and Φ_p . Temperature and solvent can also affect this value.

The efficiency of the formation of the excited state, R^* , is governed by the electron transfer between the precursors, which in the case of an annihilation reaction (Scheme 2-8) can be considered the reduced species, R^- , and its oxidised counterpart, R^+ .



Scheme 2-8: A generalised ECL annihilation mechanism.

The precursor R^+ can be described as a molecule containing a ‘hole’ in the Highest Occupied Molecular Orbital (HOMO), and R^- can be thought as having an electron existing in the Lowest Unoccupied Molecular Orbital (LUMO). As described in Figure 2-6, two possible pathways exist for the electron transfer between the R^- and R^+ species, with the electron in the LUMO of R^- being transferred directly to the HOMO of R^+ (Path B) or alternatively being transferred to the LUMO of R^+ then decaying via light emission to form the ground state (Path A). The preference for the system to decay via either mode determines the probability and hence the efficiency of the excited state formation, Φ_{ES} .

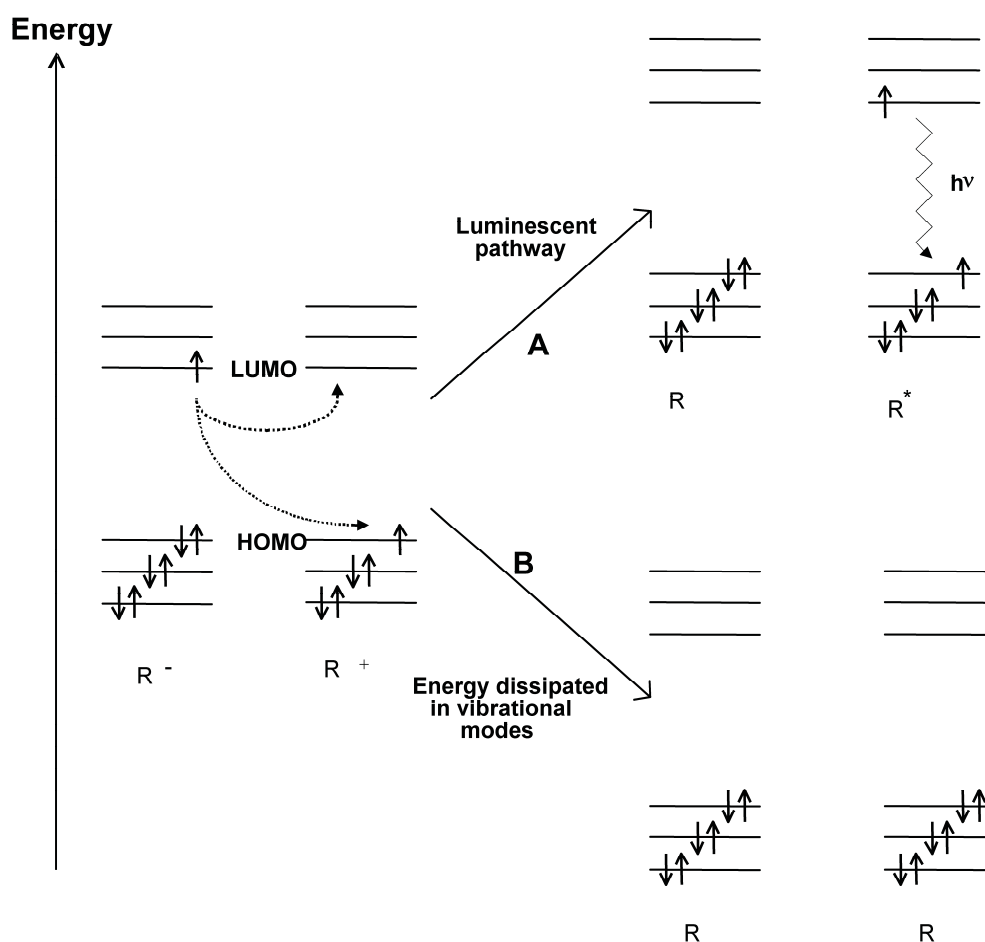


Figure 2-6: Molecular orbital diagram showing two alternative pathways for electron transfer between reduced and oxidised precursors R^- and R^+ . (A) Formation of an excited state and (B) direct production of ground state products. Redrawn from Ref [185].

An understanding of the reaction route preference can be realised through the electron transfer theory first developed by Marcus.¹⁸⁶ Briefly, for ECL to occur, the thermodynamically less favoured electron transfer shown in Path A of Figure 2-6 needs to be preferred. ECL reactions are typically characterised by fast ($\sim 10^{10} \text{ M}^{-1}\text{s}^{-1}$), highly energetic (2-4 eV) electron transfers, and as such formation of ground state products would require a large amount of energy to be rapidly dissipated through the vibrational modes to accommodate the thermodynamically favoured pathway. This difficulty is resolved by the formation of the electronically excited product and the ultimate dissipation of the excess energy in the form of a photon.¹⁸⁷ In other words, the formation

of ground state product is kinetically inhibited because the highly exergonic nature of the reaction places it in the so-called Marcus inverted region.

In ideal situations, Φ_{ECL} can be considered to approach Φ_{P} , (for example, $\text{Ru}(\text{bpy})_3^{2+}$ in deoxygenated acetonitrile) yet it is generally observed to be lower. This behaviour can be attributed to at least two causes: firstly, the instability of the reaction products (for example R^+ or R^-) results in not all electrochemically generated material participating in the reaction and secondly the competition between the reaction leading to the excited state and that directly leading to the ground state.¹⁸⁸

The excited state can be quenched by another molecule to produce the ground state without light emission, potentially reducing Φ_{ECL} significantly. The non-radiative electron transfer between the luminophore and a quencher occurs quite readily due to the excited state being easier to oxidise or reduce than the corresponding ground state by an amount essentially equal to the excitation energy of the molecule.¹⁸⁹ Quenchers are most commonly oxygen or water, although the unexcited luminophore or co-reactant can also act as a quencher, particularly in high concentrations.^{14,190} These quenchers can prove to be a limiting factor on the sensitivity of a co-reactant detection system. The effect of quenching on co-reactant detection has been demonstrated in the detection of tripropylamine, with the reducing tripropylamine radical quenched by oxygen.¹⁴

The electrode itself can also quench the reaction by allowing electron or energy transfer to occur between the electrode and the luminophore. The problem of electrode quenching can be minimised by electronically decoupling the luminophore from the electrode through the use of a semiconducting electrode such as indium tin oxide (ITO) coated glass.¹⁸⁹

2.4. ECL for Chemical Sensing

Extensive work has been undertaken in regards to the analytical suitability of ECL-based detection methods with a number of commercial detection systems now available for the identification of biomolecules.¹⁸⁰ Due to the selectivity of the method it is often employed for the sensitive detection of organic compounds containing acid or amine functionality, such as pharmaceuticals and pesticides. ECL-based detectors are typically coupled to Flow Injection Analysis (FIA), Capillary Electrophoresis (CE), or High Performance Liquid Chromatography (HPLC) systems, however batch detection and lab-on-a-chip systems can also be used.^{174,181}

When compared to other detection methods for similar compounds ECL can provide a number of benefits, including: spatial and temporal control over the reaction zone; inexpensive and simple experimental set-up; low background signals; relative insensitivity to matrix effects; large linear ranges (up to 6 orders of magnitude for some co-reactants) and excellent sensitivity, with limits of 10^{-12} M routinely achieved for luminophore tagged biomolecules and sub nanomolar sensitivity achieved for co-reactants.^{174,180,191}

2.4.1. Solution Phase ECL

Traditionally ECL-based detection has been undertaken with all required reagents in the solution phase. Solution phase ECL offers sensitive detection limits for a range of compounds while providing simple, cost-effective experimental design. Bard first demonstrated the analytical applications of ECL in 1983 by using the technique to detect and quantify the oxalate anion in aqueous solution.¹⁷⁸ Since then numerous compounds have been demonstrated to be suitable for quantification via ECL methods. Solution phase methods have proven to be highly sensitive and reliable and are now routinely used in a

number of commercial ECL systems such as the ORIGEN Analyzer¹⁸⁰ which is designed for use in clinical diagnostics.

Two operational modes exist for solution phase systems. The first mode of operation is with a large excess of luminophore present in solution when compared to the amount of co-reactant.¹⁷⁹ This operational mode is designed for the sensitive detection of the co-reactant as it can be assumed that the luminophore concentration remains effectively constant throughout the reaction and thus the amount of light produced is primarily a function of co-reactant concentration. The second mode of operation functions with a reversal of reagent concentrations, with the co-reactant being present in excess, acting as a detection mechanism for the luminophore. Typical applications involving this mode incorporate the luminescent labelling of a compound such as DNA or antibody prior to detection.¹⁸³

Both methods can provide excellent sensitivity with co-reactant concentrations of 10^{-9} M regularly being detected,^{174,180,191} and conversely 10^{-12} M for the detection of the derivatised luminophore.¹⁹² In addition to being highly sensitive, these systems also possess an excellent linear range of up to 6 orders of magnitude for the detection of the luminophore,¹⁹² and up to 8 orders of magnitude for some pharmaceuticals.¹⁷⁴ Due to this sensitivity and large linear range, solution phase ECL has proven suitable for the analysis of a large range of compounds, often finding use with many pharmaceutical and agricultural chemicals.

Despite the excellent performance of solution phase ECL, it does suffer several disadvantages, including loss of signal due to diffusion of the luminophore out of the reaction zone, limited ability to cycle electrochemically an individual luminophore

repeatedly and high consumption of the luminescent reagent.¹⁴ Further, the inclusion of extra reagents to the solution may complicate any additional sample processing. These difficulties are compounded when using solution phase ECL as a detection system for flowing stream methods such as FIA and HPLC. This is due to the requirements of additional reagent streams for the introduction of the luminophore containing solution which in turn provides more experimental variables (luminophore flow rate for example) to adjust for optimal detection.

With these disadvantages in mind, there has been considerable effort committed to the creation of modified electrodes for use in the ECL detection of co-reactants. As the luminophore is not the analyte in this detection mode and can be regenerated during the course of the reaction, it is possible to immobilise the luminescent reagent at the electrode surface and not degrade the system performance, by maintaining a similar luminophore concentration to that in the reaction zone of the equivalent solution phase experiment.¹⁹³ The use of an immobilised luminophore for ECL sensing would avoid many of the problems commonly associated with solution phase ECL detection methods, with the resulting sensor being readily compatible with existing separation techniques.

2.5. Immobilisation Methods for ECL Active Compounds

In the case of $\text{Ru}(\text{bpy})_3^{2+}$ based ECL, the luminescent reagent is regenerated during the course of the reaction and therefore can be reused for many more analyte recognition events. This feature of the reaction lends itself to the creation of ECL sensors based on modified electrodes. The immobilisation of the luminescent reagent at the electrode can offer a simple and sensitive detection arrangement requiring only a small quantity of luminescent reagent, while at the same time localising the luminophore, achieving

concentrations not normally possible in the equivalent solution phase set-up (c.f. millimolar to molar concentrations). The reduction in the quantity of reagent can reduce costs and assist in the development of ECL-based lab-on-a-chip devices and other applications.

The immobilisation of ECL active complexes, in particular $\text{Ru}(\text{bpy})_3^{2+}$ and its derivatives, has been explored with a wide range of immobilisation methods. Several immobilisation strategies for $\text{Ru}(\text{bpy})_3^{2+}$ and its derivatives have been reported, including the use of: Langmuir-Blodgett^{194,195} and Langmuir-Schaefer films;^{196,197} liquid crystals;¹⁹⁸ self-assembled monolayers;^{143,199-205} conducting polymers^{31,32} and metallopolymers^{11,206-208} - both preformed and electrodeposited varieties;²⁰⁹⁻²¹¹ hydrophobic immobilisation,^{212,213} electrostatic immobilisation in ionomers such as Nafion²¹⁴⁻²¹⁶ and Eastman AQ55D;²¹⁷ Sol-Gels;²¹⁸⁻²²⁰ and a range of composite materials²²¹⁻²²⁹ often involving the use of nanotubes²³⁰⁻²³⁴ or nanoparticles.^{217,235}

The most favoured $\text{Ru}(\text{bpy})_3^{2+}$ attachment method is through the use of a polymeric matrix to immobilise the complex to the electrode. However the use of covalently-bound monolayers remains a largely unexplored alternative for ECL sensors.¹⁴³ Both attachment methods provide a number of benefits. However, it is currently considered that most immobilisation methods lack the stability required for a commercially suitable analytical device.

2.5.1. Polymer Modified Electrodes

Polymer Modified Electrodes are a simple method of electrode modification and are often used in ECL-based sensors. A range of polymer systems have been previously investigated for ECL analysis, with redox polymers¹¹ and ionomers typically used.

The most explored of these polymer layers has been ionomers, with Rubinstein and Bard first reporting the electrostatic immobilisation of $\text{Ru}(\text{bpy})_3^{2+}$ in the perfluorinated cation-exchange polymer Nafion in 1980.²³⁶ Since then, extensive research has been undertaken in an attempt to improve and understand such polymeric systems. This Nafion-based system provides good sensitivity and linear range for the detection of oxalate and various amines in aqueous solution, with a linear range of 4 orders of magnitude being demonstrated for oxalate.²¹⁴ However, there are issues with the stability of this system as $\text{Ru}(\text{bpy})_3^{2+}$ may partition into electrochemically inaccessible hydrophobic regions of the film.^{8,214,216,237-240}

Nafion and related polymers such as Eastman AQ (a non-fluorinated version of Nafion) and polystyrene persulfonate are often considered to be a clustered network of reversed micellar structures²⁴¹⁻²⁴⁴ consisting of hydrophilic and hydrophobic domains as shown in Figure 2-7. For Nafion at least, this structure is thought to vary significantly with solvent content.^{245,246} The networking of the hydrophilic regions allows for the diffusive transport of ions throughout the layer while the hydrophobic regions provide structural integrity and prevent dissolution into aqueous media.

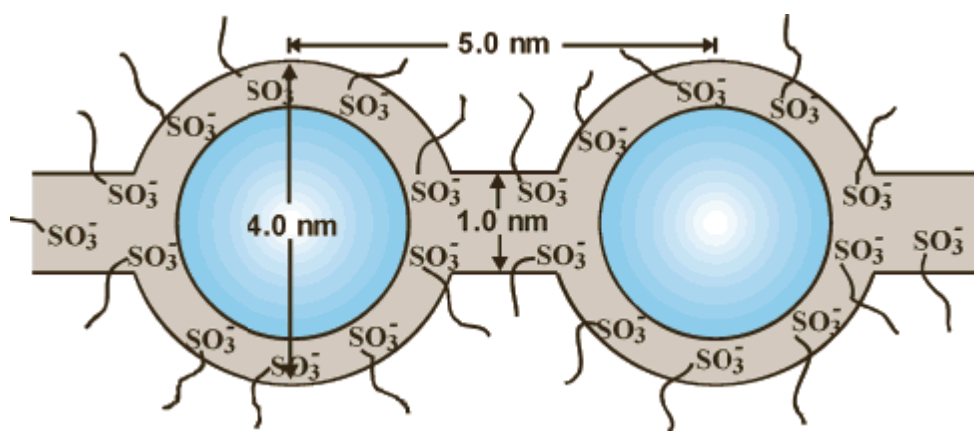


Figure 2-7: The reversed micellar structure of Nafion. Redrawn from Ref [245].

The presence of hydrophobic regions in the film can create potential difficulties in regards to the electrochemistry of hydrophobic metal complexes such as $\text{Ru}(\text{bpy})_3^{2+}$, exhibiting a slow partitioning into the electrochemically inaccessible region of the film. Studies have been undertaken to verify and understand the partitioning of compounds into the electrochemically inaccessible regions.^{238-240,247} It is normally considered that complexes like $\text{Ru}(\text{bpy})_3^{2+}$ are electrostatically bound to the sulfonate functionality, however, it is possible for the complex to exist as a neutral charge compensated entity (such as $\text{Ru}(\text{bpy})_3\text{Cl}_2$) and reside within the hydrophobic region of Nafion.²³⁹ The rate at which a complex migrates into this hydrophobic region is generally considered to be slow, occurring over a period of hours and is determined by a range of factors including solution pH, oxidation state and proton content of the complex.²³⁹ Complexes absorbed into these hydrophobic regions can be temporarily introduced into the electrochemically active areas of the Nafion by partially solvating the hydrophobic and interstitial regions of the film with the addition of a water miscible organic solvent like ethanol.^{214,239}

To overcome the limitations in stability of ionomer films such as Nafion, a range of composite materials have been developed.^{221-232,235} Previously used composites have typically blended Nafion with a range of sol-gels (including silica,²²¹ titania,²²² vanadium oxide²²⁶ and alumina²²³) and carbons (nanotubes^{230,231} and powdered graphite²²⁴). These composites have had varying success in improving the stability of the film, extending the layer viability from approximately a day for Nafion films to a number of days for most composites.¹⁷⁴ However, the current literature suggests an incomplete understanding of the layer stability improvement mechanism. It is suggested that this improvement is due to the composite co-material (nanotubes, organic silicates, etc.) providing a stronger hydrophobic interaction with the $\text{Ru}(\text{bpy})_3^{2+}$ than that of the surrounding Nafion. This

stronger interaction hinders the migration of the $\text{Ru}(\text{bpy})_3^{2+}$ into the electrochemically inaccessible regions of the Nafion.^{224,232,235}

The lack of understanding regarding stability is compounded by there being no benchmark by which the analytical stability of solid state ECL devices is measured.¹⁷⁴ Previously, stability has been estimated in relation to peak currents and ECL intensity, however the conditions, such as solvent type, storage, and duty cycle vary significantly between authors. The issue of improving layer stability while maintaining sensitivity remains an obstacle to the commercialisation of ECL sensors based on immobilised luminescent reagents.

While a large range of Nafion composites have been explored for ECL sensing, the use of Nafion/conducting polymer composites in this field is yet to be reported. Conducting polymers possess properties that make them potentially suitable for the creation of a Nafion-based ECL sensor, such as high conductivity which could allow for high charge transport throughout the layer and simple sensor synthesis via electrodeposition. As previously mentioned (Section 2.2.1.4), conducting polymer composites of Nafion are not new and have been used to improve the entrapment of the redox moiety, reduce interferences and improve sensor lifetimes. These reported benefits would be desirable for a PME-based ECL sensor.

2.5.2. Monolayer Modified Electrodes

A number of monolayer and multilayer-based ECL active systems have been developed with varying success.¹⁷⁴ The first ECL active monolayer systems were produced by Bard via the deposition of Langmuir-Blodgett films using a $\text{Ru}(\text{bpy})_3^{2+}$ based surfactant.¹⁹⁵ These films are relatively easy to produce, however they suffer significantly from poor

stability.¹⁹⁴ These type of monolayer films have been reported to collapse at the electrode surface¹⁹⁴ and also suffer from limited oxidative stability, degrading in up to 15 minutes under repetitive cyclic voltammograms.²⁴⁸

An alternate monolayer attachment chemistry is the use of alkanethiol chemistry, with a limited number of alkanethiol based monolayers being reported for ECL use.^{200,202,205,249} While excellent light output is reported, issues with layer stability are experienced. As expected, these stability issues resulted from desorption of the SAM at the high oxidising potentials required for ECL which is typically much higher than the potential window of the SAM (c.f. 1.3 V with 0.8 V). As a result of this instability such layers have not been investigated from an analytical point of view.

Aside from alkanethiols and Langmuir-Blodgett methods, a range of other monolayer chemistries exist that are potentially useful for luminophore attachment. One recently explored option has been the use of organosilane-based layers. The creation of organosilane monolayers for electrochemistry has been limited due to the requirement of an oxide layer to conduct the attachment chemistry, potentially restricting electron transfer to and from the electrode. Some researchers have used organosilane chemistries to attach potentially ECL active complexes to the surface.^{201,250,251} Investigation of both the photochemistry and electrochemistry of these complexes has been undertaken, although the ECL properties have not yet been reported.

Recently Wang's group have reported the synthesis of an ECL active organosilane monolayer on an ITO electrode.⁹⁷ This conductive oxide readily allows access to the redox properties of the layer. The ECL active layer was based on a ruthenium complex with an epoxy modified phenanthroline ligand. The ligand was attached to the substrate

via reaction with an aminated silane already immobilised at the electrode surface. To improve the solid state ECL response, a layer was formed whereby the complex was attached to gold nanoparticles through use of the epoxy chemistry, then subsequent attachment to the electrode with the use of a mercaptosilane. While both layers exhibited strong ECL, the demonstration of the layers stability was restricted to only 10 cyclic voltammograms (~8 minutes), preventing an appropriate comparison with other immobilisation methods. The absence of other relevant analytical data such as limits of detection also hampers the assessment of the layer suitability for ECL-based sensing systems.

A potential method to achieve stable ECL active monolayers is to form layers via the electroreductive absorption of aryl diazonium salts. As previously discussed, this chemistry can result in a strong carbon-carbon bond between the compound and the electrode, possibly limiting many of the degradation issues associated with monolayer chemistries. The use of the diazonium pathway has been previously used to achieve an ECL active sensor, with $\text{Ru}(\text{bpy})_3^{2+}$ being electrostatically attached to the electrode via a benzene sulfonic acid monolayer deposited from the diazonium salt.¹⁴³ The layer was reported to be stable with no loss of signal over the course of a week when stored dry, however no information about the duty cycle of the sensor during that time was provided.

At present no covalently bound ECL-based devices using diazonium based attachment chemistry have been reported. A redox active osmium compound has recently been attached using a two-step method based on the diazonium chemistry.²⁵² While no ECL was demonstrated in this paper, tris(2,2'-bipyridyl) osmium(II) complexes have been shown to undergo solution phase ECL.²⁵³ Also Lefrant's group have demonstrated the electrodeposition of a $\text{Ru}(\text{bpy})_3^{2+}$ derivative, bis(2,2'-bipyridyl)(4-phenyl-2,2'-bipyridyl)

ruthenium(II) from the isolated diazonium salt in acetonitrile.^{254,255} The complex was successfully attached to a range of substrates including glassy carbon, carbon nanotubes and boron doped diamond. The resulting layer was suggested for use in a range of possible optoelectronic applications requiring photosensitive compounds and was shown to be stable for an extended period of time with a 20 % decrease in peak height over 90 min. However the use of organic solvents for the deposition possibly limits the potential use of these devices in many developing fields such as microfluidics and screen printed electrodes where organic solvents may be detrimental for sensor construction or lifetime. In summary, these previous achievements highlight the potential for creation of a diazonium based immobilisation method for ECL active complexes.

2.6. References

- (1) Wang, J. *Analytical Electrochemistry*; VCH Publishers, Inc.: New York, 1994.
- (2) Janata, J.; Josowicz, M.; DeVaney, D. M.; *Anal. Chem.* **1994**, *66*, 207R-228R.
- (3) Koryta, J.; *Anal. Chim. Acta* **1981**, *139*, 1-51.
- (4) Merz, A. In *Electrochemistry IV*; Springer Berlin, 1990; Vol. 152, p 49-90.
- (5) Murray, R. W.; Ewing, A. G.; Durst, R. A.; *Anal. Chem.* **1987**, *59*, 379A -390A.
- (6) Wang, J.; *Electroanal.* **1991**, *3*, 255-259.
- (7) Murray, R. W. In *Electroanalytical Chemistry: A series of Advances*; Bard, A. J., Ed.; Marcel Dekker, Inc.: New York, 1984; Vol. 13, p 191-368.
- (8) Wei, H. W.; Wang, E.; *Trends in Anal. Chem.* **2008**, *27*, 447-459.
- (9) Gooding, J. J. In *Encyclopedia of Nanoscience and Nanotechnology*; Nalwa, H. S., Ed.; American Scientific Publishers: 2004; Vol. 1, p 17-49.
- (10) Hale, P. D.; Boguslavsky, L. I.; Inagaki, T.; Karan, H. I.; Lee, H. S.; Skotheim, T. A.; Okamoto, Y.; *Anal. Chem.* **1991**, *63*, 677-682.
- (11) Dennany, L.; Hogan, C. F.; Keyes, T. E.; Forster, R. J.; *Anal. Chem.* **2006**, *78*, 1412-1417.
- (12) Leech, D.; Forster, R. J.; Smyth, M. R.; Vos, J. G.; *J. Mater. Chem.* **1991**, *1*, 629-635.
- (13) Forster, R. J.; Vos, J. G.; *Macromolecules* **1990**, *23*, 4372-4377.
- (14) Forster, R. J.; Bertoncello, P.; Keyes, T. E.; *Annu. Rev. Anal. Chem.* **2009**, *2*, 1-27.
- (15) Liu, Y.; Fan, L.; Li, Y.; Xiao, S.; Li, Y.; *J. App. Poly. Sci.* **2002**, *86*, 2737-2741.
- (16) McKenna, K.; Brajter-Toth, A.; *Anal. Chem.* **1987**, *59*, 954-958.
- (17) Pickup, P. G. In *Modern Aspects of Electrochemistry*; White, R. E., Bockris, J. O. M., Conway, B. E., Eds.; Plenum Publishers: New York, 1999, p 549-591.
- (18) Yamamoto, T.; Sugiyama, K.; Kushida, T.; Inoue, T.; Kanbara, T.; *J. Am. Chem. Soc.* **1996**, *118*, 3930-3937.

- (19) Prissanaroon, W., La Trobe University, 2004.
- (20) Sadki, S.; Schottland, P.; Brodie, N.; Sabouraud, G.; *Chem. Soc. Rev.* **2000**, *29*, 283-293.
- (21) Bobaka, J.; Ivaska, A.; Lewenstam, A.; *Electroanal.* **2003**, *15*, 366-374.
- (22) Maksymiuk, K.; *Electroanal.* **2006**, *18*, 1537-1551.
- (23) Akhtar, P.; Too, C. O.; Wallace, G. G.; *Anal. Chim. Acta* **1997**, *339*, 211-223.
- (24) Bhat, N.; Geetha, P.; Pawde, S.; *Polym. Eng. & Sci.* **1999**, *39*, 1517-1524.
- (25) Dall' Antonia, L. H.; Vidotti, M. E.; Cordoba de Torresi, S. I.; Torresi, R. M.; *Electroanal.* **2002**, *14*, 1577-1586.
- (26) Álvarez-Romero, G. A.; Morales-Pérez, A.; Rojas-Hernández, A.; Palomar-Pardavé, A.; Ramírez-Silva, M. T.; *Electroanal.* **2004**, *16*, 1236-1243.
- (27) Michalska, A.; Maksymiuk, K.; *Anal. Chim. Acta* **2004**, *523*, 97-105.
- (28) Cosnier, S.; *Anal. Bioanal. Chem* **2003**, *377*, 507-520.
- (29) Razola, S. S.; Ruiz, L.; Diez, N. M.; Mark, H. B.; Kauffmann, J.-M.; *Biosens. Bioelectron.* **2002**, *17*, 921-928.
- (30) Llaudet, E.; Botting, N. P.; Crayston, J. A.; Dale, N.; *Biosens. Bioelectron.* **2003**, *18*, 43-52.
- (31) Blanchard, R. M.; Martin, A. F.; Nieman, T. A.; Guerrero, D. J.; Ferraris, J. P.; *Mikrochim. Acta* **1998**, *130*, 55-62.
- (32) Iyoda, T.; Aiba, M.; Saika, T.; Honda, K.; Shimidzu, T.; *J. Chem. Soc., Faraday Trans.* **1991**, *87*, 1765-1769.
- (33) Dennany, L.; O'Reilly, E. J.; Innis, P. C.; Wallace, G. G.; Forster, R. J.; *Electrochim. Acta* **2008**, *53*, 4599-4605.
- (34) Schuhmann, W.; *Mikrochim. Acta* **1995**, *121*, 1-29.
- (35) Roget, A.; Livache, T.; *Mikrochim. Acta* **1999**, *131*, 3-8.

- (36) Livache, T.; Roget, A.; Dejean, E.; Barthet, C.; Bidan, G.; Teoule, R.; *Nucleic Acids Res.* **1994**, *22*, 2915-2921.
- (37) Cosnier, S.; Gondran, C.; Le Pellec, A.; Senillou, A.; *Anal. Lett.* **2001**, *34*, 61-70.
- (38) Dupont-Filliard, A.; Roget, A.; Livache, T.; Billon, M.; *Anal. Chim. Acta* **2001**, *449*, 45-50.
- (39) Arora, K.; Prabhakar, N.; Chand, S.; Malhotra, B. D.; *Sensor Actuat B-Chem* **2007**, *126*, 655-663.
- (40) Cosnier, S.; *Biosensors & Bioelectronics* **1999**, *14*, 443-456.
- (41) Iwuoha, E. I.; Smyth, M. R. In *Electroactive Polymer Electrochemistry*; Lyons, M. E. G., Ed.; Plenum Press: New York, 1996; Vol. 2, p 297-328.
- (42) Whiteley, L. D.; Martin, C. R.; *Anal. Chem.* **1987**, *59*, 1746-1751.
- (43) White, H. S.; Leddy, J.; Bard, A. J.; *J. Am. Chem. Soc.* **1982**, *104*, 4811-4817.
- (44) Buttry, D. A.; Anson, F. C.; *J. Am. Chem. Soc.* **1983**, *105*, 685-689.
- (45) He, P.; Chen, X.; *J. Electroanal. Chem.* **1988**, *256*, 353-360.
- (46) Oyama, N.; Ohsaka, T.; Ushirogouchi, T.; *J. Phys. Chem.* **1984**, *88*, 5274-5280.
- (47) Oyama, N.; Anson, F. C.; *Anal. Chem.* **1980**, *52*, 1192-1198.
- (48) Beelen, E.; Riga, J.; Verbist, J. J.; *Synth. Met.* **1991**, *41*, 449-454.
- (49) Ehrenbeck, C.; Juttner, K.; *Electrochim. Acta* **1994**, *41*, 511-518.
- (50) Kuwabata, S.; Nakamura, J.; Yoneyama, H.; *J. Chem. Soc. Chem. Commun.* **1988**, 779-780.
- (51) Bidan, G.; Ehui, B.; Lapkowski, M.; *J. Phys. D: Appl. Phys.* **1988**, *21*, 1043-1054.
- (52) Yasuzawa, M.; Kunugi, A.; *Electrochem. Commun.* **1999**, *1*, 459-462.
- (53) Mailley, P.; Cosnier, S.; Coche-Guerente; *Anal. Lett.* **2000**, *33*, 1733-1753.
- (54) Liu, Y.-C.; Hwang, B.-J.; Hsu, W.-C.; *Sensor Actuat B-Chem* **2002**, *87*, 304-308.
- (55) Sata, T.; Funakoshi, T.; Akai, K.; *Macromolecules* **1996**, *29*, 4029-4035.

- (56) Langsdorf, B. L.; Sultan, J.; Pickup, P. G.; *J. Phys. Chem. B* **2003**, *107*, 8412-8415.
- (57) Park, H.; Kim, Y.; Hong, W. H.; Choi, Y. S.; Lee, H.; *Macromolecules* **2005**, *38*, 2289-2295.
- (58) Gooding, J. J.; *Electroanal.* **2007**, *20*, 573-582.
- (59) Love, J. C.; Estroff, L. A.; Kriebel, J. K.; Nuzzo, R. G.; Whitesides, G. M.; *Chem. Rev.* **2005**, *105*, 1103-1170.
- (60) McCreery, R. L.; *Chem. Rev.* **2008**, *108*, 2646-2687.
- (61) Pinson, J.; Podvorica, F.; *Chem. Soc. Rev.* **2005**, *34*, 429-439.
- (62) Maeda, H.; Yamauchi, Y.; Ohmori, H.; *Current Topics in Analytical Chemistry* **2001**, *2*, 121-133.
- (63) Vegunta, S. S. S.; Ngunjiri, J. N.; Flake, J. C.; *Langmuir* **2009**, *25*, 12750-12756.
- (64) Linford, M. R.; Chidsey, C. E. D.; *J. Am. Chem. Soc.* **1993**, *115*, 12631-12632.
- (65) Combellas, C.; Jiang, D.; Kanoufi, F.; Pinson, J.; Podvorica, F.; *Langmuir* **2009**, *25*, 286-293.
- (66) Gooding, J. J.; *Electroanal.* **2003**, *15*, 81-96.
- (67) Losic, D.; Gooding, J. J.; Shapter, J. G.; Hibbert, D. B.; Short, K.; *Electroanal.* **2001**, *13*, 1385-1393.
- (68) Creager, S.; Yu, C. J.; Bamdad, C.; O'Connor, S.; MacLean, T.; Lam, E.; Chong, Y.; Olsen, G. T.; Gozin, M.; Kayyem, J. F.; *J. Am. Chem. Soc.* **1999**, *121*, 1059-1064.
- (69) Sikes, H. D.; Smalley, J. F.; Dudek, S. P.; Cook, A. R.; Newton, M. D.; Chidsey, C. E. D.; Feldberg, S. W.; *Science* **2001**, *292*, 1519-1523.
- (70) Kelley, S. O.; Jackson, N. M.; Hill, M. G.; Barton, J. K.; *Angew. Chem. Int. Ed.* **1998**, *38*, 941-945.

- (71) Lin, W.; Xiu, Y.; Jiang, H.; Zhang, R.; Hildreth, O.; Moon, K.-S.; Wong, C. P.; *J. Am. Chem. Soc.* **2008**, *130*, 9636-9637.
- (72) Lim, J. K.; Yun, W. S.; Yoon, M. H.; Lee, S. K.; Kim, C. H.; Kim, K.; Kim, S. K.; *Synth. Met.* **2003**, *139*, 521-527.
- (73) Finklea, H. O.; Avery, S.; Lynch, M.; *Langmuir* **1987**, *3*, 409-413.
- (74) Walczak, M. M.; Popenoe, D. D.; Deinhammer, R. S.; Lamp, B. D.; Chung, C.; Porter, M. D.; *Langmuir* **1991**, *7*, 2687-2693.
- (75) Chow, E.; Hibbert, D. B.; Gooding, J. J.; *Anal. Chim. Acta* **2005**, *543*, 167-176.
- (76) Mearns, F. J.; Wong, E. L. S.; Short, K.; Hibbert, D. B.; Gooding, J. J.; *Electroanal.* **2006**, *18*, 1971-1981.
- (77) Horn, A. B.; Russell, D. A.; Shorthouse, L. J.; Simpson, T. R. E.; *J. Chem. Soc., Faraday Trans.* **1996**, *92*, 4759-4762.
- (78) Levicky, R.; Herne, T. M.; Tarlov, M. J.; Satija, S. K.; *J. Am. Chem. Soc.* **1998**, *120*, 9787-9792.
- (79) Hickman, J. J.; Ofer, D.; Labinis, P. E.; Whitesides, G. M.; Wrighton, M. S.; *Science* **1991**, *252*, 680-686.
- (80) Casero, E.; Darder, M.; Takada, K.; Abruna, H. D.; Pariente, F.; Lorenzo, E.; *Langmuir* **1999**, *15*, 127-134.
- (81) Beulen, M. W. J.; van Veggel, F. C. J. M.; Reinhoudt, D. N.; *Chem. Commun.* **1999**, 503-504.
- (82) Bardea, A.; Katz, E.; Willner, I.; *Electroanal.* **2000**, *12*, 731-735.
- (83) Turyan, I.; Mandler, D.; *Anal. Chem.* **1994**, *66*, 58-63.
- (84) Turyan, I.; Mandler, D.; *Anal. Chem.* **1997**, *69*, 894-897.
- (85) Nagaoka, T.; Chen, C. D.; Okuno, H.; Nakayama, M.; Ogura, K.; *Anal. Sci.* **1999**, *15*, 857-862.

- (86) Stora, T.; Hovius, R.; Dienes, Z.; Pachoud, M.; Vogel, H.; *Langmuir* **1997**, *13*, 5211-5214.
- (87) Rubinstein, I.; Steinberg, S.; Tor, Y.; Shanzer, A.; Sagiv, J.; *Nature* **1998**, *332*, 426-429.
- (88) Flink, S.; Boukamp, B. A.; van der Berg, A.; van Veggel, F. C. J. M.; Reinhoudt, D. N.; *J. Am. Chem. Soc.* **1998**, *120*, 4652-4657.
- (89) Gooding, J. J.; Hall, E. A. H.; Hibbert, D. B.; *Electroanal.* **1998**, *10*, 1130-1136.
- (90) Patolsky, F.; Zayats, M.; Katz, E.; Willner, I.; *Anal. Chem.* **1999**, *71*, 3171-3180.
- (91) Katz, E.; Buckmann, A. F.; Willner, I.; *J. Am. Chem. Soc.* **2001**, *123*, 10752-10753.
- (92) Umek, R. M.; Lin, S. W.; Vielmetter, J.; Terbrueggen, R. H.; Irvine, B.; Yu, C. J.; Kayyem, J. F.; Yowanto, H.; Blackburn, G. F.; Farkas, D. H.; Chen, Y.-P.; *J. Mol. Diagn.* **2001**, *3*, 74-84.
- (93) Spinke, J.; Liley, M.; Guder, H.-J.; Angermaier, L.; Knoll, W.; *Langmuir* **1993**, *9*, 1821-1825.
- (94) Rickert, J.; Beck, W. G.; Heiduschka, G. J.; *Biosens. Bioelectron.* **1995**, *11*, 757-768.
- (95) Berggren, C.; Johansson, G.; *Anal. Chem.* **1997**, *67*, 3651-3657.
- (96) Mirsky, V. M.; Riepl, M.; Wolfbeis, O. S.; *Biosens. Bioelectron.* **1997**, *12*, 977-989.
- (97) Wei, H.; Yin, J.; Wang, E.; *Anal. Chem.* **2008**, *80*, 5635-5639.
- (98) Zebda, A.; Labeau, M.; Diard, J. P.; Lavalley, V.; Stambouli, V.; *Sensor Actuat B-Chem* **2010**, *144*, 176-182.
- (99) Delmar, M.; Hitmi, R.; Pinson, J.; Savéant, J. M.; *J. Am. Chem. Soc.* **1992**, *114*, 5883-5884.
- (100) Anariba, F.; DuVall, S. H.; McCreery, R. L.; *Anal. Chem.* **2003**, *75*, 3837-3844.

- (101) Downard, A. J.; *Electroanal.* **2000**, *12*, 1085-1096.
- (102) Itoh, T.; McCreery, R. L.; *J. Am. Chem. Soc.* **2002**, *124*, 10894-10902.
- (103) Stewart, M. P.; Maya, F.; Kosynkin, D. V.; Dirk, S. M.; Stapleton, J. J.; McGuinness, C. L.; Allara, D. L.; Tour, J. M.; *J. Am. Chem. Soc.* **2004**, *126*, 370-378.
- (104) Chamoulaud, G.; Belanger, D.; *J. Phys. Chem. C* **2007**, *111*, 7501-7507.
- (105) Lehr, J.; Williamson, B. E.; Flavel, B. S.; Downard, A. J.; *Langmuir* **2009**, *25*, 13503-13509.
- (106) Price, B. K.; Hudson, J. L.; Tour, J. M.; *J. Am. Chem. Soc.* **2005**, *127*, 14867-14870.
- (107) Adenier, A.; Cabet-Deliry, E.; Chausse, A.; Griveau, S.; Mercier, F.; Pinson, J.; Vautrin-UI, C.; *Chem. Mater.* **2005**, *17*, 491-501.
- (108) Nassef, H. M.; Radi, A.-E.; O'Sullivan, C. K.; *Electrochem. Commun.* **2006**, *8*, 1719-1725.
- (109) Liu, G.; Liu, J.; Bocking, T.; Eggers, P. K.; Gooding, J. J.; *Chem. Phys.* **2005**, *319*, 136-146.
- (110) Kariuki, J. K.; McDermott, M. T.; *Langmuir* **2001**, *17*, 5947-5951.
- (111) Allongue, P.; Delmar, M.; Desbat, B.; Fagebaume, O.; Hitmi, R.; Pinson, J.; Savéant, J. M.; *J. Am. Chem. Soc.* **1997**, *119*, 201-207.
- (112) Kariuki, J. K.; McDermott, M. T.; *Langmuir* **1999**, *15*, 6534-6540.
- (113) Strano, M. S.; Dyke, C. A.; Usrey, M. L.; Barone, P. W.; Allen, M. J.; Shan, H.; Kittrell, C.; Hauge, R. H.; Tour, J. M.; Smalley, R. E.; *Science* **2003**, *301*, 1519-1522.
- (114) Dyke, C. A.; Stewart, M. P.; Maya, F.; Tour, J. M.; *Synlett.* **2004**, 155-160.
- (115) Mitchell, C. A.; Bahr, J. L.; Arepalli, S.; Tour, J. M.; Krishnamoorti, R.; *Macromolecules* **2002**, *35*, 8825-8830.

- (116) Dyke, C. A.; Tour, J. M.; *J. Am. Chem. Soc.* **2003**, *125*, 1156-1157.
- (117) Bahr, J. L.; Yang, J.; Kosynkin, D. V.; Bronikowski, M. J.; Smalley, R. E.; Tour, J. M.; *J. Am. Chem. Soc.* **2001**, *123*, 6536-6542.
- (118) Kuo, T.-C.; McCreery, R. L.; Swain, G. M.; *Electrochem. Solid State Lett.* **1999**, *2*, 288-290.
- (119) Lud, S. Q.; Steenackers, M.; Jordan, R.; Bruno, P.; Gruen, D. M.; Feulner, P.; Garrido, J. A.; Stutzmann, M.; *J. Am. Chem. Soc.* **2006**, *128*, 16884-16891.
- (120) Zhou, Y.; Zhi, J.; *Electrochem. Commun.* **2006**, *8*, 1811-1816.
- (121) Bureau, C.; Pinson, J. *Method for Modifying Insulating or Semi-Conductive Surfaces, and Resulting Products*, Patent Number: WO2007048894, France, 2007.
- (122) Chausse, A.; Chehimi, M. M.; Karsi, N.; Pinson, J.; Podvorica, F.; Vautrin-UI, C.; *Chem. Mater.* **2002**, *14*, 392-4000.
- (123) Bernard, M.-C.; Chausse, A.; Cabet-Deliry, E.; Chehimi, M. M.; Pinson, J.; Podvorica, F.; Vautrin-UI, C.; *Chem. Mater.* **2003**, *15*, 3450-3462.
- (124) Laforgue, A.; Addou, T.; Belanger, D.; *Langmuir* **2005**, *21*, 6855-6865.
- (125) Hurley, B. L.; McCreery, R. L.; *J. Electrochem. Soc.* **2004**, *151*, B252-B259.
- (126) Paulik, M. G.; Brooksby, P. A.; Abell, A. D.; Downard, A. J.; *J. Phys. Chem. C* **2007**, *111*, 7808-7815.
- (127) Downard, A. J.; Tan, E. S. Q.; Yu, S. S. C.; *New J. Chem.* **2006**, *30*, 1283-1288.
- (128) Deniau, G.; Azoulay, L.; Bougerolles, L.; Palacin, S.; *Chem. Mater.* **2006**, *18*, 5421-5428.
- (129) Maldonado, S.; Smith, T. J.; Williams, R. D.; Morin, S.; Barton, E.; Stevenson, K. J.; *Langmuir* **2006**, *22*, 2884.
- (130) de Villeneuve, C. H.; Pinson, J.; Bernard, M. C.; Allongue, P.; *J. Phys. Chem. B* **1997**, *101*, 2415-2420.

- (131) Allongue, P.; H., d. V. C.; Cherouvrier G; Cortes, R.; Bernard, M.-C.; *J. Electroanal. Chem.* **2003**, *550-551*, 161-174.
- (132) Allongue, P.; de Villeneuve, C. H.; Pinson, J.; *Electrochim. Acta* **2000**, *45*, 3241-3248.
- (133) Adenier, A.; Bernard, M. C.; Chehimi, M. M.; Cabet-Deliry, E.; Desbat, B.; Fagebaume, O.; Pinson, J.; Podvorica, F.; *J. Am. Chem. Soc.* **2001**, *123*, 4541-4549.
- (134) Jiang, D.; Sumpter, B. G.; Dai, S.; *J. Am. Chem. Soc.* **2006**, *128*, 6030-6031.
- (135) Jiang, D.; Sumpter, B. G.; Dai, S.; *J. Phys. Chem. B* **2006**, *110*, 23628-23632.
- (136) Vos, J. G.; Forster, R. J.; Keyes, T. E. *Interfacial Supramolecular Assemblies*; John Wiley & Sons, Ltd. (UK): Chichester, 2003.
- (137) Nuzzo, R. G.; Dubois, L. H.; Allara, D. L.; *J. Am. Chem. Soc.* **1990**, *112*, 558-569.
- (138) Finklea, H. O. In *Electroanalytical Chemistry: A series of Advances*; Bard, A. J., Rubinstein, I., Eds.; Marcel Dekker, Inc.: New York, 1996, p 109-335.
- (139) de la Llave, E.; Ricci, A.; Calvo, E. J.; Scherlis, D. n. A.; *J. Phys. Chem. C* **2008**, *112*, 17611-17617.
- (140) Delmar, M.; Desarmot, G.; Fagebaume, O.; Hitmi, R.; Pinson, J.; Savéant, J. M.; *Carbon* **1997**, *35*, 801-807.
- (141) D'Armours, M.; Belanger, D.; *J. Phys. Chem. B* **2003**, *107*, 4811-4817.
- (142) Shewchuk, D. M.; McDermott, M. T.; *Langmuir* **2009**, *25*, 4556-4563.
- (143) Wang, H.; Xu, G.; Dong, S.; *Talanta* **2001**, *55*, 61-67.
- (144) Downard, A. J.; *Langmuir* **2000**, *16*, 9680-9682.
- (145) Saby, C.; Ortiz, B.; Champagne, G. Y.; Belanger, D.; *Langmuir* **1997**, *13*, 6805-6813.
- (146) Doppelt, P.; Hallais, G.; Pinson, J.; Podvorica, F.; Verneyre, S.; *Chem. Mater.* **2007**, *19*, 4570-4575.

- (147) Brooksby, P. A.; Downard, A. J.; *J. Phys. Chem. B* **2005**, *109*, 8791-8798.
- (148) Adenier, A.; Combellas, C.; Kanoufi, F.; Pinson, J.; Podvorica, F. I.; *Chem. Mater.* **2006**, *18*, 2021-2029.
- (149) Solak, A. O.; Eichorst, L. R.; Clark, W. J.; McCreery, R. L.; *Anal. Chem.* **2003**, *75*, 296-305.
- (150) McCreery, R. L.; *Interface* **2004**, *13*, 46-51.
- (151) Gooding, J. J.; Chou, A.; Mearns, F. J.; Wong, E. L. S.; Jericho, K. L.; *Chem. Commun.* **2003**, 1938-1939.
- (152) Fan, C.; Plaxco, K. W.; Heeger, A. J.; *Proc. Natl. Acad. Sci.* **2003**, *100*, 9134-9137.
- (153) Liu, J.; Paddon-Row, M. N.; Gooding, J. J.; *Chem. Phys.* **2006**, *324*, 226-235.
- (154) Hess, C. R.; Juda, G. A.; Dooley, D. M.; Amii, R. N.; Hill, M. G.; Winkler, J. R.; Gray, H. B.; *J. Am. Chem. Soc.* **2003**, *125*, 7156-7157.
- (155) Oakes, J.; Gratton, P.; *J. Chem. Soc., Perkin Trans. 2*, **1998**, 1857-1864.
- (156) Hodges, G. R.; Smith, J. R. L.; Oakes, J.; *J. Chem. Soc., Perkin Trans. 2*, **1999**, 1943-1952.
- (157) Toupin, M.; Belanger, D.; *J. Phys. Chem. C* **2007**, *111*, 5394-5401.
- (158) Yang, X. H.; Hall, S. B.; Burrell, A. K.; Officer, D. L.; *Chem. Commun.* **2001**, 2628-2629.
- (159) Vaik, K.; Maeorg, U.; Maschion, F. C.; Maia, G.; Schiffrin, D. J.; Tammeveski, K.; *Electrochim. Acta* **2005**, *50*, 5126-5131.
- (160) Sarapuu, A.; Vaik, K.; Schiffrin, D. J.; Tammeveski, K.; *J. Electroanal. Chem.* **2003**, *541*, 23-29.
- (161) Polsky, R.; Harper, J. C.; Dirk, S. M.; Arango, D. C.; Wheeler, D. R.; Brozik, S. M.; *Langmuir* **2007**, *23*, 364-366.
- (162) Yang, X. H.; Hall, S. B.; Tan, S. N.; *Electroanal.* **2003**, *15*, 885-891.

- (163) Corgier, B. P.; Marquette, C. A.; Blum, L. J.; *J. Am. Chem. Soc.* **2005**, *127*, 18328-18332.
- (164) Harper, J. C.; Polsky, R.; Wheeler, D. R.; Dirk, S. M.; Brozik, S. M.; *Langmuir* **2007**, *23*, 8285-8287.
- (165) Harper, J. C.; Polsky, R.; Dirk, S. M.; Wheeler, D. R.; Brozik, S. M.; *Electroanal.* **2007**, *19*, 1268-1274.
- (166) Wang, J.; Carlisle, J. A.; *Diamond Rel. Mater.* **2006**, *15*, 279.
- (167) Radi, A.-E.; Montornes, J. M.; O'Sullivan, C. K.; *J. Electroanal. Chem.* **2006**, *587*, 140-147.
- (168) Bourdillon, C.; Delmar, M.; Demaille, C.; Hitmi, R.; Moiroux, J.; Pinson, J.; *J. Electroanal. Chem.* **1992**, *336*, 113-123.
- (169) Corgier, B. P.; Marquette, C. A.; Blum, L. J.; *Biosens. Bioelectron.* **2007**, *22*, 1522-1526.
- (170) Liu, G.; Nguyen, Q. T.; Chow, E.; Bocking, T.; Hibbert, D. B.; Gooding, J. J.; *Electroanal.* **2006**, *18*, 1141-1151.
- (171) Nassef, H. M.; Radi, A.-E.; O'Sullivan, C. K.; *J. Electroanal. Chem.* **2006**, *592*, 139-146.
- (172) Vakurov, A.; Simpson, C. E.; Daly, C. L.; Gibson, T. D.; Millner, P. A.; *Biosens. Bioelectron.* **2004**, *20*, 1118-1125.
- (173) Lee, W. Y.; *Mikrochim. Acta* **1997**, *127*, 19-39.
- (174) Gorman, B. A.; Francis, P. S.; Barnett, N. W.; *The Analyst* **2006**, *131*, 1-24.
- (175) Tokel, N. E.; Bard, A. J.; *J. Am. Chem. Soc.* **1972**, *94*, 2862-2863.
- (176) Chang, M.-M.; Saji, T.; Bard, A. J.; *J. Am. Chem. Soc.* **1977**, *99*, 5399-5403.
- (177) Rubinstein, I.; Bard, A. J.; *J. Am. Chem. Soc.* **1981**, *103*, 512-516.
- (178) Rubinstein, I.; Martin, C. R.; Bard, A. J.; *Anal. Chem.* **1983**, *55*, 1580-1582.

- (179) Miao, W.; Choi, J.-P. In *Electrogenerated Chemiluminescence*; Bard, A. J., Ed.; Marcel Dekker, Inc.: New York, 2004.
- (180) Debad, J. D.; Glezer, E. N.; Leland, J. K.; Sigal, G. B.; Wohlstadter, J. In *Electrogenerated Chemiluminescence*; Bard, A. J., Ed.; Marcel Dekker, Inc.: New York, 2004.
- (181) Danielson, N. D. In *Electrogenerated Chemiluminescence*; Bard, A. J., Ed.; Marcel Dekker, Inc.: New York, 2004.
- (182) Gerardi, R. D.; Barnett, N. W.; Lewis, S. W.; *Anal. Chim. Acta* **1999**, *378*, 1-41.
- (183) Fanhrich, K. A.; Pravda, M.; Guilbault, G. G.; *Talanta* **2001**, *54*, 531-559.
- (184) Kapturkiewicz, A.; *Chem. Phys. Lett.* **1995**, *236*, 389-394.
- (185) Velasco, J. G.; *Electroanal.* **1991**, *3*, 261-271.
- (186) Marcus, R. A.; *J. Chem. Phys.* **1965**, *43*, 2654-2657.
- (187) Kapturkiewicz, A. In *Electrogenerated Chemiluminescence*; Bard, A. J., Ed.; Marcel Dekker, Inc.: New York, 2004, p 163-213.
- (188) Bolletta, F.; Bonafede, S.; *Pure & Appl. Chem.* **1986**, *58*, 1229-1232.
- (189) Bard, A. J. In *Electrogenerated Chemiluminescence*; Bard, A. J., Ed.; Marcel Dekker: New York, 2004.
- (190) Cooke, M. M.; Doeven, E., H.; Hogan, C. F.; Adcock, J. L.; McDermott, G. P.; Conlan, X. A.; Barnett, N. W.; Pfeffer, F. W.; Francis, P. S.; *Anal. Chim. Acta* **2009**, *635*, 94-101.
- (191) Knight, A. W.; Greenway, G. M.; *Analyst* **1994**, *119*, 879-890.
- (192) Blackburn, G. F.; Shah, H. P.; Kenten, J. H.; Leland, J.; Kamin, R. A.; Link, J.; Peterman, J.; Powell, M. J.; Talley, D. B.; Tyagi, S. K.; Wilkins, E.; Wu, T.-G.; Massy, R. J.; *Clin. Chem.* **1991**, *37*, 1534-1539.
- (193) Faulkner, L. R.; *Methods Enzymol.* **1978**, *57*, 494-526.
- (194) Miller, C. J.; McCord, P.; Bard, A. J.; *Langmuir* **1991**, *7*, 2781-2787.

- (195) Zhang, X.; Bard, A. J.; *J. Phys. Chem.* **1988**, *92*, 5566-5569.
- (196) Bertoncello, P.; Dennany, L.; Forster, R. J.; Unwin, P. R.; *Anal. Chem.* **2007**, *79*, 7549-7553.
- (197) P. Bertoncello; N.R. Wilson; P. R. Unwin; *Soft Matter* **2007**, *3*, 1300-1307.
- (198) Kojima, H.; Takagi, Y.; Teramoto, H.; *Electrochim. Acta* **1988**, *33*, 1789-1793.
- (199) Xu, X.-H.; Bard, A. J.; *Langmuir* **1994**, *10*, 2409-2414.
- (200) Obeng, Y. S.; Bard, A. J.; *Langmuir* **1991**, *7*, 195-201.
- (201) Ghosh, P.; Spiro, T. G.; *J. Am. Chem. Soc.* **1980**, *102*, 5543-5549.
- (202) Bertoncello, P.; Kefalas, E. T.; Pikramenou, Z.; Unwin, P. R.; Forster, R. J.; *J. Phys. Chem. B* **2006**, *110*, 10063-10069.
- (203) D'Aleo, A.; Williams, R. M.; Chriqui, Y.; Iryer, V. M.; Belser, P.; Vergeer, F.; Ruiz, V.; Unwin, P. R.; De Cola, L.; *The Open Journal of Inorganic Chemistry* **2007**, *1*, 26-36.
- (204) Dennany, L.; O'Reilly, E. J.; Keyes, T. E.; Forster, R. J.; *Electrochem. Commun.* **2006**, *8*, 1588-1598.
- (205) Sato, Y.; Uosaki, K.; *J. Electroanal. Chem.* **1995**, *384*, 57-66.
- (206) Elliott, C. M.; Pichot, F.; Bloom, C. J.; Rider, L. S.; *J. Am. Chem. Soc.* **1998**, *120*, 6781-6784.
- (207) Lu, M.-C.; Whang, C.-W.; *Anal. Chim. Acta* **2004**, *522*, 25-33.
- (208) Lee, J.-K.; Lee, S.-H.; Kim, M.; Kim, H.; Kim, D.-H.; Lee, W. Y.; *Chem. Commun.* **2003**, 1602-1603.
- (209) Abruna, H. D.; Bard, A. J.; *J. Am. Chem. Soc.* **1982**, *104*, 2641-2642.
- (210) Maness, K. M.; Terrill, R. H.; Meyer, T. J.; Murray, R. W.; Wightman, R. M.; *J. Am. Chem. Soc.* **1996**, *118*, 10609-10616.
- (211) Lowry, R. B.; Williams, C. E.; Braven, J.; *Talanta* **2004**, *63*, 961-966.

- (212) Barbante, G. J.; Hogan, C. F.; Mechler, A.; Hughes, A. B.; *J. Mater. Chem.* **2010**, *20*, 891-899.
- (213) Zanarini, S.; Bard, A. J.; Marcaccio, M.; Palazzi, A.; Paolucci, F.; Stagni, S.; *J. Phys. Chem. B* **2006**, *110*, 22551-22556.
- (214) Downey, T. M.; Nieman, T. A.; *Anal. Chem.* **1992**, *64*, 261-268.
- (215) Martin, A. F.; Nieman, T. A.; *Biosens. Bioelectron.* **1997**, *12*, 479-489.
- (216) Rubinstein, I.; Bard, A. J.; *J. Am. Chem. Soc.* **1981**, *103*, 5007-5013.
- (217) Du, Y.; Qi, B.; Yang, X.; Wang, E.; *J. Phys. Chem. B* **2006**, *110*, 21662-21666.
- (218) Dvorak, O.; De Armond, M. K.; *J. Phys. Chem.* **1993**, *97*, 2646-2648.
- (219) Choi, H. N.; Cho, S.-H.; Park, Y.-J.; Lee, D. W.; Lee, W.-Y.; *Anal. Chim. Acta* **2005**, *541*, 47-54.
- (220) Wang, H.; Xu, G.; Dong, S.; *Electroanal.* **2002**, *14*, 853-857.
- (221) Khramov, A. N.; Collinson, M. M.; *Anal. Chem.* **2000**, *72*, 2943-2948.
- (222) Choi, H. N.; Cho, S. H.; Lee, W. Y.; *Anal. Chem.* **2003**, *75*, 4250-4256.
- (223) Su, X.; Zhuang, Z.; Lv, B.; Xiao, D.; *Sens. Lett.* **2007**, *5*, 578-583.
- (224) Shi, L. H.; Liu, X. Q.; Li, H. J.; Xu, G. B.; *Anal. Chem.* **2006**, *78*, 7330-7334.
- (225) Xu, Z.; Guo, Z.; Dong, S.; *Biosens. Bioelectron.* **2005**, *21*, 455-461.
- (226) Choi, H. N.; Lyu, Y.-K.; Lee, W. Y.; *Electroanal.* **2006**, *18*, 275-281.
- (227) Ding, S.-N.; Xu, J.-J.; Chen, H.-Y.; *Electroanal.* **2005**, *17*, 1517-1522.
- (228) Salimi, A.; Hallaj, R.; Amini, M. K.; *Anal. Chim. Acta.* **2005**, *534*, 335-342.
- (229) Wang, H.; Xu, G.; Dong, S.; *The Analyst* **2001**, *126*, 1095-1099.
- (230) Choi, H. N.; Yoon, S. H.; Lyu, Y.-K.; Lee, W.-Y.; *Electroanal.* **2007**, *19*, 459-465.
- (231) Guo, Z.; Dong, S.; *Anal. Chem.* **2004**, *76*, 2683-2688.
- (232) Choi, H. N.; Lee, J.-Y.; Lyu, Y.-K.; Lee, W. Y.; *Anal. Chim. Acta* **2006**, *565*, 48-55.

- (233) Zhang, L.; Guo, Z.; Xu, Z.; Dong, S.; *J. Electroanal. Chem.* **2006**, *592*, 63-67.
- (234) Lin, Z.; Chen, G.; *Talanta* **2006**, *70*, 111-115.
- (235) Song, H.; Zhang, Z.; Wang, F.; *Electroanal.* **2006**, *18*, 1838-1841.
- (236) Rubinstein, I.; Bard, A. J.; *J. Am. Chem. Soc.* **1980**, *102*, 6641-6642.
- (237) Shultz, L. L.; Stoyanoff, J. S.; Nieman, T. A.; *Anal. Chem.* **1996**, *68*, 349-354.
- (238) Bunker, C. E.; Rollins, H. W.; Ma, B.; Simmons, K. J.; Liu, J.-T.; Ma, J.-J.; Martin, C. W.; DesMarteau, D. D.; Sun, Y.-P.; *J. Photoch. Photobio. A* **1999**, *126*, 71-76.
- (239) Vining, W. J.; Meyer, T. J.; *J. Electroanal. Chem.* **1987**, *237*, 191-208.
- (240) Abraham John, S.; Ramaraj, R.; *J. Electroanal. Chem.* **1997**, *424*, 49-59.
- (241) Lee, P. C.; Meisel, D.; *J. Am. Chem. Soc.* **1980**, *102*, 5477-5481.
- (242) Eisenberg, A.; Hird, B.; Moore, R. B.; *Macromolecules* **1990**, *23*, 4098-4107.
- (243) Hsu, W. Y.; Gierke, T. D.; *J. Membr. Sci.* **1983**, *13*, 307-326.
- (244) Knox, C. K.; Voth, G. A.; *J. Phys. Chem. B* **2010**, *114*, 3205-3218.
- (245) Mauritz, K. A.; Moore, R. B.; *Chem. Rev.* **2004**, *104*, 4535-4586.
- (246) Gebel, G.; *Polymer* **2000**, *41*, 5829-5838.
- (247) Rubinstein, I.; *J. Electroanal. Chem.* **1985**, *188*, 227-244.
- (248) Zhang, X.; Bard, A. J.; *J. Am. Chem. Soc.* **1989**, *111*, 8098-8105.
- (249) Zanarini, S.; Rampazzo, E.; Bich, D.; Canteri, R.; Ciana, L. D.; Marcaccio, M.; Marzocchi, E.; Panciatichi, C.; Pederzoli, C.; Paolucci, F.; Prodi, L.; Vanzetti, L.; *J. Phys. Chem. C* **2008**, *112*, 2949-2957.
- (250) Abruna, H. D.; Meyer, T. J.; Murray, R. W.; *Inorg. Chem.* **1979**, *18*, 3233-3240.
- (251) Ghosh, P.; Spiro, T. G.; *J. Electroanal. Chem.* **1981**, *128*, 1281-1287.
- (252) Boland, S.; Barriere, F.; Leech, D.; *Langmuir* **2008**, *24*, 6351-6358.
- (253) Rodriguez, M.; Bard, A. J.; *Anal. Chem.* **1990**, *62*, 2658-2662.

- (254) Joussetme, B.; Bidan, G.; Billon, M.; Goyer, C.; Kervella, Y.; Guillerez, S.; Hamad, E. A.; Goze-Bac, C.; Mevellec, J.-Y.; Lefrant, S.; *J. Electroanal. Chem.* **2008**, *621*, 277-285.
- (255) Agnes, C.; Arnault, J.-C.; Omnes, F.; Joussetme, B.; Billon, M.; Bidan, G.; Mailley, P.; *Phys. Chem. Chem. Phys.* **2009**, *11*, 11647-11654.

Chapter 3: Experimental Methods and Characterisation

This chapter details the experimental methods used for the fabrication, synthesis and characterisation of all modified electrodes produced in this thesis.

3.1. Fabrication and Synthesis Methods

In this work, two different approaches for creating solid state ECL sensors were explored. The first approach involved the formation of composite films consisting of Nafion, $\text{Ru}(\text{bpy})_3^{2+}$, and polypyrrole. The second approach involved the use of aryl diazoniums to covalently attach either an ECL active complex to the electrode or a phenyl-bipyridyl ligand, which was then complexed with bis(2,2'-bipyridyl)dichloro ruthenium(II) [$\text{Ru}(\text{bpy})_2\text{Cl}_2$] at the electrode surface.

All chemicals described in this thesis were purchased from Sigma-Aldrich Pty. Ltd. unless otherwise mentioned. All chemicals were of reagent grade or better and used without further purification unless specified. Deionised water (Sybron Barnstead; resistivity $\geq 17.9 \text{ M}\Omega \text{ cm}$) was used for aqueous solutions and aqueous rinses. All acetonitrile was purified by distillation over calcium hydride.

Electrodes were polished to clean and renew the surface prior to use. Glassy carbon electrodes were polished successively with $0.3 \mu\text{m}$ and $0.05 \mu\text{m}$ alumina prior to rinsing and sonication. Platinum electrodes were polished with $0.3 \mu\text{m}$ alumina prior to rinsing. Gold electrodes used for electrochemical characterisation were polished with an aqueous cerium oxide slurry with an average particle diameter of 10 nm .

3.1.1. Fabrication of Nafion/Polypyrrole Films

Nafion/polypyrrole composite films were formed on glassy carbon and platinum substrates by the following procedure, which was modified from previous work by Downey and Nieman.¹ A Nafion solution (5 % solution in a mixture of alcohols) was drop coated onto the substrate and allowed to air dry. The resulting film was immersed in a 0.1 M H₂SO₄ solution for 1 hour to allow the film to swell. Ru(bpy)₃²⁺ was loaded into the swollen film by soaking in a 1 mM solution of the Ru(bpy)₃Cl₂ dissolved in 0.1 M H₂SO₄ for 20 minutes. Polypyrrole was then incorporated into the Nafion/Ru(bpy)₃²⁺ film by the immersion of the electrode in a solution containing pyrrole (0.05 M) and the supporting electrolyte, 0.05 M dodecylbenzenesulfonic acid (DBSA), followed by the application of a potential of 1.5 V v.s. Ag/AgCl for 5 seconds. The resulting film was rinsed thoroughly in deionised water before being characterised.

For electrochemical studies, films were deposited on 3 mm diameter glassy carbon discs embedded in a 6 mm diameter PTFE body (CH Instruments, TX, USA). For surface analysis experiments, 12 x 12 mm platinum squares were used as working electrodes. The resulting films were analysed with Cyclic Voltammetry (CV), X-ray Photoelectron Spectroscopy (XPS), Time-of-Flight Secondary Ion Mass Spectrometry (ToF-SIMS) and Atomic Force Microscopy (AFM) as described in Section 3.2.

3.1.2. Electrodeposition of Ruthenium Based Layers using Diazonium Chemistry

Bis(2,2'-bipyridyl)(4-phenyl-2,2'-bipyridyl)ruthenium(II) [Ru(bpy)₂(ph-pby)²⁺] layers were constructed through two alternate methods. The first method, discussed further in Chapter 5, involves the deposition of a layer of 4-phenyl-2,2'-bipyridine covalently attached to the substrate prior to its complexation at the surface with Ru(bpy)₂Cl₂. The

second method, which is discussed in Chapter 6, involves the synthesis of the complex bis(2,2'-bipyridyl)(para-amino-4'-phenyl-2,2'-bipyridyl) ruthenium(II) $[\text{Ru}(\text{bpy})_2(\text{apb})^{2+}]$, prior to its conversion to the diazonium and subsequent electrochemical deposition. The structures of the ligands used in this thesis are described in Figure 3-1.

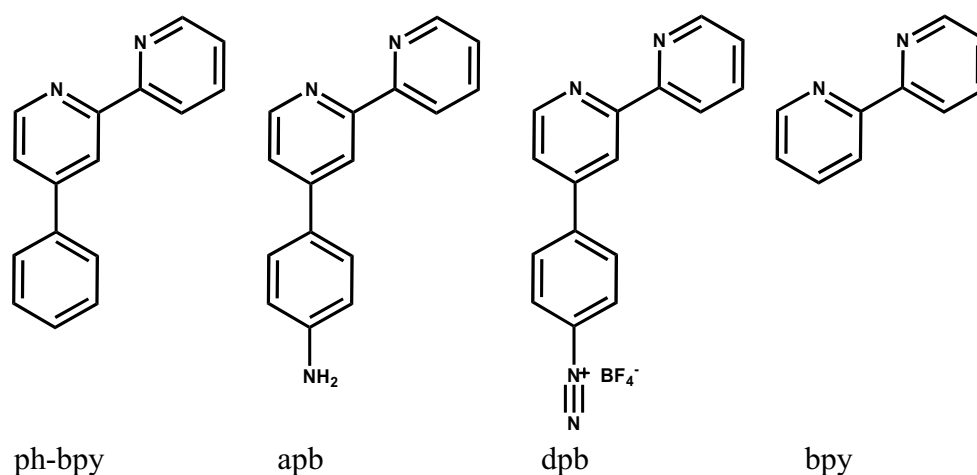


Figure 3-1: Ligands used in Chapters 4 to 7. ph-bpy is 4-phenyl-2,2'-bipyridyl, apb is 4'-(4-aminophenyl)-2,2'-bipyridyl, dpb is para-diazonium-4'-phenyl-2,2'-bipyridine and bpy is 2,2'-bipyridyl.

3.1.2.1. Two-step Synthesis of $\text{Ru}(\text{bpy})_2(\text{dpb})^{2+}$ Films

The ligand, 4-(4-aminophenyl)-2,2'-bipyridine, was synthesised by Gregory Barbante^a following the procedure described by Johansson.² Once synthesised, the ligand was converted to the diazonium salt by reaction with an equivalent quantity of NaNO_2 in acidic media and isolated through the addition of NaBF_4 . No further purification of the diazonium salt was undertaken. The electrodeposition of the diazonium onto gold or glassy carbon substrates was conducted from a fresh solution containing 3 mM of the diazonium salt ($\text{MW} = 346.1 \text{ g mol}^{-1}$) and 0.1 M tetrabutylammonium hexafluorophosphate (TBAPF_6) electrolyte in acetonitrile. Deposition was undertaken by voltammetric cycling between 0.3 and -1.8 V vs Ag wire at 100 mV s^{-1} for 3 scans.

^a Department of Chemistry, La Trobe University, Australia

The formation of the $\text{Ru}(\text{bpy})_2(\text{ph-pby})^{2+}$ layer at the electrode was attempted using a variety of experimental conditions. The method involved the *in-situ* formation of the bis(2,2'-bipyridyl)diaquo ruthenium(II) from the dichloro compound prior to attachment to the electrode. This attachment was achieved by soaking the phenyl-bipyridine coated electrode in a room temperature ethanol/water (90:10) solution containing 1 mM of $\text{Ru}(\text{bpy})_2\text{Cl}_2$ over a period of 24 hours.

Throughout the synthesis, the layer was characterised using a range of analytical techniques including CV, Electrochemical Quartz Crystal Microbalance (EQCM), XPS, ToF-SIMS, and AFM. For electrochemical studies, films were deposited on either a 3 mm diameter glassy carbon disc or 2 mm diameter gold disc embedded in a 6 mm diameter PTFE body (CH Instruments, USA). EQCM studies used a clean gold coated (1000 Å thick) AT cut quartz crystal with a fundamental frequency of 7.95 MHz and a geometrical electrode area of 0.196 cm² (CH Instruments, USA). For surface analysis (XPS, ToF-SIMS, or AFM), 15 mm diameter glassy carbon discs (active deposition area of 0.503 cm²) and the gold coated quartz crystals described above were used.

3.1.2.2. Direct Electrodeposition of $\text{Ru}(\text{bpy})_2(\text{apb})^{2+}$ Films

To form the complex $\text{Ru}(\text{bpy})_2(\text{apb})^{2+}$ the following procedure was used. The ligand, 4-(4-aminophenyl)-2,2'-bipyridine (94 mg, 0.4 mmol), was reacted with bis(2,2'-bipyridyl)dichloro ruthenium(II) (100 mg, 0.38 mmol) by heating at reflux under a nitrogen atmosphere for 5 hrs in a mixture of ethanol and water (20 ml, 1:1). Once a deep red solution had formed the solvent was evaporated under reduced pressure. The solid was redissolved in deionised water (20 mL) and the resulting solution filtered through a sintered funnel; the filter cake was rinsed with deionised water (5 mL). The filtrate was treated with a saturated aqueous solution of KPF_6 , which gave an orange precipitate. The resulting solid was collected by filtration and washed with deionised water (2 x 5 mL) and

diethyl ether (2 x 5 mL). The red precipitate was recrystallised from an acetone-water mixture to give a dark red powder and then dried under vacuum at 50 °C (0.150 g, 42 %). ^1H NMR (300 MHz, DMSO- d_6) δ 5.81 (s, 2H), 6.64-6.68 (m, 3H), 7.43-7.61 (m, 8H), 7.68-7.82 (m, 7H), 8.13 (t, 4H, J 7.8 Hz), 8.81 (d, 3H, J 8.4 Hz), 8.91 (s, 1H), 9.1 (d, 1H, J 8.10 Hz); ESI-MS: m/z $[\text{Ru-PF}_6+\text{H}^+]^+$ 806.0 (Calculated: 805.7), $[\text{Ru-2PF}_6+2\text{H}^+]^+$ 663.1 (Calculated: 660.74), $[\text{Ru-2PF}_6]^{2+}$ 330.6 (Calculated: 330.37).

Layers were deposited onto electrodes (Section 3.1.2.1) from a 0.5 M HCl solution containing 1.2 mM of $\text{Ru}(\text{bpy})_2(\text{apb})$ and 1.5 mM NaNO_2 which was allowed to react for at least 2 minutes prior to electrochemical deposition. The electrochemical cell was kept in ice prior to and during the deposition. Deposition solutions were used up to 10 times before disposal. Films were deposited via 6 sequential potential scans between 0.5 and -0.7 V v.s. Ag/AgCl at a scan rate of 100 mV/s. After deposition the resulting films were characterised using CV, XPS, ToF-SIMS, and AFM.

3.1.3. Spontaneous Deposition of $\text{Ru}(\text{bpy})_2(\text{apb})^{2+}$ Films

The formation of layers of $\text{Ru}(\text{bpy})_2(\text{apb})^{2+}$ by spontaneous deposition of diazonium salt onto both glassy carbon and patterned Diamond Like Carbon (DLC) surfaces was undertaken. Thin films of $\text{Ru}(\text{bpy})_2(\text{apb})^{2+}$ were prepared by soaking substrates in a room temperature solution of 0.5 M HCl containing 1.2 mM of $\text{Ru}(\text{bpy})_2(\text{apb})(\text{PF}_6)_2$ and 1.5 mM NaNO_2 for a period of one hour. DLC surfaces were prepared in a Scanning Electron Microscope (SEM) by electron beam deposition of residual hydrocarbons (from a diffusion pump) onto a silicon nitride substrate.³ To obtain a 2 by 2 pattern of DLC squares (3 x 3 μm squares 25 nm high with each block separated by 3 μm) a 4555 μs dwell time (100 nm beam diameter) was used with an accelerating voltage of 10.0 kV and an emission current of 40 pA on a JEOL JSM 840 SEM. After the deposition of

$\text{Ru}(\text{bpy})_2(\text{apb})^{2+}$, layers were rinsed in both water and ethanol. Layers on DLC substrates were also briefly sonicated in ethanol prior to analysis. The layers were characterised using CV, XPS, ToF-SIMS and AFM.

3.2. Characterisation Methods

Several analysis methods were used to characterise the films produced in this thesis. This section provides essential background information to the techniques and the experimental conditions used in the analysis of the films manufactured in accordance with Section 3.1 described above. The analysis methods chosen to characterise the thin films produced in the thesis provide complementary information about the composition, structure and electrochemical response of the film. Table 3-1 provides a brief overview of the analysis method and the information it provides.

Technique	Incident probe	Analysed response	Analysis Depth	Information available
XPS	X-ray photons	Photoelectron energy	5-10 nm	<ul style="list-style-type: none"> • Surface elemental composition • Chemical bonding • Elemental/chemical distribution
ToF-SIMS	Ion beams	Ion Mass	1-2 nm	<ul style="list-style-type: none"> • Surface elemental and molecular composition • Molecular distribution • Isotope distribution
AFM	Mechanical Force	Topography	Not Applicable	<ul style="list-style-type: none"> • Surface topography • Film thickness • Film stiffness
CV	Electromotive Force	Current	Up to whole film	<ul style="list-style-type: none"> • Reaction thermodynamics • Reaction kinetics • Mass transport
EQCM	Electromotive Force	Mass change and Current	Whole film	<ul style="list-style-type: none"> • Mass deposition and transport

Table 3-1: An overview of the characterisation techniques used in this work.

3.2.1. X-ray Photoelectron Spectroscopy

3.2.1.1. Basic Concepts

X-ray Photoelectron Spectroscopy (XPS) is a powerful surface analysis technique that can determine both the elemental and chemical composition of solid surfaces via use of the photoelectric effect. A sample is irradiated with X-rays of a known energy, $h\nu$, resulting in photoelectron emission with a kinetic energy, E_K . The relationship between E_K and $h\nu$ can be expressed as shown in Equation 3.1,

$$E_k = h\nu - E_B - \phi \quad (3.1)$$

where E_B is the binding energy of the photoelectrons in the sample and ϕ is the spectrometer work function. This work function is a combination of the surface work function of the sample and the analyser work function. An energy level diagram of this process is shown in Figure 3-2. The work function can be measured and compensated for and in practice, Equation 3.1 becomes:

$$E_k = h\nu - E_B \quad \text{or} \quad E_B = h\nu - E_k \quad (3.2)$$

Einstein first described this relationship in 1905,⁴ and by measuring the kinetic energy of the ejected electrons, the binding energy can be determined.

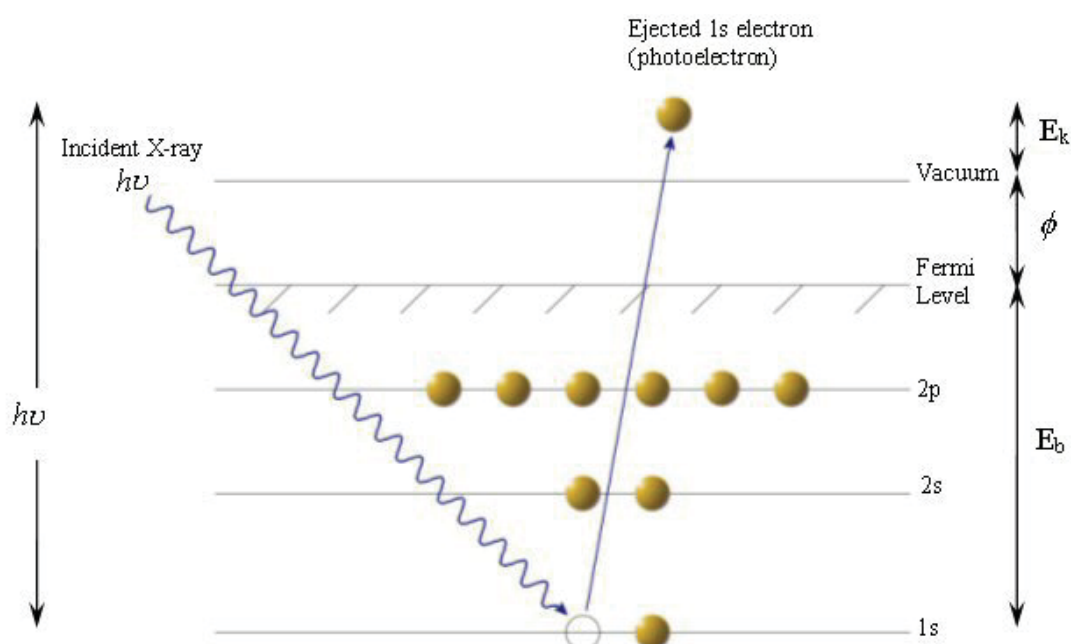


Figure 3-2: Energy diagram of photoelectron formation. Redrawn from Ref [5].

The binding energy is the energy required to release the electron from an atomic or molecular orbital and as such each element possesses a unique set of core electron binding energies, allowing for all elements present in concentrations above the limit of detection to be identified. The photon energies used in XPS enable it to be sensitive to core electron binding energies for all elements except for H and He.

The main advantage of XPS is its ability to obtain information about the chemical state of the surface in addition to elemental information. This ability originates from the binding energy of the electron being dependent on the bonding state of the associated atom. For example, a shift to more electronegative environments for a carbon atom results in the binding energy of the C 1s photoelectron shifting to higher values ($E_B(\underline{\text{C}}-\text{C}) = 285.0 \text{ eV}$ c.f. $E_B(\underline{\text{C}}\text{FO}) \approx 289 \text{ eV}$ c.f. $E_B(\underline{\text{C}}\text{HF}) \approx 291 \text{ eV}$ c.f. $E_B(\underline{\text{C}}\text{F}_3) \approx 293 \text{ eV}$).^{6,7} This shift in binding energies can readily be observed in a Nafion film as shown in Figure 3-3.

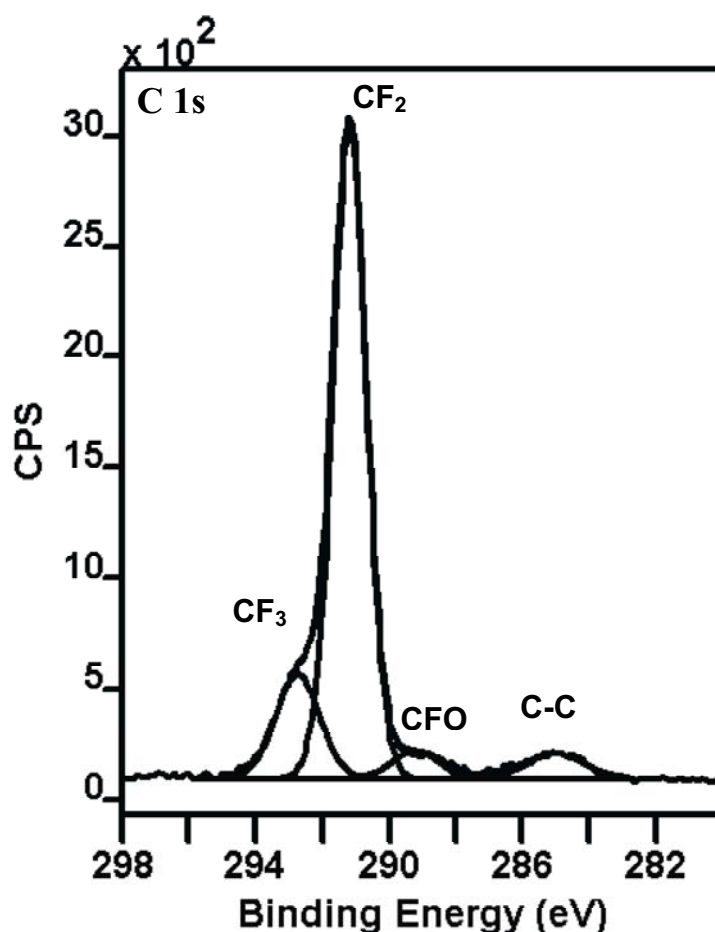


Figure 3-3: XPS spectrum of the C 1s photoelectron region in Nafion.

The observed photoelectron flux, I , is directly dependent on a range of factors. For a homogeneous sample, the photoelectron flux can be described simply by

$$I = J\rho\sigma K\lambda \quad (3.3)$$

where J is the photon flux, ρ is the concentration of the chemical species on the solid surface, σ is the photoelectron cross-section which is dependent on the element and photon energy considered, K is an instrument dependent term that takes into account factors like instrument geometry, electron transmission and detection efficiency and λ is the inelastic mean free path of the photoelectrons.⁸

The inelastic mean free path of an electron is described as the thickness of material that will result in the intensity of an unscattered electron beam to be reduced by $1/e$. As a result, 95% of unscattered photoelectrons ejected from the material originate from within a distance of 3λ from the surface. Depending on the E_k of the photoelectron and the material assessed, values for λ can range between 5 and 100 \AA as shown in Figure 3-4, however if the E_k of the photoelectrons is kept to over 50 eV this upper limit reduces to 20 \AA . The incident X-ray energies used in XPS (eg. the Al $K\alpha$ line at 1486.6 eV) ensure that the E_k of the photoelectron is over 50 eV and as a result, only photoelectrons within $\sim 50 \text{ \AA}$ of the surface escape without being inelastically scattered, limiting the analysis depth of XPS to this value.⁹

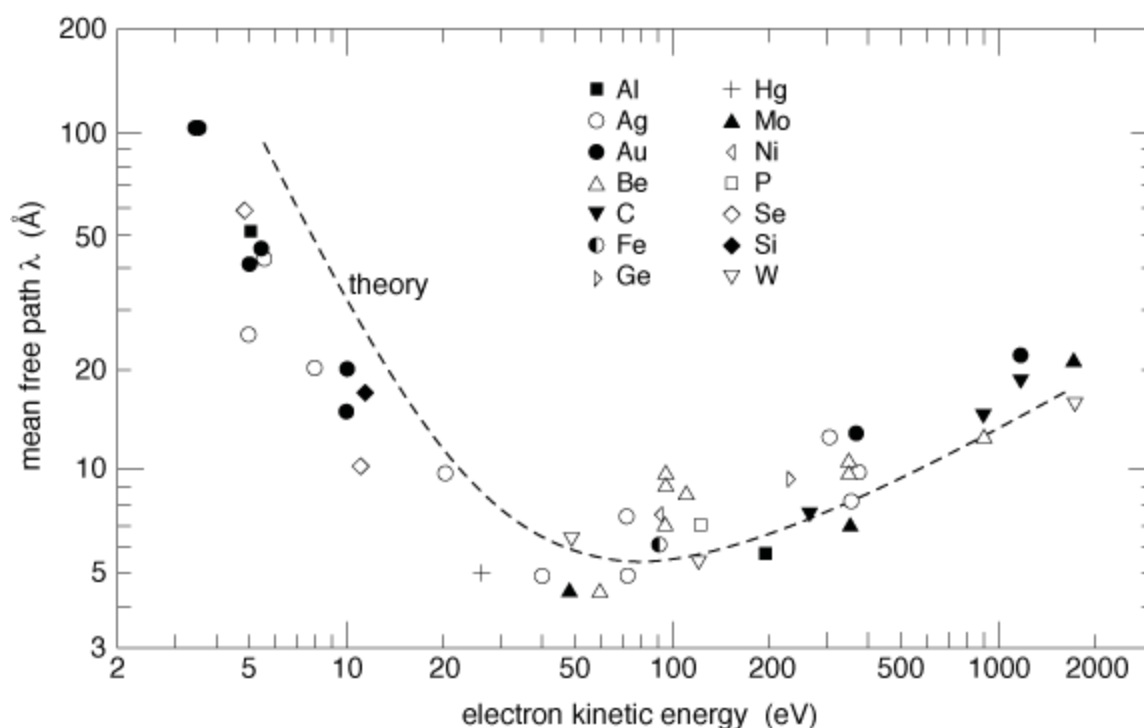


Figure 3-4: The universal curve of electron mean free path. Redrawn from Ref [10].

The photoelectron intensity in Equation 3.3 is considered to be the integrated peak area after background subtraction has been performed (background subtraction is either a linear background or a function that takes into account the background inelastic scattering

of the photoelectrons upon which the peak sits). Equation 3.3 allows for the direct quantification of chemical species present on the surface however experimentally determined sensitivity factors, F , are more often employed and incorporate terms such as σ , λ , and K . If during the course of an experiment the photon flux and analysis area are held constant, an atomic percentage of the species of interest can be derived by dividing the normalised peak area by the sum of all normalised peak intensities as demonstrated in Equation 3.4

$$[A]_{atomic \%} = 100 \times \frac{\left(\frac{I_A}{F_A} \right)}{\sum \left(\frac{I}{F} \right)} \quad (3.4)$$

3.2.1.2. Instrumentation

Figure 3-5 shows the principal components for an XPS system: an X-ray source, charge neutraliser, electron energy analyser, and detector, and a computerised control and data acquisition system. To minimise electron scattering and to preserve sample surfaces, all of these components, excluding the control system, operate under ultra-high vacuum (UHV).

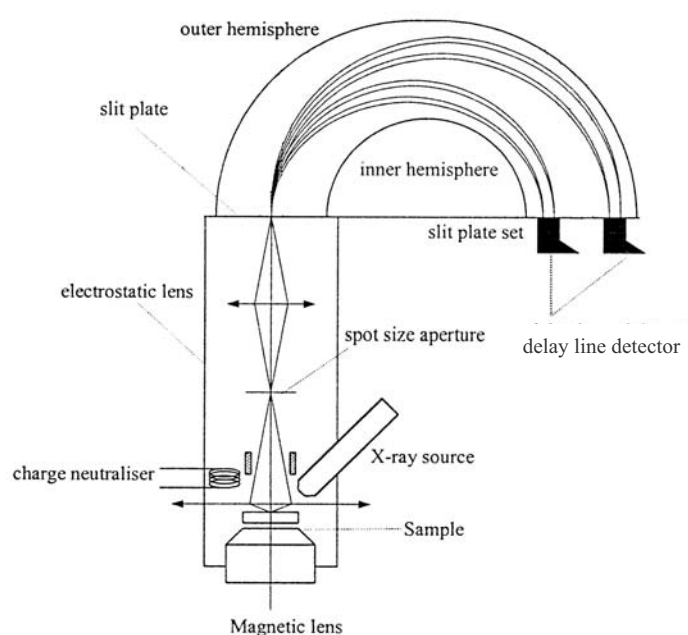


Figure 3-5: Schematic of a XPS system with essential components shown. Redrawn from Ref [11].

In laboratory-based XPS systems, X-rays are generated by X-ray fluorescence. This fluorescence is achieved by the acceleration of electrons onto a metallic target causing the emission of a photon with an energy that is characteristic of the target material. In most XPS systems, X-rays generated are from Al or Mg sources, with primary $K\alpha$ emissions of 1486.6 eV and 1253.6 eV respectively.⁷ These principal X-ray lines and other less intense peaks exist on a background of Bremsstrahlung radiation. The X-ray sources also have line widths greater than 0.7 eV limiting spectral resolution. X-ray sources are often monochromated using quartz crystal arrays to remove the Bremsstrahlung and to reduce X-ray line width and can reduce the X-ray line width to 0.16 eV.⁵

Photoelectrons are energy analysed as shown in Figure 3-5, before being counted and converted into usable spectra. Several different types of energy analysers are currently in use; currently, variants of the Concentric Hemispherical Analyser (CHA) are most common. The CHA as shown in Figure 3-5 consists of two concentric metal hemispheres with a voltage (V) applied between them. These hemispheres guide electrons of pre-defined kinetic energy (referred to as pass energy) through the analyser to the detector. Only electrons within 10 % of that pass energy will navigate the analyser successfully to be detected. All other electrons will collide with the CHA walls or miss the detector. The relationship between the applied voltage and pass energy is given by:

$$E_{pass} = \frac{eV}{\left[\left(\frac{R_o}{R_i} \right) - \left(\frac{R_i}{R_o} \right) \right]} \quad (3.5)$$

Where R_o and R_i are the radius of the outer and inner hemispheres, respectively. The following equation for the energy resolution then holds:

$$\frac{dE}{E_{pass}} = \frac{dS}{2R} \quad (3.6)$$

Where dS is the average slit width and R is the mean radius of the spectrometer. This equation indicates that improved absolute energy resolution can be achieved using smaller slits or pass energy. The conventional mode of analyser operation is referred to constant energy analysis with the pass energy fixed (values typically range between 5 to 160 eV) by use of a retarding potential applied prior to the CHA, ensuring constant energy resolution during analysis.

3.2.1.3. Experimental

XPS experiments were conducted using an Axis Ultra DLD (Kratos, UK) spectrometer equipped with a radial distribution chamber as shown in Figure 3-6. A monochromatised Al K α X-ray source was used ($h\nu = 1486.6$ eV) operated with a power output of 150 W. The analyser was operated in a hybrid mode that combines the use of electrostatic and magnetic lenses. The photoelectrons were energy analysed using a CHA and detected with a delay line detector system. The analysis area was 700 μm by 300 μm .

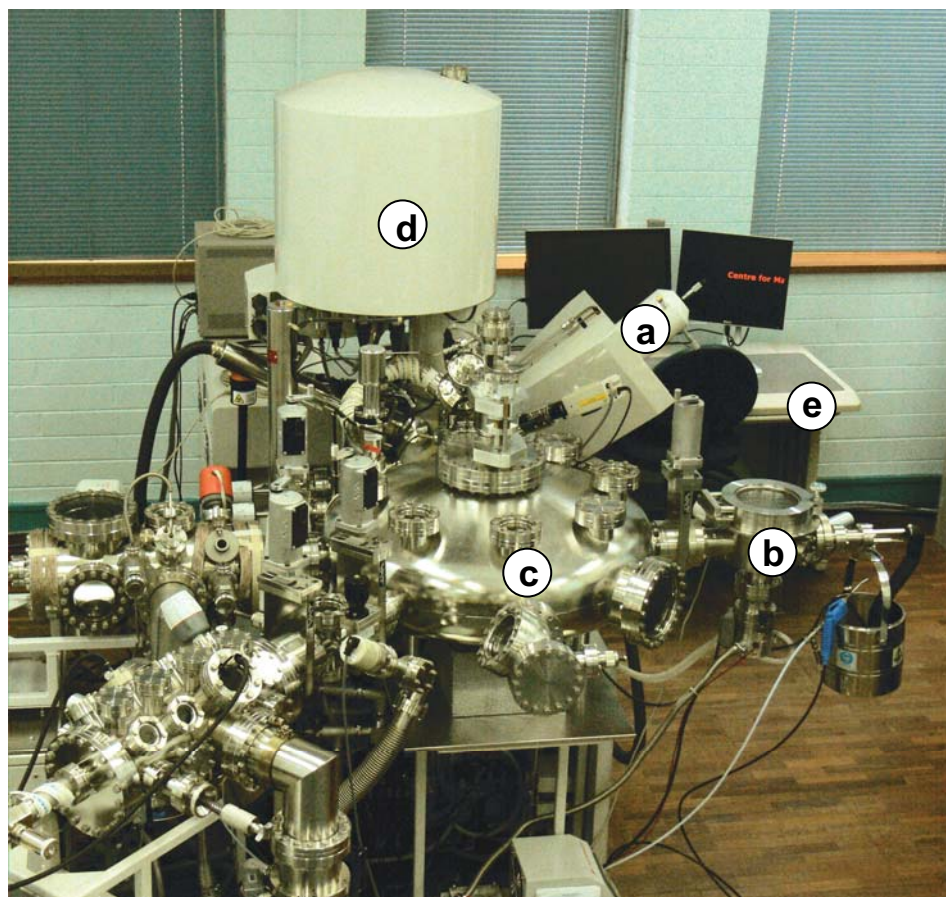


Figure 3-6: The Kratos AXIS Ultra DLD XPS spectrometer with components, monochromatised Al K α X-ray source (a), sample introduction system (b) sample transfer chamber (c), CHA energy analyser (d) and control instrumentation (e).

Survey and high-resolution region spectra were collected using 160 eV and 20 eV pass energies respectively. The spectrometer energy scale was calibrated using the Au 4f_{7/2} ($E_B = 84.0$ eV), Ag 3d_{5/2} ($E_B = 368.3$ eV) and Cu 2p_{3/2} ($E_B = 933.6$ eV) photoelectron peaks. A surface charge neutraliser was utilised to improve resolution. Spectra were charge corrected to a reference of 284.6 eV for the aromatic peak in the C 1s spectra⁶ or to the Au 4f_{7/2} photoelectron peak at 84.0 eV.

Spectra were quantified using the CasaXPS software program (version 2.3.10, Casa Software Ltd., UK). Unless otherwise mentioned, relative atomic concentrations were determined by applying the associated peak sensitivity factor (supplied by Kratos), after background subtraction (Shirley background shape) and the fitting of

gaussian (70 %) / lorentzian (30 %) synthetic peaks.¹²⁻¹⁴ Atomic concentration uncertainties for all fitted spectra were estimated to be ± 10 % of the measured value.

3.2.2. Time-of-Flight Secondary Ion Mass Spectrometry

3.2.2.1. Basic Concepts

Secondary Ion Mass Spectrometry (SIMS) is a mass spectrometry technique that is ideal for analysis of solid surfaces. SIMS is performed by bombarding the surface with high energy ions (primary ions), and mass analysing the secondary ions created in the bombardment. This mass analysis can allow for both elemental and structural information to be obtained from the top 1-2 nm of the surface.

In SIMS primary ions of keV energies are used to disrupt the surface, and with the resulting collisions, cause a cascade of secondary collisions that eject low energy (ca 20 eV) secondary particles from the surface¹⁵ as demonstrated in Figure 3-7. These particles consist of positive, negative, and neutral species. The overwhelming majority (90 %) of species emitted are neutral, however only the secondary ions are mass analysed in a SIMS instrument.

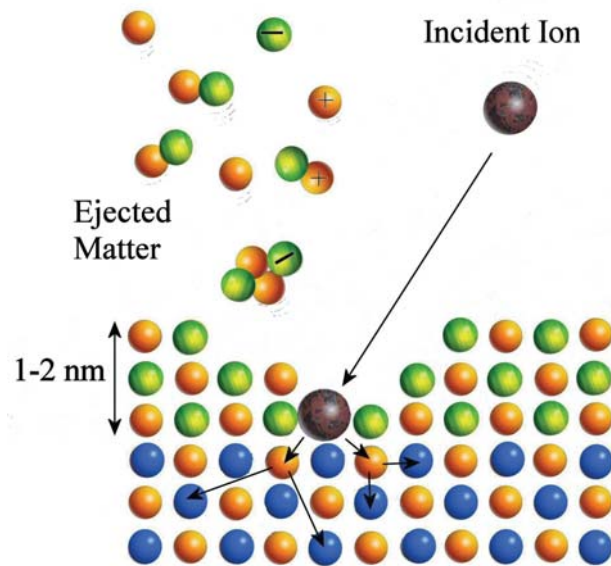


Figure 3-7: Secondary ion generation in SIMS, note the minimal penetration depth. Redrawn from Ref [16].

If a surface is bombarded with a low dose of ions during the experiment ($< 10^{13}$ ions cm^{-2}), the surface damage remains minimal as statistically no point in the analysis area would be impacted more than once.¹⁵ The information derived from an experiment of this type is considered to be directly representative of the outermost layers of the surface and is known as static SIMS due to the limited change in surface composition experienced.

In ToF-SIMS a Time-of-Flight (ToF) mass analyser is used for mass discrimination and secondary ion detection. ToF mass analysers have many advantages over other SIMS analysers. ToF analysers can provide excellent sensitivity (as low as ng cm^{-2} or parts per trillion) while providing good mass resolution ($> 10^3$ $m/\Delta m$) and with a theoretically limitless mass range (practically up to 10^4 m/z).¹⁷ Further to this, ToF mass analysers allow for parallel detection of all masses in the selected range. This parallel detection makes it ideal for SIMS by minimising the fluence a sample is exposed to, reducing damage by primary ions. As an example of the data obtained, a detailed ToF-SIMS mass

spectrum obtained from a glassy carbon disc using Bi^+ primary ions is presented in Figure 3-8.

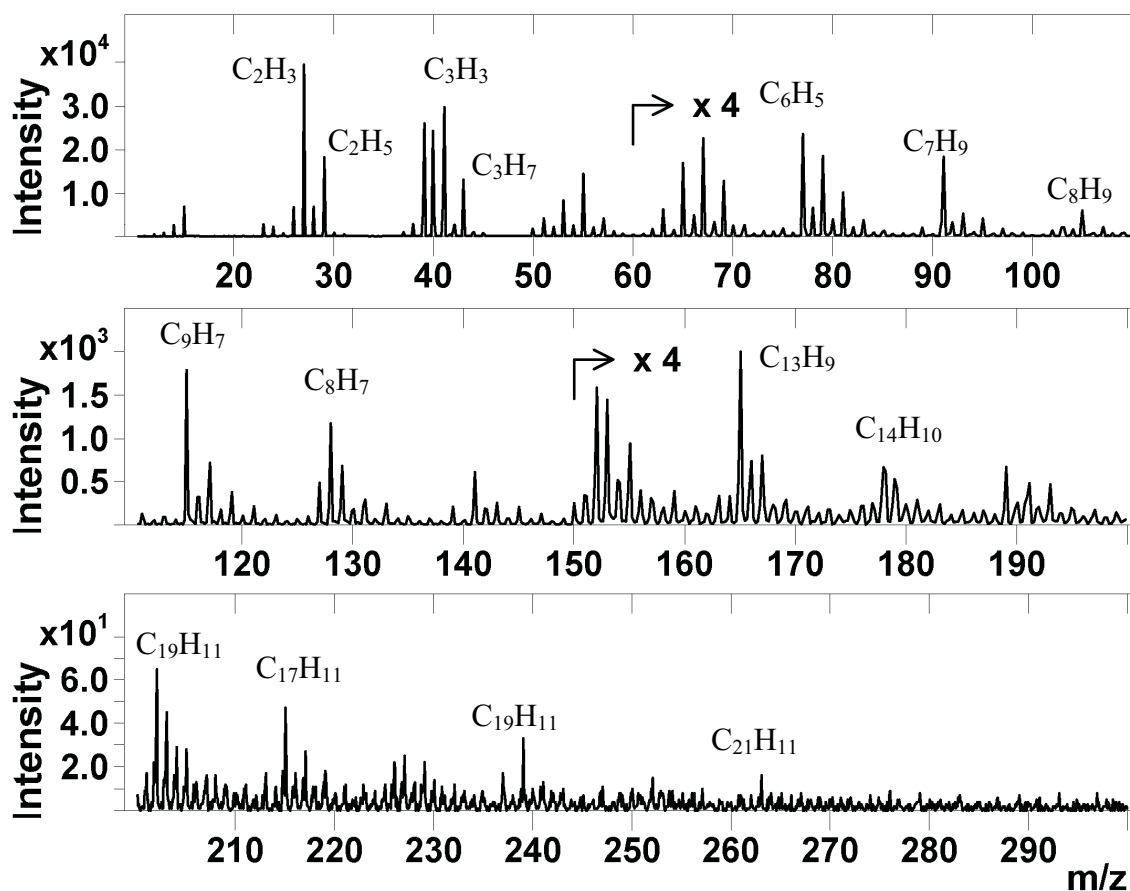


Figure 3-8: A typical positive ion ToF-SIMS spectrum of glassy carbon with major peaks labeled.

While SIMS techniques, in particular ToF-SIMS, provide excellent qualitative information about a surface, they are usually unable to provide quantitative information. This is due to difficulties in the modelling of the sputtering and ionisation events as chemical species tend to sputter and ionise with differing rates and probabilities.¹⁸ Even with this difficulty in quantification, the high quality chemical data SIMS provides is of great value in surface characterisation.

3.2.2.2. Instrumentation

A ToF analyser is shown in Figure 3-9. The analyser primarily consists of ion extraction optics, flight tube and detector, all maintained in a UHV environment. A low energy

electron flood gun is required for non-conducting samples, such as polymers, to neutralise surface charging thereby preserving efficient secondary ion production.

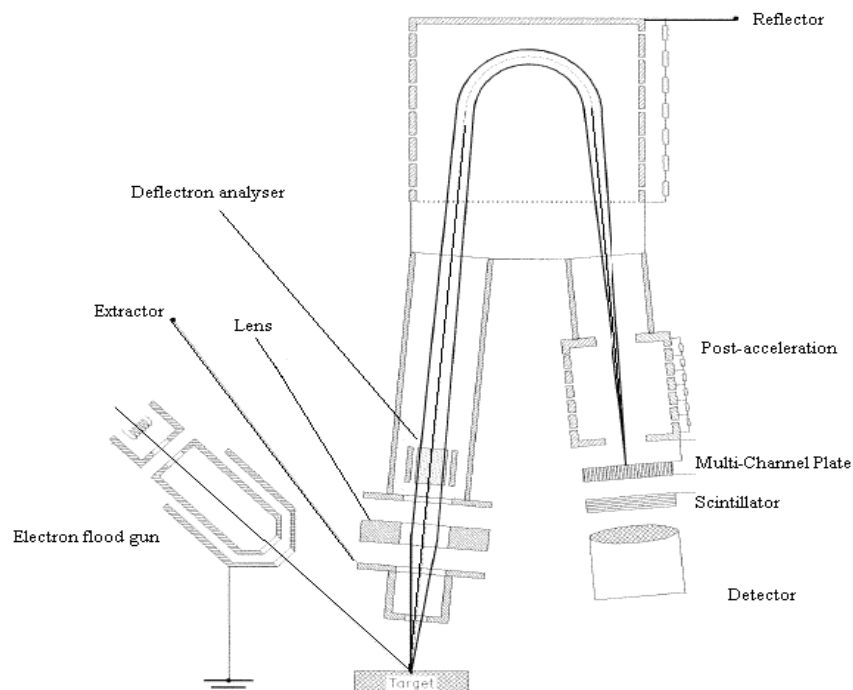


Figure 3-9: Schematic of a reflectron ToF analyser. Redrawn from Ref [19].

In a ToF-SIMS instrument, the secondary ions generated are extracted using the extraction assembly before passing through a flight tube which is shielded from external electric fields. After extraction, the ions will have a kinetic energy of E_k , and a velocity of v . The velocity of the ions is given by Equation 3.7. Thus the velocity and hence the time of flight is dependant on the mass of ion, m .

$$E_k = \frac{1}{2}mv^2 \quad (3.7)$$

$$\text{or} \quad v = \sqrt{\frac{2E_k}{m}}$$

Equation 3.7 demonstrates that the smaller the mass of the ions, the faster they will traverse the flight path and hence be detected with a shorter flight time than heavier ions. Ions of all masses will eventually reach the detector, thus allowing the mass range of a ToF instrument to be limited only by the duty cycle period.

Not all the secondary ions extracted have the same initial velocities due to variations in the ion sputtering processes, which results in a broadening of spectral peaks. To remove this effect, an electrostatic mirror (or reflectron) and second field free region are used, ensuring that the time of flight is only dependent on ion mass. The electrostatic mirror decelerates, stops and then accelerates the ions towards the detector. Ions with larger initial velocities penetrate deeper into the mirror resulting in a longer trajectory and longer flight time. Careful adjustment of reflectron conditions compensates for and removes the effect of initial velocity spread improving mass resolution in the resulting spectrum.

For detection, ion mass is discriminated through the use of the relation given by Equation 3.8.¹⁵ The time, t , is defined as the time taken for the ion to travel the length of the analyser, L , from the point of primary ion impact to the detector.

$$t = \frac{L}{v} = L \sqrt{\frac{m}{2E_k}} \quad (3.8)$$

3.2.2.3. Experimental

ToF-SIMS analysis was performed using a ToF-SIMS IV (Ion-TOF GmbH, Germany) instrument, as shown in Figure 3-10. A Bismuth cluster liquid metal ion gun operating at 25 keV was used as the primary ion source. The source was capable of producing a range of ion clusters including $^{209}\text{Bi}^+$, Bi_3^+ , Bi_3^{++} , Bi_5^{++} , Bi_7^{++} ions. $^{209}\text{Bi}^+$ was the primary ion

used with Bi_3^+ used for high m/z (> 800 Da) investigations. The instrument was operated with a $100 \mu\text{s}$ acquisition cycle time and a 10.5 ns ion pulse width, resulting in a current of 2.5 pA at the sample surface. The analysis time was 100 s and the analysis area was $100 \mu\text{m} \times 100 \mu\text{m}$. The primary ion dose density kept below the static SIMS limit of $10^{13} \text{ ions cm}^{-2}$. Surface charge neutralisation was performed with the use of an electron flood gun pulsed out of phase with the ion source during data acquisition. The analysis chamber pressure was kept at or below 10^{-9} torr. High mass resolution spectra (> 7500 at $m/z = 29$) were recorded.

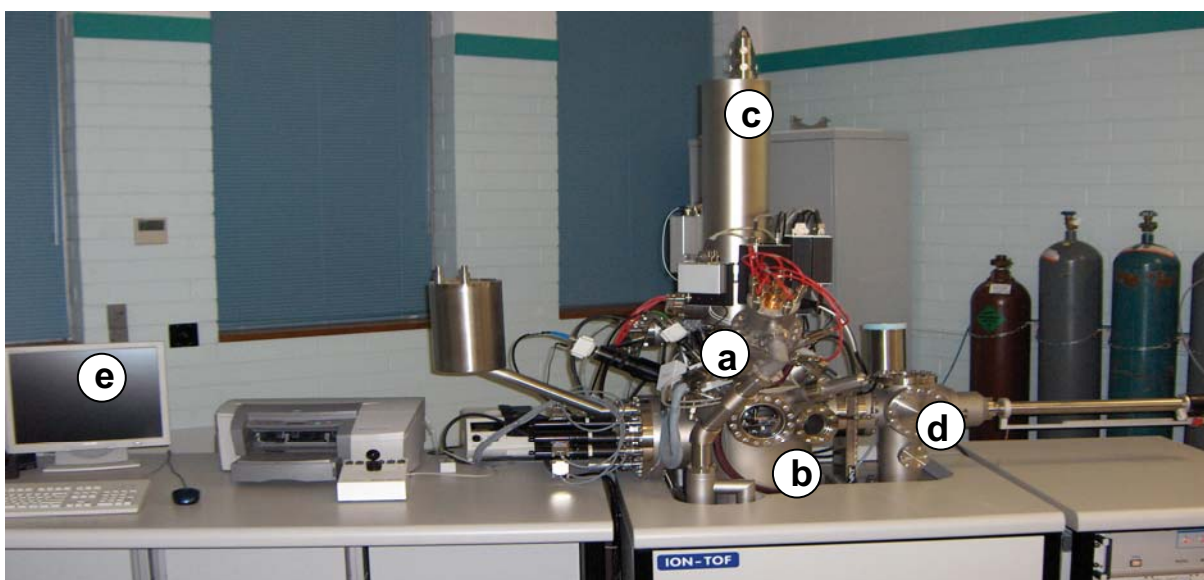


Figure 3-10: The ToF-SIMS IV instrument showing: the Bi ion source (a), analysis chamber (b), Time of Flight analyser with reflectron (c), sample loading chamber (d) and control electronics (e).

3.2.3. Atomic Force Microscopy

3.2.3.1. Basic Concepts

Atomic Force Microscopy (AFM) is a versatile and sensitive scanning probe technique that can be used to provide high resolution images of a surface. AFM works by measuring the forces between the surface and a microscale probe that is rastered across the surface to form an image. A typical AFM probe consists of a small cantilever with a sharp tip

(< 50 nm depending on application) attached at one end. When an AFM tip is brought into close proximity of a surface, the tip will experience deflection due to the attractive or repulsive forces between it and the surface. By measuring the deflection of the cantilever, the height of the tip relative to the surface can be determined.²⁰ The deflection of the cantilever can be measured with use of a laser reflected off the back of the cantilever and onto a position sensitive photodiode as shown in Figure 3-11.

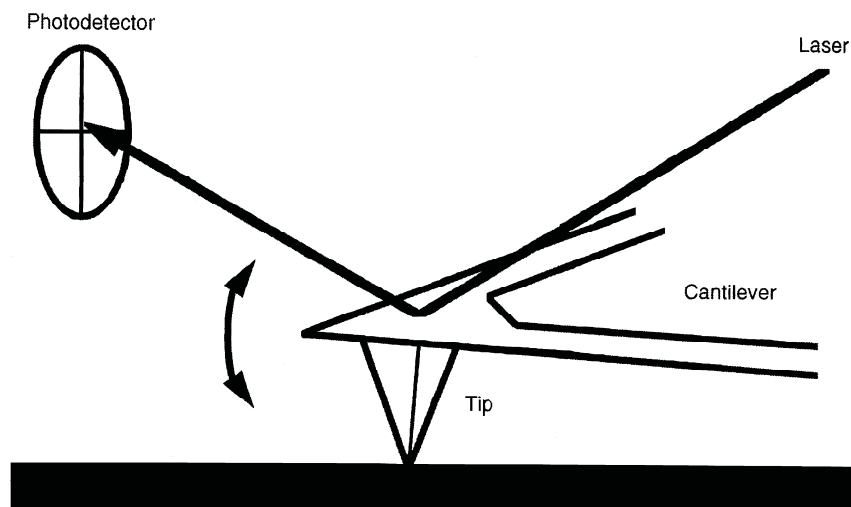


Figure 3-11: A schematic illustrating the measurement of cantilever deflection. Redrawn from Ref [21].

AFM provides many advantages over other high resolution imaging techniques. As it uses mechanical transduction, AFM can be run in many types of environments including vacuum, air, and liquid allowing for a wide range of samples to be analysed with minimal sample preparation. Another advantage is that the tip itself can be modified to measure and map a range of physical and chemical parameters such as conductivity, magnetism, force measurements, surface adhesion and various electrochemical processes.

An AFM can be run in a variety of modes each providing a range of benefits. The two most common modes are static and dynamic modes. In static mode, the probe is lowered

until there is physical contact between the tip and surface before the probe is scanned across the surface while being allowed to maintain either a constant cantilever deflection or constant height above the surface. Static mode is a conceptually simple technique, however it is generally used for hard flat samples²² as it can often cause unwanted indents in the surface or potentially damage the AFM tip. In dynamic AFM, described by instrument manufacturers as tapping or AC mode, the probe is driven at or near its resonance frequency causing it to oscillate. As the tip is lowered closer to the surface the amplitude of the oscillation is damped by interaction with the surface. As with static mode, the tip is scanned across the surface while maintaining either constant height or constant damping. Dynamic mode is considered a potentially less damaging technique that is well suited to the analysis of softer surfaces.²³

3.2.3.2. Experimental

AFM images were acquired using MFP-3D Atomic Force Microscopes (Asylum Research, USA) as shown in Figure 3-12. To minimise noise and drift, the sample stage and head were positioned on a TS-150 active isolation table (Herzan, USA) which was then enclosed in an environmental isolation enclosure (Asylum Research / TMC, USA). Two types of AFM cantilevers were used; PPP-NCHR PointProbe-plus monolithic silicon tips (Nanosensors, Switzerland) with a maximum tip radius of 10 nm and PPP-NCHR tips modified in house by the electron beam deposition of Diamond Like Carbon (DLC) in a SEM (15 minute deposition at an accelerating voltage of 10.0 kV and an emission current of 5 pA on a JEOL JSM 840). To obtain images, the instrument was operated in dynamic mode with a minimum image resolution of 256 by 256 points. Images were corrected with a first order plane fit prior to presentation or further analysis. Scratching experiments were undertaken by imaging a region of interest with a PPP-NCHR tip in contact mode with a high applied force (a setpoint of 4 V which corresponds to a force of 17 μ N) over an area of 2.5 x 2.5 μ m at a scan rate of 1.0 Hz. Two sweeps of the scratched area were

conducted to ensure complete removal of loose material from the scratched area. A minimum image resolution of 256 by 256 pixels was used. Force curves were measured using a PPP-NCHR tip with the point of contact defined by the deflection observed prior to the extension of the tip to the surface.²⁴ An estimate of the force applied with the tip was determined by using the mean force constant of 42 N m^{-1} for the PPP-NCHR tip as determined by the manufacturer.²⁵

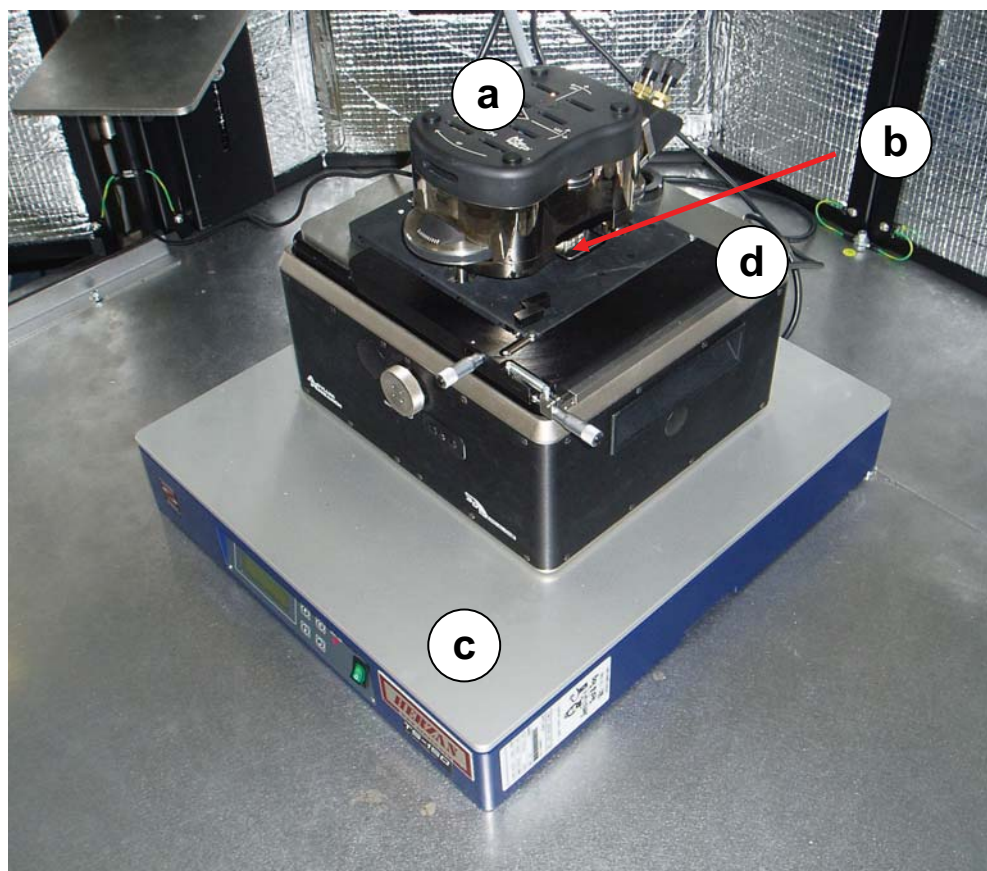


Figure 3-12: The Asylum MFP-3D atomic Force Microscope including the microscope head (a), cantilever (b), sample stage (c) and active dampening table (d). The entire setup is enclosed in an environmental isolation enclosure.

3.2.4. Cyclic Voltammetry

3.2.4.1. Basic Concepts:

Cyclic voltammetry (CV) is a versatile electrochemical analysis technique that can provide a wealth of information regarding redox reactions occurring at or near the working electrode. The technique involves the controlled cyclic sweep of the potential E (V), of a working electrode with respect to a reference potential as shown in Figure 3-13 where the resulting current, i (A), is then measured. The observed current is characteristic of the properties of the solution and contacting electrode.

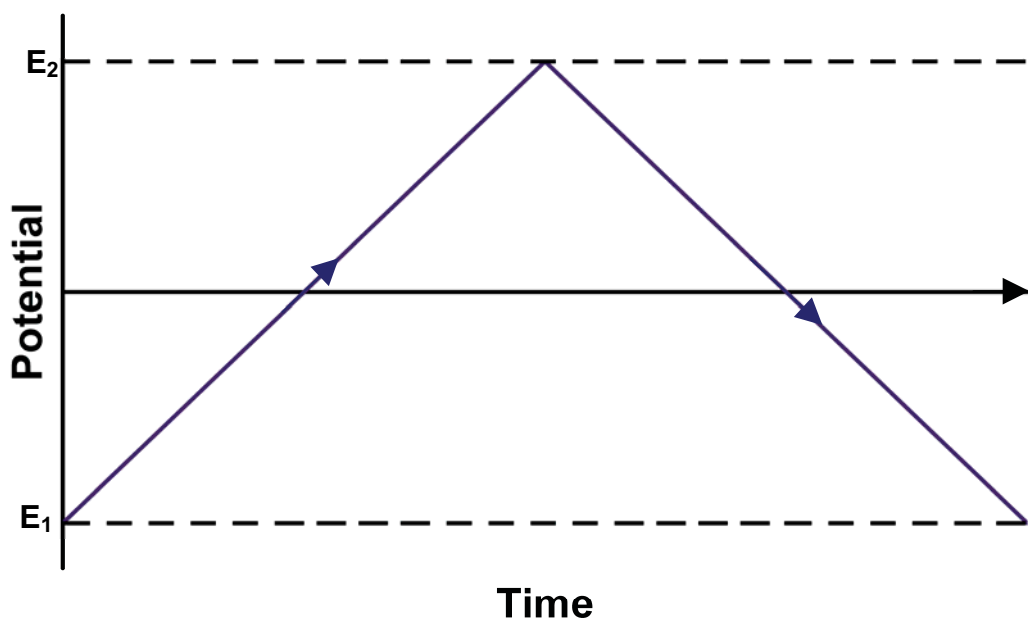


Figure 3-13: An example of the triangular waveform used in CV.

Figure 3-14 shows a simulated voltammogram of a reversible one electron solution phase redox reaction under ideal conditions. In this voltammogram the potential is swept from E_1 to E_2 and back at a scan rate of v ($V s^{-1}$). The initial current at E_1 is due to the non-faradaic (capacitive) charging of the electrode / solution interface which increases linearly with scan rate. As the potential is moved towards E_2 the current increases due to the oxidation of the redox active species with a peak in current response observed at a

potential E_p^a , with a magnitude, i_p^a . After the potential moves past E_p^a , the current falls away as the un-oxidised species cannot diffuse fast enough into the region adjacent to the electrode to maintain the rate of the electrochemical reaction. On the returning sweep, a peak in current, i_p^c , at a potential, E_p^c , corresponding to the reverse reaction, the reduction of the previously oxidised species, is observed before again tailing off due to a depletion in reagents.

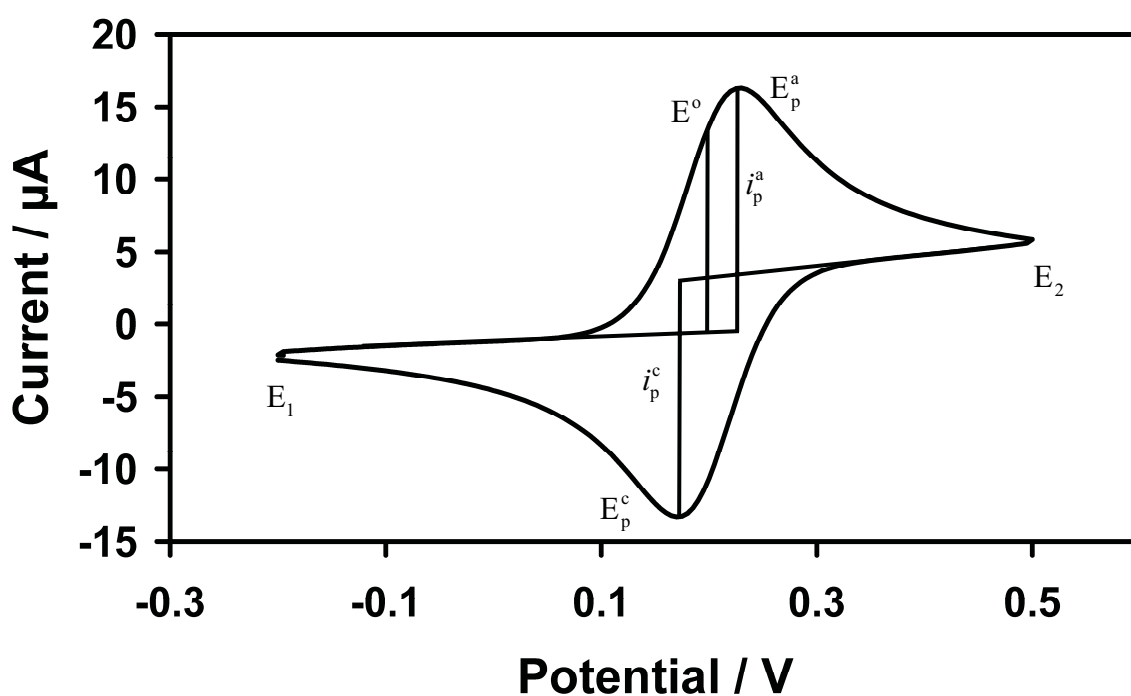


Figure 3-14: A typical voltammogram showing the important parameters. E_1 and E_2 are the lower and upper scan limits with E_p^c and i_p^c being the cathodic response and E_p^a and i_p^a being the anodic response.

Even under ideal conditions for solution phase reactions a hysteresis in the voltammogram is observed, with E_p^a and E_p^c being split by a potential difference, ΔE_p , of 57 mV for a one electron transfer.²⁶ This potential difference presents an issue as thermodynamically a reaction cannot have two different energies (one for the forward and one for the reverse reaction). Consequently, a formal potential, E^o , can be defined as the true potential at which the redox reaction occurs (under standard conditions of 25 ° C at

an effective concentration of 1 M and gases at a pressure of 1 bar) can be related to the peak potentials via the Equation 3.9.²⁶

$$E^o = \frac{E_p^a + E_p^c}{2} \quad (3.9)$$

Subsequently the difference between the peak potentials and E^o , $\Delta E_p/2$, can be considered as an overpotential which is analogous to the activation energy required to transfer an electron from the electrode to the redox active species. Under non-ideal conditions higher values of ΔE_p are often observed due to slow heterogeneous kinetics, though values of $\Delta E_p > 57$ mV can also arise as a result of the resistance of the cell.

CV measurements can provide a substantial amount of information regarding the electrochemical process of interest, in particular, information about thermodynamics and kinetics, charge and mass transport and reagent concentrations. For example, when the electroactive species is not surface confined and the current is limited by diffusion, the use of the Randles-Sevcik equation (Equation 3.10), can provide information about the electrochemical system at hand²⁷ including the concentration of the electroactive species, C (mol cm^{-3}), the diffusion coefficient, D ($\text{cm}^2 \text{s}^{-1}$), the stoichiometric number of electrons transferred, n , or the electrode area, A (cm^2).

$$i_p = 2.69 \times 10^5 n^{3/2} AD^{1/2} C\nu^{1/2} \quad (3.10)$$

If the scan rate is varied or multiple cycles are run, further information about heterogeneous or homogeneous reaction kinetics may be obtained. Also, the observation of new peaks (or conversely the absence of existing peaks) in the voltammogram can indicate formation of new chemical species or layers. This makes the technique ideal for the monitoring of growth or degradation polymers and other thin films.

3.2.4.2. Instrumentation

Cyclic voltammetry is typically performed using a three electrode setup as shown in Figure 3-15 below. The three electrodes are: a working electrode, where the electrochemistry of interest takes place; a counter or auxiliary electrode, which supplies current and completes the electrical circuit; and a reference electrode, where a secondary redox couple with a defined potential provide a reference point for the applied potential. The three electrode types are typically made from different materials. Working electrodes are traditionally metals (typically inert metals e.g. Au or Pt) or carbon based materials (often glassy carbon or graphite). Counter electrodes are normally constructed of inert materials such as platinum to avoid interferences. Reference electrodes typically consist of a silver wire coated with silver chloride the half reaction for which is shown in equation 3.11 below, although other systems such as mercury/mercury chloride can be used.^{27,28} The reference electrode is typically encased in a glass capillary with a porous frit at one end providing electrical contact between the reference electrode and the remainder of the electrochemical cell.^{28,29}



The reference electrode embodied in equation 3.11 only occurs in aqueous solutions. For work in non-aqueous solutions a quasi-reference electrode (QRE) is often employed. Usually this consists of a silver wire immersed in an appropriate solvent/electrolyte system.²⁷ QREs are considered more unstable than their aqueous counterparts and to compensate are often referenced to an internal standard such as ferrocene.²⁷

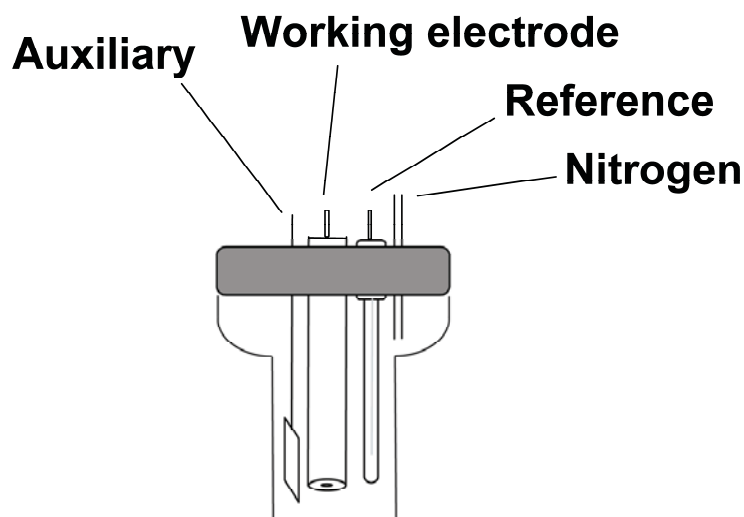


Figure 3-15: The standard three electrode cell set-up used for cyclic voltammetry and other electrochemical procedures

3.2.4.3. Experimental

Cyclic voltammetry was performed using a μ -Autolab Type II (Eco Chemie, Netherlands) potentiostat/galvanostat. A three electrode cell consisting of a reference electrode, counter electrode, and working electrode was used. The counter electrode was a platinum wire. For aqueous systems a Ag/AgCl (3 M KCl) reference electrode with a standard electrode potential of 0.233 V with respect to a standard hydrogen electrode was used. In organic solvents a Ag wire pseudo reference was used, which was referenced to the ferrocene E^0 potential of 0.265 V v.s. Ag/AgCl.²⁷ All reference potentials are referred back to the Ag/AgCl reference unless otherwise mentioned. The working electrode used was either a 3 mm diameter glassy carbon or 2 mm gold disc embedded in a 6 mm diameter PTFE body (CH Instruments, USA). For experiments involving surface analysis 12 x 12 mm Pt flags (Goodfellow, USA), glassy carbon discs of 15 mm diameter (HTW, Germany), or gold coated QCM discs (Section 3.2.5.2) were used as electrodes. The EQCM cell described in Figure 3-17 was used for electrochemical experiments involving both the glassy carbon and QCM discs. Contacting solutions were degassed with nitrogen gas

(99.999% Linde) for a minimum of 5 minutes prior to commencing an experiment unless otherwise mentioned. To minimise electrical noise, experiments were conducted in a grounded Faraday Cage.

For ECL experiments, a quartz bottomed glass cell as shown in Figure 3-16 was used, and positioned in a holder designed to allow a reproducible distance between the working electrode and photodetector. Light emission was detected using a photomultiplier tube (PMT) (9828SB, Electron Tubes, UK) biased at + 500 V positioned directly under the cell. The output signal was amplified using a transimpedance amplifier (D7280, Ames Photonics, USA) and acquired using the auxiliary channel of the potentiostat with the GPES software package (version 4.9, Eco Chemie, Netherlands). Experiments were conducted in a light tight Faraday Cage. Whenever possible the light signal was given time to relax between experiments to minimise background noise.

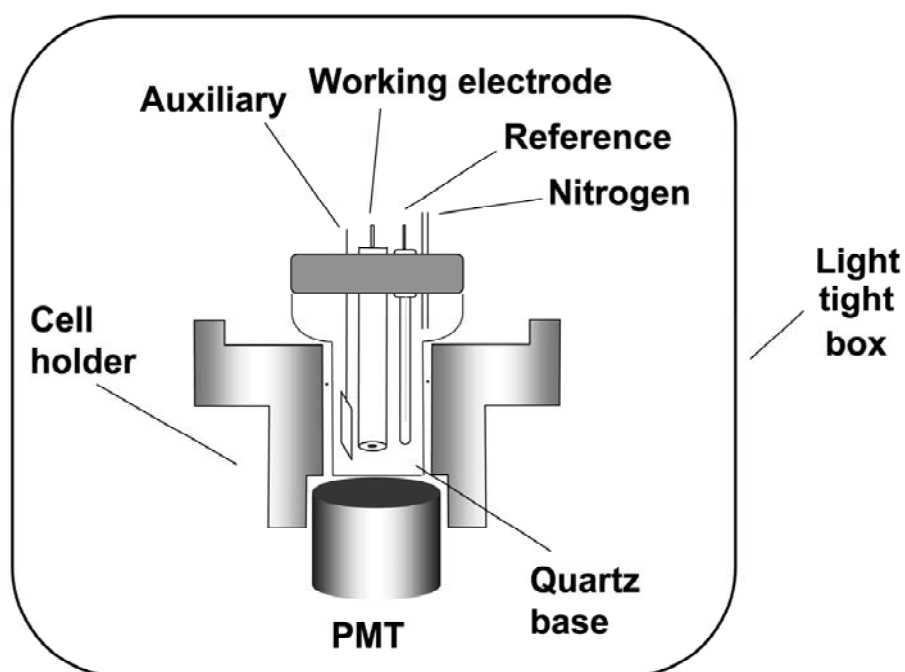


Figure 3-16: Diagram of electrochemical set up for ECL experiments.

3.2.5. Electrochemical Quartz Crystal Microbalance

3.2.5.1. Basic Concepts

Quartz Crystal Microbalance (QCM) techniques allow for measurement of small mass changes via the measurement of the corresponding change in resonant frequency of a crystal oscillator. In QCM a quartz crystal is electrically oscillated in a shear mode at a resonant frequency, f_0 (Hz), and as a mass, Δm (g), is deposited on the crystal surface the resonant frequency of the crystal will decrease according to the Sauerbrey Equation as given in Equation 3.12

$$\Delta f = -2f_0^2 \Delta m / A \sqrt{\mu_q \rho_q} \quad (3.12)$$

where Δf is the frequency shift of the quartz oscillator in Hz, A is the area of the quartz covered by the electrode in cm^2 , μ_q is the shear modulus of quartz ($2.947 \times 10^{11} \text{ g cm}^{-1} \text{ s}^2$) and ρ_q is the density of quartz (2.648 g cm^{-3}).³⁰

Electrochemical Quartz Crystal Microbalance (EQCM) uses an electrode on the quartz crystal as a working electrode, allowing for electrochemistry to be performed while the QCM is running. This technique provides a unique opportunity to analyse the electrodeposition of material onto the electrode surface *in-situ*.

3.2.5.2. Experimental

EQCM studies were performed on a CH Instruments 420A Potentiostat (CH Instruments, USA) using a 3 electrode EQCM cell, a diagram describing the EQCM cell and its connection to the potentiostat is shown in Figure 3-17. The working electrode was a gold coated (100 nm thick) AT cut quartz crystal with a fundamental frequency of 7.95 MHz

and a geometrical electrode area of 0.196 cm^2 . Working electrodes were cleaned electrochemically by cycling between 0.4 and 1.4 V vs Ag/AgCl in 0.1 M H_2SO_4 at a scan rate of 10 mV/s until there was no change in CV. The counter electrode consisted of a platinum wire, with the reference electrode being a Ag wire pseudo reference in acetonitrile, which was regularly referenced to the ferrocene ($E^0 = 0.265 \text{ V}$ v.s. Ag/AgCl).²⁷ The EQCM cell and QCM signal generator were housed in a grounded Faraday Cage to minimise electrical noise and dampen acoustic interference. To further dampen any undue noise, the EQCM cell was located on a marble table in a temperature controlled room (22°C).

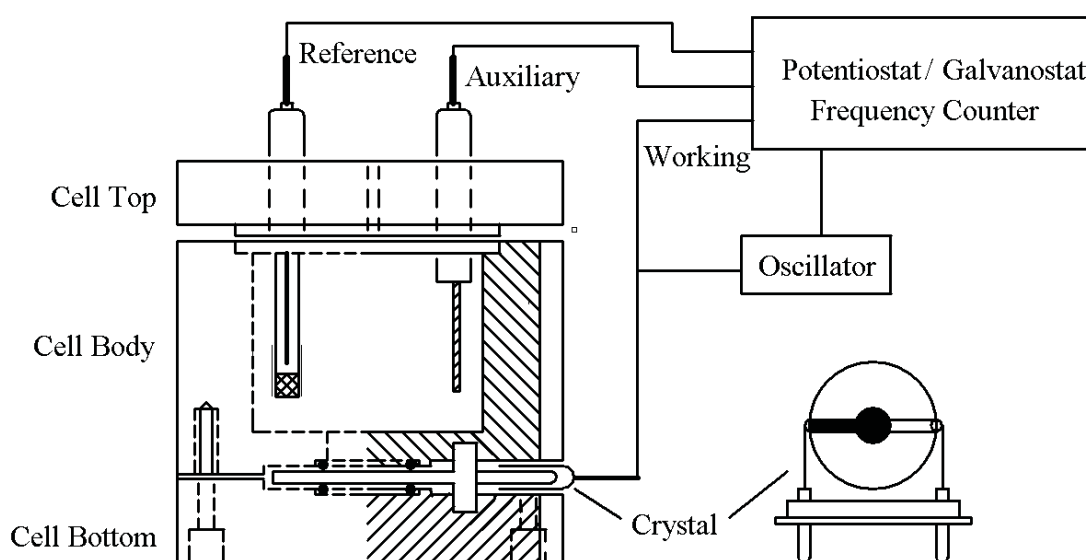


Figure 3-17: Diagram of the EQCM cell used. Redrawn from Ref [31].

3.3. References

- (1) Downey, T. M.; Nieman, T. A.; *Anal. Chem.* **1992**, *64*, 261-268.
- (2) Johansson, O.; Borgstrom, M.; Lomoth, R.; Palmblad, M.; Bergquist, J.; Hammarstrom, L.; Sun, L.; Åkermark, B.; *Inorg. Chem.* **2003**, *42*, 2908-2918.
- (3) Balaur, E.; Peele, A. G.; *Thin Solid Films* **2009**, *517*, 6520-6526.
- (4) Einstein, A.; *Annalen der Physik* **1905**, *17*, 132-148.
- (5) Kibel, M. H. In *Surface Analysis Methods in Materials Science*; O'Connor, D. J., Sexton, B. A., Smart, R. S. C., Eds.; Springer-Verlag: New York, 1992, p 175.
- (6) Moulder, J. F.; Stickle, W. F.; Sobol, P. E.; Bomben, K. D. *Handbook of X-ray Photoelectron Spectroscopy*; Perkin-Elmer Corporation Physical Electronics Division: Eden Prairie, 1992.
- (7) Ratner, B. D.; Castner, D. G. In *Surface Analysis: The principle techniques*; Vickerman, J. C., Ed.; John Wiley & Sons.: Chichester, 1997, p 43-98.
- (8) Watts, J. F. *An Introduction to Surface Analysis by Electron Spectroscopy*; Oxford University Press: New York, 1990.
- (9) Seah, M. P.; Dench, W. A.; *Surf. Inter. Anal.* **1979**, *1*, 2-11.
- (10) Zangwill, A. *Physics at Surfaces*; Cambridge University Press: Cambridge, 1988.
- (11) Fulghum, J. E.; *Journal of Electron Spectroscopy & Related Phenomena* **1999**, *100*, 331-355.
- (12) Fairley, N.; Carrick, A. *The Casa Cookbook Part 1: Recipes for XPS Data Processing*; Pelican Press: Manchester, 2005.
- (13) Fairley, N.; 2.3.10 ed. 2005.
- (14) *CasaXPS User's Manual: Version 1.0*; Casa Software Ltd.: Uk, 2000.
- (15) Vickerman, J. C.; Swift, A. J. In *Surface Analysis: The principle techniques*; Vickerman, J. C., Ed.; John Wiley & Sons.: Chichester, 1997, p 43-98.
- (16) Prissanaroon, W., La Trobe University, 2004.

- (17) Vickerman, J. C. In *ToF-SIMS: Surface Analysis by Mass Spectrometry*; Vickerman, J. C., Briggs, D., Eds.; IM Publications and Surface Spectra Limited: Manchester, 2001.
- (18) Eynde, X. V. In *ToF-SIMS: Surface Analysis by Mass Spectrometry*; Vickerman, J. C., Briggs, D., Eds.; IM Publications and Surface Spectra Limited: Manchester, 2001.
- (19) ION-TOF (GmbH).
- (20) Bhushan, B. In *Springer Handbook of Nanotechnology*; Bhushan, B., Ed.; Springer: Heidelberg, 2007.
- (21) Leggett, G. In *Surface Analysis: The principle techniques*; Vickerman, J. C., Ed.; John Wiley & Sons.: Chichester, 1997, p 43-98.
- (22) Hafner, J. H. In *Springer Handbook of Nanotechnology*; B. Bhushan, Ed.; Springer: Heidelberg, 2007.
- (23) Zhong, Q.; Inniss, D.; Kjoller, K.; Elings, V. B.; *Surf. Sci. Lett.* **1993**, *290*, L688-L692.
- (24) In *MPF 3D Manual*; Asylum Research: Santa Barbara, 2007, p 262-283.
- (25) NanoWorld AG: Neuchatel, Switzerland; Vol. 2011, p <http://www.nanosensors.com/PPP-NCHR.htm>.
- (26) Compton, R. G.; Banks, C. E. *Understanding Voltammetry*; World Scientific Publishing Co. Pty. Ltd.: Singapore, 2007.
- (27) Bard, A. J.; Faulkner, L. R. *Electrochemical methods: fundamentals and applications*; 2nd ed.; John Wiley: New York, 2001.
- (28) Monk, P. M. *Fundamentals of electroanalytical chemistry*; Wiley: Chichester, 2001.
- (29) Hawkrige, F. M. In *Laboratory Techniques in Electroanalytical Chemistry*; Kissinger, P. T., Heineman, W. R., Eds.; Marcel Dekker Inc.: New York, 1984.

- (30) Sauerbrey, G.; *Z. Phys.* **1959**, *155*, 206-222.
- (31) Instruments, C. H. *Electrochemical Instrumentation*; C.H. Instruments, Inc.: Austin, Texas, 2007.

Chapter 4: Nafion/Polypyrrole composites for ECL sensing

4.1. Introduction

The immobilisation of ECL active compounds on electrodes can be achieved through a variety of methods such as the use of Langmuir-Blodgett^{1,2} and Langmuir-Schaefer films,³ self-assembled monolayers,⁴⁻⁹ and the electrostatic attachment into polymer films.^{10,11} The advantages of each method are discussed in Chapter 2. The electrostatic attachment method provides a number of benefits over other immobilisation techniques. In particular, such systems are characterised by an enlarged reaction volume compared to 2D monolayer systems, often resulting in better sensitivity due to greater analyte turnover. Ionomers such as Nafion have shown promise for the electrostatic immobilisation of $\text{Ru}(\text{bpy})_3^{2+}$,^{11,12} however they tend to suffer from instability related to the migration of $\text{Ru}(\text{bpy})_3^{2+}$ into electrochemically inactive regions of the polymer.¹³ Nafion composites have been shown to be successful in improving the stability of the $\text{Ru}(\text{bpy})_3^{2+}$ loaded film while maintaining excellent sensitivity.¹⁴ It is suggested that the enhanced stability of these composites is due to the co-material (nanotubes, sol-gels, etc.) providing a stronger hydrophobic interaction with the $\text{Ru}(\text{bpy})_3^{2+}$, than that of the surrounding Nafion, hindering the migration of $\text{Ru}(\text{bpy})_3^{2+}$ into the electrochemically inaccessible (hydrophobic) regions of the Nafion.¹⁵⁻¹⁷

A number of Nafion-based composites have been investigated for use in ECL sensing, however the use of conducting polymer blends remains unexplored. Conducting polymers possess qualities that make them potentially suitable for the creation of a modified electrode-based ECL sensor. These qualities include good electron transport properties and simple, easily controlled synthesis via electrodeposition. As discussed in Chapter 2

(Section 2.2.1.4.) conducting polymer composites of Nafion have been reported previously and were used to improve the entrapment of the redox moiety, reduce interferences and improve sensor lifetimes.^{18,19} These reported benefits are desirable for a PME-based ECL sensor.

In this chapter, a Nafion/polypyrrole composite for the immobilisation of ECL reagents, in particular $\text{Ru}(\text{bpy})_3^{2+}$, is described. The structure and function of the composite film are compared with pure Nafion using a combination of electrochemical and surface analytical techniques, such as CV, XPS and ToF-SIMS, with a view to understanding the factors that influence the overall performance of the film.

4.2. Results and Discussion

The fabrication methods of the Nafion films described in this section are discussed in Section 3.1.1.

4.2.1. Layer Thickness

Atomic Force Microscopy (AFM) measurements were used to determine the thickness of the deposited Nafion layer. A typical AFM image of a fractured fully hydrated $\text{Ru}(\text{bpy})_3^{2+}$ loaded Nafion film on a silicon substrate is shown in Figure 4-1. The average thickness of the film (d), is estimated to be $\sim 1.5 \mu\text{m}$. The AFM measurements are consistent with estimates based on the previous measurements of charge transport rates in similar films.^{10,20} The film thickness, coupled with the surface coverage ($\Gamma = 18.2 \text{ nMol cm}^{-2} \pm 1.9 \text{ nmol cm}^{-2}$) from slow scan CV experiments under conditions of exhaustive electrolysis of the ruthenium centres within the layer allows for the estimation of the concentration of electroactive sites within the film ($c = \Gamma / d$). These experiments suggest a $\text{Ru}(\text{bpy})_3^{2+}$ concentration of $0.12 \text{ M} \pm 0.013 \text{ M}$.

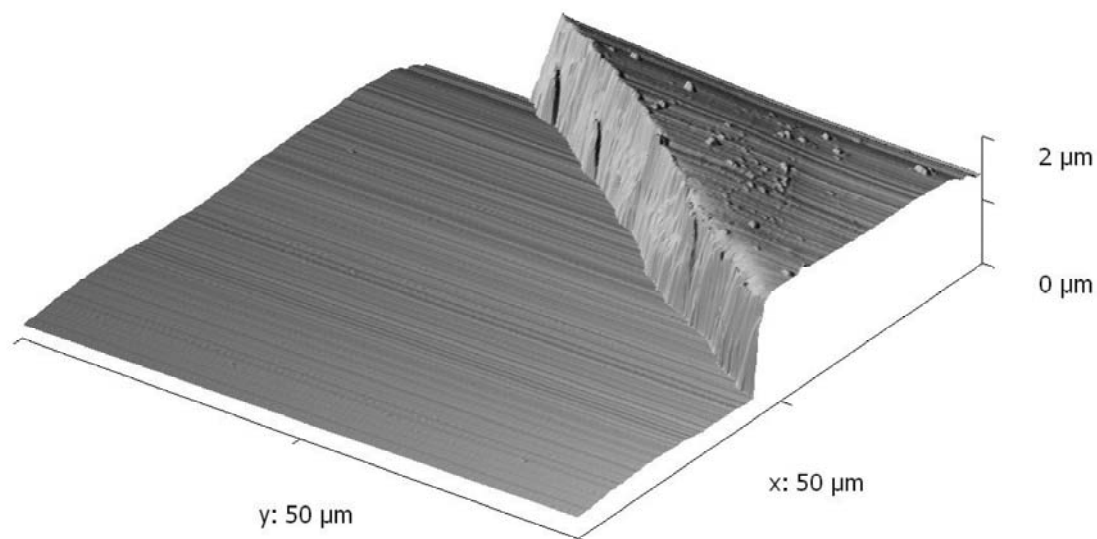


Figure 4-1: An AFM image showing a created step edge (top right hand corner) on a hydrated Nafion film loaded with $\text{Ru}(\text{bpy})_3^{2+}$ on a silicon substrate. Average film thickness was measured to be $\sim 1.5 \mu\text{m}$.

4.2.2. Ruthenium Absorption and Polypyrrole Deposition

Figure 4-2 shows a series of CVs following the absorption of $\text{Ru}(\text{bpy})_3^{2+}$ from solution into the immobilised Nafion layer over time. The increase in peak current associated with each successive scan is attributed to $\text{Ru}(\text{bpy})_3^{2+}$ diffusing into the layer. Distinctive peak tailing in the CVs is observed which is consistent with semi-infinite diffusional charge transport where the thickness of the depletion layer is less than that of the film ($\sim 1.5 \mu\text{m}$). The increase in peak current, i_p , over time is demonstrated in the insert of Figure 4-2. It is observed that i_p starts to plateau after 45 minutes of immersion indicating that the Nafion film becomes fully loaded with $\text{Ru}(\text{bpy})_3^{2+}$ in this period. It is important to establish the loading rate for the Nafion film to ensure sufficient SO_3^- sites are still available for the incorporation of the cationic polymer, polypyrrole (PPy), into the film. Therefore the film was only partially loaded with $\text{Ru}(\text{bpy})_3^{2+}$ by immersing the film in solution for 20 minutes.

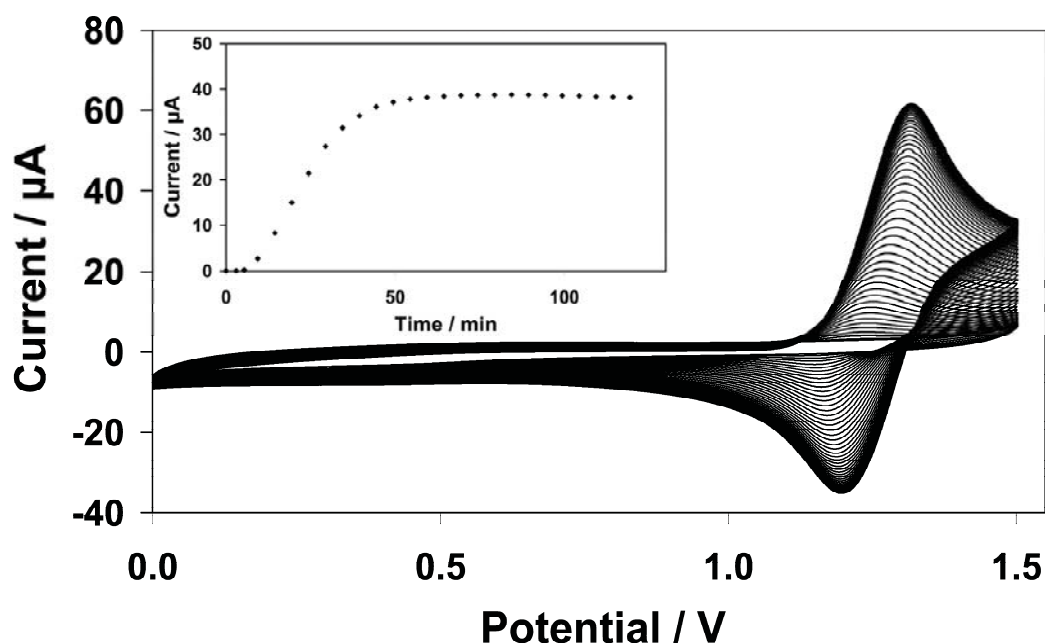


Figure 4-2: Consecutive CVs demonstrating the absorption of $\text{Ru}(\text{bpy})_3^{2+}$ into the Nafion film. The first 40 scans are shown. The insert demonstrates the increase in peak current over time, with the plateau indicating that the film is fully loaded. Scan rate was 100 mV s^{-1} .

The amount of PPy deposited into the Nafion layer was estimated by measuring the charge passed during polymerisation in a control experiment where no $\text{Ru}(\text{bpy})_3^{2+}$ complex was present in the layer. The absence of $\text{Ru}(\text{bpy})_3^{2+}$ in the film avoids the contribution of the $\text{Ru}^{2+}/\text{Ru}^{3+}$ oxidation to the measured charge. In these experiments, $0.5 \text{ mC} \pm 0.17 \text{ mC}$ of charge was passed and as the polymerisation of pyrrole may be considered a one electron transfer,²¹ this corresponds to the polymerisation of $5.2 \pm 1.8 \text{ nmol}$ ($83.4 \text{ nM cm}^{-2} \pm 25.4 \text{ nM cm}^{-2}$) of pyrrole monomer into the film.

4.2.3. Electrochemical Characterisation of Films

Figure 4-3 shows a typical CV for an electrode modified with the Nafion/PPy composite and loaded with $\text{Ru}(\text{bpy})_3^{2+}$ (Nf/Ru/PPy). A cyclic voltammogram of a film containing only Nafion and $\text{Ru}(\text{bpy})_3^{2+}$ (Nf/Ru) prior to the incorporation of the PPy is provided for comparison. The 10th cycle is shown in each case. The Nf/Ru/PPy and Nf/Ru films exhibit similar voltammetric behaviour, with the $\text{Ru}^{2+}/\text{Ru}^{3+}$ redox couple observed at approximately 1.1 V. Distinctive tailing of the voltammetric peak is observed for both

electrodes at these relatively short experimental time scales. Under these conditions the peak current varies linearly with the square root of scan rate (Figure 4-4). This response is consistent with semi-infinite diffusional charge transport where the thickness of the depletion layer is less than that of the film ($\sim 1.5 \mu\text{m}$). An additional irreversible peak (not shown) was observed at 1.0 V for the Nf/Ru/PPy system which appeared only in the first scan and was attributed to the oxidation of residual pyrrole monomer present in the film.^{22,23} The reversible electrochemistry of Nafion/PPy composites is normally observed between -0.4 to -0.54 vs Ag/AgCl depending on the electrolyte present in the contacting solution.²⁴ This redox couple is notably absent in the Nf/Ru/PPy film. This absence has been reported previously for Nafion/PPy composites produced in a similar manner.²⁵ The reason for this is unclear but may be related to the polymeric nature of the Nafion dopant which being immobile, inhibits the charge compensation process relative to systems doped with freely diffusing anions.

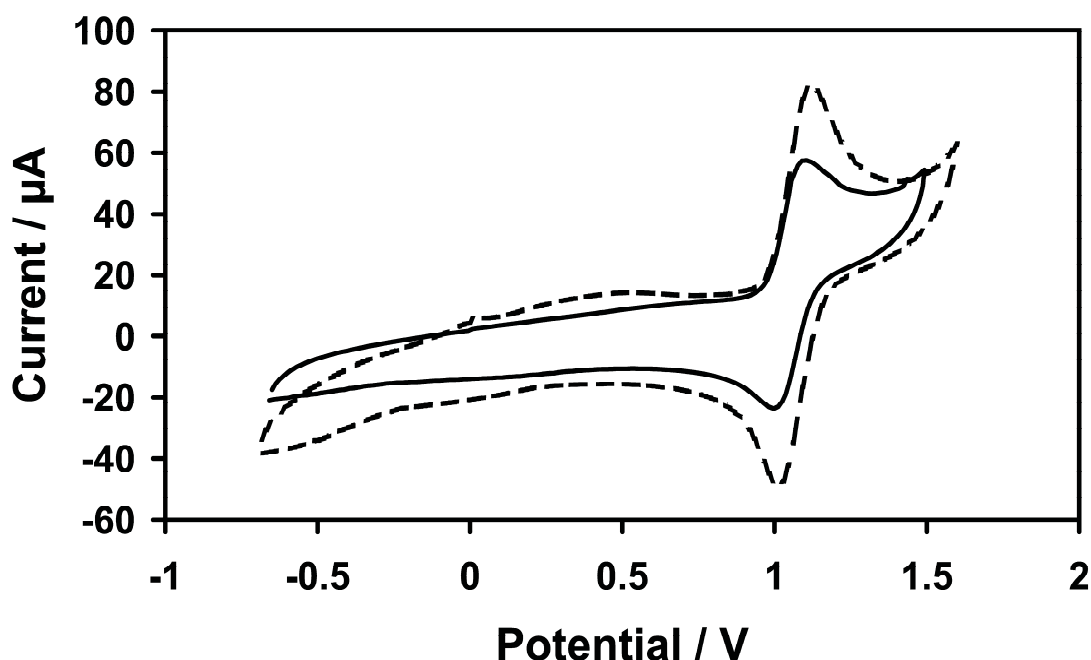


Figure 4-3: Voltammetric response of Nf/Ru film in 95:5 0.2 M Na_2SO_4 /Acetonitrile before (----), and after (—), the incorporation of PPy. The scan rate was 100mV/s.

At relatively fast scan rates and under identical conditions to the pure Nafion system, the peak currents associated with the oxidation and reduction of $\text{Ru}(\text{bpy})_3^{2+}$ in the film were

consistently 20 to 30 % smaller after the incorporation of PPy. However, slow scan rate studies, where the layer was exhaustively oxidised (scan rates less than 1 mV s⁻¹), revealed that the surface coverage (Γ) of the ruthenium complex remained identical ($\Gamma = 18.2 \text{ nmol cm}^{-2} \pm 1.9 \text{ nmol cm}^{-2}$).

As the total amount of $\text{Ru}(\text{bpy})_3^{2+}$ is constant, the most likely explanation for the decrease in peak currents on incorporation of PPy is a decrease in the rate of charge transport through the film. It has been previously shown that charge transport in thin films of redox polymers, including Nafion-based systems,^{26,27} is a diffusion-like process^{28,29} and hence the voltammetric response obeys the Randles-Sevcik equation,³ as given below.

$$i_p = 2.69 \times 10^5 n^{3/2} AD^{1/2} C \nu^{1/2} \quad (4.1)$$

where i_p is the peak current (A), n is the electron stoichiometry, A is the electrode area (cm²), D is the diffusion coefficient of the system (cm² s⁻¹), C is the concentration of the electroactive species (mol cm⁻³) and ν is the scan rate (V s⁻¹). Figure 4-4 shows that the peak current scales linearly with the square root of the scan rate for both film types, allowing information regarding the charge transport characteristics of the film to be extracted. Table 4-1 provides further information regarding the gradients presented in Figure 4-4. By measuring the voltammetric response of the Nf/Ru layer at various scan rates before and after polymerising PPy into the layer, any variations in response due to differences in $\text{Ru}(\text{bpy})_3^{2+}$ concentration were minimised. Figure 4-4 shows how the slope of the i_p versus square root of scan rate varies depending on the composition of the layer and that of the contacting solution. Comparison of graph (a) with (b) and graph (c) with (d) suggests a decrease in the rate at which charge is transported through the layer by a factor of approximately two upon incorporation of PPy.

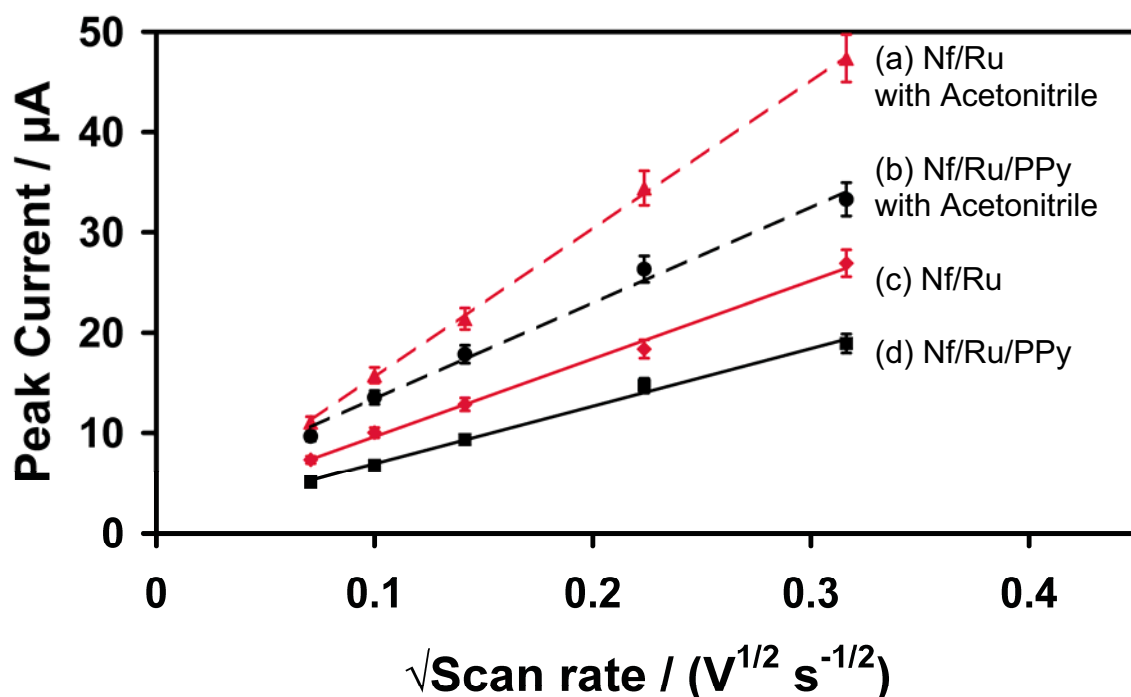


Figure 4-4: Comparison of charge transport rates through Nf/Ru and Nf/Ru/PPy films with and without the presence of acetonitrile. (a) Nf/Ru in 0.2 M Na₂SO₄ with 5 % acetonitrile, (b) Nf/Ru/PPy in 0.2 M Na₂SO₄ with 5 % acetonitrile, (c) Nf/Ru in 0.2 M Na₂SO₄, (d) Nf/Ru/PPy in 0.2 M Na₂SO₄. All trendlines presented have a R² > 0.99.

Series	Gradient (A V ^{1/2} s ^{-1/2})	Intercept (µA)	D _{CT} (cm ² s ⁻¹)
a) Nf/Ru in 95:5 0.2 M Na ₂ SO ₄ /Acetonitrile	1.48 x 10 ⁻⁴ ± 1.0 x 10 ⁻⁵	0.73 ± 0.27	4.12 x 10 ⁻⁹ ± 1.0 x 10 ⁻⁹
b) Nf/Ru/PPy in 95:5 0.2 M Na ₂ SO ₄ /Acetonitrile	9.59 x 10 ⁻⁵ ± 4.8 x 10 ⁻⁶	3.79 ± 0.83	1.73 x 10 ⁻⁹ ± 4.20 x 10 ⁻¹⁰
c) Nf/Ru in 0.2 M Na ₂ SO ₄	7.77 x 10 ⁻⁵ ± 5.4 x 10 ⁻⁶	1.86 ± 0.23	1.13 x 10 ⁻⁹ ± 2.76 x 10 ⁻¹⁰
d) Nf/Ru/PPy in 0.2 M Na ₂ SO ₄	5.75 x 10 ⁻⁵ ± 1.8 x 10 ⁻⁶	1.16 ± 0.19	6.22 x 10 ⁻¹⁰ ± 1.51 x 10 ⁻¹⁰

Table 4-1: Values for D_{CT}, along with gradients and intercepts for data presented in Figure 4-4. The surface coverage (Γ) for these layers was 1.82 ± 0.2 x 10⁻⁸ cm²s⁻¹ and the layer thickness was 1.5 µm.

The value of the apparent charge transport diffusion coefficient (D_{CT}) for the Nf/Ru/PPy film in 0.2 M Na₂SO₄ is 6.22 x 10⁻¹⁰ cm² s⁻¹ and can be compared with a value of 1.14 x 10⁻⁹ cm²s⁻¹ for the Nf/Ru films prepared. The measured value of D_{CT} for Nf/Ru is within the range of previously reported values for this system.^{20,27,30} Since exhaustive electrolysis (1 mV s⁻¹) of the layers before and after incorporation of PPy reveal no change in the total number of moles of Ru(bpy)₃²⁺ in the layer and if the layer thickness and thus ruthenium concentration (0.12 M), are assumed not to vary significantly on

incorporation of PPy, the apparent decrease in D_{CT} cannot be ascribed to variations in Ru intersite separation or to loss of $Ru(bpy)_3^{2+}$ from the layer. Redox switching in these layers requires influx and efflux of counter ions from the supporting electrolyte in order to maintain charge neutrality. Therefore, the most likely explanation for the observed decrease in signal is an impeded ion flux as a result of partial blocking of the ion channels present in the Nafion by PPy resulting in slow charge transport.

Figure 4-4 also illustrates the effect of the acetonitrile content of the contacting solution on the apparent rate of charge transport through the films. The increase in D_{CT} , by a factor of approximately three, manifested by the greater slope of the graph, may be attributed to the partial solvation of hydrophobic and interstitial regions within the layer, allowing for improved ion transport through these regions of the Nafion. Apart from inhibiting the movement of charge compensating counter-ions, another explanation for the observed effect of PPy on the layer is a decrease in the ruthenium concentration due to displacement from the layer. However, the recovery in voltammetric response on exposure of the same films to acetonitrile solution supports the conclusion that the effect of PPy on the film is to slow the rate charge transport by impeding ion flux.

4.2.4. Surface Characterisation of Films

Figure 4-5 shows a comparison of the C 1s and N 1s photoelectron region spectra for the Nf/Ru and Nf/Ru/PPy films. Table 4-2 provides a comparison between the concentrations of film constituents as atomic % and normalised to the Ru 3d photoelectron component. XPS analyses are required to confirm the presence of PPy, at least at the surface of the films, as no PPy electrochemistry is observed.

The C 1s spectra of both films (Figs. 4-5(a) and 4-5(b)) are complex due to the different chemical environments associated with the Nafion film, Ru(bpy)₃²⁺ and PPy. The presence of Ru(bpy)₃²⁺ in both films is confirmed by the observation of the Ru 3d_{5/2} photoelectron peak at 280.9 eV. The Ru 3d_{3/2} peak occurs at a binding energy 4.17 eV higher than the Ru 3d_{5/2} peak and lies underneath the aliphatic C 1s component (E_B = 285.0 eV). Other peaks observed in both films include CF₃ (E_B = 293.3 eV), CF₂ (E_B = 291.6 eV), both associated with Nafion, C=O (E_B = 289.6 eV), C-O (E_B = 287.6 eV) associated with Nafion and PPy and C-N (E_B = 286.0 eV) associated with PPy and Ru(bpy)₃²⁺. These peak assignments are consistent with those previously reported.³¹ The aromatic C 1s component (E_B = 284.6 eV) is associated with both PPy and Ru(bpy)₃²⁺ and was fitted by taking into account the contributions expected from both species.

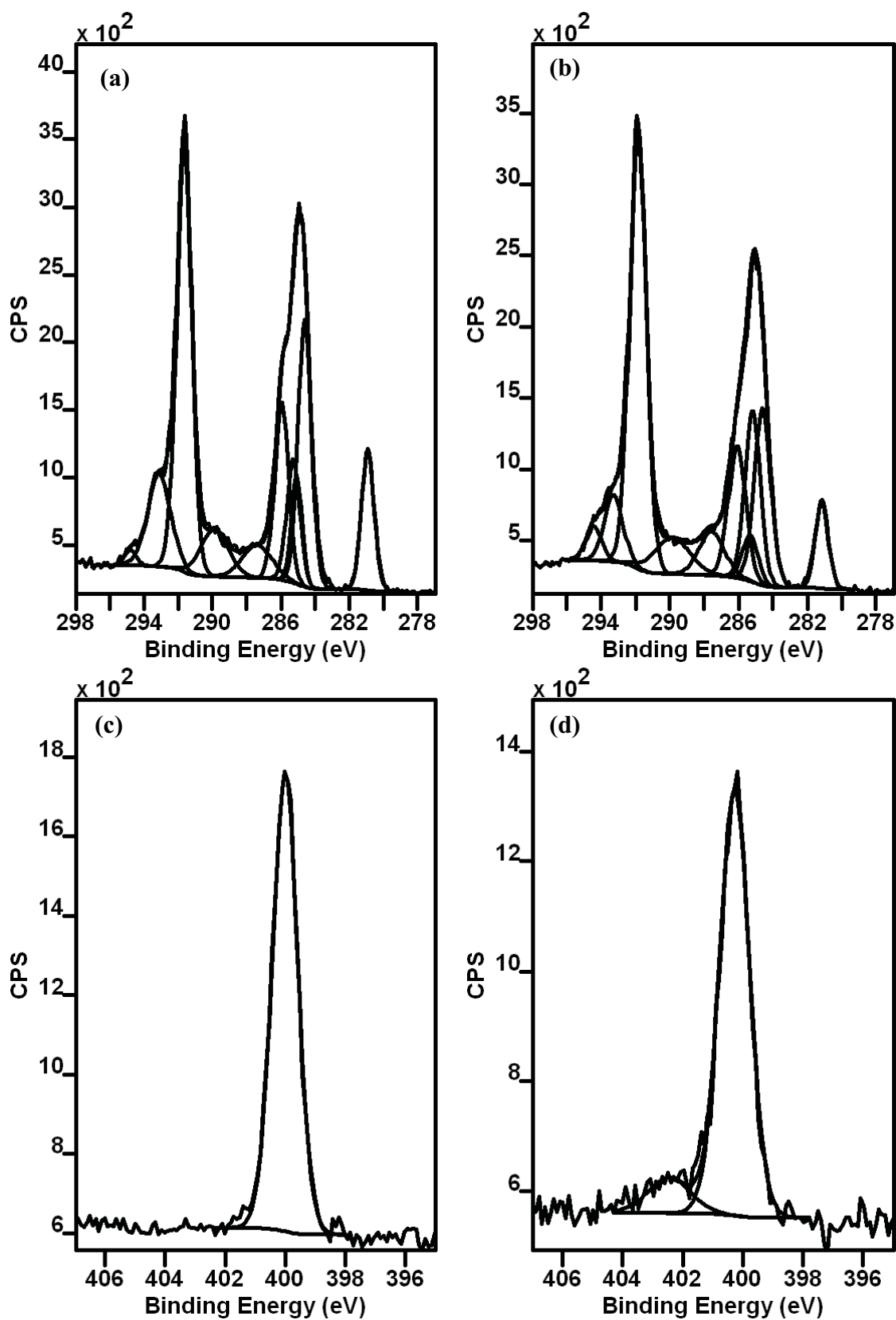


Figure 4-5: Comparison of high resolution C 1s and Ru 3d XPS spectra for Nf/Ru (a) and Nf/Ru/PPy (b) films. High resolution N 1s XPS spectra of Nf/Ru (c) and Nf/Ru/PPy (d) films are also compared. Tables 4-2 and 4-3 provide peak assignments and quantification of this data.

Element	Component	Binding Energy (eV)	Nf/Ru Film		Nf/Ru/PPy Film	
			Atomic %	Normalised to Ru 3d	Atomic %	Normalised to Ru 3d
F 1s	C-F	688.8	45.0	112.5	47.3	175.6
O 1s	CF-O-CF	535.2	3.5	7.9	2.6	9.8
	C=O	532.2	0.7	1.6	0.6	2.1
	C-O-C	533.3	0.1	0.2	0.1	0.3
	-SO ₃ ⁻	531.4	3.7	8.5	3.0	11.3
N 1s	N ⁺	402.1	0.0	0.0	0.3	1.0
	-NH-	400.0	2.9	6.5	2.3	8.7
C 1s	-CF ₃	294.6	0.4	0.8	0.4	1.3
	CF ₃ -CFO, CF ₂ O	293.3	4.8	11.0	2.8	10.4
	-CF ₂	291.6	14.8	33.6	16.2	60.2
	-C=O	289.6	3.0	6.7	2.7	10.4
	-C-O	287.6	2.2	5.0	2.5	9.2
	-C-N	286.0	5.7	12.9	5.2	19.1
	-C-C	285.0	3.3	7.5	6.1	22.5
	Aromatic carbon	284.6	8.5	19.4	6.6	24.5
S 2p _{3/2}	-SO ₃ ⁻	167.8	0.9	2.1	0.8	3.0
Ru 3d _{5/2}	Ru ²⁺	280.9	0.4	1.0	0.3	1.0

Table 4-2: Comparison of XPS % atomic concentration for Nf/Ru and Nf/Ru/PPy films. Components have been normalised to Ru 3d intensity.

The N 1s region spectra for both films include a component at 400.0 eV, consistent with the bipyridine ligand in Ru(bpy)₃²⁺. However, in Fig. 4-5(d) a weak contribution from a higher binding energy component (402.1 eV) is observed and is assigned as N⁺ from the cationic form of PPy³² confirming the presence of PPy in the layer. The presence of PPy at the film surface is further supported by the increase in the ratios of C-N : Ru (10.6 to 19.1), N : Ru (6.5 to 8.7) and aromatic carbon : Ru (15.9 to 24.5) in the Nf/Ru/PPy film, which is expected due to the structure of the pyrrole monomer as shown in Figure 4-6. These changes are greater than the uncertainties assigned to the XPS data and therefore statistically significant.

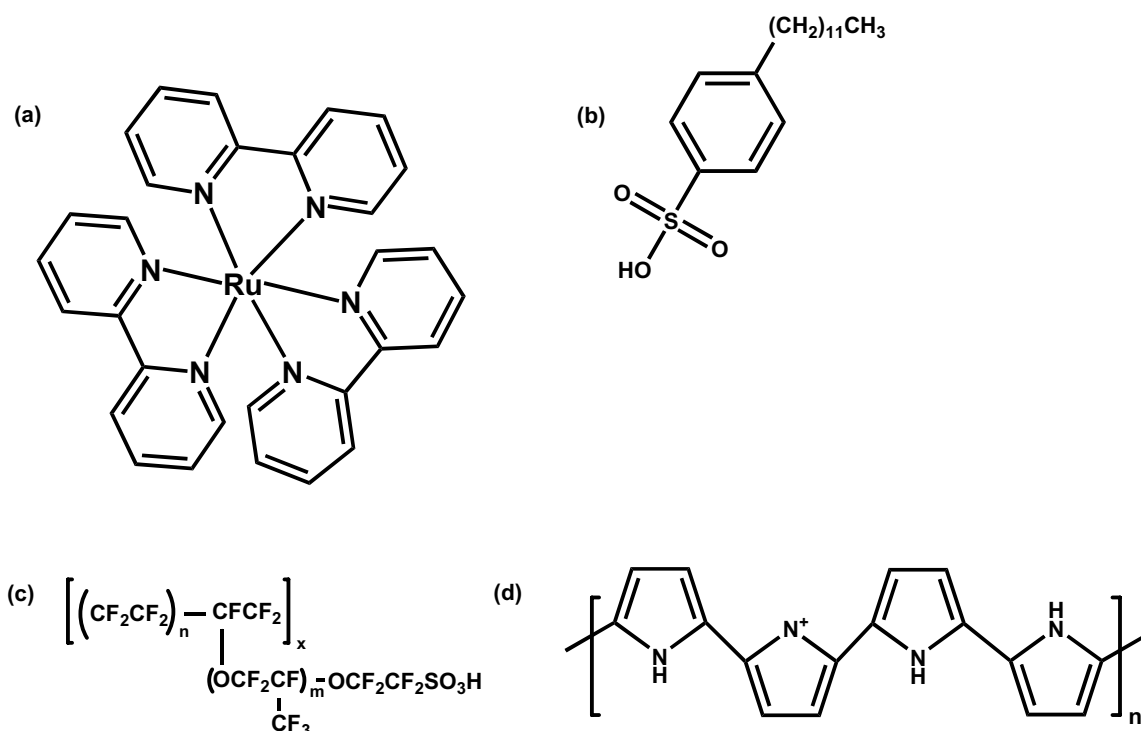


Figure 4-6: The structures of (a) Ru(bpy)₃²⁺, (b) DBSA, and (c) Nafion and (d) Cationic Polypyrrole.

The surface composition of the films was determined by first normalising the XPS components to the Ru 3d peak, and then subtracting the expected contributions from the Ru(bpy)₃²⁺ (as determined from the N : Ru ratio) to account for the nitrogen and carbon present in the complex. This correction was performed on the N 1s region spectra and C-N and aromatic components of the C 1s spectra. The adjusted ratios are presented in Table 4-3 and allow for a direct comparison between the concentrations of pyrrole monomer, Ru(bpy)₃²⁺ and SO₃⁻ sites in each film.

Component	Binding Energy (eV)	Ratio of Component _{corrected} :Ru Nf/Ru/ Film	Ratio of Component _{corrected} :Ru Nf/Ru/PPy Film
N ⁺	402.1	0.0	1.0
-NH-	400.0	0.5	2.7
-C-N	286.0	0.9	7.1
Aromatic carbon	284.5	1.4	6.5

Table 4-3: XPS components from Table 4-2 with ratios corrected for contributions due to Ru(bpy)₃²⁺.

The surface composition of the films may be further explored by considering these corrected atomic ratios in conjunction with the empirical structures of the PPy ([C₄H₃N]_n)

and Nafion. The structure of Nafion consists of a poly(tetrafluoroethene) backbone with sulfonic acid functionalised side chains, thus the Ru : S ratio provides a ratio of $\text{Ru}(\text{bpy})_3^{2+}$ to SO_3^- sites present in the Nafion. In the Nf/Ru films the Ru : S ratio is 1 to 2.1, which corresponds to the stoichiometric ratio expected from the formal charges assigned to the $\text{Ru}(\text{bpy})_3^{2+}$, and thus suggests that the $\text{Ru}(\text{bpy})_3^{2+}$ is electrostatically bound to the Nafion. The Ru : S ratio for the Nf/Ru/PPy, in contrast, is 1 : 3.0 and this result is attributed to the combined electrostatic binding of the PPy to the SO_3^- sites present in the Nafion. If the electrostatic binding of $\text{Ru}(\text{bpy})_3^{2+}$ to the Nafion (Ru : S ratio of 1 : 2) is considered, the remaining sulfur component provides an indication of the relative concentration of PPy present at the surface. In the Nf/Ru/PPy film, the S : N ratio when adjusted for the binding of $\text{Ru}(\text{bpy})_3^{2+}$ into the Nafion (by subtracting the two SO_3^- equivalents bound to the $\text{Ru}(\text{bpy})_3^{2+}$), is 1 to 3.7 suggesting that there are 3.7 pyrrole monomers present in the film for every SO_3^- group. These results also indicate that in the Nf/Ru/PPy film the PPy is electrostatically attached to the Nafion, and are consistent with previous studies of PPy doped with large docdeylbenzenesulfonic acid (DBSA) surfactant compounds.²² XPS analysis of the Nf/Ru/PPy films indicates that the surface composition comprises approximately one $\text{Ru}(\text{bpy})_3^{2+}$ complex for every 3.0 SO_3^- groups and 3.7 pyrrole monomer units. This result is in agreement with the electrochemical measurements ($\text{Ru}(\text{bpy})_3 : \text{pyrrole} \approx 1 : 4.5$) presented herein.

Figures 4-7a and 4-7b show the positive and negative static secondary ion mass spectra respectively, obtained from the surface of the Nf/Ru/PPy layer. Spectra for Nafion and Nf/Ru films are presented in Appendix I (Figures I-1 and I-2). The data confirms the presence of $\text{Ru}(\text{bpy})_3^{2+}$ in both the Nf/Ru and Nf/Ru/PPy layers with characteristic peaks present at m/z 96, 98-102, and 104, corresponding to the isotope pattern of ruthenium. In addition, clusters of peaks are observed at m/z 570, 414, and 258 corresponding to the

complete $\text{Ru}(\text{bpy})_3^{2+}$ molecular ion and its fragmentation products after the loss of successive bipyridine groups; other significant peaks are indicated in Figures 4-7a and 4-7b.

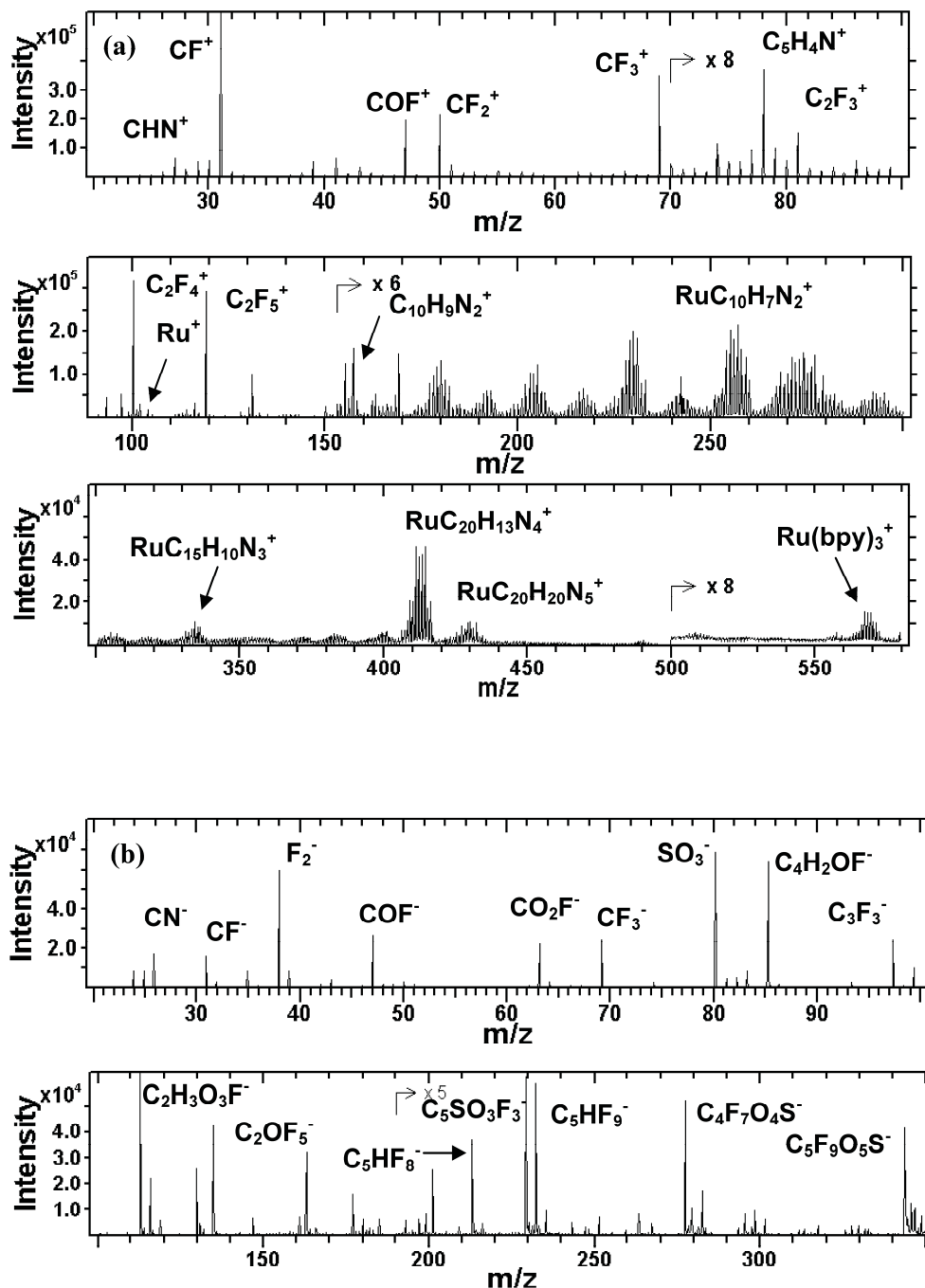


Figure 4-7: Positive (a) and negative (b) ion ToF-SIMS spectra for the Nf/Ru/PPy layer. Relevant high intensity mass fragments are labelled.

The presence of PPy in the layer is difficult to determine definitively via ToF-SIMS as the ionisation process results in changes in the polymer. However, several minor peaks

corresponding to oligomeric fragments of PPy were detected, including $C_4H_4N^+$ ($m/z = 66$), $C_8H_7N_2^+$ ($m/z = 131$) and $C_{12}H_7N_3^+$ ($m/z = 193$). In addition, nitrogen-containing fragments, including CN^- ($m/z = 26$), CH_2N^+ ($m/z = 28$) and $C_2H_3N^+$ ($m/z = 41$), that are often associated with pyrrole,³³⁻³⁵ were detected. These may also be associated with the bipyridine ligands of $Ru(bpy)_3^{2+}$.

Previous ToF-SIMS studies of doped PPy have detected mass fragments consistent with the dopant.^{34,35} In the present study, the Nf/Ru/PPy layers are formed in the presence of Nafion and DBSA, both with the potential to dope the electropolymerised PPy. Figure 4-6b shows a range of significant peaks consistent with Nafion as expected. However, the well-defined mass fragmentation pattern of DBSA³⁶ is not observed. DBSA was chosen as the supporting electrolyte in the electropolymerisation step because diffusion of this large anion into the layer is inhibited, ensuring that Nafion remains the primary dopant for the PPy. The results presented in Figure 4-6(b) confirm that DBSA does not play a role in the doping of the PPy and as such the PPy present is exclusively associated with the Nafion ionomer.

AFM images of both the Nf/Ru and Nf/Ru/PPy films were acquired to assess any morphological differences between the films. Typical images of each film are presented in Figure 4-8. The images indicate no change in morphology on incorporation of PPy into the film. Both types of film exhibited roughness not exceeding 15 nm. Often the electrodeposition of pyrrole results in a rough nodular surface stemming from the nucleation of PPy on the surface.^{22,37} The absence of this roughness suggests that the PPy nucleation takes place within the Nafion network, or directly at the electrode surface. Further, the presence of PPy at the surface, as detected by XPS, indicates that the PPy network propagates from the bulk to the surface of the film.

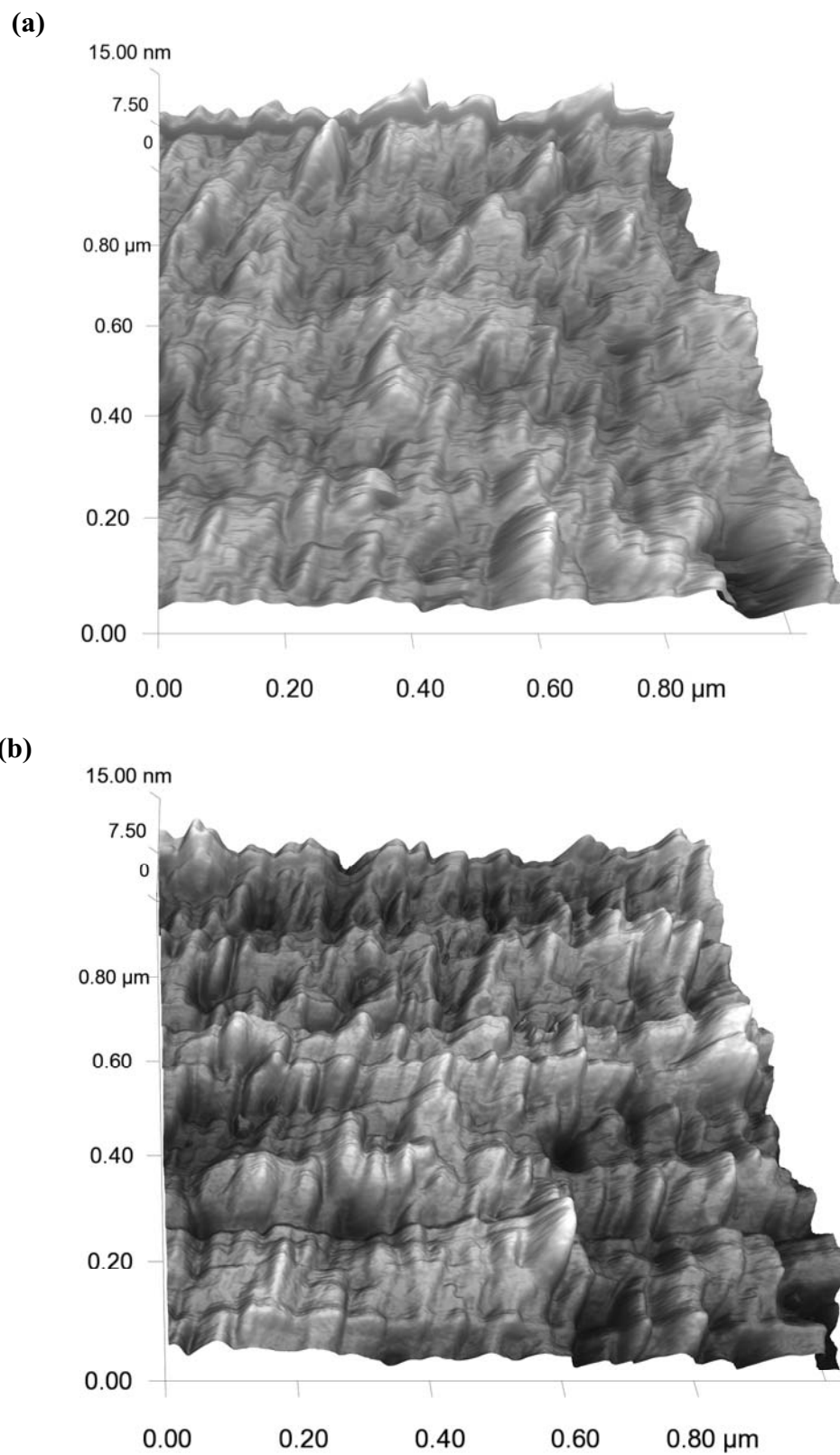


Figure 4-8: AFM images of Nf/Ru (a) and Nf/Ru/PPy (b) films. No significant changes in morphology can be observed. A DLC modified PPP-NCHR tip was used.

4.2.5. ECL Response

The application of an oxidising potential to electrodes coated with Nf/Ru/PPy films in the presence of suitable co-reactants resulted in an ECL emission which was similar to the corresponding Nf/Ru layers both in intensity and in wavelength ($\lambda_{\text{max}} = 610 \text{ nm}$). The ECL response was investigated using cyclic voltammetry with the addition of oxalate and tripropylamine as model analytes. The layer was found to be sensitive to both analytes and a typical cyclic voltammogram with simultaneously detected ECL emission in the presence of sodium oxalate is shown in Figure 4-9 (the response of the Nf/Ru/PPy layer to tripropylamine is shown in Figure I-3). The response from the Nf/Ru film is shown in Figure 4-10 for comparison. The voltammetric response in both cases is consistent with an electrochemical reaction in which the analyte oxidation is mediated by $\text{Ru}(\text{bpy})_3^{3+}$. Specifically, the anodic peak during the forward sweep is enhanced relative to the response in the absence of analyte (also shown), whereas the cathodic peak current is diminished. Figure 4-9 also shows that in both cases the emission of light is coincident with the generation of $\text{Ru}(\text{bpy})_3^{3+}$ within the layer. Since virtually no light is emitted in the absence of the analyte, this indicates that the excited state $[\text{Ru}(\text{bpy})_3^{2+}]^*$ is created during the cross reaction with the analyte.

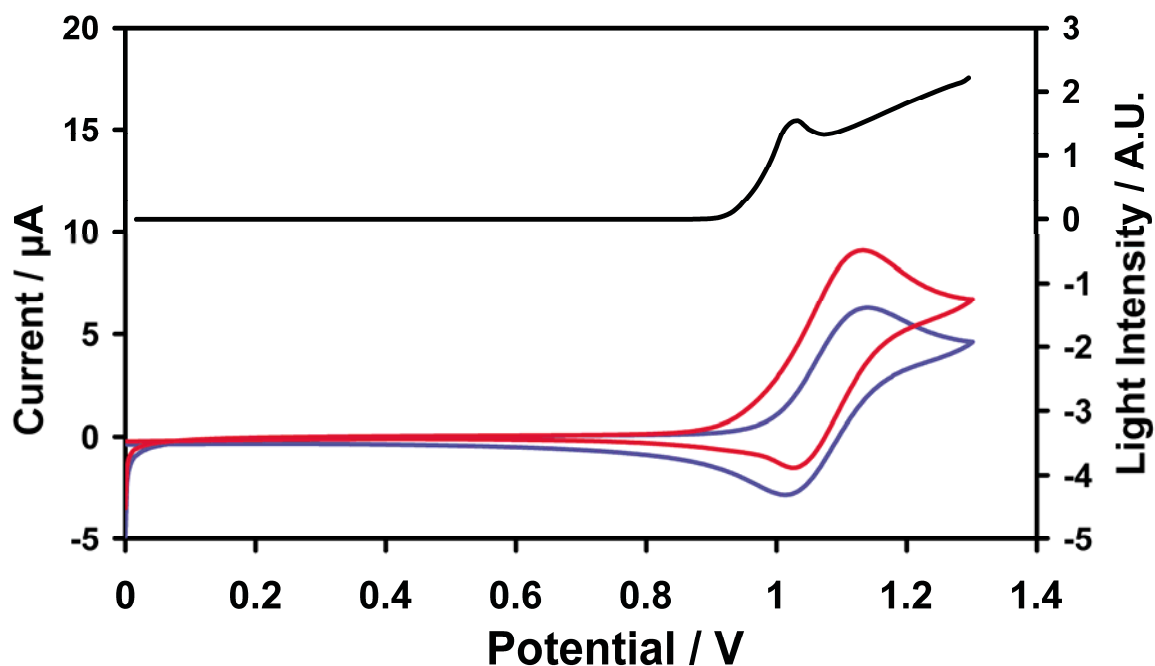


Figure 4-9: Typical voltammetric (red line) and light emission (upper trace) response of a Nf/Ru/PPy film in aqueous solutions containing 50 mM sodium oxalate and 0.2 M Na_2SO_4 electrolyte. Voltammograms of solutions without oxalate are shown for comparison (blue line). The scan rate was 10 mV s^{-1} .

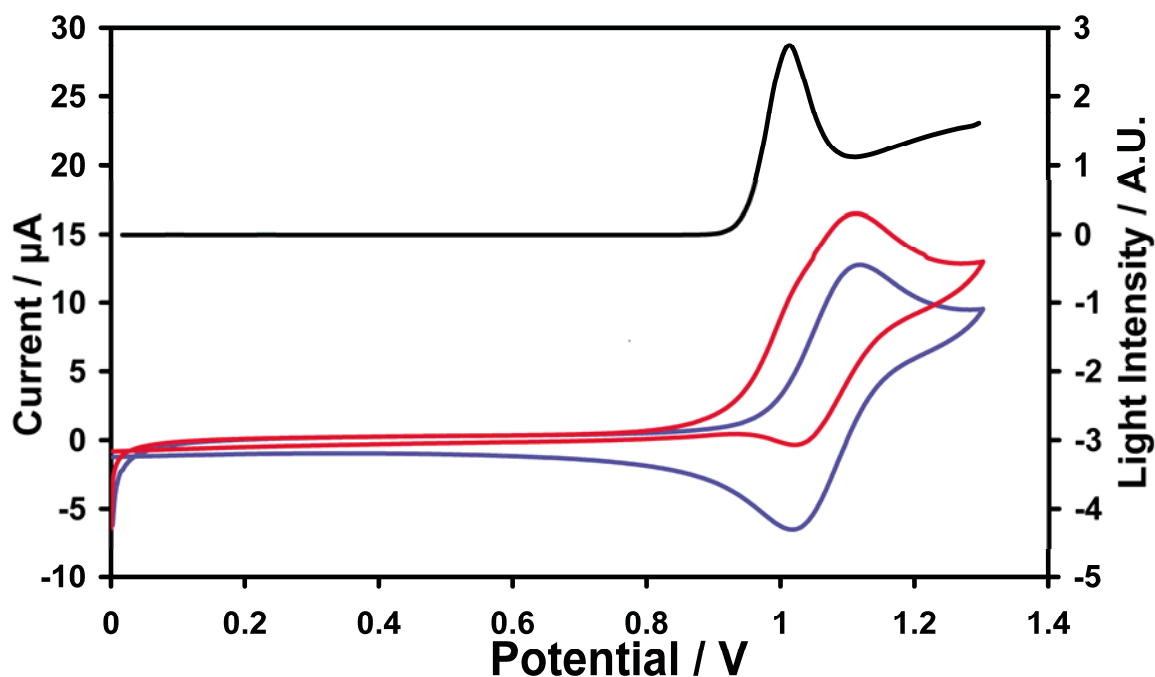


Figure 4-10: Typical voltammetric (red line) and light emission (upper trace) response of a Nf/Ru film in aqueous solutions containing 50 mM sodium oxalate and 0.2 M Na_2SO_4 electrolyte. Voltammograms of solutions without oxalate are shown for comparison (blue line). The scan rate was 10 mV s^{-1} .

A decrease in ECL signal is observed from the Nf/Ru/PPy film when compared to the Nf/Ru films; this may be attributed to the difference in the charge transport characteristics of the films or differences in the rate of transport of analyte within the layer. The limits of detection (signal-to-noise ratio = 3) for the Nf/Ru/PPy film in the absence of acetonitrile were found to be 10 μM and 100 nM for oxalate and tripropylamine respectively. This difference in detection limits between the two analytes is expected due to the greater efficiency of tripropylamine in generating the excited state.³⁸ The system exhibited a linear response for oxalate concentrations (Figure 4-11) in the range of 100 μM to 100 mM and tripropylamine concentrations (see Figure I-4) in the range of 100 nM to 1 mM. The use of a 5 % acetonitrile solution improves the detection limit by an order of magnitude, providing detection limits of 1 μM and 10 nM, respectively. This decrease in detection limits, observed alongside an increase in peak current, suggests that the improved sensitivity is due to the acetonitrile allowing more facile access and congress of charge compensating counterions by solvating the hydrophobic and interstitial regions of the Nafion. The limits of detection achieved are comparable to those achieved by Downy and Neiman with Nf/Ru films, who reported detection limits of 1 μM and 10 nM for oxalate and tripropylamine in flowing streams.¹²

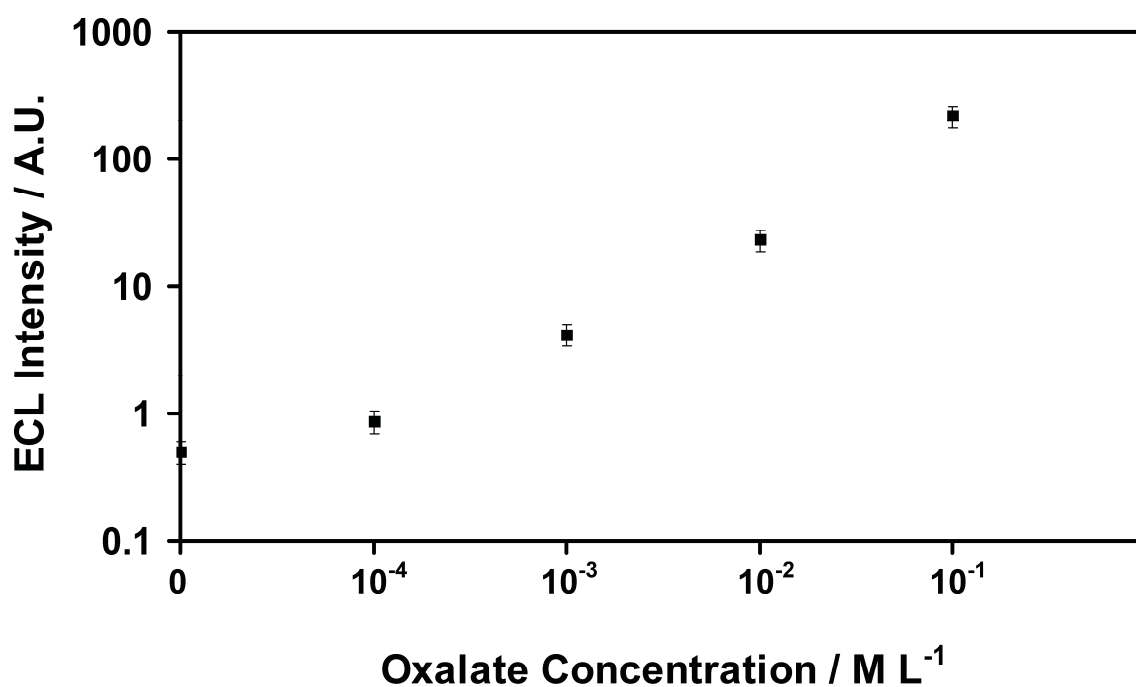


Figure 4-11: Dependence of ECL intensity on the concentration of the model analyte sodium oxalate for a Nf/Ru/PPy modified electrode. The error bars represent the maximum difference in response for three measurements.

4.2.6. Layer Stability

The stability of the Nf/Ru/PPy films to electrochemical cycling was investigated and compared with Nf/Ru films. Both film types were continuously scanned in electrolyte with oxidative peak currents ($I_{p,ox}$) measured with respect to time. All films remained macroscopically stable for the duration of the experiment, with no delamination or cracking occurring. $Ru(bpy)_3^{2+}$ was not detectable in the contacting electrolyte by UV-VIS absorption or luminescence spectroscopy at the end of these experiments, even when a small volume ($< 1 \text{ cm}^3$) electrochemical cell was used. This suggests that rather than being lost from the layer, the ruthenium complex partitions into inaccessible regions of the film with time. Films were investigated in two solvent systems: an aqueous 0.2 M Na_2SO_4 solution and a 95:5 mix by volume of 0.2 M Na_2SO_4 aqueous solution and acetonitrile. In both instances, Nf/Ru/PPy films showed an enhanced stability over Nf/Ru films. In the aqueous solution a useful lifetime (a decrease to 90 % of maximum electrochemical signal) of 7 hrs may be observed for the Nf/Ru/PPy films, whereas the

useful lifetime of the Nf/Ru films tested was 4.5 hrs, an increase of over 50 % (see Figure I-5). Bard et. al. have previously observed a 5 % decrease after 1.5 hrs and a 16 % decrease after 6.6 hrs for Nf/Ru films,¹⁰ and this is consistent with the results presented here.

As shown in Figure 4-12, when scanned in the solution containing acetonitrile, the useful lifetime of Nf/Ru/PPy and Nf/Ru films were shortened considerably, to 135 min and 108 min, respectively. This reduction in lifetime results from the partial solvation of the film in the presence of acetonitrile, which may accelerate the transport of $\text{Ru}(\text{bpy})_3^{2+}$ into the electrochemically inaccessible regions of the Nafion associated with the fluorocarbon backbone. These results are consistent with the results of Vining and Meyer, where the addition of organic solvent enhances the rate of exchange between the various regions within the Nafion film.¹³

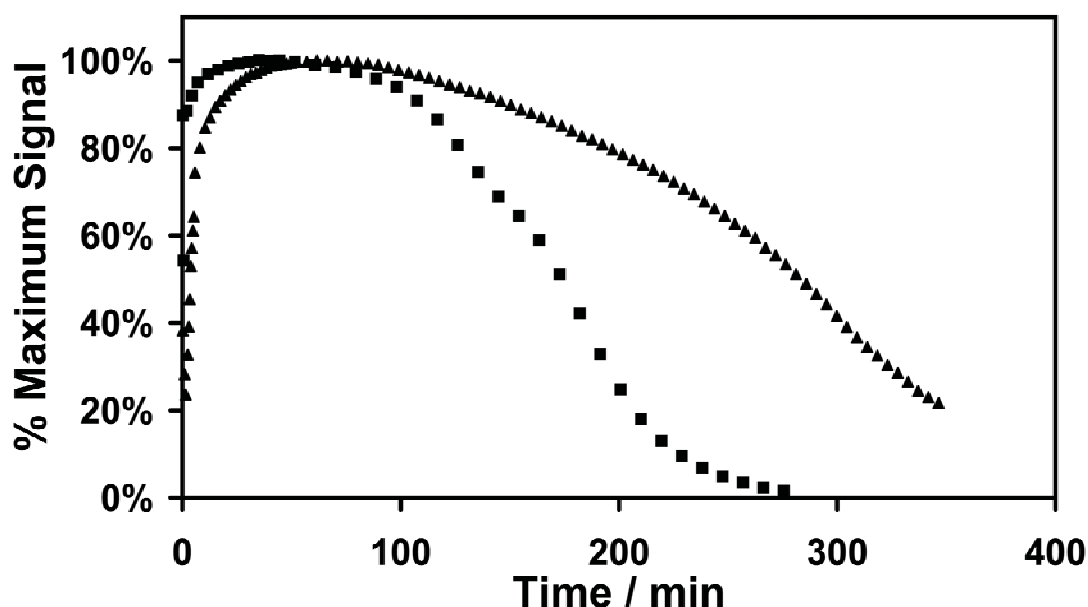


Figure 4-12: Comparative response of Nf/Ru (■) and Nf/Ru/PPy (▲) films mean oxidative peak currents over time in 95:5 0.2 M Na_2SO_4 /Acetonitrile. Films were continuously scanned at between 0.6 V and 1.5 V at a scan rate of 100 mV s^{-1} .

The structure of Nafion is believed to resemble that of a reversed micelle,³⁹⁻⁴¹ consisting of a porous assembly of hydrophilic ion clusters connected by ion channels. The observed

increase in stability of Nf/Ru/PPy over Nf/Ru may be due to the formation of an interpenetrating network of PPy within the Nafion film that partially blocks the ion channels and in so doing impedes the transport of the $\text{Ru}(\text{bpy})_3^{2+}$ from the ion clusters into the hydrophobic and interstitial regions of the Nafion film. Also the increase in the time taken to initially reach 90 % of the maximum electrochemical signal (break-in time), as observed in Figure 4-12, provides further evidence for the PPy existing in the interstitial regions of the Nafion film.

The change in 'break-in' time (4 min for Nf/Ru and 15 min for Nf/Ru/PPy) may be due to the PPy impeding the transport of solvent and electrolyte into the layer by blocking the ion channels and interstitial regions in the Nafion. While the lifetimes of the films are shortened with the use of acetonitrile, the addition of PPy provides a compensating extension in film lifetime of 24 %.

The proposed stabilisation mechanism provided by the PPy contrasts to the mechanism suggested with other Nafion composites described previously. Literature suggests that the improvement is due to the composite co-material (nanotubes, organic silicates, etc.) providing a stronger hydrophobic interaction with the $\text{Ru}(\text{bpy})_3^{2+}$ than that of the surrounding Nafion. This stronger interaction hinders the migration of the $\text{Ru}(\text{bpy})_3^{2+}$ into the electrochemically inaccessible regions of the Nafion.¹⁵⁻¹⁷ In contrast, the addition of PPy is thought to stabilise the $\text{Ru}(\text{bpy})_3^{2+}$ within the film by physically impeding its migration to the more hydrophobic and hence electrochemically inaccessible regions of the Nafion film.

4.3. Conclusions

The use of Nafion/PPy composites for the immobilisation of $\text{Ru}(\text{bpy})_3^{2+}$ at a working electrode has been shown to be effective in producing stable films for use in an ECL-based sensor. Surface characterisation of the film correlates well to electrochemical measurements and suggests that the PPy present is distributed homogeneously within the layer. ToF-SIMS studies demonstrate that PPy is exclusively doped with the Nafion ionomer.

Although the presence of PPy impedes charge transport through the layer ($D_{\text{CT}} = 1.13 \times 10^{-9} \text{ cm}^2 \text{ s}^{-1}$ for Nf/Ru c.f. $6.22 \times 10^{-10} \text{ cm}^2 \text{ s}^{-1}$ for Nf/Ru/PPy), it also appears to slow the rate of transport of $\text{Ru}(\text{bpy})_3^{2+}$ into the electrochemically inaccessible, hydrophobic regions of the film. This provides an improvement to the usable lifetime of the film when compared to the use of pure Nafion films. In aqueous solution, the Nf/Ru/PPy film has been shown to be stable to electrochemical cycling for 7 hrs, which is an improvement of 50 % over the pure Nafion-based film. In the presence of acetonitrile, this stability is somewhat reduced; however, the addition of acetonitrile provides an improvement in the ECL sensitivity by an order of magnitude, resulting in the detection of oxalate to a concentration of 1 μM and tripropylamine to a concentration of 10 nM.

4.4. References

- (1) Miller, C. J.; McCord, P.; Bard, A. J.; *Langmuir* **1991**, *7*, 2781-2787.
- (2) Zhang, X.; Bard, A. J.; *J. Phys. Chem.* **1988**, *92*, 5566-5569.
- (3) Bertonecello, P.; Dennany, L.; Forster, R. J.; Unwin, P. R.; *Anal. Chem.* **2007**, *79*, 7549-7553.
- (4) Wang, H.; Xu, G.; Dong, S.; *Talanta* **2001**, *55*, 61-67.
- (5) Obeng, Y. S.; Bard, A. J.; *Langmuir* **1991**, *7*, 195-201.
- (6) Sato, Y.; Uosaki, K.; *J. Electroanal. Chem.* **1995**, *384*, 57-66.
- (7) Ghosh, P.; Spiro, T. G.; *J. Electroanal. Chem.* **1981**, *128*, 1281-1287.
- (8) Bertonecello, P.; Kefalas, E. T.; Pikramenou, Z.; Unwin, P. R.; Forster, R. J.; *J. Phys. Chem. B* **2006**, *110*, 10063-10069.
- (9) Zanarini, S.; Rampazzo, E.; Bich, D.; Canteri, R.; Ciana, L. D.; Marcaccio, M.; Marzocchi, E.; Panciatichi, C.; Pederzoli, C.; Paolucci, F.; Prodi, L.; Vanzetti, L.; *J. Phys. Chem. C* **2008**, *112*, 2949-2957.
- (10) Rubinstein, I.; Bard, A. J.; *J. Am. Chem. Soc.* **1980**, *102*, 6641-6642.
- (11) Martin, A. F.; Nieman, T. A.; *Biosens. Bioelectron.* **1997**, *12*, 479-489.
- (12) Downey, T. M.; Nieman, T. A.; *Anal. Chem.* **1992**, *64*, 261-268.
- (13) Vining, W. J.; Meyer, T. J.; *J. Electroanal. Chem.* **1987**, *237*, 191-208.
- (14) Gorman, B. A.; Francis, P. S.; Barnett, N. W.; *The Analyst* **2006**, *131*, 1-24.
- (15) Shi, L. H.; Liu, X. Q.; Li, H. J.; Xu, G. B.; *Anal. Chem.* **2006**, *78*, 7330-7334.
- (16) Choi, H. N.; Lee, J.-Y.; Lyu, Y.-K.; Lee, W. Y.; *Anal. Chim. Acta.* **2006**, *565*, 48-55.
- (17) Song, H.; Zhang, Z.; Wang, F.; *Electroanal.* **2006**, *18*, 1838-1841.
- (18) Mailley, P.; Cosnier, S.; Coche-Guerente; *Anal. Lett.* **2000**, *33*, 1733-1753.
- (19) Liu, Y.-C.; Hwang, B.-J.; Hsu, W.-C.; *Sensor Actuat B-Chem* **2002**, *87*, 304-308.
- (20) Rubinstein, I.; Bard, A. J.; *J. Am. Chem. Soc.* **1981**, *103*, 5007-5013.

- (21) E.M. Genies; G. Bidan; A. F. Diaz; *J. Electroanal. Chem.* **1983**, *149*, 101-113.
- (22) Prissanaroon, W.; Brack, N.; Pigram, P. J.; Liesegang, J.; Cardwell, T.; *Surf. Interface Anal.* **2002**, *33*, 653-662.
- (23) Otero, T. F.; Tejada, R.; Elola, A. S.; *Polymer* **1987**, *28*, 651-658.
- (24) Bidan, G.; Ehui, B.; Lapkowski, M.; *J. Phys. D: Appl. Phys.* **1988**, *21*, 1043-1054.
- (25) Fan, F.-R. F.; Bard, A. J.; *J. Electrochem. Soc.* **1986**, *133*, 301-304.
- (26) Jensen, M. H.; Osvath, P.; Sargeson, A. M.; Ulstrup, J.; *J. Electroanal. Chem.* **1994**, *377*, 131-141.
- (27) White, H. S.; Leddy, J.; Bard, A. J.; *J. Am. Chem. Soc.* **1982**, *104*, 4811-4817.
- (28) Joo, P.; Chambers, Q.; *J. Electrochem. Soc.* **1985**, *132*, 1345-1349.
- (29) Dempirova, L.; Adamcova, X.; *Collection of Czechoslovak Chem. Comm.* **1989**, *54*, 3154-3161.
- (30) Martin, C. R.; Rubinstein, I.; Bard, A. J.; *J. Am. Chem. Soc.* **1982**, *104*, 4817-4824.
- (31) Susac, D.; Kono, M.; Wong, K. C.; Mitchell, K. A. R.; *App. Surf. Sci.* **2001**, *174*, 43-50.
- (32) Kupila, E.-L.; Lukkari, J.; Kankare, J.; *Synth. Met.* **1995**, *74*, 207-215.
- (33) Perruchot, C.; Chehimi, M. M.; Delamar, M.; Eccles, J. A.; Steele, T. A.; Mair, C. D.; *Synth. Met.* **2000**, *113*, 53-63.
- (34) Abel, M. L.; Leadley, S. R.; Brown, A. M.; Petitjean, J.; Chehimi, M. M.; Watts, J. F.; *Synth. Met.* **1994**, *66*, 85-88.
- (35) Grunden, B.; Iroh, J. O.; *Polymer* **1995**, *36*, 559-563.
- (36) Prissanaroon, W.; Brack, N.; Pigram, P. J.; Liesegang, J.; *Synth. Met.* **2004**, *142*, 25-34.
- (37) Su, W.; Iroh, J. O.; *Synth. Met.* **1998**, *95*, 159-167.

- (38) Miao, W.; Choi, J.-P. In *Electrogenerated Chemiluminescence*; Bard, A. J., Ed.; Marcel Dekker, Inc.: New York, 2004.
- (39) Lee, P. C.; Meisel, D.; *J. Am. Chem. Soc.* **1980**, *102*, 5477-5481.
- (40) Eisenberg, A.; Hird, B.; Moore, R. B.; *Macromolecules* **1990**, *23*, 4098-4107.
- (41) Hsu, W. Y.; Gierke, T. D.; *J. Membr. Sci.* **1983**, *13*, 307-326.

Chapter 5: Covalently bound ECL active films - a two-step approach

5.1. Introduction

An alternative approach to the use of polymer films for the immobilisation of ECL active complexes is the covalent attachment of an ECL active complex to the surface. As described in Chapter 2, a number of covalent attachment methods for ECL active complexes have previously been investigated including those based on surfactants,^{1,2} alkanethiols,^{3,4} silane and epoxy chemistries.⁵

The electroreduction of aryl diazonium salts has previously been used for the construction of amperometric sensors for a variety of analytes.⁶⁻⁸ In this chapter, a two-step approach to immobilisation of an ECL active ruthenium complex is investigated. The initial step involves the electrodeposition of the ligand, para-diazonium-4'-phenyl-2,2'-bipyridine tetrafluoroborate (referred to as dpb), via the electroreduction of the diazonium. After the deposition of dpb, the complex was assembled on the electrode by complexation with Ru(bpy)₂Cl₂. The layer was characterised at each stage using CV, EQCM, AFM, XPS and ToF-SIMS.

5.2. Results and Discussion

The synthesis and deposition methods used to create the films described in this section are discussed in Section 3.1.2.1.

5.2.1. Phenyl-bipyridine Layer Deposition

Glassy carbon (GC) electrodes were modified via the electrochemical reduction of dpb in an acetonitrile solution containing 3 mM dpb and 0.1 M TBAPF₆ as the supporting electrolyte. The cyclic voltammogram obtained from the deposition solution is presented in Figure 5-1a. Two broad cathodic peaks are observed in the initial scan, at -0.2 V and -1.0 V. In subsequent scans the peak at -0.2 V is not observed, whereas the reductive peak at -1.0 V shifts to more negative potentials (-1.35 V). A similar situation is also observed at a gold electrode (Figure 5-1b), with peaks initially being observed at -0.3 V and -0.9 V. In subsequent scans, the peak at -0.3 V is not present while the peak at -0.9 V shifts to more negative potentials. Also observed in the second sweep is a peak at -1.5 V that shifts to a more negative potential (-1.7 V) on the third sweep.

With most aryl diazoniums, a single reduction peak in the CV is observed,⁹⁻¹¹ which correlates to a one-electron reduction of the diazonium and the resulting attachment to the substrate. The diazonium reduction typically occurs at or near 0 V,^{11,12} although for diazotized ruthenium complexes this reduction potential can exist as low as -1.17 V.¹³ In some cases multiple reduction peaks have been reported for diazoniums on a range of substrates¹⁴⁻¹⁹ including gold,¹⁵ and have been attributed to the slight difference in work function associated with each crystalline face of the substrate present at the surface.¹⁵

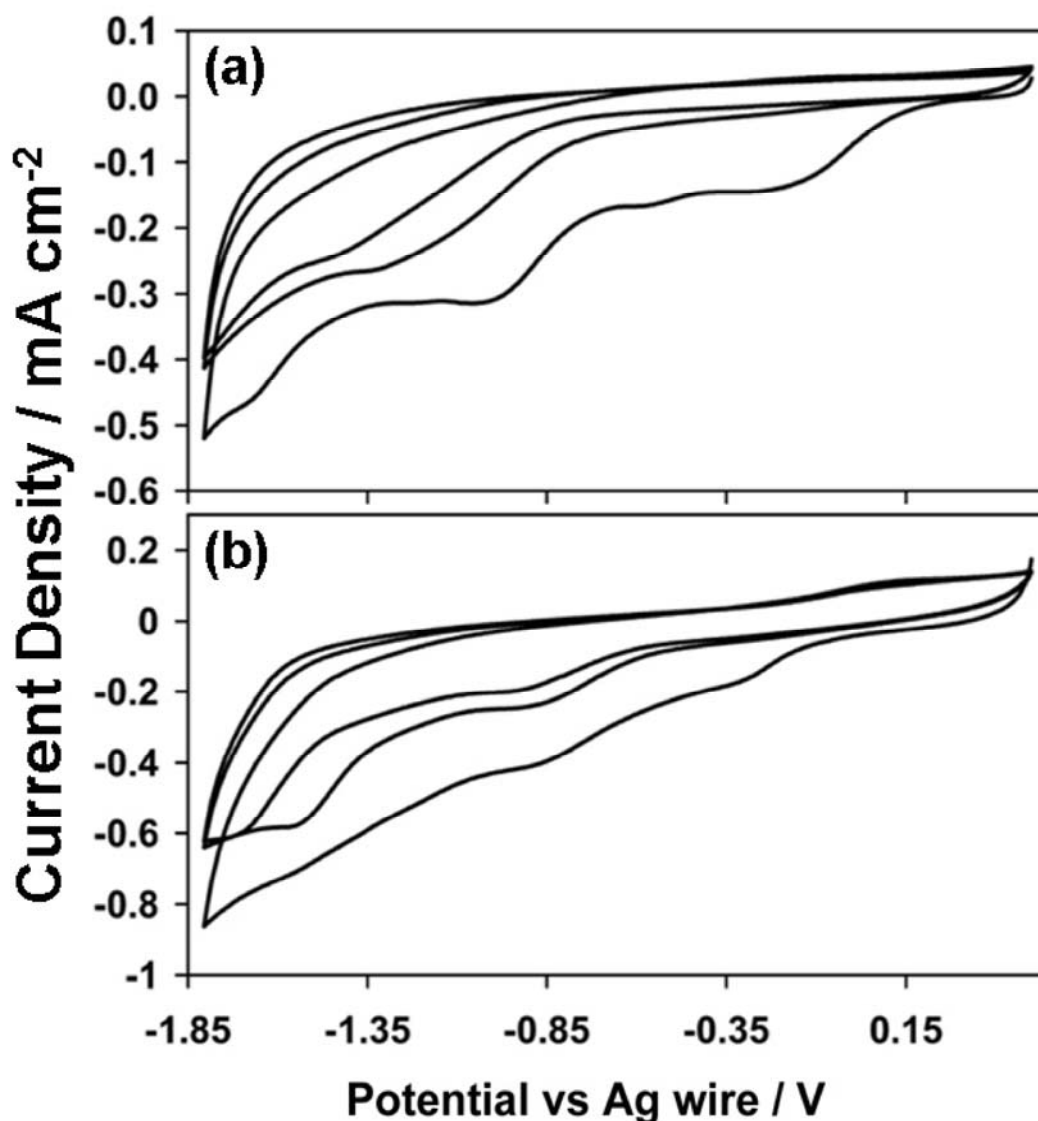


Figure 5-1: The electroreduction of dpb onto glassy carbon (a) and gold (b) substrates from acetonitrile. Scan rate was 100 mV s^{-1} .

To assist in determining which reduction was responsible for the attachment of dpb to the surface, EQCM experiments were undertaken. Figure 5-2 shows the electrodeposition of dpb onto a gold electrode and the associated change in mass with applied potential. The mass increase prior to -0.6 V may be associated with the spontaneous deposition of the diazonium as observed previously in other systems.^{20,21} To minimise the influence of spontaneous deposition on the experiment, the CV was undertaken promptly and without degassing. By not degassing the solution the cathodic peaks described in Figure 5-1b are masked and broadened, however the peak previously described at -0.9 V is still observed. The total mass deposited at the gold substrate after 3 scans is $4.2 \times 10^{-7} \text{ g}$ and is the

equivalent to a surface coverage of 9.5×10^{-9} mol cm⁻². The number of monolayers that this coverage correlates with may be determined by assuming that 50 % of the dpb reductions result in the loss of N₂ in accordance with the results from Section 5.2.2.2 and the dpb is packed in a close-packed manner (calculated monolayer surface coverage of 6.9×10^{-10} mol cm⁻²). This calculation suggests a film thickness that is equivalent to 12.4 monolayers. The result demonstrates the presence of a multilayered system where the diazonium is bound not only to the substrate but also to the previously deposited dpb.

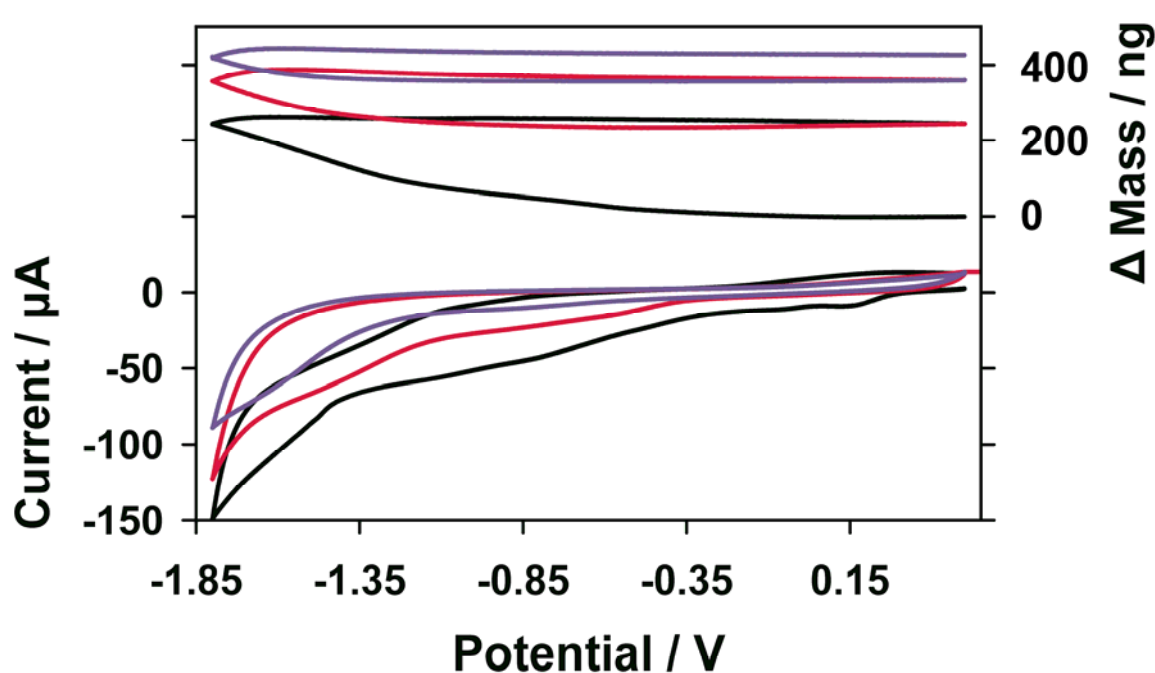


Figure 5-2: EQCM cyclic voltammogram and associated mass-potential curve for the deposition of dpb onto a gold electrode. The potential was swept between 0.5 V to -1.8 V in acetonitrile at a scan rate was 100 mV s^{-1} . The 1st scan is the black line, the 2nd scan is red and the 3rd scan is blue.

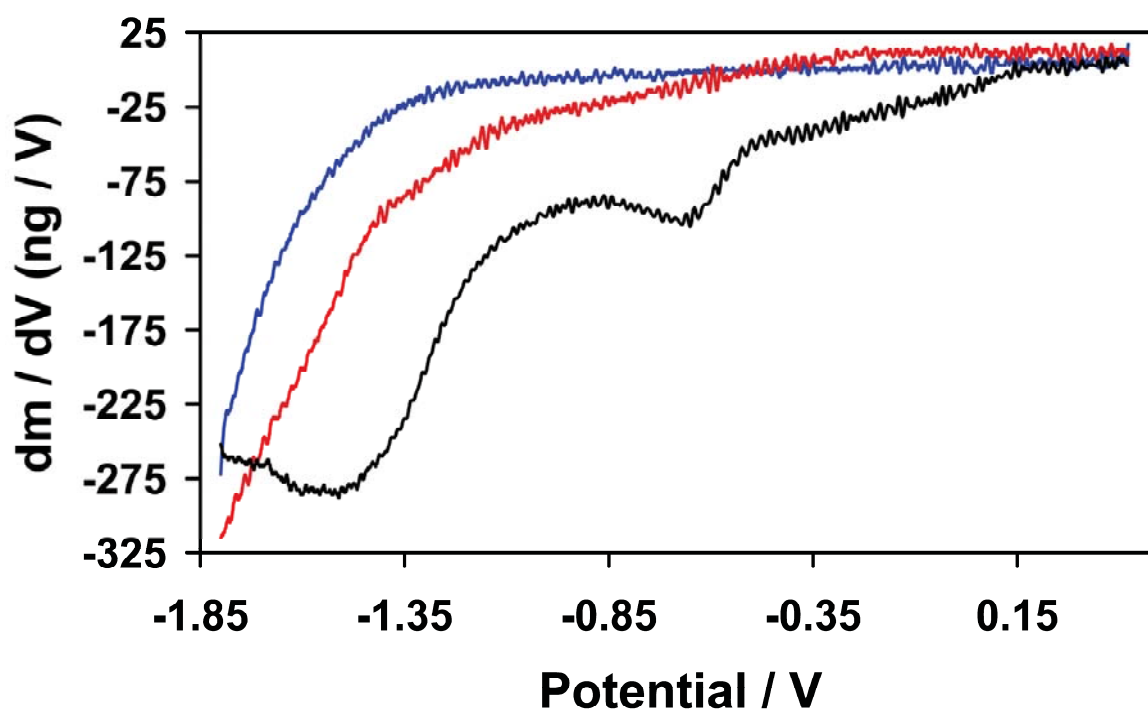
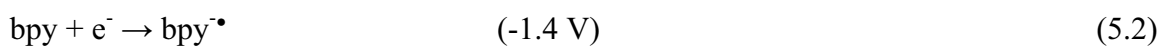
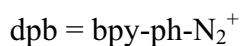


Figure 5-3: Rate of mass deposition with respect to potential. For clarity, only forward scans (0.5 V to -1.8 V) are presented. The 1st scan is the black line, the 2nd scan is red and the 3rd scan is blue.

The rate of mass deposition observed varies with applied potential (Figure 5-3) and provides a clearer understanding of the deposition process. In Figure 5-3 two distinct peaks are observed, at -0.65 V and -1.4 V. The position of the peaks correlate well to the onset of the voltammetric peaks observed in Figure 5-1b, and demonstrate that each reduction results in attachment of dpb to the electrode. Immediately following each peak in Figure 5-3 the rate of mass transfer decreases, demonstrating that each peak is related to a process that is diffusion-limited during the scan. Interestingly, a second larger peak in the deposition rate is observed at -1.45 V which corresponds to the reduction of the bipyridine moiety. It is hypothesised that the deposition of the diazonium at this more negative potential may be attributed to the mediated reduction of the diazonium by the bipyridine already deposited on the surface (or by freely diffusing bipyridine).



According to equations 5.1 and 5.2 above, the reaction between the bipyridine radical anion and the diazonium is thermodynamically favorable with a free energy (ΔG) of -0.75 eV.

The faradaic efficiency of the deposition process (moles of diazonium deposited per mole of electrons) can also be determined from Figure 5-3, and varies with the applied potential, reaching a maximum efficiency of 0.11 at a potential of -1.6 V. This low faradaic efficiency has been previously observed for other bulky diazoniums when deposited on gold such as 4-diethylanilinediazonium⁹ with the remaining portion of diazonium radicals formed reacting with each other in solution.

5.2.1.1. AFM of dpb Layers

To determine the layer thickness and morphology of dpb deposited on the substrate, AFM imaging and scratching experiments were conducted on glassy carbon substrates. Figure 5-4a and 5-4b show typical AFM images of dpb deposited onto glassy carbon, and a polished glassy carbon substrate for comparison. As a result of polishing, clean glassy carbon substrates have track marks up to 10 nm deep present on the surface. In comparison, substrates deposited with dpb (Figure 5-4) show a clear smoothing of the surface resulting from the filling in of scratch marks which leaves only the deepest marks

visible. Under these deposition conditions no nucleation sites are observed at the surface of the film resulting in a homogeneous coverage.

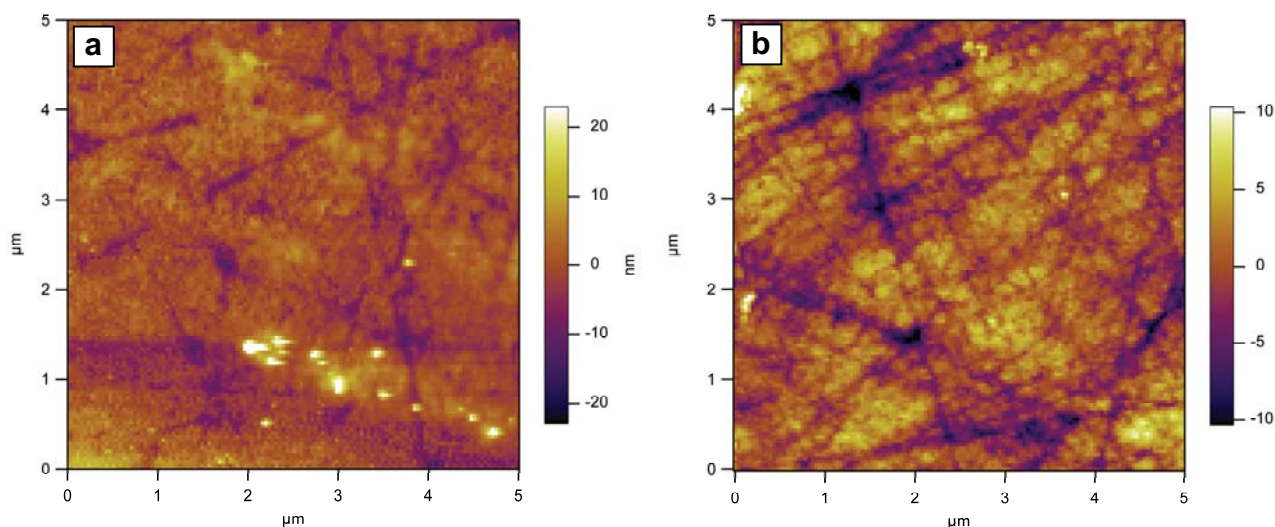


Figure 5-4: AFM image dpb deposited onto a glassy carbon substrate (a). A blank substrate is shown for comparison (b). A PPP-NCHR tip was used for imaging.

To determine film thickness scratching experiments were undertaken, as described in Section 3.2.3.3. After imaging in dynamic mode, a section of the surface was scratched using contact mode with a high set point (4 V or ~ 17 μN of applied force), prior to the re-imaging in dynamic mode. Due to the possibility of removing some of the substrate during these experiments only glassy carbon substrates were used due to their previously demonstrated resistance to scratching from a silicon nitride tip.²² Figure 5-5a presents a typical result of dpb scratched from the surface of glassy carbon. The average height profile over the scratched area is shown in Figure 5-5b. The height profile in Figure 5-5b shows an average difference in height between the two regions of 6 nm.

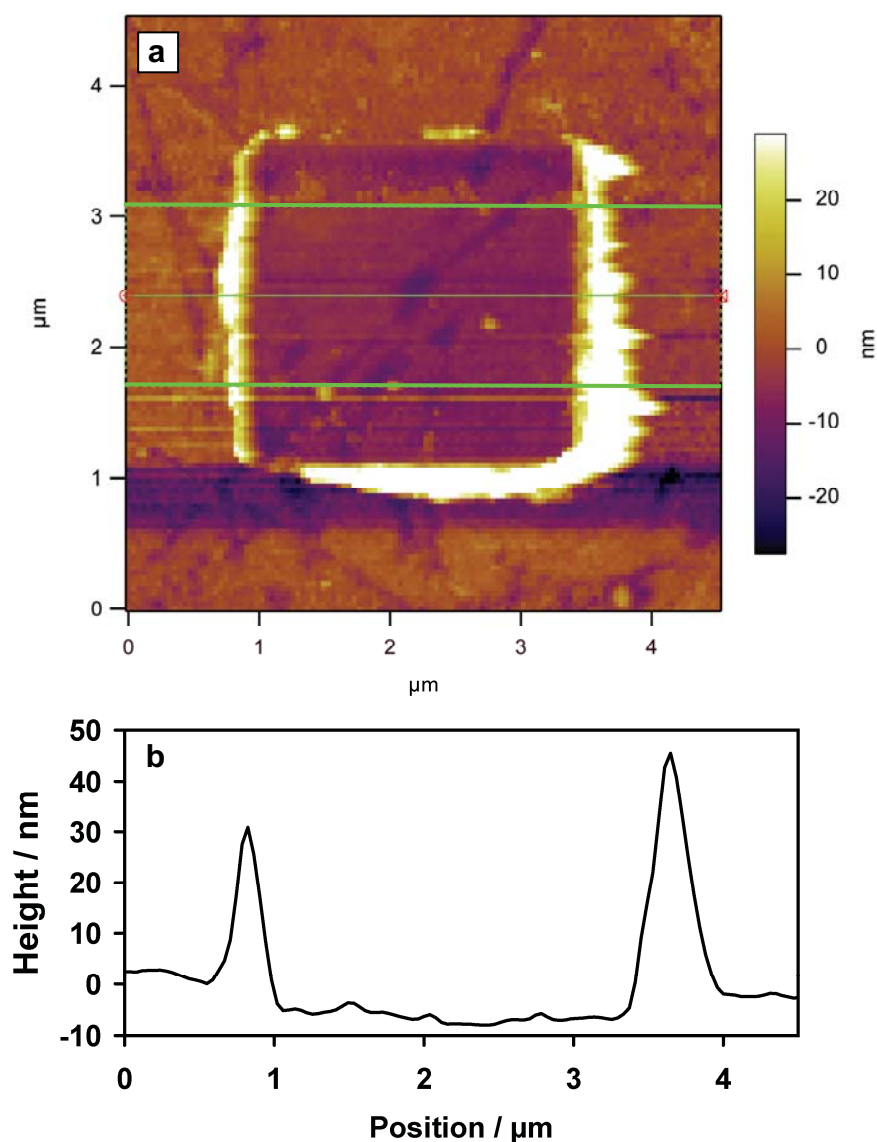


Figure 5-5: Typical scratched surface of a dpb coated glassy carbon substrate (a). The average cross section, within the area defined by the green lines, is shown below in (b) with an average dpb film thickness of 6 nm.

To confirm that the exposed surface was glassy carbon, force curves prior to and after scratching were taken, with typical results displayed in Figure 5-6. Prior to scratching (Figure 5-6a), a clear hysteresis is observed between the forward and return curves, indicating a compressible surface capable of undergoing large scale plastic deformation.²³ After scratching (Figure 5-6b) this hysteresis is no longer observed. This lack of hysteresis shows that the underlying surface is much harder than the deposited layer suggesting that the freshly exposed surface is the glassy carbon substrate. Figure 5-6b is

also consistent with force curves acquired on sections of glassy carbon where the dpb ligand was not deposited.

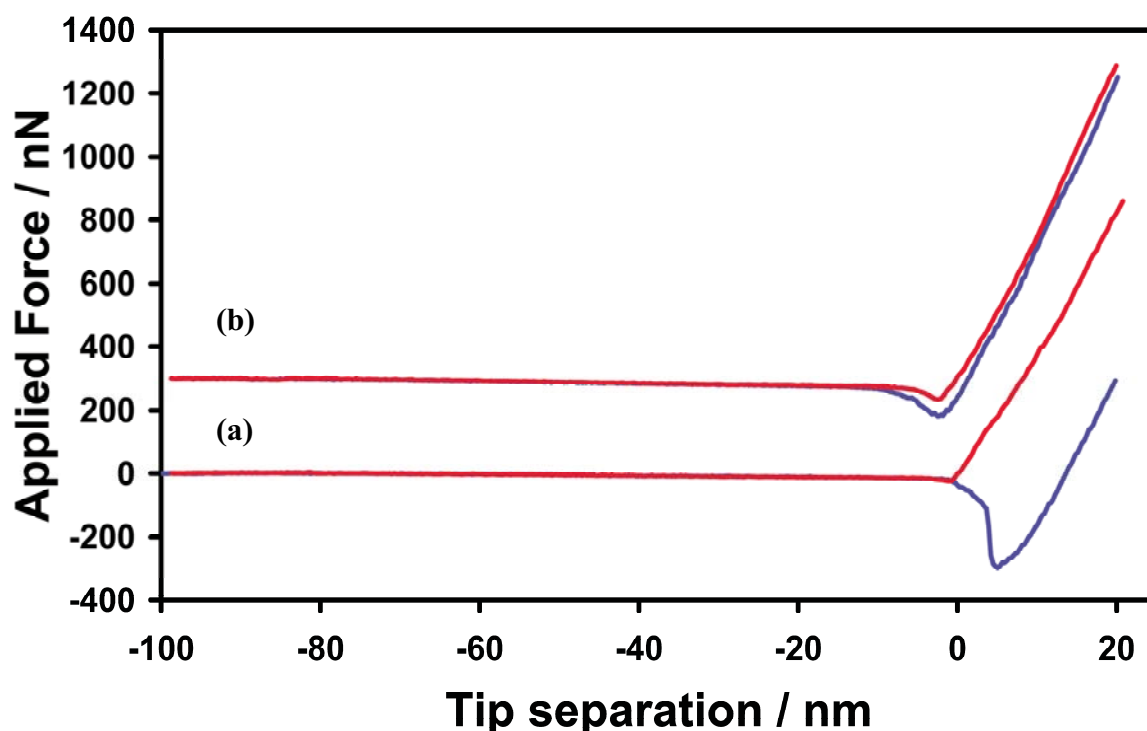


Figure 5-6: Force curves for the dpb surface (a), and the exposed glassy carbon substrate (b). Tip extension (red) and retraction (blue) are shown in both cases. For clarity, the glassy carbon force curve is offset by 300 nN.

5.2.2. dpb Layer Characterisation

5.2.2.1. Electrochemical Characterisation of dpb Layers

Cyclic voltammograms of the layer deposited onto both glassy carbon and gold substrates are presented in Figure 5-7. On both substrates, the reduction of the bipyridyl ligand is observed ($E_p = -1.5$ V for GC and -1.1 V for Au). The Gaussian shape of these peaks (after background subtraction) suggests complete reduction of the surface-immobilised material and that the layer is indeed surface-confined. On glassy carbon this peak is irreversible and degrades into two components ($E_p = -1.7$ V and -1.25 V) by the second scan; the peak on the gold substrate ($E_p = -1.1$ V) is reversible. The electrochemistry of the bipyridyl ligand is known to vary significantly depending on its environment. For example, bipyridyl absorbed onto Au(111) surfaces can undergo a reversible

electrochemistry at -0.3 V (v.s. Ag/AgCl),²⁴ however, when bound in a metal complex such as Ru(bpy)₃²⁺ this reduction shifts to -1.1 V (v.s. Ag/Ag⁺).²⁵

The surface confined nature of these peaks enables a determination of the electroactive surface coverage area present after deposition. On glassy carbon, this electroactive surface coverage is 9.2×10^{-10} mol cm⁻² while on gold a lower figure of 4.5×10^{-10} mol cm⁻² is obtained. A close-packed monolayer has a theoretical coverage of 6.9×10^{-10} mol cm⁻². On both gold and glassy carbon electrodes the amount of bipyridyl that is reduced during the CV is significantly less than the surface coverage determined by the EQCM measurements (9.5×10^{-9} mol cm⁻²), suggesting that the layer is not uniformly electrochemically accessible.

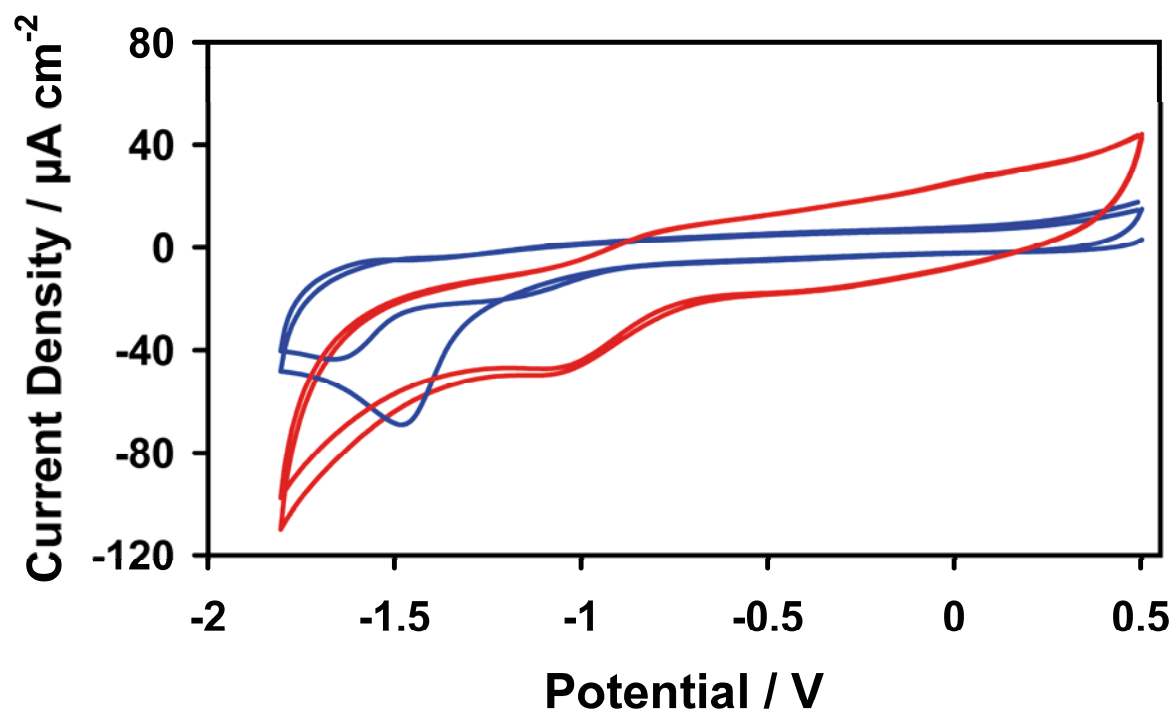


Figure 5-7: The anodic electrochemistry of 3 mm diameter glassy carbon (blue) and 2 mm diameter gold (red) electrodes modified with dpb. The electrode was tested in acetonitrile with a TBAPF₆ electrolyte, scan rate was 100 mV s^{-1} .

5.2.2.2. XPS Analysis of dpb Layers

To confirm the electrochemical and AFM results, the complementary techniques of XPS and ToF-SIMS were used to determine the chemical structure of the deposited dpb film. Figure 5-8 presents XPS survey spectra of glassy carbon discs before (Figure 5-8a) and after (Figure 5-8b) the electrochemical deposition of dpb. In both spectra, a strong C 1s photoelectron peak is observed at a binding energy of 284.0 eV, in addition an O 1s photoelectron peak is observed ($E_B = 533.0$ eV) corresponding to a partially oxidised surface that is often associated with glassy carbon substrates.^{26,27} Trace amounts of nitrogen ($E_B = 400.0$ eV) and silicon (Si 2p $E_B = 102.0$ eV) were observed on the blank glassy carbon discs which are attributed to the manufacturing process used.^{26,28} After the deposition of dpb, two distinct changes are observed in the survey spectrum: the appearance of fluorine and an increase in the nitrogen signal. Low levels of sodium, sulfur and zinc are also observed at the surface after deposition. The appearance of the F 1s photoelectron peak ($E_B = 686.0$ eV) is due to residual electrolyte, tetrabutylammonium hexafluorophosphate (TBAPF₆), being present on the surface. The increase in the N 1s signal is associated with the nitrogen present in both dpb and TBAPF₆ as the nitrogen to fluorine ratio is higher than expected from TBAPF₆ alone (N : F would be 1 : 6 for TBAPF₆, c.f. an observed ratio of 15.9 : 1), confirming the presence of dpb on the surface.

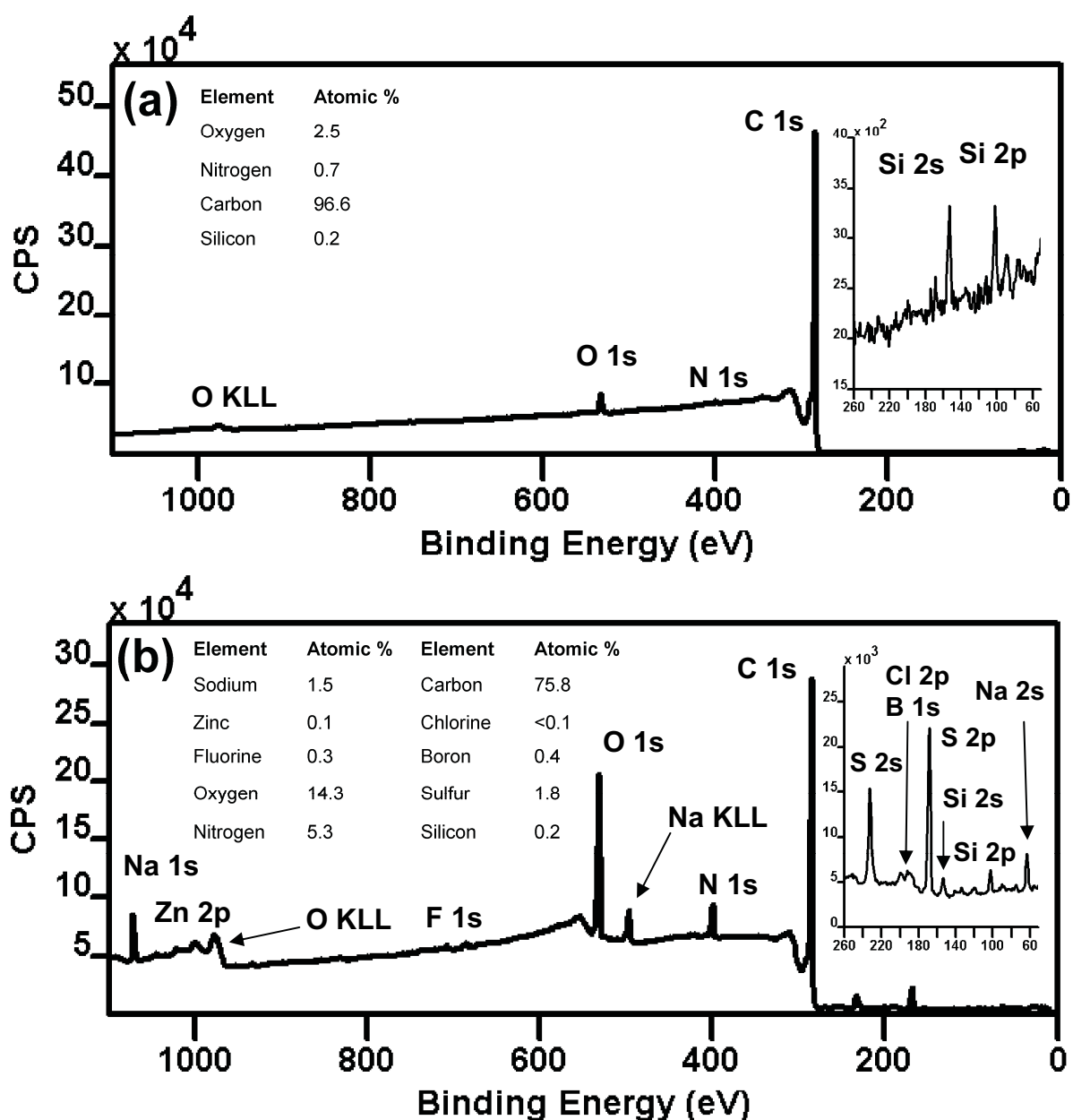


Figure 5-8: XPS survey spectra of a glassy carbon substrate before (a) and after the deposition of dpb (b). Relevant photoelectron and Auger lines are labelled.

To determine the nature of the bonding of dpb to the substrate, high resolution XPS spectra of the C 1s and N 1s photoelectron regions of dpb attached to glassy carbon and gold were investigated and are presented in Figures 5-9 and 5-10. Table 5-1 provides a comparison between the relative concentrations of the layer components as atomic percent. In addition to the C 1s and N 1s results presented in Figures 5-9 and 5-10, the analysis of high resolution photoelectron regions reveals the presence of fluorine, oxygen, chlorine, sulfur and zinc components, with the binding energies and relative

concentrations of these species also presented in Table 5-1. The fluorine component ($E_B = 686.0$ eV for GC) is from both the BF_4^- anion associated with the starting material (boron $E_B = 189.0$ eV for GC) and the PF_6^- anion in the electrolyte TBAPF₆ used during deposition, however the associated phosphorus is not observed, possibly due to its concentration being below the limit of detection for the technique. The oxygen observed at the surface ($E_B = 532.2$ eV for GC and 532.6 eV for Au) is expected to be due to surface oxides present on the substrate. The chlorine, sulfur, sodium and zinc components present are possibly caused by impurities in the starting materials or possible surface contamination during either layer deposition or sample transfer. The binding energies of the chlorine ($E_B = 199.6$ eV for Cl 2p_{3/2} on GC) and sulfur ($E_B = 168.3$ eV for S 2p_{3/2} on GC) components suggest that these elements may exist as anions (Cl^- and SO_4^{2-}) electrostatically attached to the film.²⁹

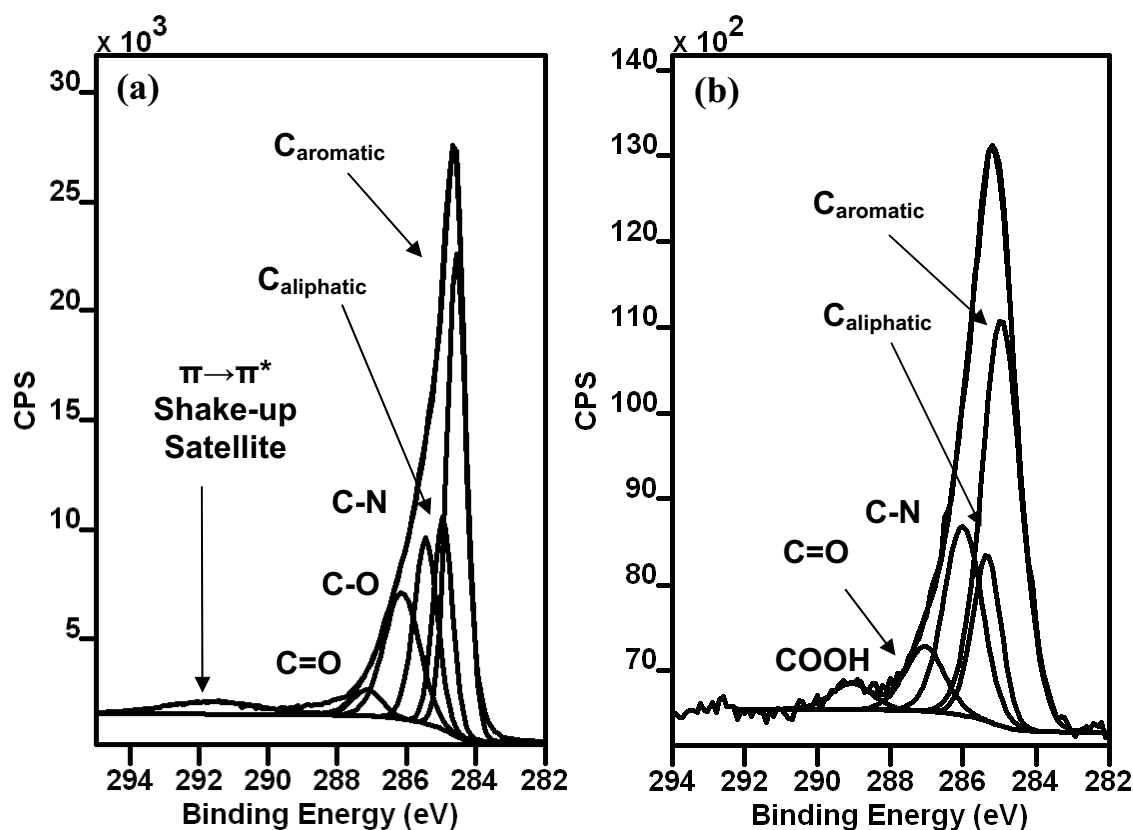


Figure 5-9: C 1s photoelectron region spectra for dpb deposited onto glassy carbon (a), and gold, (b), substrates.

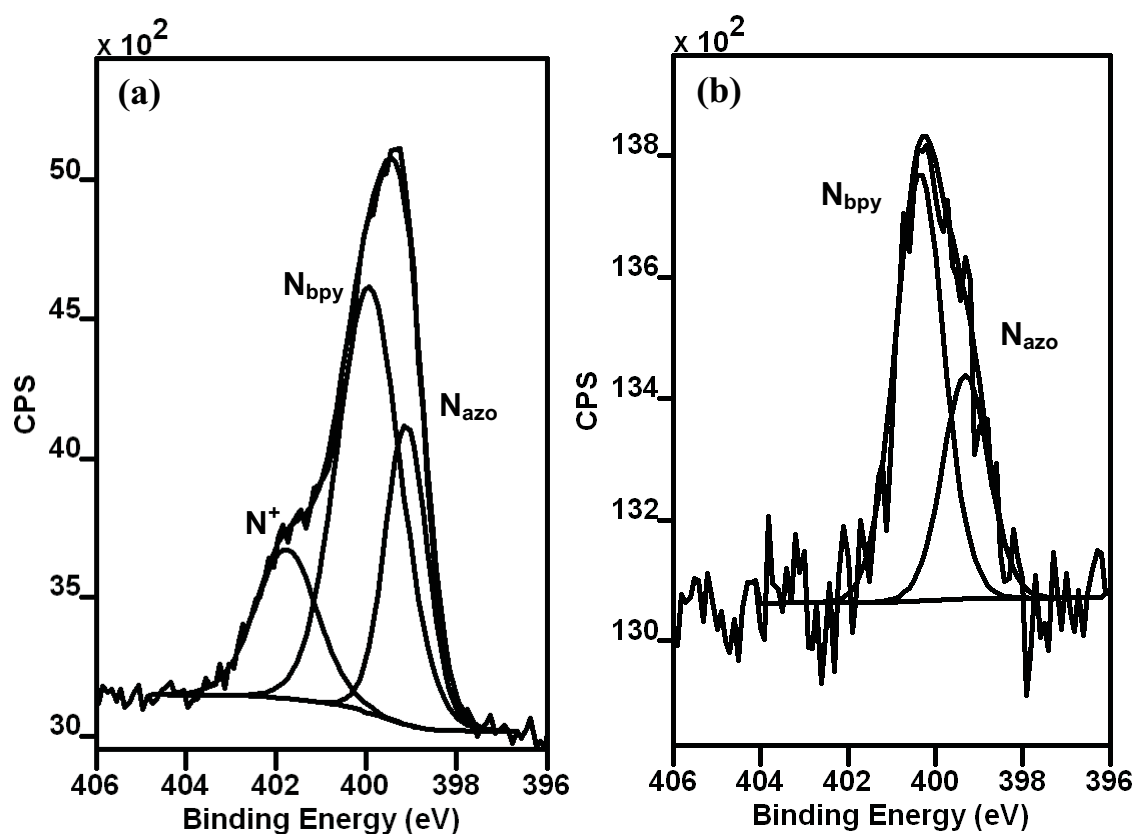


Figure 5-10: N 1s photoelectron region spectra for dpb deposited onto glassy carbon (a), and gold (b), substrates.

Element	Component	Binding Energy (eV)		Concentration (Atomic %)	
		GC	Au	GC	Au
Na 1s	Na ⁺	1071.0	ND	1.5	ND
Zn 2p _{3/2}	Zn ⁰	1021.5	1021.8	0.1	0.3
F 1s	BF ₄ ⁻ , PF ₆ ⁻	686.0	ND	0.3	ND
O 1s	Oxides	532.2	532.6	14.3	19.8
N 1s	N ⁺	401.8	ND	1.0	ND
	N _{bpy}	399.9	400.4	2.9	2.8
	N _{azo}	399.1	399.3	1.4	1.4
C 1s	π→π* Satellite	291.6	ND	3.7	ND
	-COOH	ND	289.1	ND	1.4
	-C=O	287.4	287.1	2.1	5.3
	-C-O	286.4	ND	9.0	ND
	-C-N	285.4	286.0	22.0	14.3
	-C-C	285.0	285.3	4.3	9.4
	Aromatic carbon	284.6	284.9	34.7	32.4
Cl 2p _{3/2}	Cl ⁻	199.6	ND	<0.1	ND
B 1s	BF ₄ ⁻	189.0	ND	0.4*	ND
S 2p _{3/2}	SO ₄ ²⁻	168.3	ND	1.8	ND
Si 2p	SiO ₂	102.0	ND	0.4	ND
Au 4f _{7/2}	Au ⁰	N/A	84.0	N/A	12.9
Al 2p _{3/2}	Al ₂ O ₃	74.6	ND	<0.1	ND

Table 5-1: XPS components of a dpb film on both GC and Au substrates. ND = Not Detected. The B 1s peak is broad and may contain contributions from other elements such as phosphorus and iodine.

Figure 5-9 shows the C 1s photoelectron region for dpb deposited on both glassy carbon and gold. The spectra appear similar with peaks observed for the aromatic carbon ($E_B = 284.6$ eV for GC and 284.9 eV both Au) and C-N bonds ($E_B = 285.4$ eV for GC and 286.0 eV for Au) from the dpb. The difference in binding energy between these components is a result of dpb on Au sample being charge corrected to the Au 4f_{7/2} ($E_B = 84.0$ eV) photoelectron line. The peak intensities of these components were fitted to match the concentration of nitrogen observed from the N 1s photoelectron line. In addition to components expected from the deposition of dpb, components associated with surface oxides and adventitious carbons are observed. These components can be attributed to C-O ($E_B = 286.4$ eV for GC), C=O ($E_B = 287.3$ eV for GC and 287.2 eV for Au), COOH ($E_B = 289.1$ eV for Au) and aliphatic carbon ($E_B = 285.0$ eV for GC and 285.3 eV for Au) from surface oxides and other adventitious material present on the surface.

Figure 5-10 shows the N 1s XPS region spectra for dpb deposited onto both glassy carbon and gold substrates. The spectra appear similar with two low binding energy peaks present on both substrates. An additional peak at 401.8 eV is observed on glassy carbon and is attributed to the presence of charged nitrogen species, N⁺. The ratio of N⁺ to fluorine is 3 : 1 and is greater than the 1 : 6 ratio expected from only TBAPF₆ alone, suggesting that the bipyridyl ligand may be partially protonated. The low binding energy components are attributed to bipyridyl nitrogen ($E_B = 399.9$ eV for GC and 400.4 eV for Au) present in dpb and azo functionality ($E_B = 399.1$ eV for GC and 399.3 eV for Au) formed from the incomplete loss of N₂ during the electrodeposition of the starting material.^{30,31} Crucially, no peak corresponding to the positively charged nitrogen in the diazonium functional group ($E_B \approx 406$ eV) is observed, confirming that the film is not physisorbed to the electrode surface.^{32,33} The ratio of bipyridyl to azo nitrogen present at

the surface is approximately 2.1 : 1 on Au and 2.9 : 1 on GC. This ratio suggests that approximately 50 % of the dpb present on gold is bound via azo bonds with 35 % of dpb bound to a glassy carbon substrate via azo bonding. On gold, the ratio of the bipyridyl peak to the other components is also consistent with the stoichiometry of dpb with 50 % of the film bound via azo bonds.

5.2.2.3. ToF-SIMS Analysis of dpb Layers

ToF-SIMS was undertaken to confirm the presence of dpb on the surface. Figure 5-11 shows both positive (a) and negative (b) ion spectra of dpb on gold with major peaks labelled. The use of a gold substrate provides a simpler background compared to glassy carbon. The modified gold surfaces were cleaned in acetonitrile via an overnight Soxhlet extraction, to ensure a pristine surface free of residual electrolyte from the deposition process.

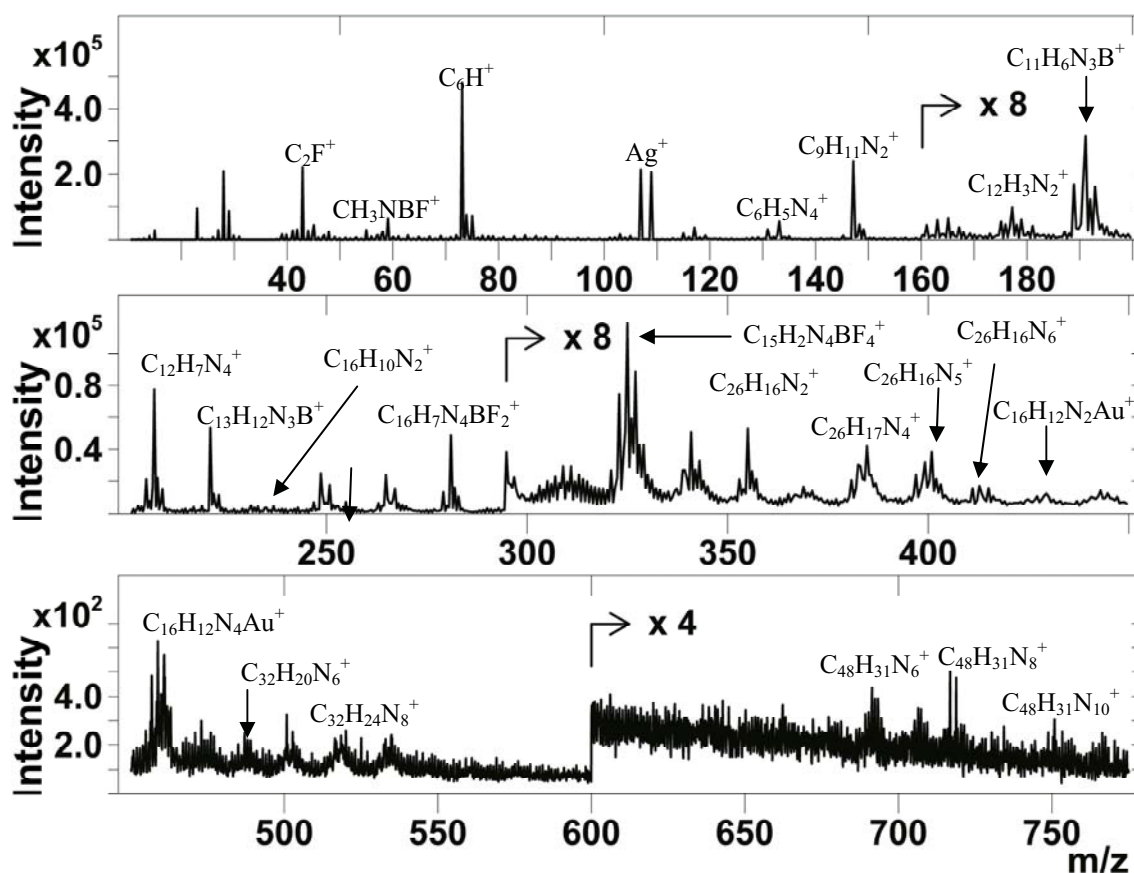


Figure 5-11a: Positive ion ToF-SIMS spectrum of a dpb modified surface with major relevant peaks labelled.

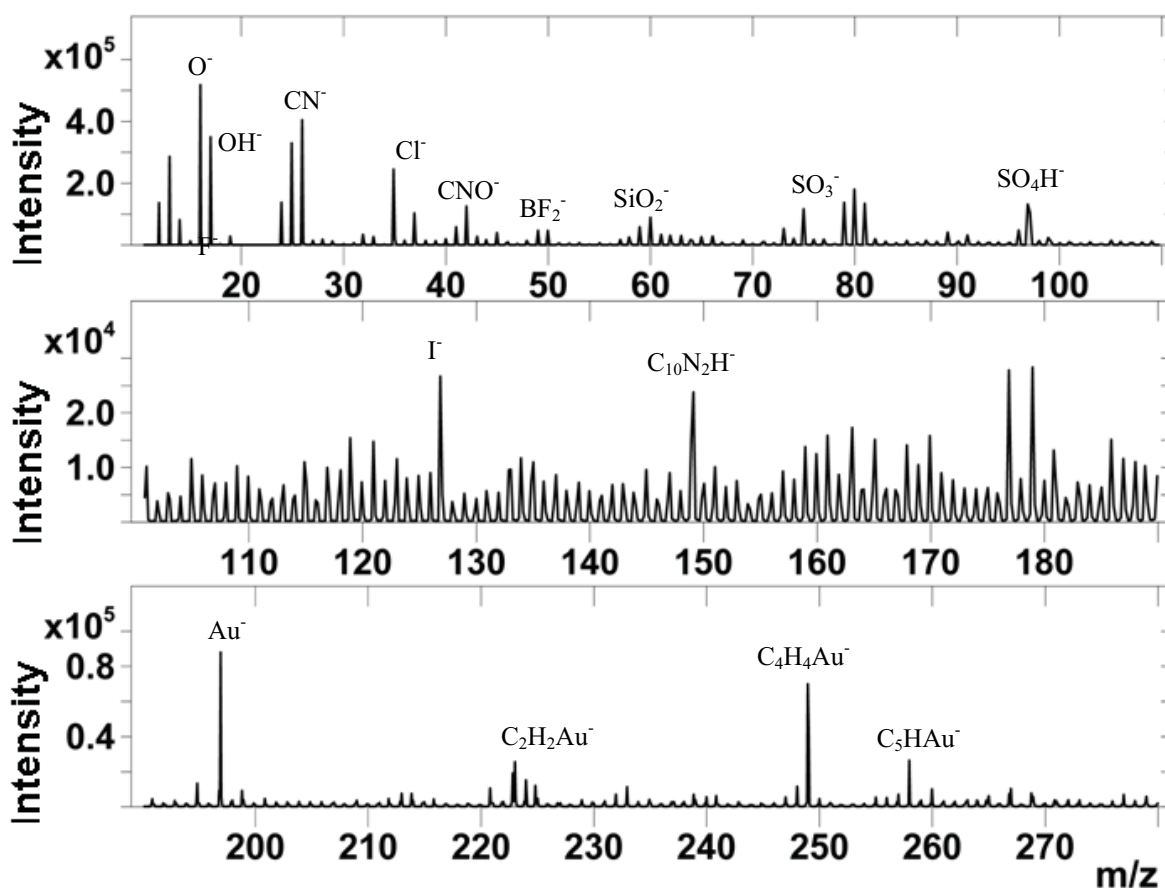


Figure 5-11b: Negative ion ToF-SIMS spectrum of a dpb modified gold surface with relevant peaks labelled.

Many peaks associated with dpb are observed, and assigned in Tables 5-2 and 5-3. ToF-SIMS confirms the presence of dpb on the surface with fragments associated with phenylbipyridine ($C_{16}H_{12}N_2^+$), bipyridine ($C_{10}H_7N_2^+$), pyridine ($C_5H_5N^+$), and benzene ($C_6H_6^+$) detected (see Table 5-2 for details). In many cases, fragments of the tetrafluoroborate anion (BF_4^-) from the original diazonium salt are present. These BF_4^- fragments and other anions are observed in the ToF-SIMS spectra despite the Soxhlet extraction. This result is in contradiction to the XPS results which did not show evidence of fluorine or boron following Soxhlet extraction. The reason for this discrepancy lies with the detection limits of each technique, with ToF-SIMS having a detection limit in parts per billion whilst XPS can only detect concentrations of parts per thousand. This result suggests that the phenylbipyridine surface is partially protonated with the BF_4^- and other anions (for example, Cl^- and SO_4^{2-}) acting as counterions that are electrostatically attached to the surface.

Component	Positive Ions			
	Gold		GC	
	Ion	Mass (m/z)	Ion	Mass (m/z)
Benzene	$C_6H_3^+$	75.025	$C_6H_5^+$	77.038
	$C_6H_4^+$	76.026	$C_6H_6^+$	78.045
	$C_6H_6^+$	78.046	$C_6H_7^+$	79.054
Pyridine	$C_5H_4N^+$	78.035	$C_5H_5N^+$	79.040
Bipyridine	$C_{10}H_7N_2^+$	155.063	$C_{10}H_7N_2^+$	155.061
Phenyl-bipyridine	$C_{16}H_{11}N_2^+$	231.090	$C_{16}H_{11}N_2^+$	231.090
	$C_{16}H_{12}N_2^+$	232.104	$C_{16}H_{12}N_2^+$	232.103
	$C_{16}H_{13}N_2^+$	233.116	$C_{16}H_{13}N_2^+$	233.105
Azobenzene	$C_6H_5N_2^+$	105.053	$C_6H_5N_2^+$	105.045
Azophenylpyridine	Not present		$C_{11}H_8N_3^+$	182.080
Azophenylbipyridine	$C_{16}H_{12}N_4^+$	260.730	$C_{16}H_{12}N_4^+$	260.116
	$C_{16}H_{13}N_4^+$	261.173	$C_{16}H_{13}N_4^+$	261.115
Bipyridine tetrafluoroborate	$C_{10}H_7N_2BF_4^+$	242.054	$C_{10}H_7N_2BF_4^+$	242.048
Phenyl-bipyridine tetrafluoroborate	$C_{16}H_{10}N_2BF_4^+$	317.009	$C_{16}H_{10}N_2BF_4^+$	317.050
Azophenylbipyridine tetrafluoroborate	$C_{15}H_{10}N_4BF_4^+$	333.042	$C_{15}H_{10}N_4BF_4^+$	333.042
	$C_{16}H_{13}N_4BF_4^+$	348.088	$C_{16}H_{13}N_4BF_4^+$	348.132
Substrate	$^{107}Ag^+$	106.906	$C_{10}H_8^+$	128.056
	$^{109}Ag^+$	108.905	$C_{14}H_{10}^+$	178.061
			$C_{20}H_{10}^+$	250.067
Substrate + phenylbipyridine	$C_{16}H_{12}N_2Au^+$	429.158	$C_{26}H_{20}N_2^+$	360.130
			$C_{30}H_{22}N_2^+$	410.145
Substrate + azophenylbipyridine	$C_{16}H_{12}N_4Au^+$	457.036	Not clearly observed	
Di(phenylbipyridine)	$C_{32}H_{22}N_4^+$	462.184	$C_{32}H_{22}N_4^+$	462.144
Di(azophenylbipyridine)	$C_{32}H_{21}N_8^+$	517.113	$C_{32}H_{21}N_8^+$	517.113
	$C_{32}H_{24}N_8^+$	520.132	$C_{32}H_{24}N_8^+$	520.132
Phenylbipyridine + azophenylbipyridine	$C_{32}H_{19}N_6^+$	487.194	$C_{32}H_{19}N_6^+$	487.168
	$C_{32}H_{20}N_6^+$	488.264	$C_{32}H_{20}N_6^+$	488.175
	$C_{32}H_{21}N_6^+$	489.306	$C_{32}H_{21}N_6^+$	489.183
Tri(phenylbipyridine)	$C_{48}H_{33}N_6^+$	691.261	Not clearly observed	
Di(azophenylpyridine)+ phenylbipyridine	$C_{48}H_{33}N_{10}^+$	749.289		

Table 5-2: Positive ion mass fragments associated with dpb deposited onto gold and glassy carbon substrates.

Component	Negative Ions			
	Gold		GC	
	Ion	Mass (m/z)	Ion	Mass (m/z)
Substrate	Au ⁻	196.997	C ₁₂ ⁻ C ₁₃ ⁻ C ₁₅ ⁻	143.998 155.996 179.992
Substrate + phenylbipyridine	C ₂ H ₂ Au ⁻ C ₄ H ₄ Au ⁻ C ₅ HAu ⁻	222.957 248.997 257.924	Not clearly observed	
Bipyridine	C ₁₀ HN ₂ ⁻	148.999	C ₁₀ HN ₂ ⁻	149.032
Counterions	³⁵ Cl ⁻	34.967	³⁵ Cl ⁻	34.969
	³⁷ Cl ⁻	36.964	³⁷ Cl ⁻	36.966
	BF ₂ ⁻	49.008	BF ₂ ⁻	49.009
	SO ₃ ⁻	79.954	SO ₃ ⁻	79.964
	SO ₄ H ⁻	96.955		
	I ⁻	126.896		

Table 5-3: Negative ion mass fragments associated with dpb deposited onto gold and glassy carbon substrates.

The presence of both gold and silver ions in the ToF-SIMS spectrum (Figure 5-11) suggests that the layer is either thinner than the 2 nm analysis depth that ToF-SIMS provides or is inhomogeneous with inconsistent coverage across the surface exposing the gold substrate. This inhomogeneity may be due to damage caused by the Soxhlet process where any loosely-bound material such as physisorbed dimers are removed. This process would be similar to the damage caused by sonication and has been well characterised by Shewchuk and McDermott.³⁴

ToF-SIMS can assist in determining the nature of the bonding between dpb and the substrate. Several fragments in both positive and negative ion spectra provide evidence of the covalent bonding of dpb to the surface through both proposed modes of binding, these being the gold carbide bond (Au-C) and the azo bond (Au-N=N-C). A schematic of the binding regime of dpb to the substrate is presented in Figure 5-12. Peaks including C₄H₄Au⁻, C₁₆H₁₂Au⁺ and C₁₆H₁₂N₂Au⁺, suggest the presence of bonding via a gold carbide link, whereas peaks such as C₁₆H₁₂N₄Au⁺ demonstrate that the layer is also bound

to the surface via azo bonds. The presence of peaks such as $C_6H_5N_2^+$, $C_{16}H_{12}N_4^+$, $C_{16}H_{13}N_4BF_4^+$ further confirms the presence of azo bonding within the film.

Several high mass fragments observed in Figure 5-11, can be attributed to the presence of dimers and trimers of dpb on the gold surface providing strong evidence for multilayer film formation. These oligomeric fragments contain m/z ratios that indicate the presence of both carbon-carbon bonds and azo bonds between the individual dpb moieties. For example, the trimer, tri(phenylbipyridine), is observed with zero ($C_{48}H_{31}N_6^+$, m/z = 691.260), one ($C_{48}H_{31}N_8^+$, m/z = 719.261), or two ($C_{48}H_{31}N_{10}^+$, m/z = 749.289) azo groups present.

Two forms of bonding between dpb monomers can exist with the diazonium either attacking the phenyl or bipyridyl group in the dpb molecule and are described in Figure 5-12. ToF-SIMS shows that both bonding configurations are present within the film. The observation of fragments corresponding to diazobenzene ($C_6H_4N_4^+$, m/z = 132.034), diphenylazide ($C_{12}H_8N_2^+$, m/z = 180.082) and biphenyl ($C_{12}H_{10}^+$, m/z = 154.063) demonstrates bonding to the phenyl group via both azo and carbon-carbon bonds. Fragments corresponding to azobipyridine ($C_{10}H_6N_4^+$, m/z = 182.077) and di(bipyridyl)benzene ($C_{26}H_{17}N_4^+$, m/z = 385.146) show the bonding of the diazonium to the bipyridyl component.

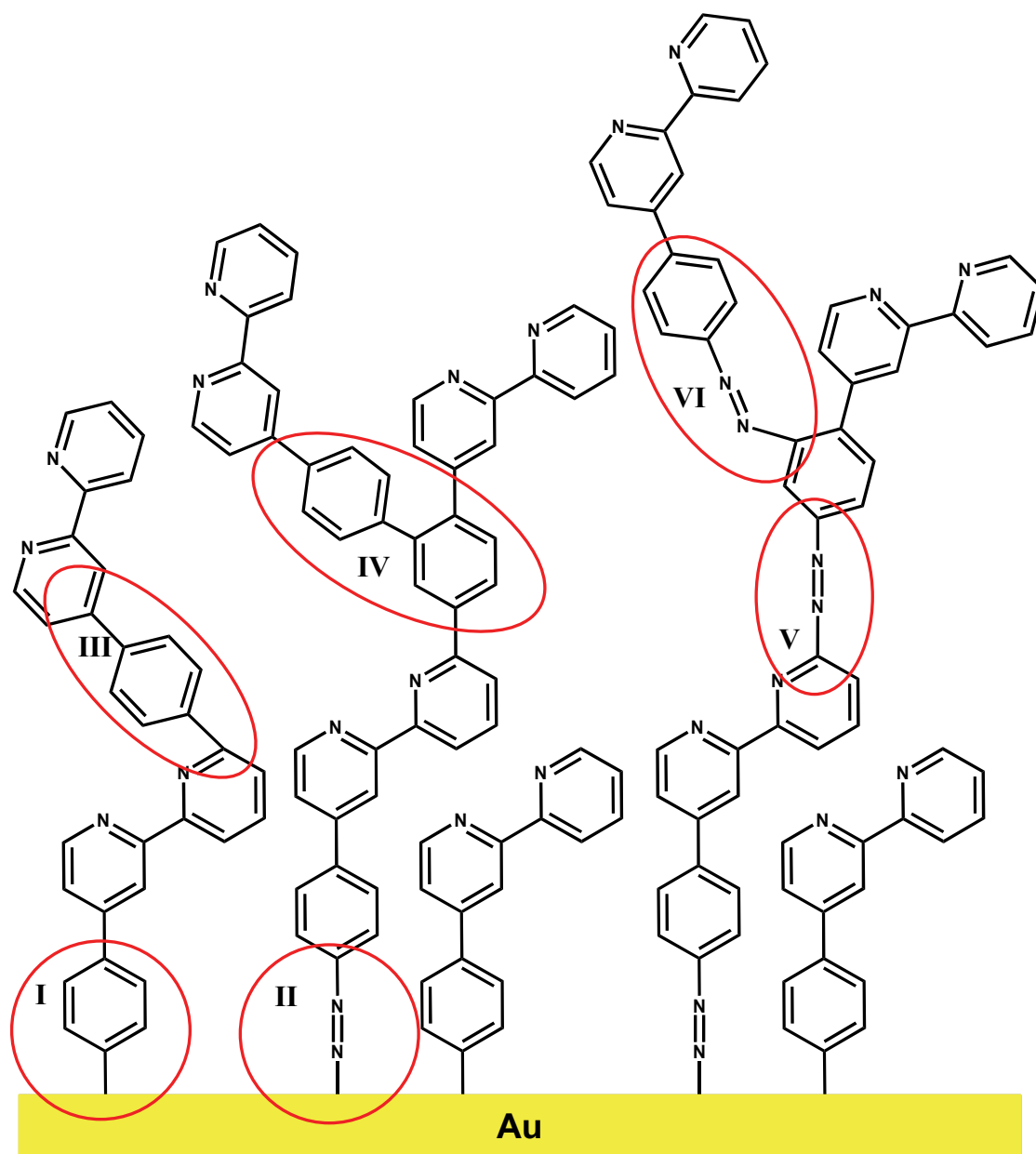


Figure 5-12: Schematic representation of the electrodeposited dpb layer on gold showing some of the bonding configurations detected via ToF-SIMS. Bonds of note are labelled, I, dpb to gold via carbide bonds, II, via azo bonds, III and IV, dpb to dpb with complete loss of nitrogen, V and VI, dpb to dpb without loss of nitrogen.

ToF-SIMS results of dpb deposited on glassy carbon are shown in Figure 5-13, with relevant peaks listed in Tables 5-2 and 5-3. The spectra appear similar to the dpb layer deposited onto gold (Figure 5-11), however fragments from the glassy carbon substrate mask the contribution from the dpb layer. As with gold, peaks associated with dpb (such as bipyridyl and phenyl bipyridine, fragments) are observed, although often with different amounts of dehydrogenation and as with the gold substrate, these fragments can have an

associated counter ion (including $C_{10}H_7N_2BF_4^+$, $C_{16}H_{10}N_2BF_4^+$, $C_{15}H_{10}N_4BF_4^+$, $C_{16}H_{13}N_4BF_4^+$) again suggesting protonation of the surface. Evidence for dpb directly bound to the surface through carbon-carbon or azo bonds is ambiguous due to the aromatic nature of both the film and underlying substrate. This ambiguity is due to many of the surface-bound fragments being equivalent to those associated with a multilayered system. The direct observation of mass fragments corresponding to a multilayered system however is possible, with peaks corresponding to the dimer di(phenylbipyridine) in its various bonding arrangements observed (see Table 5.2).

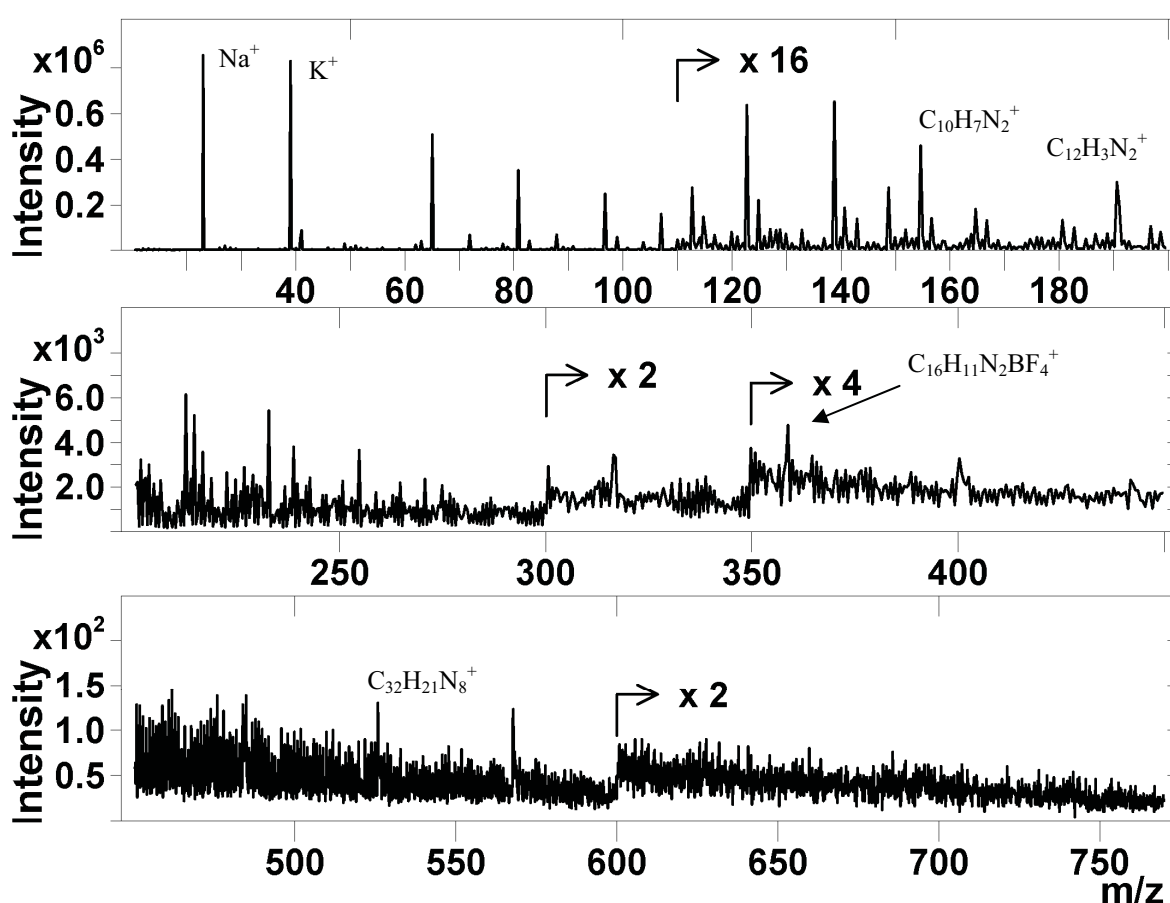


Figure 5-13: Positive ion ToF-SIMS spectrum of a dpb modified glassy carbon surface with relevant peaks labelled.

5.2.3. Attachment of Ru(bpy)₂Cl₂ to dpb Films and Subsequent Characterisation

As described in Section 3.1.2.1, the dpb functionalised surface was reacted with Ru(bpy)₂Cl₂ to form an ECL active electrode. After soaking the electrode in a 1 mM solution of Ru(bpy)₂Cl₂ in ethanol/water (90:10) for 24 hrs the surface was thoroughly rinsed and investigated using a range of electrochemical and surface characterisation techniques to determine both the success of the complexation at the surface and the electrode suitability for use as an ECL sensor.

5.2.3.1. Electrochemistry of Ru(bpy)₂(dpb) Films

Figure 5-14 presents a CV of a dpb modified glassy carbon electrode after refluxing in Ru(bpy)₂Cl₂ for 24 hrs. A bare electrode refluxed in the same solution is shown for comparison. The modified electrode presents a broad reversible peak at 0.9 V which is attributable to the Ru²⁺/Ru³⁺ redox couple of the attached complex.³⁵⁻³⁹ The bare electrode shows no redox activity in this region suggesting that the redox couple observed on the dpb modified electrode is not due to any residual Ru(bpy)₂Cl₂ present at the surface. The low redox potential of the Ru²⁺/Ru³⁺ couple bound to the layer compared to that of solution phase Ru(bpy)₃²⁺ (1.32 V in acetonitrile with 0.1 M TBAPF₄ vs Ag/Ag⁺)⁴⁰ and other similar ruthenium diimine complexes, suggests that this electrochemistry may be due to the formation of a ruthenium complex with only 5 nitrogens datively bound to the metal centre (referred to as N5) as opposed to the more common 6 dative bonds (N6).

The voltammetric peaks presented in Figure 5-14 have a Gaussian shape after the subtraction of the faradaic background, verifying that the redox couple is surface-confined and the complex is bound to the electrode. Integration of the charge under the background-corrected voltammetric peaks reveals that the surface coverage (Γ) of the

complex on the electrode surface is $1.4 \times 10^{-10} \pm 0.76 \times 10^{-10} \text{ mol cm}^{-2}$ (average value from 5 electrodes). This value is equivalent to the estimated theoretical coverage for a close-packed monolayer for the complex ($1.4 \times 10^{-10} \text{ mol cm}^{-2}$) and demonstrates an effective coupling of the $\text{Ru}(\text{bpy})_2$ to the surface. This data also suggests that the ruthenium complex interacts only with the outermost layer of dpb.

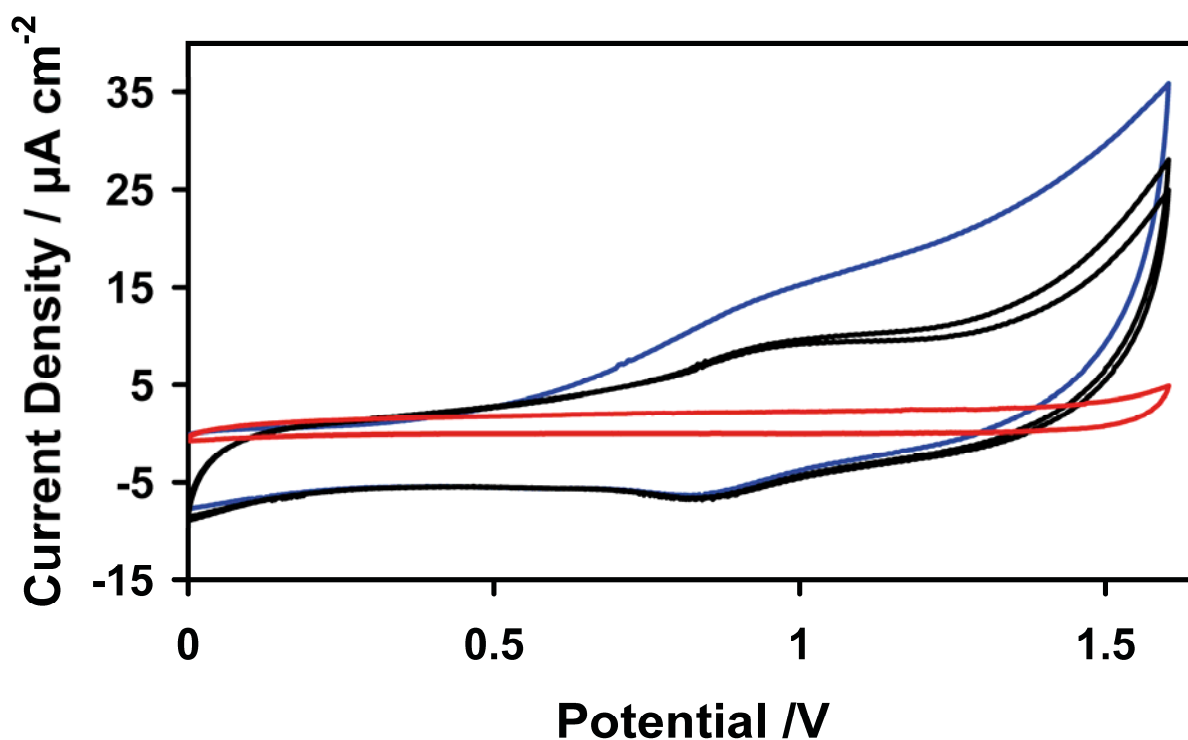


Figure 5-14: Anodic electrochemistry of a modified dpb layer after complexation with $\text{Ru}(\text{bpy})_2$. The electrode was tested in acetonitrile with TBAPF_6 (0.1 M) as electrolyte, scan rate was 100 mV s^{-1} . The first scan is shown in blue, with subsequent scans in black. An unmodified electrode refluxed in the same manner is shown (red) for comparison.

5.2.3.2. XPS Characterisation of $\text{Ru}(\text{bpy})_2(\text{dpb})$ Films

The surface characteristics of $\text{Ru}(\text{bpy})_2(\text{dpb})$ films were investigated using XPS and ToF-SIMS to confirm the presence of the ruthenium compound at the surface. Figure 5-15 presents a XPS survey spectrum of the complexed layer. Carbon, oxygen, nitrogen, fluorine, sulfur and chlorine were detected as with the dpb layer, and in addition, photoelectron lines attributed to ruthenium were observed. The presence of ruthenium on

the surface indicates successful complexation, confirming that the observed electrochemistry (Figure 5-14) is due to the ruthenium metal centre.

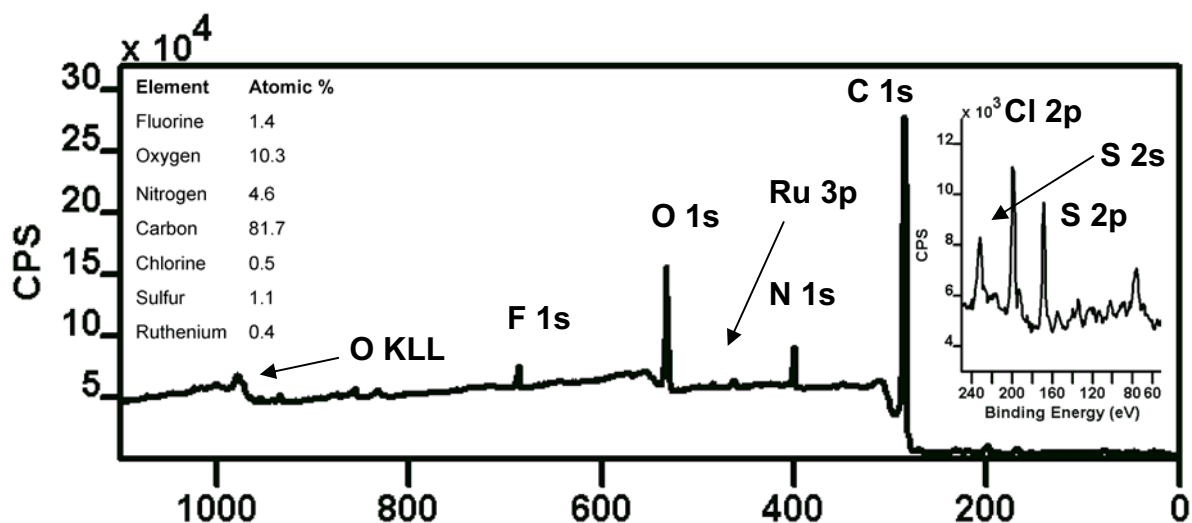


Figure 5-15: A typical XPS survey spectrum of a $\text{Ru}(\text{bpy})_2(\text{dpb})$ layer on glassy carbon with major photoelectron lines labelled.

The photoelectron region scans of the complexed layer provide a detailed view of the chemical environment present at the surface and assists in determining the bonding environment of the ruthenium. Figure 5-16 shows high resolution C 1s and N 1s photoelectron regions of the complexed layer on a glassy carbon substrate. Table 5-4 provides atomic concentrations of the components discussed. The C 1s region is comprised of contributions from aliphatic ($E_B = 285.0$ eV) and aromatic ($E_B = 284.6$ eV) carbons, $\text{C}-\text{N}$ ($E_B = 285.6$ eV), $\text{C}-\text{O}$ ($E_B = 286.2$ eV), and $\text{C}=\text{O}$ ($E_B = 288.1$ eV) bonds. The peak intensities of these components were fitted to match the concentration of nitrogen observed from the N 1s photoelectron line. The C 1s region is complicated by the presence of the Ru 3d photoelectron peak that is partially obscured by the main carbon peak (Ru $3d_{5/2}$ $E_B = 281.0$ eV, Ru $3d_{3/2}$ $E_B = 285.2$ eV). The position of the Ru $3d_{5/2}$ photoelectron line is consistent with the ruthenium being in the 2+ oxidation state.⁴¹ Two peaks are observed in the N 1s region with these peaks corresponding to contributions from bipyridyl ligands ($E_B = 400.4$ eV) and the azo bonding between dpb ligands and to

the substrate ($E_B = 398.8$ eV). This peak assignment is consistent with XPS results observed for dpb films and other diazonium systems.²⁰

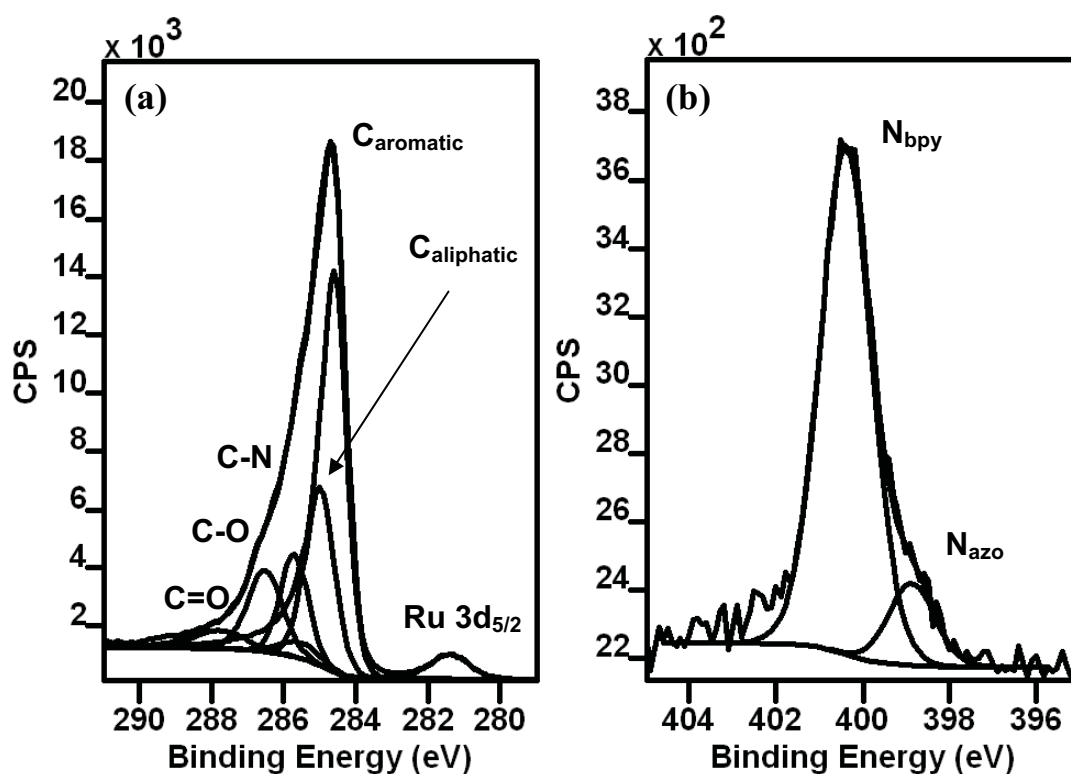


Figure 5-16: XPS region scans of the C 1s (a) and N 1s (b) photoelectron peaks in a Ru(bpy)₂(dpb) film on a glassy carbon substrate.

Element	Component	Binding Energy (eV)	Atomic %	Normalised to Ru 3d
F 1s	PF ₆ ⁻	686.6	1.4	3.5
O 1s	Oxides	532.9	7.4	18.8
	SO ₄ ²⁻	531.6	2.9	7.2
N 1s	N _{bpy}	400.4	3.9	10.0
	-N=N-	398.9	0.6	1.5
C 1s	-C=O	287.8	3.3	8.2
	-C-O	286.5	10.7	26.9
	-C-N	285.7	10.5	26.6
	-C-C	285.0	19.4	48.9
	Aromatic carbon	284.6	37.9	95.6
Cl 2p _{3/2}	-O-Cl	200.5	0.2	0.6
	Cl ⁻	198.2	0.3	0.9
S 2p _{3/2}	SO ₄ ²⁻	168.9	1.1	2.7
Ru 3d _{5/2}	Ru ²⁺	281.4	0.4	1.0

Table 5-4: Binding energy and relative concentration of components for the complexed layer as determined by XPS. Binding energy for Ru 3d peak is given from the 3d_{5/2} component with the 3d_{3/2} existing at a binding energy 4.17 eV higher. Both components are included as one peak for quantification.

By normalising the atomic concentrations in the film to the ruthenium content present in the film, its composition becomes more apparent (Table 5-4). From the ratio of Ru to N_{bpy} (1 to 13.3), it is observed that all the bipyridine present on the surface is not complexed to ruthenium. If all ruthenium was bound, then a ratio Ru to N_{bpy} of 1 to 6 would be expected. This lower ratio suggests that only about 55 % of the bipyridyl groups are complexed to ruthenium. As the complexing agent, $\text{Ru}(\text{bpy})_2$, contains bipyridyl ligands, it is estimated that ~22 % of the phenyl-bipyridine ligand previously deposited onto the surface is complexed to $\text{Ru}(\text{bpy})_2$. This figure of 22 % derived from XPS results is also in agreement with the ratio determined from electrochemical measurements of surface coverage which suggest that 15 % of the phenyl-bipyridine ligand is complexed with $\text{Ru}(\text{bpy})_2$.

Table 5-4 also shows that when compared to the dpb surface presented in Table 5-1, the ratio of the N 1s components associated with bipyridyl and azo functionality is significantly different to the $\text{Ru}(\text{bpy})_2(\text{dpb})$ surface, with the N_{azo} to N_{bpy} ratio, changing from approximately 1 : 2 to 1 : 6.6. In part, this change in ratio can be accounted for by the extra bipyridyl nitrogens associated with the binding of $\text{Ru}(\text{bpy})_2$ to the surface, however when this is considered, a N_{azo} to N_{bpy} ratio of 1 : 4 exists on the complexed surface.

5.2.3.3. ToF-SIMS of the Complexed Layer

To assist in determining the chemical structure of the complexed film, XPS was complemented with ToF-SIMS. Figure 5-17 displays a typical positive ion spectrum of the complexed film on glassy carbon. The presence of dpb is observed on the surface with peaks corresponding to phenyl-bipyridine ($m/z = 232.093$), and azophenylpyridine ($m/z = 182.079$). In addition, peaks associated with $\text{Ru}(\text{bpy})_2$, such as the presence of

ruthenium isotopes at m/z 96, 98-102, and 104, are present, with the corresponding isotope pattern also observed for fragments relating to $\text{Ru}(\text{bpy})^+$ ($m/z = 255.964$) and $\text{Ru}(\text{bpy})_2^+$ ($m/z = 414.039$). Peaks such as $(\text{bipyridine} + \text{H})^+$ ($m/z = 157.070$) are associated with both dpb and $\text{Ru}(\text{bpy})_2$.

The observation of groups of peaks with intensities characteristic of the ruthenium isotope distribution appear at masses higher than that of $\text{Ru}(\text{bpy})_2$, suggesting that the ruthenium present on the surface is not exclusively associated with $\text{Ru}(\text{bpy})_2$ and is instead complexed to the surface. The lack of evidence for any of the starting material, $\text{Ru}(\text{bpy})_2\text{Cl}_2$ ($m/z = 484$), or possible reaction intermediates such as $\text{Ru}(\text{bpy})_2(\text{H}_2\text{O})_2$ ($m/z = 450$) and $\text{Ru}(\text{bpy})_2(\text{H}_2\text{O})\text{Cl}$ ($m/z = 467$), on the surface further suggests that all the ruthenium observed is complexed to the surface. Peaks corresponding to the desired compound, $\text{Ru}(\text{bpy})_2(\text{dpb})$ ($m/z = 645$), are not clearly observed in either the positive or negative ion spectra on a glassy carbon substrate. However, peaks associated with $\text{Ru}(\text{dpb})^+$ ($m/z = 333.013$), $\text{Ru}(\text{dpb} + \text{N}_2)^+$ ($m/z = 361.003$) and $\text{C}_{32}\text{H}_{23}\text{N}_5\text{Ru}^+$, ($m/z = 579.100$) suggest a complexation of $\text{Ru}(\text{bpy})_2$ to the surface. The lack of peaks associated with the $\text{Ru}(\text{bpy})_2(\text{dpb})$ compound may suggest that the complex is in the N5 form instead of the N6 form. The existence of the N5 complex is further evidenced by related films of $\text{Ru}(\text{bpy})_3$ and $\text{Ru}(\text{bpy})_2(\text{dpb})$ not showing this fragmentation pattern³ (see Chapters 4 and 6) and instead presenting a clear molecular ion. However no peaks exclusively associated with the N5 complex, such as $\text{Ru}(\text{bpy})_2(\text{dpb})\text{Cl}$ ($m/z = 680$) are observed.

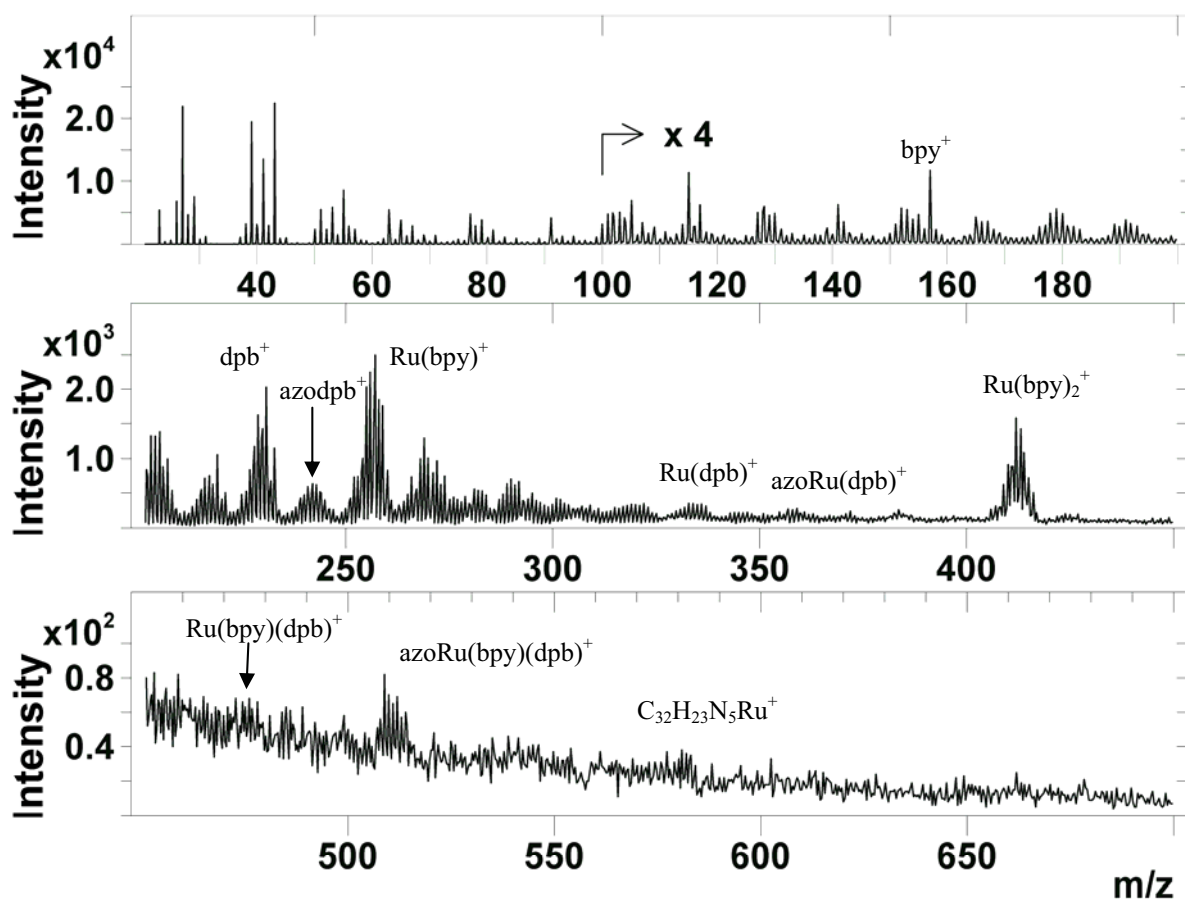


Figure 5-17: Positive ion ToF-SIMS spectra of a $\text{Ru}(\text{bpy})_2(\text{dpb})$ modified glassy carbon surface.

From the results of the electrochemical and surface analysis presented above the structure of the $\text{Ru}(\text{bpy})_2(\text{dpb})$ layer may be inferred to be similar to the structure proposed in Figure 5-18 with a thin layer (~ 6 nm) of dpb ligand covered by a monolayer of $\text{Ru}(\text{bpy})_2(\text{dpb})$ bound in the N5 coordination as shown. The creation of the N5 coordinated complex at the surface may be due to a steric hindrance provided by the disordered layer of dpb created prior to reaction with $\text{Ru}(\text{bpy})_2$. This steric hindrance may prevent the binding of the second bipyridyl nitrogen to the metal centre.

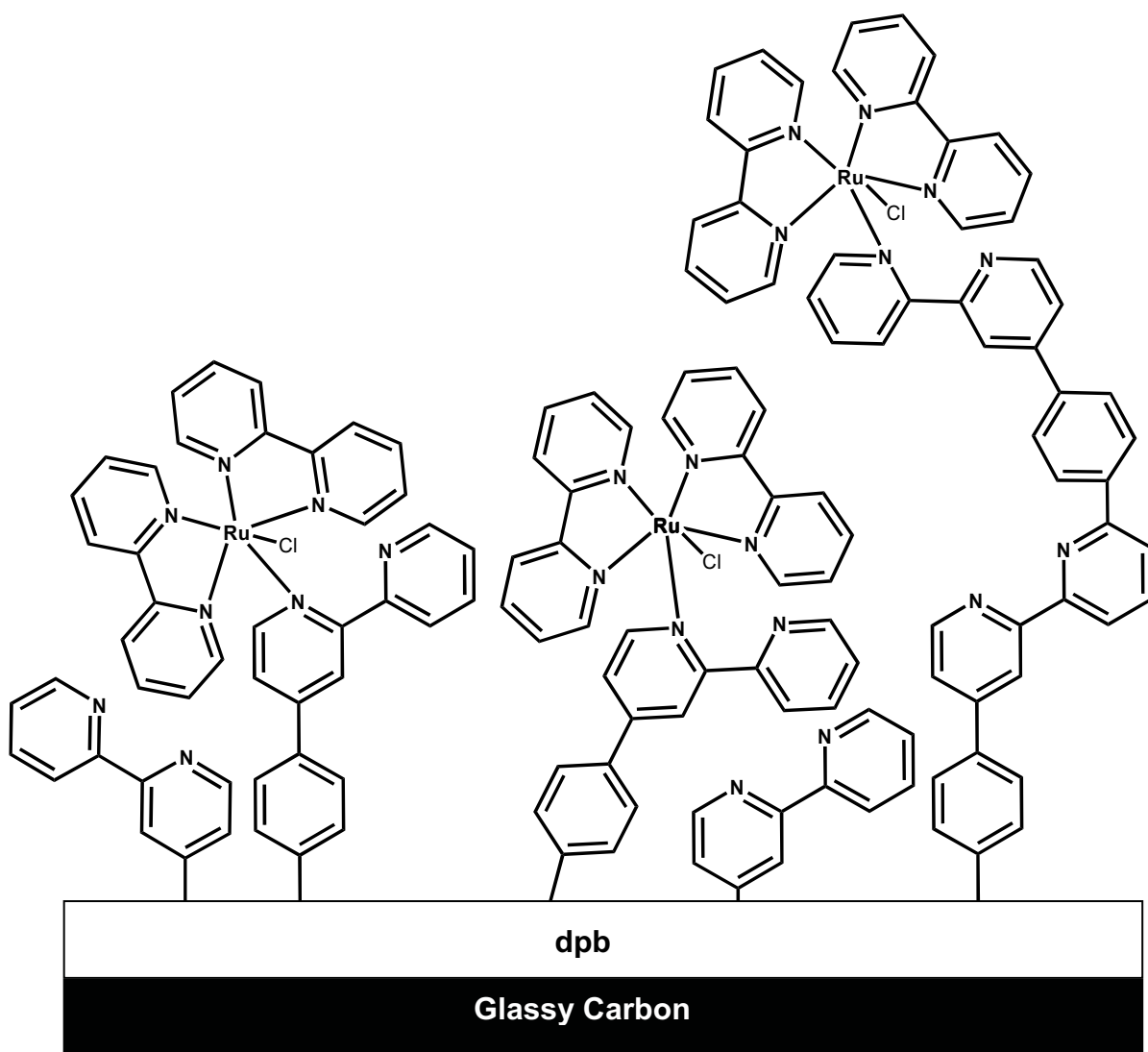


Figure 5-18: Proposed structure of the complexed film, with a monolayer of Ru(bpy)₂(dpb) in the N5 binding configuration on top of a thicker dpb film.

5.2.3.4. Electrochemiluminescence

Figure 5-19 demonstrates the ECL response of the complexed layer when used with the co-reactant tripropylamine (TPA) in an acetonitrile solution. It is observed that the light emitted from the layer is coincident with the onset of the oxidation of the ruthenium centre at < 1 V, demonstrating that the light emission is due to the reaction of TPA with the complexed surface. The layer produces a low intensity of light emission compared to other model systems (see Chapters 4 and 6) with a relatively high concentration of TPA required for a detectable response. For comparison, the electrodeposited layer presented in Chapter 6 produces approximately 150 times more light emission for the same

experimental conditions. A direct comparison with the Nafion-based film produced in Chapter 4 is not possible as the film dissolves in acetonitrile, however, the equivalent aqueous system produces a maximal light intensity approximately 6×10^4 greater than the film presented in Figure 5-19. N5 coordinated ruthenium complexes are known to possess significantly lower photoluminescent quantum yields than the corresponding N6 species. As ECL intensity is governed by the quantum yield, this low level of light produced may provide further evidence for the film existing in N5 state.³⁹

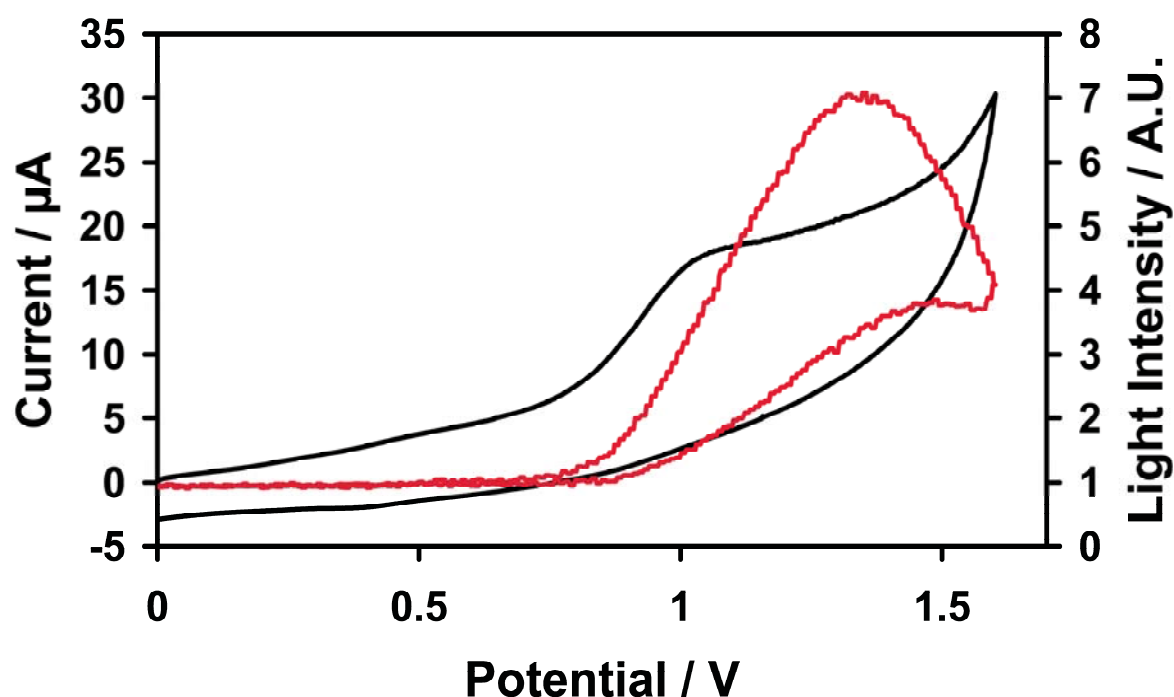


Figure 5-19: ECL emission from the complexed layer (red), in a solution of 5 mM TPA in acetonitrile with 0.1M TBAPF₆ electrolyte. The layers electrochemical response is also shown (black). Scan rate was 100 mV s⁻¹.

5.3. Conclusions

The successful deposition of thin phenyl-bipyridine films onto gold and glassy carbon substrates from the associated diazonium salt, para-diazonium-4'-phenyl-2,2'-bipyridine tetrafluoroborate, has been achieved. The direct electrodeposition of the diazonium salt can be achieved with a reduction potential of -0.65 V. In addition, this deposition can be achieved via the mediated electrolysis of the diazonium by previously bound bipyridine at a potential of -1.4 V.

The deposited film has been characterised by various electrochemical and surface analysis techniques. Characterisation of the film shows that it is a multilayered structure of approximately 6 nm in thickness which is bound with both carbon-carbon and azo bonds between the individual dpb molecules. ToF-SIMS data shows that both bonding types also bind the film to the underlying substrate. XPS results estimate that approximately 50 % of the dpb in the film is bound through an azo bond.

The subsequent complexation of this film using the reagent $\text{Ru}(\text{bpy})_2\text{Cl}_2$ to form an ECL active layer was partially successful. XPS and ToF-SIMS analysis confirms the binding of $\text{Ru}(\text{bpy})_2$ to the film, though electrochemical experiments and ToF-SIMS suggest that the complexation reaction may be incomplete with the Ru bound to 5 pyridine groups instead of the desired 6 with the second chloride remaining coordinated to the metal. Cyclic voltammetry demonstrates that the film is electroactive and capable of co-reactant ECL with TPA. However, further ECL experiments show that the film is not highly responsive to the co-reactant, emitting low levels of light compared to other films discussed in this thesis (see Chapters 4 and 6). This low level of light emission is related to the relatively poor oxidising power of the $\text{Ru}(\text{N})_5$ species and to its low quantum yield. Therefore, although the study produced some interesting insights into the behavior of diazonium

species, the results suggest that the film is not well suited to a role as an ECL-based sensor.

5.4. References

- (1) Obeng, Y. S.; Bard, A. J.; *Langmuir* **1991**, *7*, 195-201.
- (2) Zhang, X.; Bard, A. J.; *J. Phys. Chem.* **1988**, *92*, 5566-5569.
- (3) Zanarini, S.; Rampazzo, E.; Bich, D.; Canteri, R.; Ciana, L. D.; Marcaccio, M.; Marzocchi, E.; Panciatichi, C.; Pederzoli, C.; Paolucci, F.; Prodi, L.; Vanzetti, L.; *J. Phys. Chem. C* **2008**, *112*, 2949-2957.
- (4) Sato, Y.; Uosaki, K.; *J. Electroanal. Chem.* **1995**, *384*, 57-66.
- (5) Wei, H.; Yin, J.; Wang, E.; *Anal. Chem.* **2008**, *80*, 5635-5639.
- (6) Gooding, J. J.; *Electroanal.* **2007**, *20*, 573-582.
- (7) Nassef, H. M.; Radi, A.-E.; O'Sullivan, C. K.; *J. Electroanal. Chem.* **2006**, *592*, 139-146.
- (8) Yang, X. H.; Hall, S. B.; Burrell, A. K.; Officer, D. L.; *Chem. Commun.* **2001**, 2628-2629.
- (9) Laforgue, A.; Addou, T.; Belanger, D.; *Langmuir* **2005**, *21*, 6855-6865.
- (10) Combellas, C.; Jiang, D.; Kanoufi, F.; Pinson, J.; Podvorica, F.; *Langmuir* **2009**, *25*, 286-293.
- (11) Delmar, M.; Desarmot, G.; Fagebaume, O.; Hitmi, R.; Pinson, J.; Savéant, J. M.; *Carbon* **1997**, *35*, 801-807.
- (12) Liu, G.; Nguyen, Q. T.; Chow, E.; Bocking, T.; Hibbert, D. B.; Gooding, J. J.; *Electroanal.* **2006**, *18*, 1141-1151.
- (13) Jouselme, B.; Bidan, G.; Billon, M.; Goyer, C.; Kervella, Y.; Guillerez, S.; Hamad, E. A.; Goze-Bac, C.; Mevellec, J.-Y.; Lefrant, S.; *J. Electroanal. Chem.* **2008**, *621*, 277-285.
- (14) Brooksby, P. A.; Downard, A. J.; *Langmuir* **2004**, *20*, 5038-5045.
- (15) Benedetto, A.; Balog, M.; Viel, P.; Le Derf, F.; Sallé, M.; Palacin, S.; *Electrochim. Acta* **2008**, *53*, 7117-7122.

- (16) Itoh, T.; McCreery, R. L.; *J. Am. Chem. Soc.* **2002**, *124*, 10894-10902.
- (17) Cline, K. K.; Baxter, L.; Lockwood, D.; Saylor, R.; Stalzer, A.; *J. Electroanal. Chem.* **2009**, *633*, 283-290.
- (18) Baranton, S.; Belanger, D.; *J. Phys. Chem. B* **2005**, *109*, 24401-24410.
- (19) Baranton, S.; Belanger, D.; *Electrochim. Acta* **2008**, *53*, 6961-6967.
- (20) Lehr, J.; Williamson, B. E.; Flavel, B. S.; Downard, A. J.; *Langmuir* **2009**, *25*, 13503-135-9.
- (21) Stewart, M. P.; Maya, F.; Kosynkin, D. V.; Dirk, S. M.; Stapleton, J. J.; McGuinness, C. L.; Allara, D. L.; Tour, J. M.; *J. Am. Chem. Soc.* **2004**, *126*, 370-378.
- (22) Kishi, A.; Umeda, M.; *App. Surf. Sci.* **2009**, *255*, 9154-9158.
- (23) Burnham, N. A.; Colton, R. J.; Pollock, H. M.; *Nanotechnology* **1993**, *4*, 64-80.
- (24) Dretschkow, T.; Wandlowski, T.; *Electrochim. Acta* **1999**, *45*, 731-740.
- (25) Tokel, N. E.; Bard, A. J.; *J. Am. Chem. Soc.* **1972**, *94*, 2862-2863.
- (26) McCreery, R. L.; *Chem. Rev.* **2008**, *108*, 2646-2687.
- (27) Dekanski, A.; Stevanovic, J.; Stevanovic, R.; Nickolic, B.; Jovanovic, V.; *Carbon* **2001**, *39*, 1195-1205.
- (28) Dübgen, A., Quote from HTW, Germany.
- (29) Moulder, J. F.; Stickle, W. F.; Sobol, P. E.; Bomben, K. D. *Handbook of X-ray Photoelectron Spectroscopy*; Perkin-Elmer Corporation Physical Electronics Division: Eden Prairie, 1992.
- (30) Toupin, M.; Belanger, D.; *J. Phys. Chem. C* **2007**, *111*, 5394-5401.
- (31) Zhou, Y.; Zhi, J.; *Electrochem. Commun.* **2006**, *8*, 1811-1816.
- (32) Finn, P.; Jolly, W. L.; *Inorg. Chem.* **1972**, *11*, 1434-1435.
- (33) Brant, P.; Feltham, R. D.; *J. Organomet. Chem.* **1976**, *120*, C53-C57.
- (34) Shewchuk, D. M.; McDermott, M. T.; *Langmuir* **2009**, *25*, 4556-4563.

- (35) Leech, D.; Forster, R. J.; Smyth, M. R.; Vos, J. G.; *J. Mater. Chem.* **1991**, *1*, 629-635.
- (36) Barisci, J. N.; Wallace, G. G.; Wilke, E. A.; Meaney, M.; Smyth, M. R.; Vos, J. G.; *Electroanal.* **1989**, *1*, 245-250.
- (37) Moyer, B. A.; Meyer, T. J.; *Inorg. Chem.* **1981**, *20*, 436-444.
- (38) Forster, R. J.; Figgemeier, E.; Lees, A. C.; Hjelm, J.; Vos, J. G.; *Langmuir* **2000**, *16*, 7867-7870.
- (39) Curtis, J. C.; Bernstein, J. S.; Meyer, T. J.; *Inorg. Chem.* **1985**, *24*, 385-397.
- (40) Bard, A. J.; Faulkner, L. R. *Electrochemical methods: fundamentals and applications*; 2nd ed.; John Wiley: New York, 2001.
- (41) Susac, D.; Kono, M.; Wong, K. C.; Mitchell, K. A. R.; *App. Surf. Sci.* **2001**, *174*, 43-50.

Chapter 6: The Electrodeposition of Ru(bpy)₂(apb)²⁺ films.

6.1. Introduction

The results presented in Chapter 5 suggest that some of the problems of side products and low surface coverage, encountered in the multi-step approach to electrode modification with ruthenium complexes, may be overcome by adopting a more direct single step modification strategy. During the course of the work described here, Jouselme et al. have demonstrated the successful deposition of the diazonium derivative of the complex Ru(bpy)₂(apb)(PF₆)₂, from organic solvent.^{1,2} However, *in-situ* formation and deposition of the diazonium complex from aqueous media was not explored nor were the ECL properties. This deposition method can provide a useful single step aqueous attachment to electrodes in environments sensitive to organic solvents such as screen printed electrodes and lab-on-a-chip devices.

In this chapter the creation and use of an ECL active film from Ru(bpy)₂(apb)²⁺ is demonstrated. The Ru(bpy)₂(apb)²⁺ layer is electrodeposited from a solution of the hexafluorophosphate salt, via the diazotisation of the amine with nitrous acid (HNO₂). The film is subsequently characterised with electrochemical and surface analysis techniques, including CV, XPS and ToF-SIMS. The film is assessed for its suitability as an ECL-based sensor with the model analyte 2-(dibutylamino)ethanol (DBAE), and the stability of the film and the mechanism of its degradation is investigated.

6.2. Results and Discussion

The synthesis and deposition methods used to create the films described in this section are discussed in Section 3.1.2.2.

6.2.1. Layer Deposition

Glassy carbon electrodes were modified via the electrochemical reduction of a 0 °C 1.2 mM $[\text{Ru}(\text{bpy})_2(\text{apb})](\text{PF}_6)_2$ solution containing 1.5 mM NaNO_2 and 0.5 M HCl . A typical cyclic voltammogram obtained from the deposition is presented in Figure 6-1. The deposition gives rise to a broad reduction wave, unlike aryl diazonium salts in organic media where a sharp deposition peak is observed.^{3,4} In similar systems it is reported that the reduction peak for this diazonium occurs at -0.6 V v.s. Ag/AgCl in organic media.² However, the observed response is consistent with the reduction of the diazonium and subsequent formation of a covalent bond with the substrate through either a carbon-carbon or azo ($-\text{N}=\text{N}-$) bond as shown previously.² This cathodic current is not observed unless NaNO_2 is present. After the initial scan, the current drops to background levels in subsequent potential sweeps. The loss of the large cathodic current observed in the first scan indicates that the electrode is largely covered during the timescale of one voltammetric cycle.

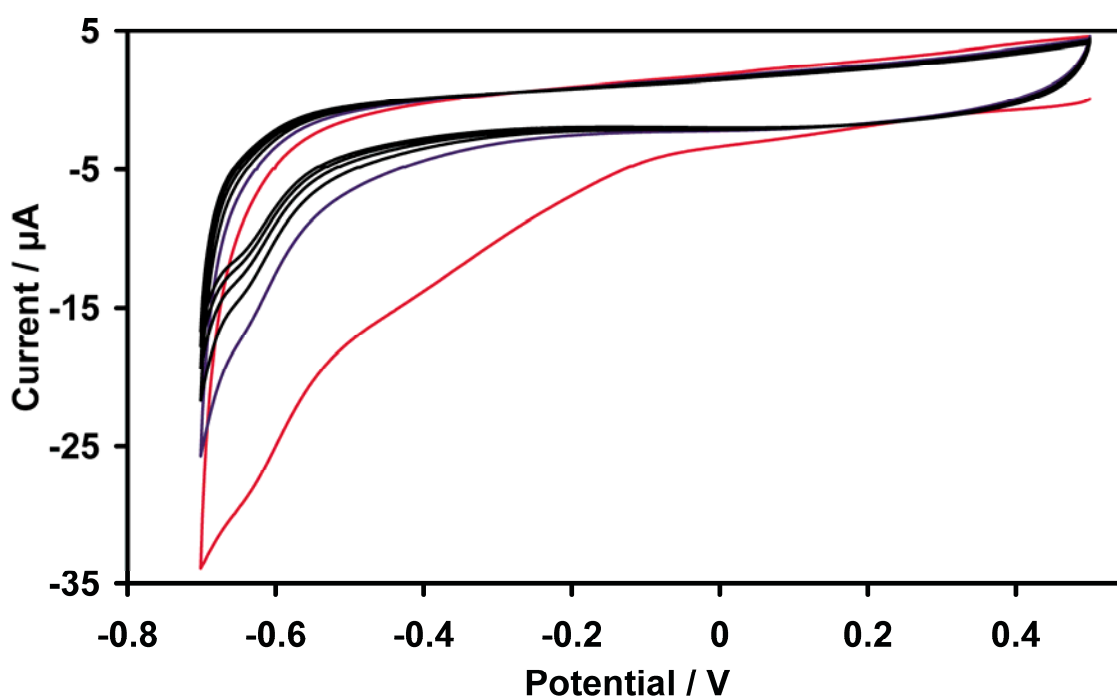


Figure 6-1: Deposition CV for $\text{Ru}(\text{bpy})_2(\text{apb})^{2+}$ from a solution containing 1.5 mM NaNO_2 and 0.5 M HCl , the first 6 scans are shown. The initial scan is shown in red with the second scan shown in blue, the remainder of the scans are presented in black. The scan rate was 100 mV s^{-1} .

6.2.2. Layer Characterisation

6.2.2.1. Electrochemical Characterisation

The cyclic voltammetric response of the electrodeposited layer of the ruthenium complex in blank electrolyte is presented in Figure 6-2 and is compared with the response from an electrode treated in exactly the same way with the exception of the addition of NaNO_2 to the solution. A reversible redox couple centred around 1.15 V is observed and can be attributed to the $\text{Ru}^{2+}/\text{Ru}^{3+}$ couple of the deposited complex and is consistent with the solution phase voltammetry of the complex and with electrochemistry obtained from other immobilised forms of $\text{Ru}(\text{bpy})_3^{2+}$.^{1,5,6}

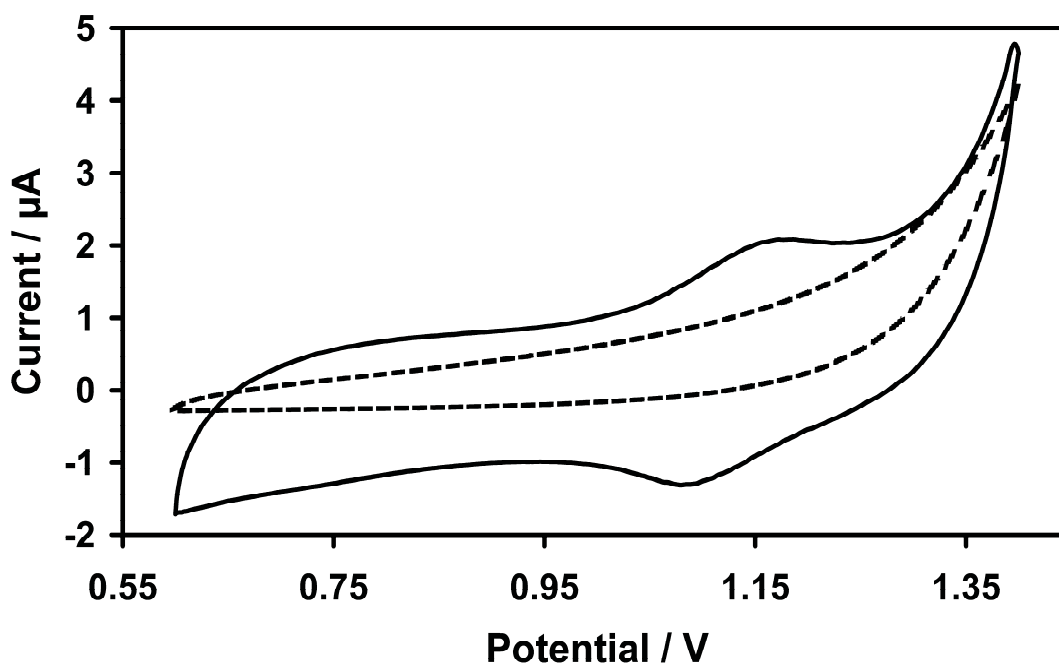


Figure 6-2: Electrochemical response of a GC electrode after reaction with $\text{Ru}(\text{bpy})_2(\text{apb})^{2+}$ and NaNO_2 (solid line), and with only $\text{Ru}(\text{bpy})_2(\text{apb})^{2+}$ (dashed line). Scan rate was 100 mV s^{-1} .

Figure 6-3 shows the voltammetric response for a similar layer at a range of scan rates with the insert showing the dependence of peak current on scan rate. After background subtraction is performed on the voltammetric peaks, a Gaussian peak shape is observed. The absence of peak tailing and the linear dependence of peak current (see insert of Figure 6-3) on scan rate proves that the wave observed for the $\text{Ru}^{2+}/\text{Ru}^{3+}$ redox couple is due to a surface-confined species bound to the electrode. Integration of the charge under

the background-corrected voltammetric peaks reveals that the surface coverage (Γ) of the complex is $4.8 \times 10^{-10} \pm 2.2 \times 10^{-10} \text{ mol cm}^{-2}$ (average value from seven electrodes). This value is greater than the estimated theoretical coverage for a close packed monolayer for the complex ($1.4 \times 10^{-10} \text{ mol cm}^{-2}$), indicating the presence of a multilayered system equivalent to between two and five monolayers.

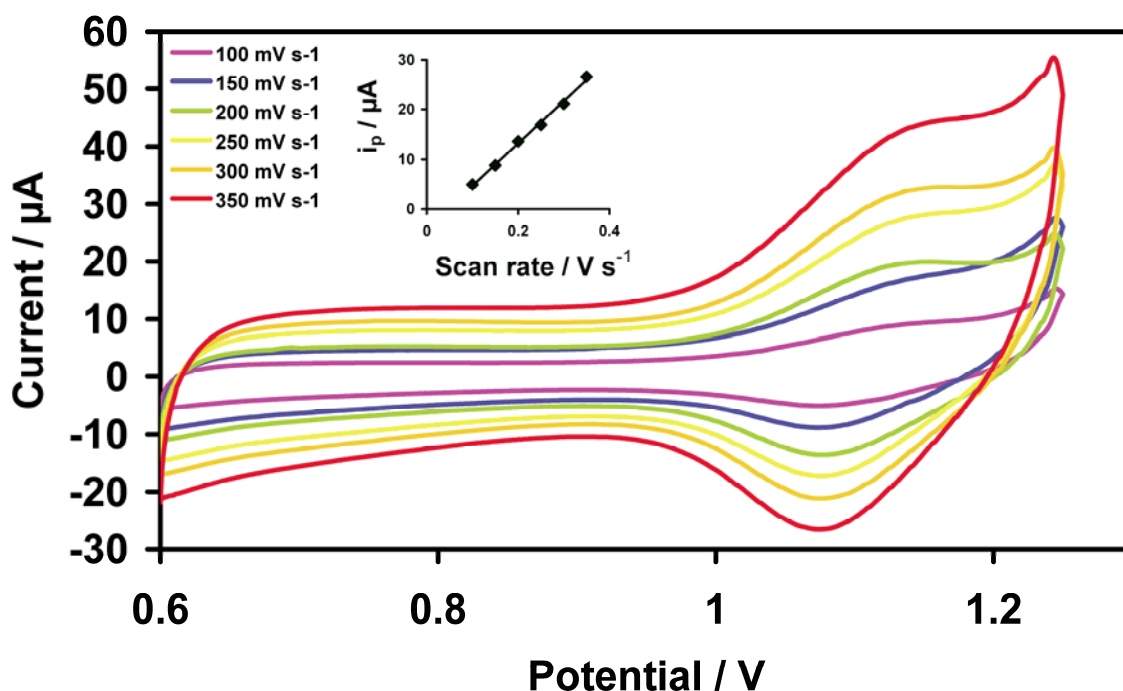


Figure 6-3: Scan rate dependence of 3 mm diameter glassy carbon electrode modified with a layer of $\text{Ru}(\text{bpy})_2(\text{apb})^{2+}$ in blank electrolyte solution (0.1 M LiClO_4). The insert demonstrates the linear dependence of the $\text{Ru}^{2+}/\text{Ru}^{3+}$ peak current on scan rate.

6.2.2.2. Surface Analysis

The nature of the bonding in the layer and the functional groups involved in bonding to the substrate (carbon-carbon or azo-carbon bonding) were examined using XPS and ToF-SIMS. An XPS survey spectrum of the layer is shown in Figure 6-4, with contributions observed from fluorine, oxygen, nitrogen, carbon and ruthenium. Trace amounts of chlorine, silicon and phosphorus are also present. The nitrogen, carbon and ruthenium can be attributed to the attached $\text{Ru}(\text{bpy})_2(\text{apb})^{2+}$ with the fluorine and phosphorus present from the hexafluorophosphate (PF_6^-) counterion used during the deposition. The presence of chlorine is also expected to be a counterion for the $\text{Ru}(\text{bpy})_2(\text{apb})^{2+}$. The silicon

observed may be a contaminant from the purification of the complex, being present in the form of silica, accounting for some of the oxygen present, with the remainder of the oxygen contribution resulting from either adventitious hydrocarbons or oxidation of the surface prior to deposition.

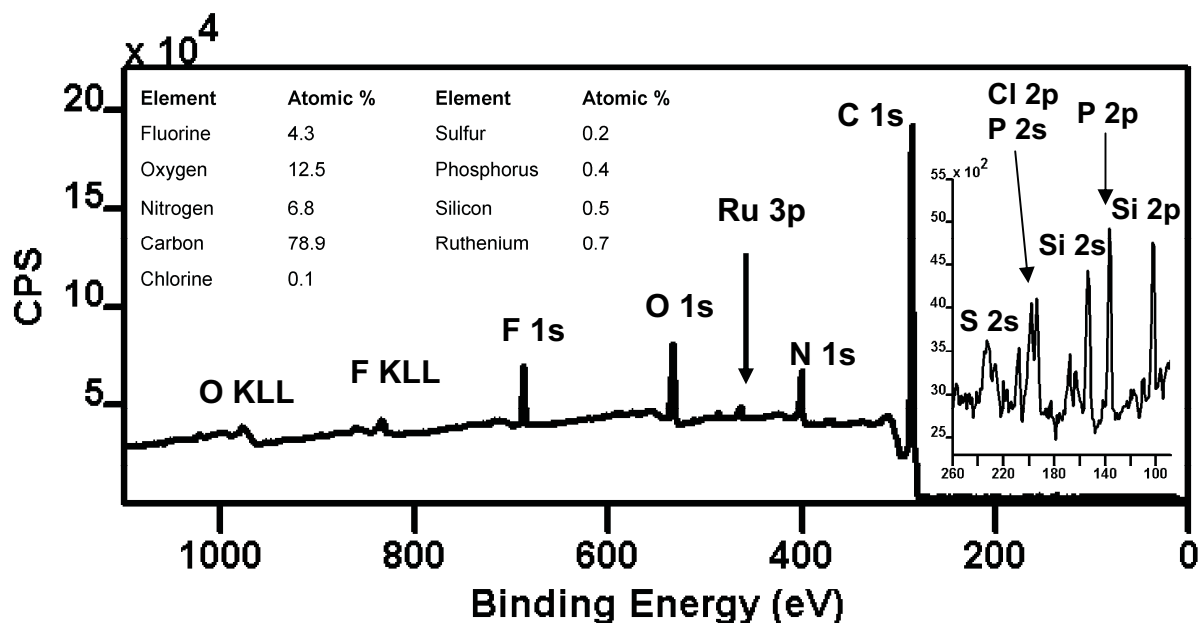


Figure 6-4: XPS survey spectrum of a $\text{Ru}(\text{bpy})_2(\text{apb})^{2+}$ layer deposited onto a glassy carbon substrate.

Typical C 1s and N 1s photoelectron region spectra for the layer are shown in Figure 6-5. The presence of $\text{Ru}(\text{bpy})_2(\text{apb})^{2+}$ on the electrode surface is confirmed by the observation of the Ru $3d_{5/2}$ photoelectron peak at 281.2 eV and corresponds to Ru in the 2+ oxidation state.⁷ The Ru $3d_{3/2}$ peak occurs at a binding energy 4.17 eV higher than the Ru $3d_{5/2}$ peak and lies underneath the aliphatic C 1s component. Other peaks observed in the C 1s region of both films include $\underline{\text{C}}\text{-N}$ ($E_B = 286.0$ eV), aromatic and aliphatic carbon ($E_B = 284.6$ and 285.0 eV respectively), $\underline{\text{C}}\text{=O}$ ($E_B = 289.6$ eV), $\underline{\text{C}}\text{-O}$ ($E_B = 287.6$ eV) and a $\pi \rightarrow \pi^*$ shake up peak ($E_B = 289.6$ eV). These peak assignments are consistent with those previously reported.^{8,9}

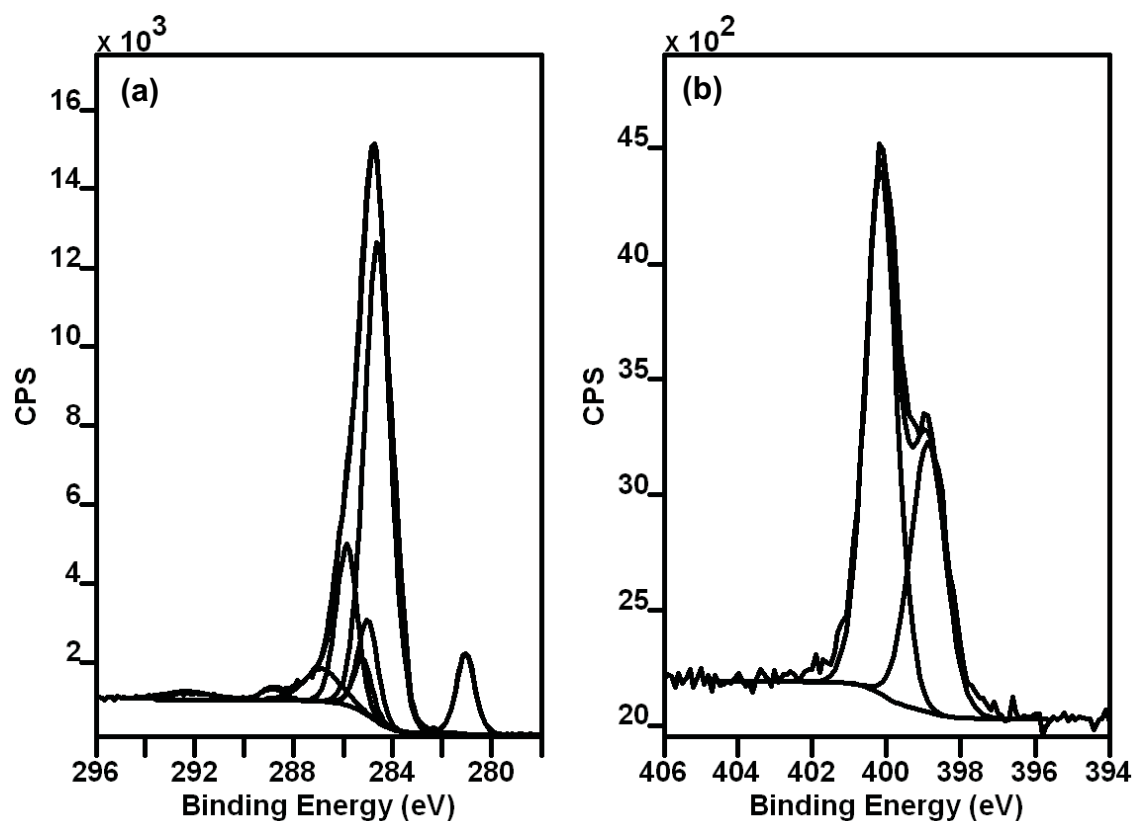


Figure 6-5: XPS region spectra for the C 1s (a) and N 1s (b) photoelectron regions of the Ru(bpy)₂(apb)²⁺ film.

Element	Component	Binding Energy (eV)	Atomic %	Normalised to Ru 3d
F 1s	PF ₆ ⁻	686.4	4.3	6.6
O 1s	Oxides	532.2	8.1	12.5
N 1s	N _{amine/bpy}	400.3	4.3	6.7
	-N=N-	399.0	1.5	2.1
C 1s	π→π* Satellite	292.5	1.3	2.1
	-C=O	287.6	0.9	1.4
	-C-O	286.6	4.6	7.1
	-C-N	285.9	13.2	20.3
	-C-C-	285.0	7.6	11.7
	Aromatic carbon	284.6	52.3	80.6
Cl 2p _{3/2}	Cl ⁻	198.2	0.1	0.2
S 2p _{3/2}	SO ₄ ²⁻	167.6	0.2	0.2
P 2p _{3/2}	PF ₆ ⁻	137.0	0.4	0.6
Si 2p	SiO ₂	103.0	0.5	0.8
Ru 3d _{5/2}	Ru ²⁺	281.2	0.7	1.0

Table 6-1: Binding energy and relative concentration of components for the Ru (bpy)₂(apb)²⁺ film as determined by XPS. Binding energy for Ru 3d peak is given from the 3d_{5/2} component with the 3d_{3/2} existing at a binding energy 4.17 eV higher. Both components are included as one peak for quantification.

Two peaks at 399.0 and 400.3 eV are observed in the N 1s region spectrum (Figure 6-5b). The peak at higher binding energy (400.3 eV) can be attributed to the pyridyl nitrogen present in the complex.^{2,10} No peak corresponding to the positively charged nitrogen in the diazonium functional group ($E_B \approx 406$ eV) is observed, confirming that the film is not physisorbed to the electrode surface.^{11,12} In previous XPS studies of diazonium derived films, the peak at 399.0 eV has often been discounted or ignored as a by-product of the reaction or possible surface contamination.^{13,14} However, as first suggested by Belanger,¹³ this peak is due to the formation of azo (R-N=N-R) bonds in the layer. Recently it has been shown by Doppelt, et. al. that through the use of ToF-SIMS and IR spectroscopy that this is the case for a range of aryl diazonium salts.¹⁵ Doppelt suggested that the formation of the azo bonds on a multi-layered system is related to the steric crowding of the layer. As such, a large complex such as Ru(bpy)₂(apb)²⁺ would encourage the formation of azo bonds in the system under study here. The ratio of Ru to N_{azo} atoms observed via XPS is 1 to 2 suggesting that through the analysis depth probed by XPS (5-10 nm), the layer is exclusively bound via the azo functionality.

ToF-SIMS was undertaken to further investigate the bonding within the layer. Figure 6-6 shows a typical positive ion ToF-SIMS mass spectrum for a layer electrodeposited from a Ru(bpy)₂(apb)²⁺ solution, with a selection of relevant mass fragments listed in Table 6-2. A number of peaks associated with the deposited complex Ru(ph-bpy)(bpy)₂, where ph-bpy is 4-phenyl-2,2'-bipyridyl, are present, with the compound fragmenting most typically through the loss of a ligand from the complex, resulting in groups of peaks associated with Ru(bpy)₂(ph-bpy), Ru(bpy)₂, Ru(ph-bpy)(bpy), Ru(ph-bpy) and Ru(bpy) fragments. These broad peak groupings are attributed to the multiple stable isotopes of Ru present in the sample. Significantly, no peaks exclusively associated with the starting material Ru(bpy)₂(apb)²⁺ are observed in the spectra. In contrast to the positive ion

spectrum, the negative ion mass spectrum for the layer provides little discernible information regarding the structure of the layer with the most notable peak present associated with the counter-ion used (PF_6^-).

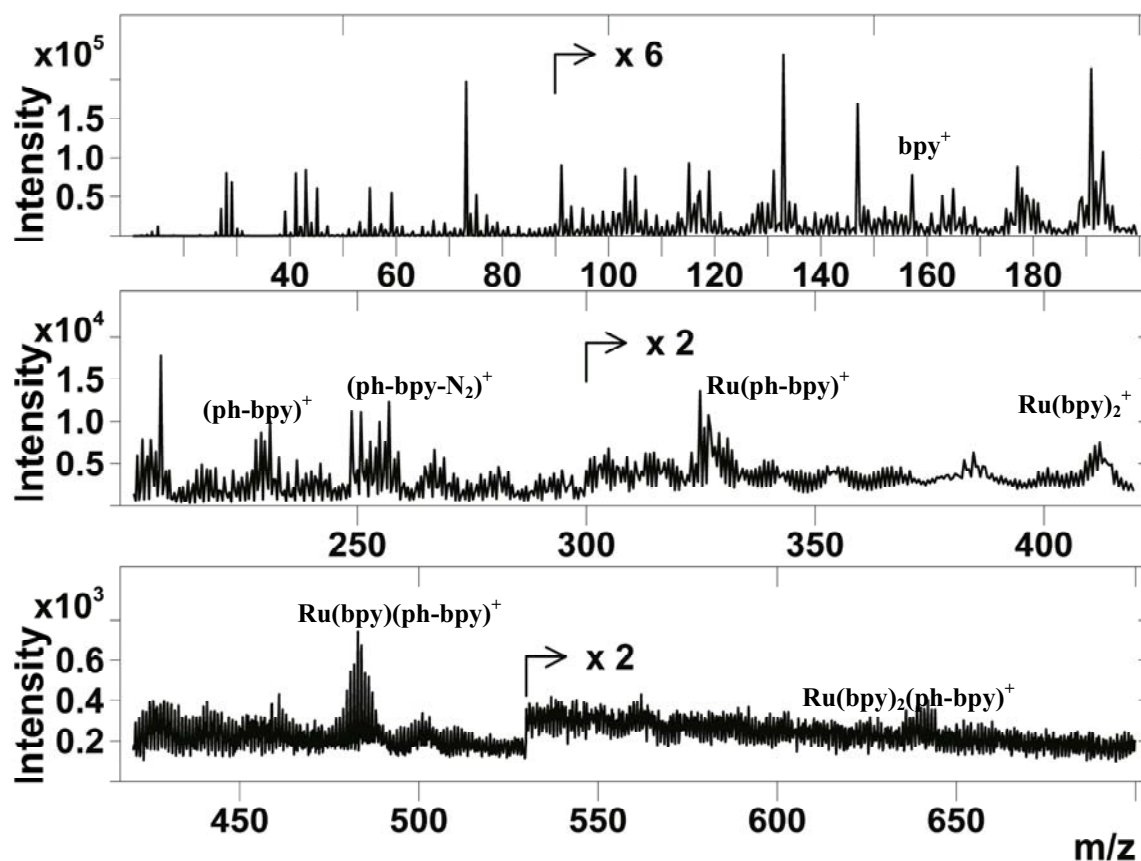


Figure 6-6: Positive ion ToF-SIMS spectrum of the deposited $\text{Ru}(\text{bpy})_2(\text{apb})^{2+}$ film.

m/z	Ion fragment	m/z	Ion fragment
101.908	$^{102}\text{Ru}^+$	260.122	$[(\text{ph-bpy})-\text{N}=\text{N}]^+$
105.048	$\text{C}_6\text{H}_5-\text{N}=\text{N}^+$	308.116	$[(\text{C}_6\text{H}_4)_2-\text{bpy}]^+$
153.062	$\text{C}_6\text{H}_5-\text{C}_6\text{H}_4^+$	331.992	$[\text{Ru}(\text{ph-bpy})]^+$
157.076	$[\text{bpy}+1\text{H}]^+$	411.995	$[\text{Ru}(\text{bpy})_2-2\text{H}]^+$
180.949	$\text{C}_6\text{H}_4-\text{N}=\text{N}-\text{C}_6\text{H}_4^+$	483.985	$[\text{Ru}(\text{bpy})(\text{ph-bpy})-4\text{H}]^+$
230.087	$[\text{ph-bpy}-1\text{H}]^+$	641.049	$[\text{Ru}(\text{bpy})_2(\text{ph-bpy})-2\text{H}]^+$
256.974	$[\text{Ru}(\text{bpy})-1\text{H}]^+$	144.965	PF_6^-

Table 6-2: Relevant ToF-SIMS peaks from Figure 6-6. The most common ruthenium isotope, ^{102}Ru is used where no mass number is listed.

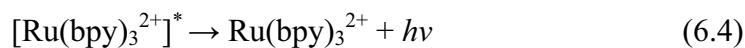
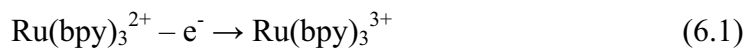
ToF-SIMS provides further evidence for the nature of the bonding between molecules of $\text{Ru}(\text{bpy})_2(\text{apb})^{2+}$ and between $\text{Ru}(\text{bpy})_2(\text{apb})^{2+}$ and the substrate. Peaks associated with the azo functionality are present, including fragment ions such as $\text{C}_6\text{H}_5-\text{N}_2^+$ and $\text{ph-bpy}-\text{N}_2^+$, confirming the azo bonding suggested by XPS analysis in this study and the

previous work of Doppelt.¹⁵ Other fragments such as C₆H₅-N=N-C₆H₄⁺ can be associated with the azo bonding to both the substrate and other ruthenium complexes within the film. Further investigation of the spectra reveals the presence of peaks that can be attributed to carbon-carbon bonding between complexes and the substrate. These fragments include C₆H₅-C₆H₄⁺, (C₆H₄)₂-bpy⁺ and (ph-bpy)₂⁺ confirming both modes of bonding in the layer. Because of the aromatic nature of the glassy carbon substrate, it is difficult to discriminate the bonding between monomers and bonding between monomer and substrate, with many of the fragments related to the intermonomer binding also consistent with fragments from either the substrate or the complex.

A long ToF-SIMS cycle time (150 μs) was employed to generate mass spectra with a mass range of about 3000 m/z in an attempt to detect oligomers of the complex at the surface. The presence of oligomers can be interpreted as consistent with a multilayered system. While no oligomers were observed, it is possible that these larger fragments are not produced in sufficient quantities to allow for detection via ToF-SIMS.

6.2.3. Electrochemiluminescence

The ECL activity of the attached Ru(bpy)₂(apb)²⁺ was investigated using the co-reactant DBAE as a model analyte. As shown in Figure 6-7, the electrochemical response features a broad peak at about 0.8 V due to the direct oxidation of DBAE. The voltammetric response for the Ru^{2+/3+} redox couple is somewhat ill-defined compared to Figure 6-2 because of the presence of the co-reactant. However, the ECL signal shows a large increase at precisely the potential corresponding to the oxidation of the Ru²⁺. This indicates that the ECL mechanisms previously suggested for Ru(bpy)₃²⁺ in the presence of tertiary amines, as given below, are also applicable in this case.^{16,17}



The slight increase in ECL signal at ~0.7 V prior to the main peak may be due to traces of the Ru(N)₅ complex in the layer produced by photolysis or as a side product during synthesis. The absence of a corresponding peak in the voltammogram (Figure 6-2) highlights the sensitivity of the ECL signal compared with the electrochemical signal. The ECL response of the modified electrode to varying concentrations of DBAE is presented in Figure 6-8. The layer is highly sensitive to the coreactant, achieving a low limit of detection 10 nM, and has a linear response to DBAE between concentrations of 10⁻⁸ and 10⁻⁴ M (R² = 0.99). These results show that this system is among the best to be reported to date in terms of sensitivity compared with previous work on ECL from modified electrodes.¹⁸

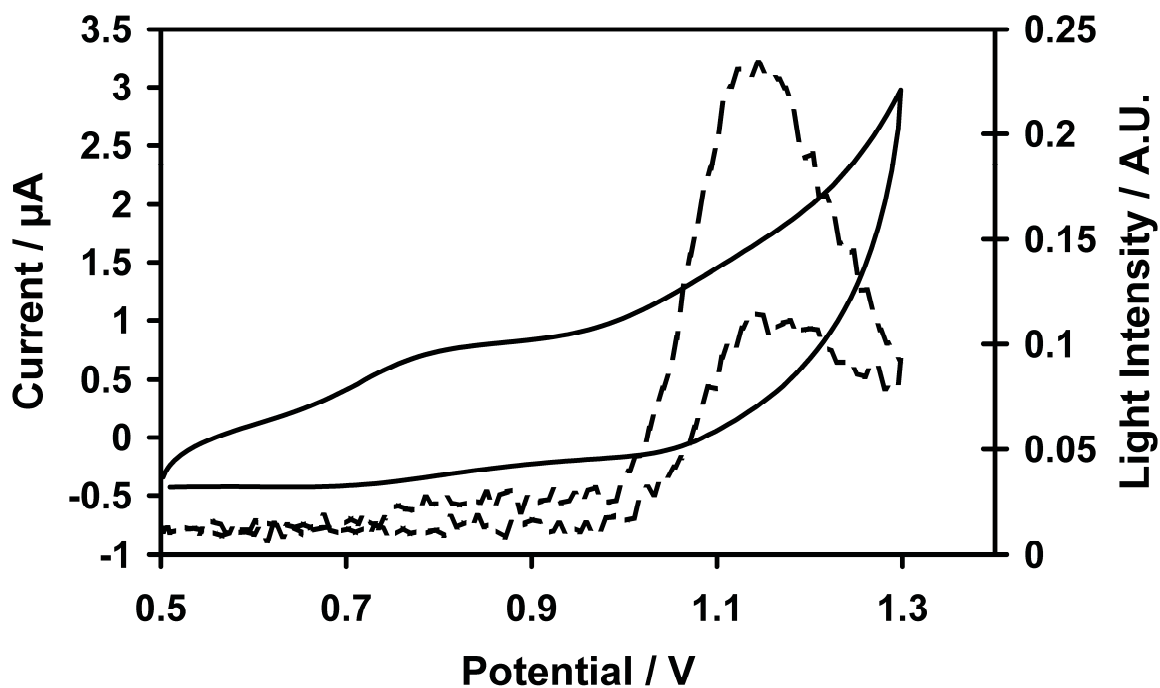


Figure 6-7: A CV showing the ECL activity (solid line) of the layer with a $10 \mu\text{M}$ solution of DBAE in 0.1 M LiClO_4 . The onset of light emission (dashed line) is co-incident with the oxidation potential of the ruthenium complex which is masked by the oxidation of the DBAE. Scan rate was 100 mV s^{-1} .

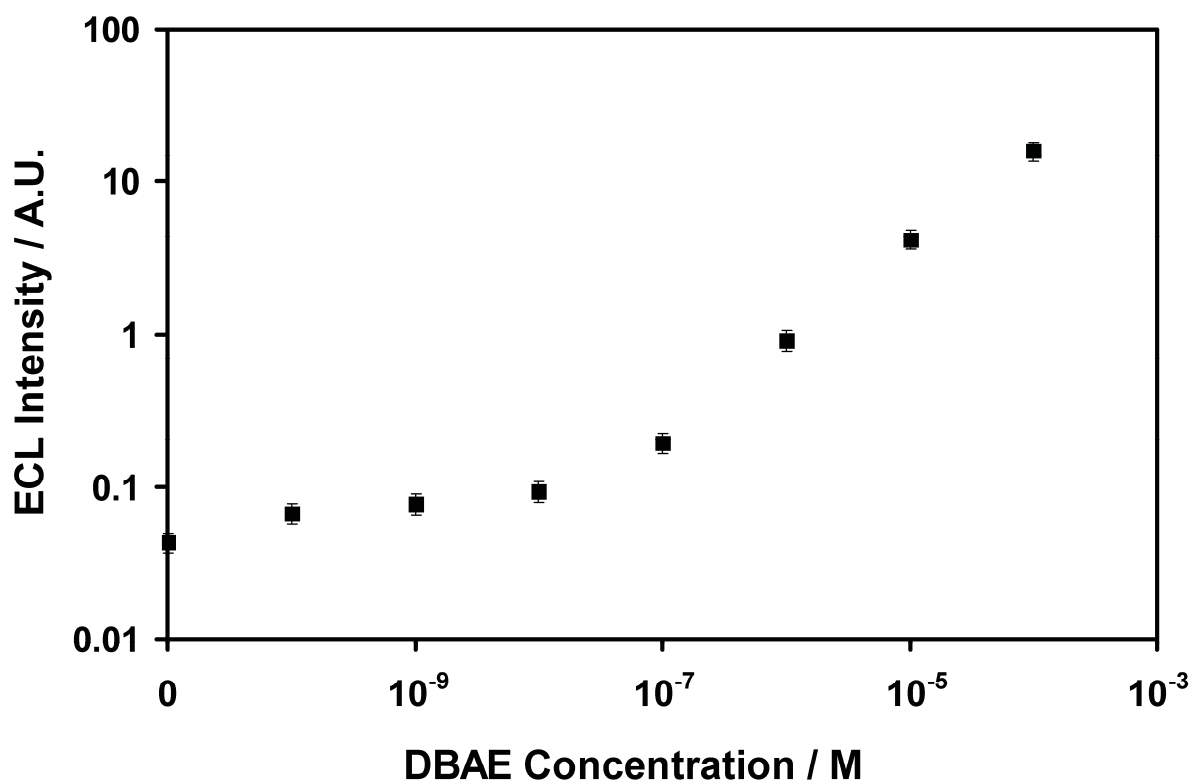


Figure 6-8: Dependence of ECL intensity on the concentration of the model analyte DBAE for a layer of $\text{Ru}(\text{bpy})_2(\text{apb})^{2+}$ deposited on GC. The error bars represent the maximum difference in response for three measurements.

6.2.4. Stability

Stability is a recurring issue with modified electrodes used for ECL-based sensing, chiefly because of the strongly oxidising conditions required to produce light emission. In order to investigate the long term stability of this layer, a series of CV experiments were run over a number of hours (1000 scans at 100 mV s⁻¹ between 0.5 and 1.25 V) to expose the film to the maximum oxidative stress possible in a period of use, with the resulting Ru²⁺/Ru³⁺ peak current shown in Figure 6-9. As the light emission from the film is dependent on the number of electrochemically active ruthenium centres present, this cycling can be used as a simple measure of the films performance over time. The data in Figure 6-9 shows an initial sharp degradation of the film which was followed by a gradual decrease in the peak current. Over the analysis period of 1000 scans (5 hrs) the film degraded to 90 % of the initial value. This degradation in performance is likely to be due to the removal of any complex that is physisorbed or trapped in the covalently bound film.¹⁹ The ECL signal from the layer after this period was also within 15 % of the initial value, demonstrating that any physisorbed material does not contribute significantly to the light emission. It should be noted that the stringent conditions under which the stability of the layer was tested (5 hrs of continuous cycling to potentials > 1 V) were chosen in order to emphasise the high level of stability of the system. The stress imposed on the layer under these conditions significantly exceeds that which would be expected in any normal period of use in a sensing context.

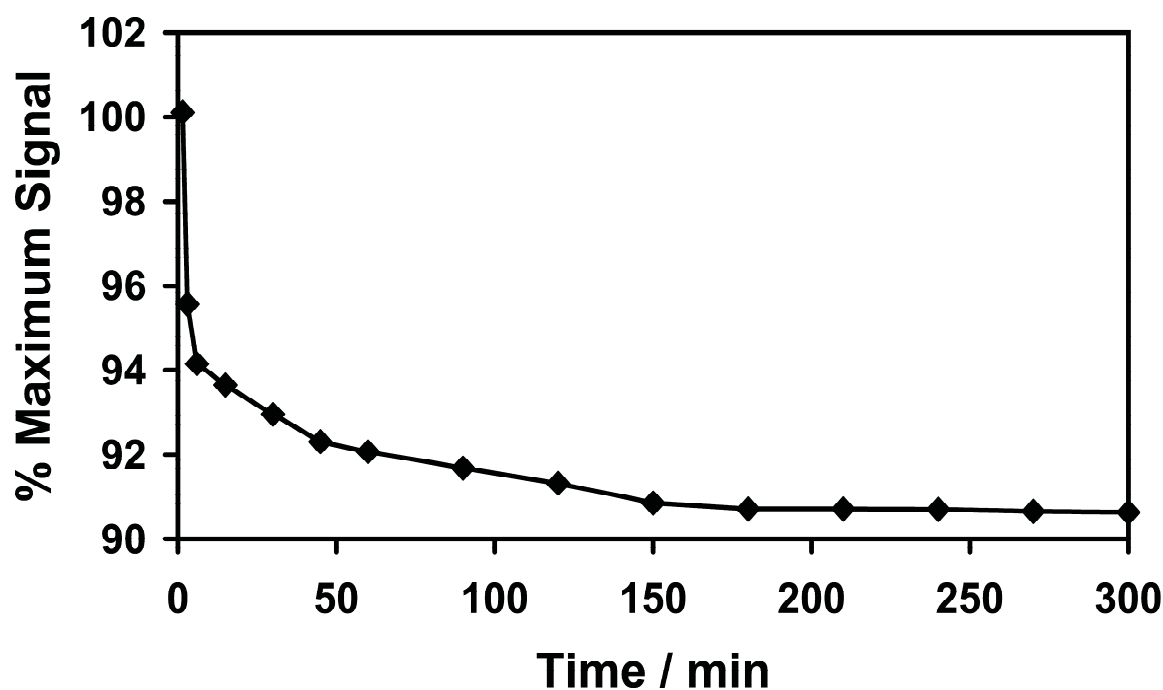


Figure 6-9: Stability of $\text{Ru}(\text{bpy})_2(\text{apb})^{2+}$ film to continuous voltammetric cycling in 0.1 M LiClO_4 between 0.5 and 1.3 V at a scan rate of 100mV/s. The graph shows the change in the peak oxidation current ($i_{p,ox}$) over time.

It has been suggested the reduction in peak current in $\text{Ru}(\text{bpy})_3^{2+}$ containing solid state devices is caused by either the removal of ruthenium redox sites from the surface,¹⁹ possibly through the cleaving of the azo bond,^{20,21} or its degradation into electrochemically inactive forms.²²⁻²⁴ To assist in determining the mechanism for ageing, XPS was conducted on samples before and after electrochemical degradation for a period of 5 hrs corresponding to a 10 % decrease in peak current. Figure 6-10 shows the C 1s and N 1s photoelectron regions before and after electrochemical degradation with Table 6-3 presenting the change in concentration and binding energy of each chemical species before and after the degradation. Unlike other XPS analyses discussed in this thesis, data in Table 6-3 cannot be presented effectively as normalised to the atomic concentration of ruthenium as the concentration of ruthenium could then not be described.

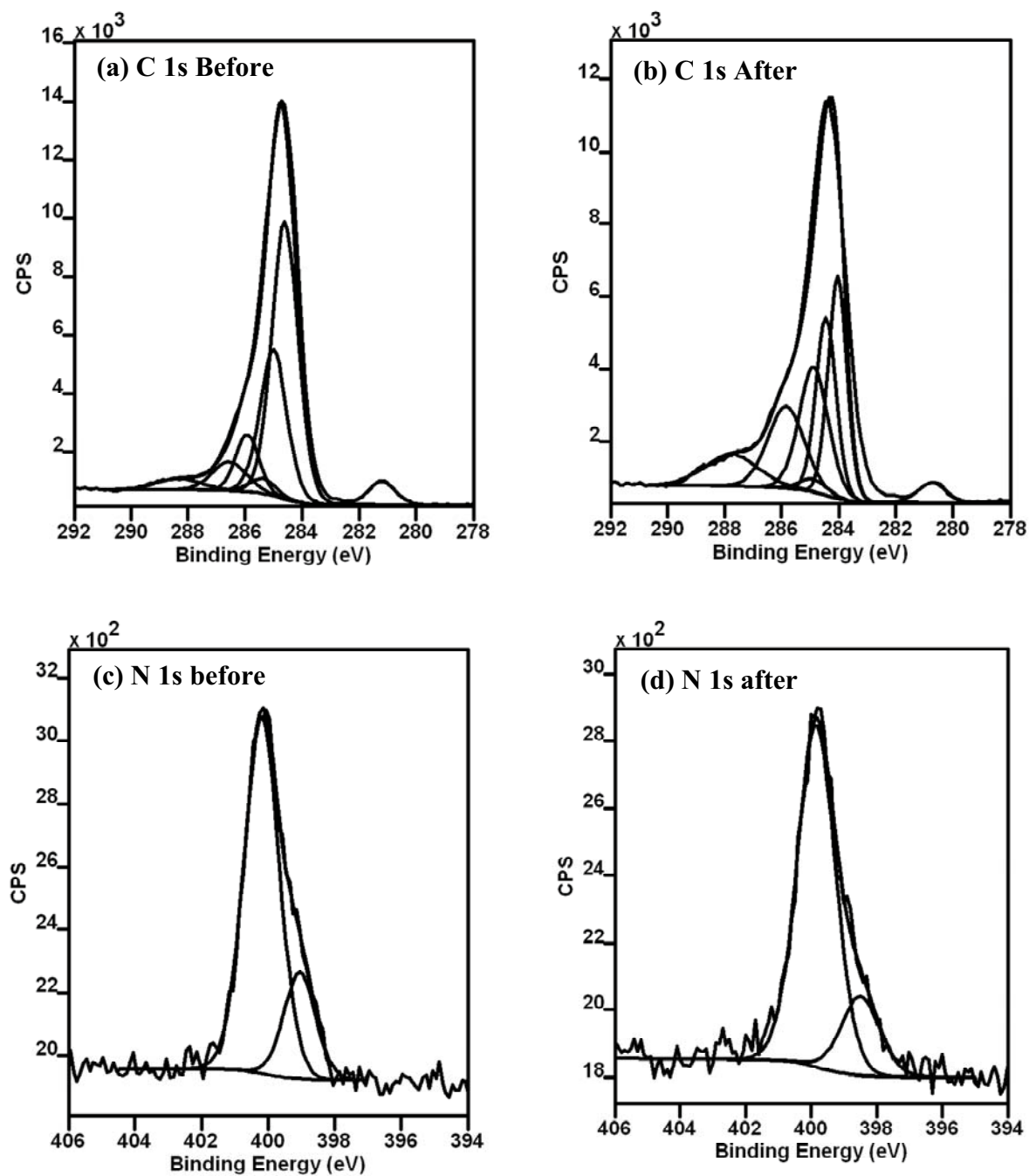


Figure 6-10: XPS spectra of C 1s and N 1s photoelectron regions before (images a and c) and after (images b and d) electrochemical cycling.

Element	Component	Before		After	
		BE (eV)	Atom %	BE (eV)	Atom %
F 1s	PF ₆ ⁻	686.4	0.9	N/A	N/A
O 1s	Oxides	532.2	18.9	532.2	25.8
N 1s	N _{bpy}	400.2	2.9	400.2	2.8
	-N=N-	399.1	0.8	399.0	0.6
C 1s	-COOH	ND	ND	289.2	1.4
	-C=O	288.2	3.3	287.9	4.5
	-C-O	286.5	6.0	286.4	9.1
	-C-N	285.7	8.6	285.6	8.0
	-C-C	285.0	14.2	285.0	6.1
	Aromatic carbon	284.6	44.1	284.6	40.5
Cl 2p_{3/2}	ClO ₄ ⁻	ND	ND	207.5	0.3
	ClO ₃ ⁻	ND	ND	200.3	0.5
	Cl ⁻	ND	ND	197.8	0.2
Ru 3d_{5/2}	Ru ²⁺	281.3	0.3	281.1	0.2

Table 6-3: Comparison of XPS components of Ru(bpy)₂(apb)²⁺ film before and after electrochemical ageing in 0.1 M LiClO₄. ND = Not Detected.

Table 6-3 shows that several changes occur with the ageing of the layer, with a large increase in oxygen concentration and corresponding decreases in ruthenium and nitrogen observed. The decrease in ruthenium concentration suggests the removal of Ru(bpy)₂(apb)²⁺ from the surface, which is further suggested by the decrease in the N_{azo} component. The partial decrease in the N_{azo} concentration may be due to the removal of ruthenium from the surface in the form of physisorbed dimers of Ru(bpy)₂(apb)²⁺ bound by an azo bridge as suggested previously.¹⁹ The increase in oxygen functionalisation can be attributed to the exposure of the modified electrode to highly oxidising potentials during electrochemical cycling. These high potentials can result in the degradation of the electrolyte, LiClO₄, increasing oxygen functionalisation at the surface. After electrochemical cycling, multiple chlorine species are observed at the surface, providing evidence for this mode of action. In comparison, a layer that was only stored in 0.1 M LiClO₄ over the same time period did not undergo any reduction in ruthenium concentration, with minimal increase in oxygen functionalisation and associated degradation of the perchlorate electrolyte ([ClO₄⁻] : [ClO₃⁻] + [Cl⁻] = 5.4 : 1 for the control film c.f. 0.4 : 1 for electrochemically cycled film).

6.3. Conclusions

The *in-situ* formation of the diazonium salt of Ru(bpy)₂(apb)²⁺ prior to its subsequent attachment to an electrode in aqueous media has been shown to be effective in producing stable highly responsive films for use in an ECL-based sensor. This strategy leads to highly stable, covalently-bound layers which will not desorb or degrade at the moderately high positive potentials required to oxidise the ruthenium complexes in the ECL cycle. Instability of, for example, thiol based monolayers on gold has been an obstacle to the creation of ECL active layers suitable for real-world sensing applications. The electrochemistry of the system is consistent with a surface-confined species with a surface coverage equivalent to up to 5 monolayers. Surface characterisation of the film correlates well to electrochemical measurements and suggests that the deposited multilayered film is attached to the surface almost exclusively via azo bonding.

The layer provides excellent ECL detection limits for the model analyte DBAE with a low limit of detection of 10 nM while providing a linear response over 4 orders of magnitude (10⁻⁸ M to 10⁻⁴ M). This performance may be related to the multilayer nature of the film with a large proportion of the ruthenium centres effectively isolated from quenching by the electrode surface. The film is also shown to be highly stable for example, the current response from the layer only decreases by < 10 % after redox cycling in supporting electrolyte for 5 hrs. This aqueous-based deposition method of an ECL active complex and the resulting film provides an excellent opportunity for the synthesis of sensitive and stable ECL-based sensors.

6.4. References

- (1) Joussetme, B.; Bidan, G.; Billon, M.; Goyer, C.; Kervella, Y.; Guillerez, S.; Hamad, E. A.; Goze-Bac, C.; Mevellec, J.-Y.; Lefrant, S.; *J. Electroanal. Chem.* **2008**, *621*, 277-285.
- (2) Agnes, C.; Arnault, J.-C.; Omnes, F.; Joussetme, B.; Billon, M.; Bidan, G.; Mailley, P.; *Phys. Chem. Chem. Phys.* **2009**, *11*, 11647-11654.
- (3) Liu, G.; Nguyen, Q. T.; Chow, E.; Bocking, T.; Hibbert, D. B.; Gooding, J. J.; *Electroanal.* **2006**, *18*, 1141-1151.
- (4) Delmar, M.; Desarmot, G.; Fagebaume, O.; Hitmi, R.; Pinson, J.; Savéant, J. M.; *Carbon* **1997**, *35*, 801-807.
- (5) Obeng, Y. S.; Bard, A. J.; *Langmuir* **1991**, *7*, 195-201.
- (6) Zanarini, S.; Rampazzo, E.; Bich, D.; Canteri, R.; Ciana, L. D.; Marcaccio, M.; Marzocchi, E.; Panciatichi, C.; Pederzoli, C.; Paolucci, F.; Prodi, L.; Vanzetti, L.; *J. Phys. Chem. C* **2008**, *112*, 2949-2957.
- (7) Susac, D.; Kono, M.; Wong, K. C.; Mitchell, K. A. R.; *App. Surf. Sci.* **2001**, *174*, 43-50.
- (8) Beamson, G.; Briggs, D. *High Resolution XPS of Organic Polymers: The Scienta ESCA300 Database*; John Wiley & Sons: Chichester, 1992.
- (9) Moulder, J. F.; Stickle, W. F.; Sobol, P. E.; Bomben, K. D. *Handbook of X-Ray Photoelectron Spectroscopy*; Perkin-Elmer Corporation - Physical Electronics Division: Eden Prairie, 1992.
- (10) Lui, G.; Klien, A.; Thissen, A.; Jaegermann, W.; *Surf. Sci.* **2003**, *539*, 37-48.
- (11) Finn, P.; Jolly, W. L.; *Inorg. Chem.* **1972**, *11*, 1434-1435.
- (12) Brant, P.; Felthan, R. D.; *J. Organometallic. Chem.* **1976**, *120*, C53-C57.
- (13) Laforgue, A.; Addou, T.; Belanger, D.; *Langmuir* **2005**, *21*, 6855-6865.

- (14) Saby, C.; Ortiz, B.; Champagne, G. Y.; Belanger, D.; *Langmuir* **1997**, *13*, 6805-6813.
- (15) Doppelt, P.; Hallais, G.; Pinson, J.; Podvorica, F.; Verneyre, S.; *Chem. Mater.* **2007**, *19*, 4570-4575.
- (16) Miao, W.; Choi, J.-P. In *Electrogenerated Chemiluminescence*; Bard, A. J., Ed.; Marcel Dekker, Inc.: New York, 2004.
- (17) Liu, X.; Shi, L.; Niu, W.; Li, H.; Xu, G.; *Angew. Chem. Int. Ed.* **2007**, *46*, 421-424.
- (18) Li, Y.; Yang, F.; Yang, X.; *Analyst* **2009**, *134*, 2100-2105.
- (19) Shewchuk, D. M.; McDermott, M. T.; *Langmuir* **2009**, *25*, 4556-4563.
- (20) Oakes, J.; Gratton, P.; *J. Chem. Soc., Perkin Trans. 2*, **1998**, 1857-1864.
- (21) Hodges, G. R.; Smith, J. R. L.; Oakes, J.; *J. Chem. Soc., Perkin Trans. 2*, **1999**, 1943-1952.
- (22) Bernhard, S.; Barron, J. A.; Houston, P. L.; Abruna, H. D.; Ruglovksy, J. L.; Gao, X.; Malliaras, G. G.; *J. Am. Chem. Soc.* **2002**, *124*, 13624-13628.
- (23) Kalyuzhny, G.; Buda, M.; McNeill, J.; Barbara, P.; Bard, A. J.; *J. Am. Chem. Soc.* **2003**, *125*, 6272-6283.
- (24) Gao, F. G.; Bard, A. J.; *Chem. Mater.* **2002**, *14*, 3465-3470.

Chapter 7: The Spontaneous Deposition of $\text{Ru}(\text{bpy})_2(\text{apb})^{2+}$ Films

7.1. Introduction

Diazonium salts have recently been reported to undergo binding to a substrate without the application of a potential.¹⁻⁶ This deposition method provides opportunities for the creation of both electrochemiluminescent (ECL) and chemiluminescent (CL) based sensing interfaces, allowing for relatively facile attachment. The simplification in the deposition step is attractive for a number of reasons, not least because it is expected to significantly reduce sensor manufacturing costs. In addition, the spontaneous deposition of diazoniums extends the applicability of the approach allowing for attachment to electrically isolated substrates as encountered with the fabrication of micropatterned surfaces and some CL based sensors.

In this chapter the deposition of an ECL active film of $\text{Ru}(\text{bpy})_2(\text{apb})^{2+}$ via the spontaneous deposition of the diazonium salt from acidic media is demonstrated. The film is subsequently characterised with electrochemical and surface analysis techniques, including CV, XPS and ToF-SIMS. The creation of micropatterned layers of $\text{Ru}(\text{bpy})_2(\text{apb})^{2+}$ is demonstrated and assessed via AFM. This chapter is deliberately limited in its scope with the objective of demonstrating a proof-of-concept for the development of sensing devices via spontaneously deposited diazonium films.

7.2. Spontaneous Deposition of $\text{Ru}(\text{bpy})_2(\text{apb})^{2+}$ onto Glassy Carbon

Glassy carbon electrodes were modified by the immersion of the electrode in a room temperature solution containing 1.2 mM $\text{Ru}(\text{bpy})_2(\text{apb})^{2+}$, 1.5 mM NaNO_2 and 0.5 M HCl. Electrodes were immersed in the solution in darkness for a period of up to 2 hrs. The open circuit potential (OCP) of the electrode was measured relative to an Ag/AgCl reference electrode to monitor the deposition. The OCP is a function of the change in surface charge and as such can be successfully used to probe changes at the electrode solution interface resulting from deposition and other phenomena. Previous studies have shown this technique to be potentially suitable for the monitoring of the spontaneous deposition of diazonium cations in acetonitrile.¹ Figure 7-1 demonstrates the change in OCP at the electrode surface while immersed in the aqueous deposition solution. As the deposition progresses a small constant decrease of 15 mV is observed over the measured period.

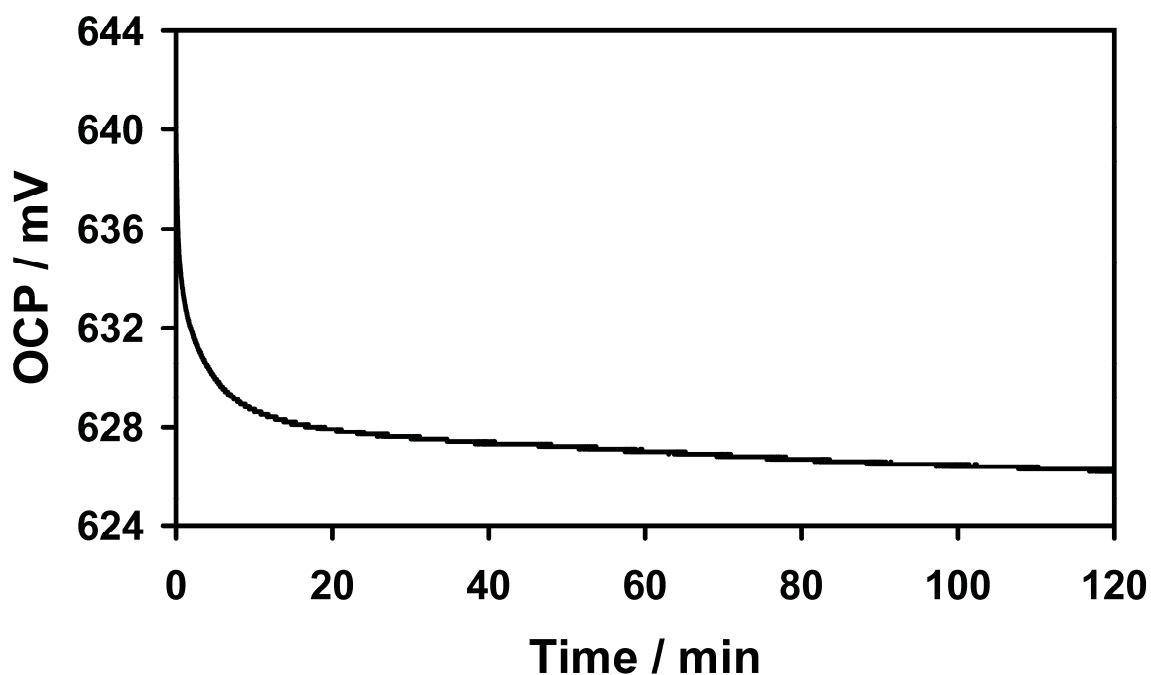


Figure 7-1: Measurement of Open Circuit Potential during the spontaneous deposition of $\text{Ru}(\text{bpy})_2(\text{apb})^{2+}$ from a 0.5 M HCl solution containing 1.5 mM NaNO_2 .

This constant decrease in potential is in contrast to the behaviour observed for nitrobenzenediazonium cations in acetonitrile at a gold electrode.¹ Downard et al. having previously observed the accumulation of positive charge and then subsequent discharging of the gold surface while exposed to nitrobenzenediazonium. This behaviour was tentatively attributed to the gold surface mediating electron transfer between adventitious impurities in the reaction solution and the diazonium cation, resulting in film formation.¹ In Figure 7-1 however, no accumulation of positive charge is observed with only a small constant reduction in OCP measured. This constant change in surface potential suggests that the insulating effect of the deposited diazonium limiting film formation¹ are not applicable in this system, with the results presented below suggesting multilayered film formation is possible. Furthermore, the differences in OCP measurements between aqueous and aprotic media may be due to the changes in experimental conditions (acetonitrile and Au substrate compared with aqueous solution. and GC substrate) required to measure the OCP for a diazonium cation generated *in-situ*.

Figure 7-2 presents a CV of the resulting electrode in blank electrolyte after deposition confirming the attachment of Ru(bpy)₂(apb)²⁺ to the electrode. An oxidation peak at 1.1 V is observed and is representative of the Ru²⁺/Ru³⁺ redox couple. This oxidation peak is consistent with observations from the electrodeposited layer formed from the same compound (Chapter 6).⁷ After background subtraction is performed on the voltammetric peak, a Gaussian peak shape is observed. The absence of peak tailing and the linear dependence of peak current on scan rate proves that the wave observed for the Ru²⁺/Ru³⁺ redox couple is due to a surface-confined species and is bound to the electrode. The redox couple is stable and is maintained even after rinsing in 0.5 M HCl, suggesting the surface confinement is not exclusively caused by any physisorbed material but is instead due to a

covalent attachment. The integration of the charge under the background corrected voltammetric peaks reveals that the surface coverage (Γ) of the complex on the electrode surface is $2.7 \times 10^{-10} \pm 0.98 \times 10^{-10} \text{ mol cm}^{-2}$ (average value from 8 electrodes). This value is greater than the estimated theoretical coverage for a close packed monolayer for the complex ($1.4 \times 10^{-10} \text{ mol cm}^{-2}$) indicating the presence of a multilayered system equivalent to 1.9 ± 0.7 monolayers. These results show that the spontaneously deposited film results in a thinner film than the equivalent electrodeposited version (average thickness of 3.4 monolayers).

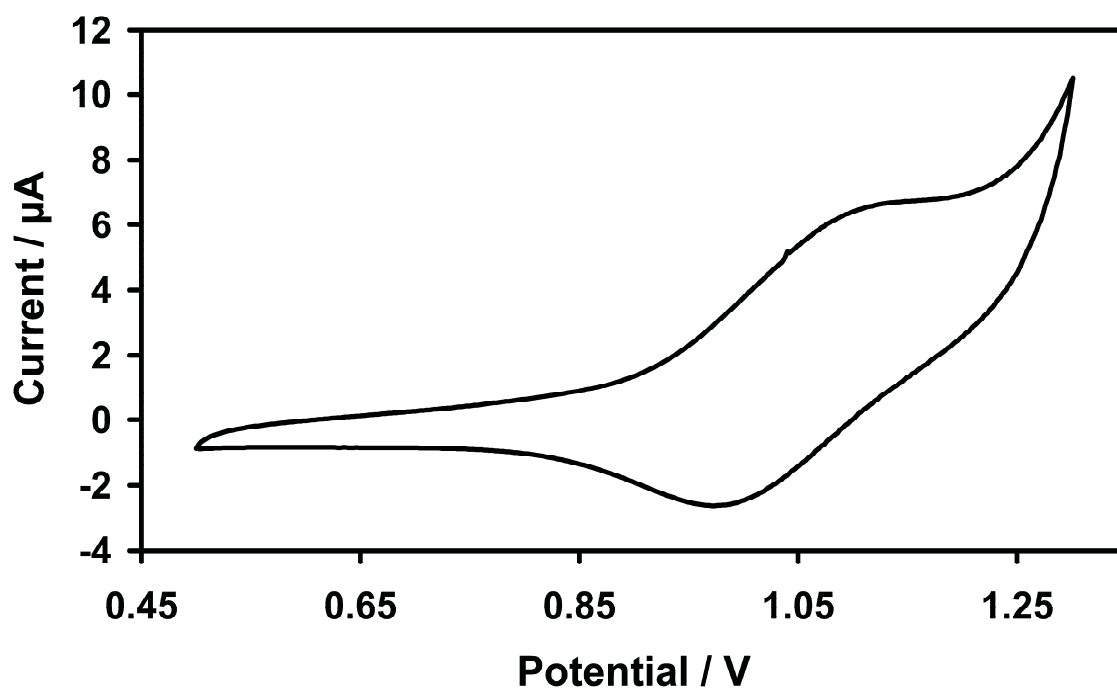


Figure 7-2: Electrochemical response of a GC electrode in 0.1 M LiClO_4 after immersion in a solution containing $\text{Ru}(\text{bpy})_2(\text{apb})^{2+}$ and NaNO_2 for a period of 2 hours. Scan rate was 100 mV s^{-1} .

7.2.1. Surface Analysis

The spontaneously deposited film was analysed with XPS to investigate bonding of $\text{Ru}(\text{bpy})_2(\text{apb})^{2+}$ to the electrode. Figure 7-3 presents high resolution C 1s and N 1s photoelectron spectra of the spontaneously deposited $\text{Ru}(\text{bpy})_2(\text{apb})^{2+}$ film. The relative atomic concentrations of each chemical environment within the film are described in

Table 7-1. The presence of $\text{Ru}(\text{bpy})_2(\text{apb})^{2+}$ on the electrode surface is confirmed by the observation of the Ru $3d_{5/2}$ photoelectron peak at 281.3 eV and corresponds to Ru in the $2+$ oxidation state.⁸ The Ru $3d_{3/2}$ peak occurs at a binding energy 4.17 eV higher than the Ru $3d_{5/2}$ peak and lies underneath the aliphatic C 1s component. Other peaks assigned in the C 1s region of both films include aromatic and aliphatic carbon ($E_B = 284.6$ and 285.0 eV respectively), C-N ($E_B = 285.5$ eV), C-O ($E_B = 286.0$ eV), C=O ($E_B = 286.6$ eV). The peak intensities of these components were fitted to match the concentrations of nitrogen and oxygen observed from the N 1s and O 1s photoelectron lines respectively. These peak assignments are consistent with those previously reported.^{9,10}

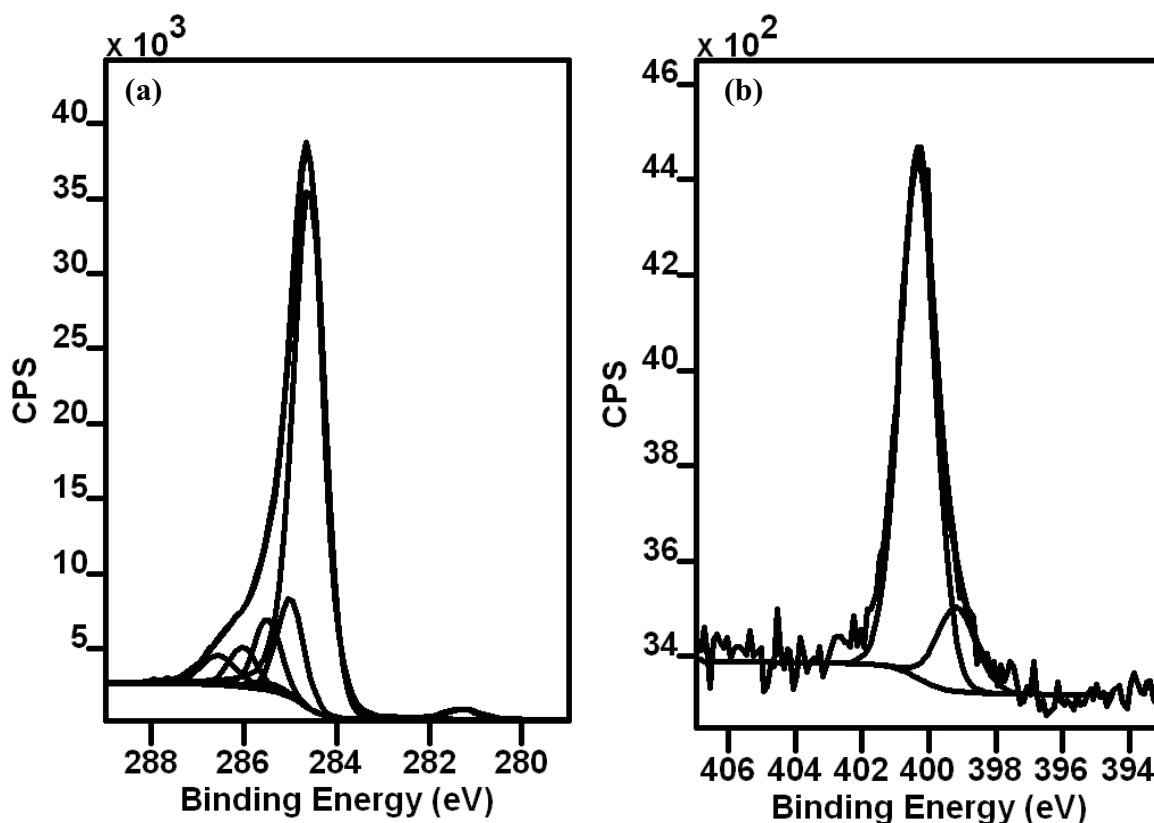


Figure 7-3: XPS spectra of C 1s (a) and N 1s (b) photoelectron regions for the spontaneously deposited $\text{Ru}(\text{bpy})_2(\text{apb})^{2+}$ film.

Element	Component	Binding Energy (eV)	Atomic %	Normalised to Ru 3d
O 1s	Oxides	532.5	11.0	68.2
N 1s	N _{bpy}	400.5	1.8	11.5
	-N=N-	399.0	0.3	2.0
C 1s	-C=O	286.6	4.0	24.9
	-C-O	286.0	4.2	26.0
	-C-N	285.5	7.1	43.9
	-C-C	285.0	10.0	62.0
	Aromatic carbon	284.6	60.7	376.8
Cl 2p _{3/2}	-O-Cl	200.3	0.3	1.8
	Cl ⁻	198.2	0.2	1.2
S 2p _{3/2}	SO ₄ ²⁻	167.7	0.4	2.3
Ru 3d _{5/2}	Ru ²⁺	281.3	0.2	1.0

Table 7-1: Binding energy and relative concentration of components for the Ru(bpy)₂(apb)²⁺ film as determined by XPS. Binding energy for Ru 3d peak is given from the 3d_{5/2} component with the 3d_{3/2} existing at a binding energy 4.17 eV higher. Both components are included as one peak for quantification.

Two peaks at 399.0 and 400.5 eV are observed in the N 1s region spectrum (Figure 7-3b). As discussed in previous chapters, the peak at higher binding energy (400.5 eV) can be attributed to the pyridyl nitrogen present in the complex,^{11,12} while the peak at 399.0 eV is associated with azo bonding.¹³ Importantly, no peak corresponding to the positively charged nitrogen in the diazonium functional group ($E_B \approx 406$ eV) is observed, confirming that the film is not physisorbed to the electrode surface.^{11,14} The ratio of Ru to N_{azo} atoms observed via XPS is 1 to 2 suggesting that the layer is exclusively bound through the azo functionality. The ratio of Ru to N_{bpy} at the surface is 1 to 11.5 which is in excess to that expected from the deposited complex. This excess nitrogen may be a contribution from the underlying glassy carbon substrate. When contributions expected from Ru(bpy)₂(apb)²⁺ are subtracted, a N_{bpy} concentration of 0.8 atom % is obtained. In comparison the concentration of nitrogen observed at a pristine glassy carbon surface was 0.7 atom % (Section 5.2.2.2.).

In comparison to the electrodeposited film (Chapter 6) the XPS results show a decrease in both ruthenium and N_{azo} concentration (0.7 to 0.2 atom % for Ru and 2.5 to 0.3 atom % for N_{azo}). This reduction in overall ruthenium concentration is consistent with electrochemical results that suggest a lower surface coverage (4.8×10^{-10} mol cm⁻² for the electrodeposited film c.f. 2.7×10^{-10} mol cm⁻² for the spontaneously deposited film).

ToF-SIMS was undertaken to further assess the binding of the deposited layer. The resulting positive mass spectrum is presented in Figure 7-4, with a list of the relevant mass fragments presented in Table 7-2. A number of peaks associated with Ru(bpy)₂(apb)²⁺ are detected, with the compound fragmenting most typically through the loss of a ligand from the complex, resulting in groups of peaks associated with Ru(bpy)₂(ph-bpy)⁺ (m/z = 638), Ru(bpy)₂⁺ (m/z = 412), Ru(bpy)(ph-bpy)⁺ (m/z = 485), Ru(ph-bpy)⁺ (m/z = 332) and Ru(bpy)⁺ (m/z = 257) fragments.

Figure 7-4 also confirms the bonding of the complex to the substrate with no residual amine detected. As with the electrodeposited species, peaks corresponding to Ru(bpy)₂(apb)²⁺ bound within the layer and to the substrate via both carbon-carbon bonds and azo bonds are observed (Table 7-2). Due to the aromatic nature of the glassy carbon substrate it is difficult to distinguish between bonding linking individual complexes and bonding of complex to substrate, with peaks including; C₆H₅-C₆H₄⁺ (m/z = 153), C₆H₅-N=N-C₆H₄⁺ (m/z = 181), Ru(ph-bpy)₂⁺ (m/z = 564) and Ru(ph-bpy)₂N₂⁺ (m/z = 592) being attributable to binding to substrate and between complexes. The presence of several fragments containing two ruthenium centres provides evidence for the formation of a multilayered film structure. Peaks including Ru₂(bpy)(ph-bpy)⁺ (m/z = 590) and Ru₂(ph-bpy)₂⁺ (m/z = 666) provide direct evidence for carbon-carbon

bonding between ruthenium centres. Equivalent binding arrangements for the azo functionality are inferred through the observation of peaks relating to $\text{Ru}_2(\text{bpy})(\text{ph-bpy})\text{N}_2^+$ ($m/z = 620$) and $\text{Ru}_2(\text{bpy})(\text{ph-bpy})\text{N}^+$ ($m/z = 606$) mass fragments.

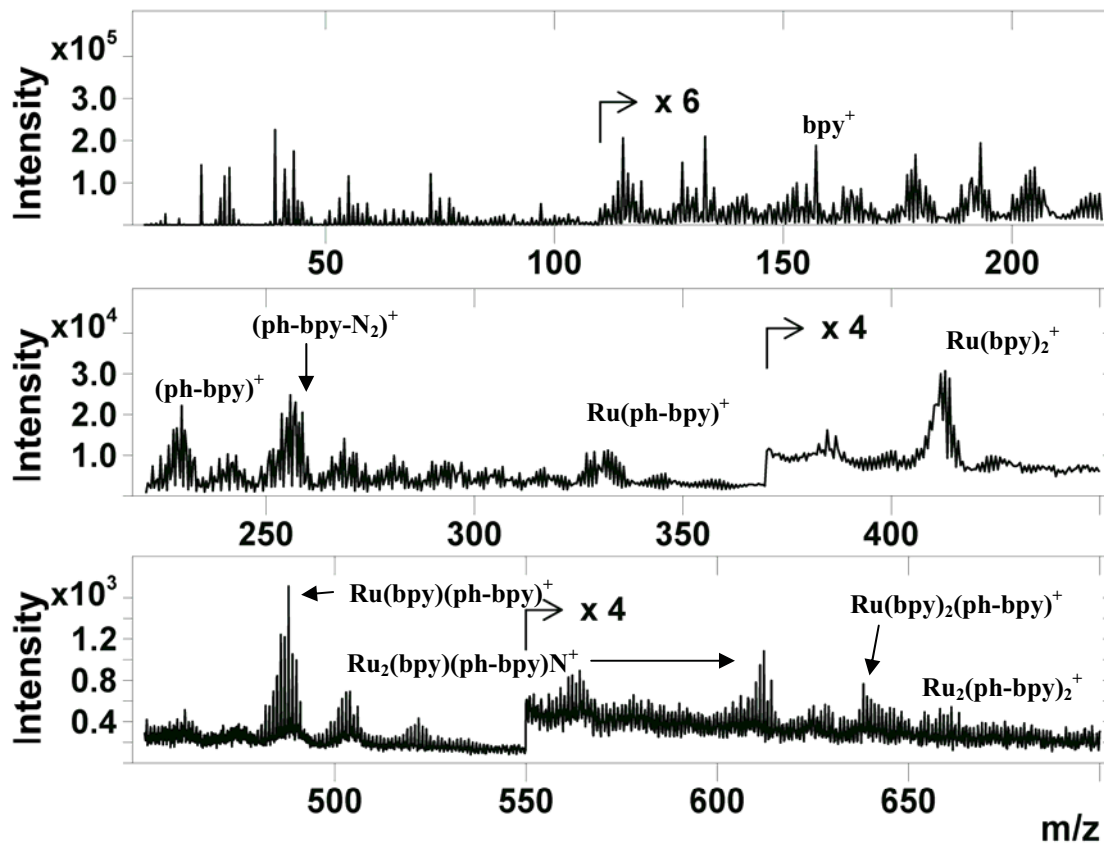


Figure 7-4: ToF-SIMS spectrum of a spontaneously deposited $\text{Ru}(\text{bpy})_2(\text{apb})^{2+}$ film onto a glassy carbon substrate.

m/z	Ion fragment	m/z	Ion fragment
102.908	$^{102}\text{Ru}^+$	412.026	$\text{Ru}(\text{bpy})_2^+$
105.048	$\text{C}_6\text{H}_5\text{-N}=\text{N}^+$	485.980	$\text{Ru}(\text{bpy})(\text{ph-bpy})^+$
153.057	$\text{C}_6\text{H}_5\text{-C}_6\text{H}_4^+$	641.106	$[\text{Ru}(\text{bpy})_2(\text{ph-bpy})\text{-2H}]^+$
157.077	$[\text{bpy}+\text{H}]^+$	564.060	$\text{Ru}(\text{ph-bpy})_2^+$
181.072	$\text{C}_6\text{H}_5\text{-N}=\text{N-C}_6\text{H}_4^+$	590.068	$\text{Ru}_2(\text{bpy})(\text{ph-bpy})^+$
231.101	$[\text{ph-bpy}]^+$	591.987	$\text{Ru}(\text{ph-bpy})_2\text{N}_2^+$
256.967	$[\text{Ru}(\text{bpy})\text{-1H}]^+$	606.107	$\text{Ru}_2(\text{bpy})(\text{ph-bpy})\text{N}^+$
259.124	$[(\text{ph-bpy})\text{-N}=\text{N}]^+$	619.970	$\text{Ru}_2(\text{bpy})(\text{ph-bpy})\text{N}_2^+$
333.004	$\text{Ru}(\text{ph-bpy})^+$	664.982	$[\text{Ru}_2(\text{ph-bpy})_2\text{-1H}]^+$
361.002	$[\text{Ru}(\text{ph-bpy})\text{-N}=\text{N}]^+$	144.971	PF_6^-

Table 7-2: Relevant mass fragments from the ToF-SIMS spectrum presented in Figure 7-4. The most common ruthenium isotope, ^{102}Ru is used where no mass number is listed.

7.2.2. ECL Response

The ECL activity of the spontaneously attached $\text{Ru}(\text{bpy})_2(\text{apb})^{2+}$ was investigated using the co-reactant 2-dibutylaminoethanol (DBAE). Figure 7-5 shows the electrochemical response of the film and resultant light emission in a solution containing 100 μM DBAE. The oxidation of Ru^{2+} to Ru^{3+} is observed at a potential of 1.0 V. The diminished peak current observed for the Ru^{3+} reduction in the scan suggests that the Ru^{3+} is being chemically reduced. The increase in light emission observed in Figure 7-5 corresponds to the oxidation potential of the immobilised ruthenium complex observed in Figure 7-2 with light emission peaking at potential of ~ 1.10 V. The co-incident emission of light at the $\text{Ru}^{2+}/\text{Ru}^{3+}$ redox couple suggests that the ECL mechanisms previously suggested for $\text{Ru}(\text{bpy})_3^{2+}$ are also applicable in this case (Section 6.2.3).^{7,15} The films response to various concentrations of DBAE is presented in Figure 7-6. The layer is reasonably sensitive to the model analyte achieving a limit of detection 10^{-5} M. The layer has a linear response to DBAE between concentrations of 10^{-5} and 10^{-2} M. The reduced response of the spontaneously deposited film when compared to the electrodeposited film (linear range between 10^{-8} and 10^{-4} M) may be due to the lower surface coverage of the spontaneously deposited film, reducing the number of reaction centres available to emit light.

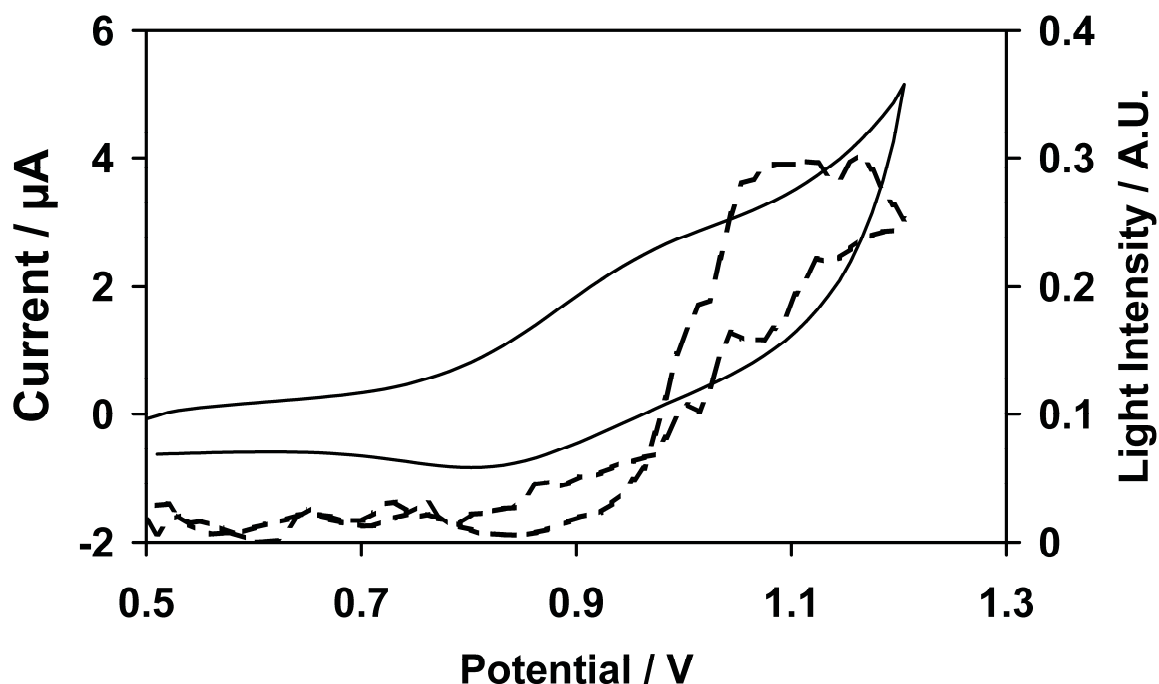


Figure 7-5: A CV (solid line) showing the ECL activity of the layer with a 100 μM solution of DBAE in 0.1M phosphate buffer solution (pH = 7.5). The onset of light emission (dashed line) is co-incident with the oxidation potential of the ruthenium complex. Scan rate was 100 mV s^{-1} .

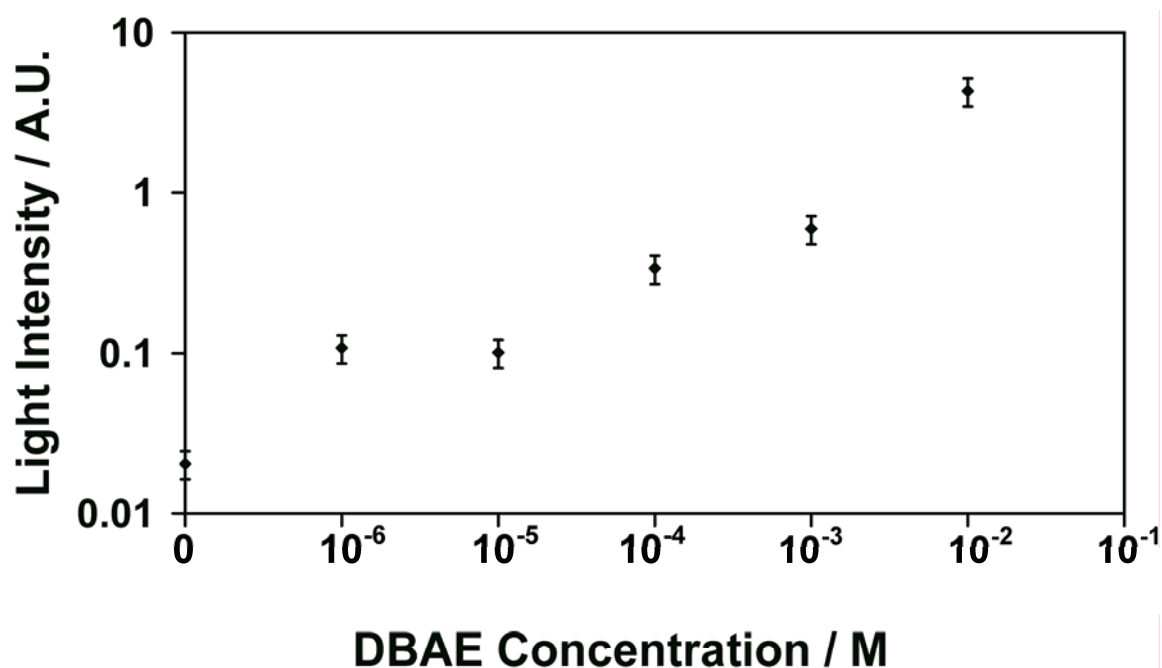


Figure 7-6: Dependence of ECL intensity on the concentration of DBAE for a spontaneously deposited layer of $\text{Ru}(\text{bpy})_2(\text{apb})^{2+}$ on a GC electrode. The error bars represent the maximum difference in response for three measurements.

7.2.3. Stability

The stability of the film was assessed using the constant cycling method described in Chapters 4 and 6. This method provides a film with a high level of oxidative stress over a short period of time, hastening any degradation processes. Figure 7-7 shows the change in the peak $\text{Ru}^{2+}/\text{Ru}^{3+}$ oxidation current of the film with respect to time (2000 scans at 100 mV s^{-1} between a potential of 0.5 V and 1.25 V in 0.1 M LiClO_4). As with the electrodeposited layer presented in Chapter 6, there is a gradual decrease in peak current over the course of several hours. The layer starts to plateau at $\sim 35\%$ of the initial peak current after 150 minutes (2.5 hrs, 600 scans) before a slow degradation reduces the response of the layer to 30 % of the initial value after 500 minutes (8.3 hrs, 2000 scans). The initial degradation phase could possibly be attributed to removal of physisorbed material, including unbound oligomers as previously discussed in the literature.^{1,7,16} This degradation also occurs over a similar time period to the electrodeposited films described in Chapter 6. The large decrease in peak current over this timescale (65 % decrease c.f. 10 % for the electroreduced film) suggests that a greater proportion of the film is in the form of physisorbed oligomers as observed in similar systems.¹ This difference in layer make-up may be due to a difference in the deposition kinetics between the two types of film with the spontaneous deposition pathway having a smaller driving force. The second slower stage of film degradation may be a result of the breakdown of the $\text{Ru}(\text{bpy})_2(\text{apb})^{2+}$ remaining at the electrode surface.

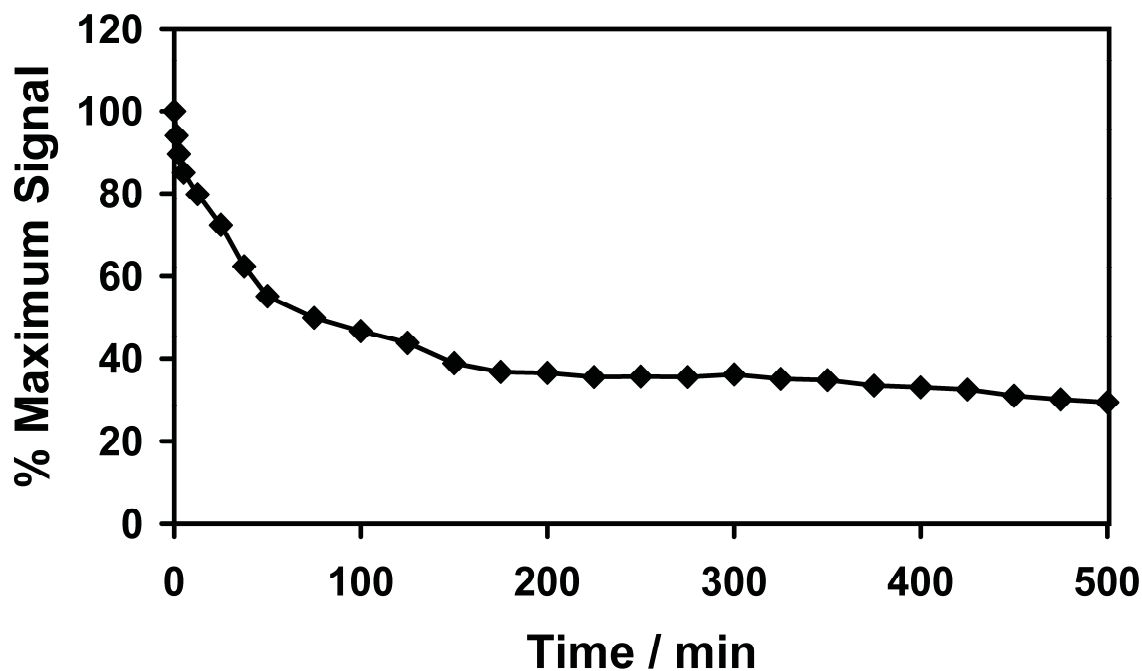


Figure 7-7: Oxidative response over time of a spontaneously deposited $\text{Ru}(\text{bpy})_2(\text{apb})^{2+}$ layer. Films were continuously scanned at between 0.5 V and 1.25 V at a scan rate of 100 mV s^{-1} , in 0.1 M LiClO_4 .

7.3. Spontaneous Deposition of $\text{Ru}(\text{bpy})_2(\text{apb})^{2+}$ onto Diamond Like Carbon

The spontaneous deposition of diazoniums can be used to modify patterned surfaces by the selective deposition onto conductive regions of the surface. This deposition approach may prove useful for the development of micro-arrays and other related sensing technologies. To assess the suitability of this deposition method for the patterning of surfaces, the complex was deposited onto a surface of silicon nitride micropatterned with Diamond Like Carbon (DLC) features as shown in Figures 7-8 and 7-9. Diazoniums have been shown to deposit on a range of conductive materials including carbon allotropes such as doped diamond and glassy carbons. DLC is a conductive carbonaceous material that can be deposited via electron beam irradiation in the presence of a carbon source with well characterised and controlled properties.¹⁷ In contrast silicon nitride is a highly insulating material with a high surface resistivity of $10^{13} \text{ } \Omega \text{ cm}^{-2}$.¹⁸ The resulting

micropatterned surface provides an excellent platform to assess the suitability of spontaneous deposition of ruthenium complexes for the modification of patterned surfaces.

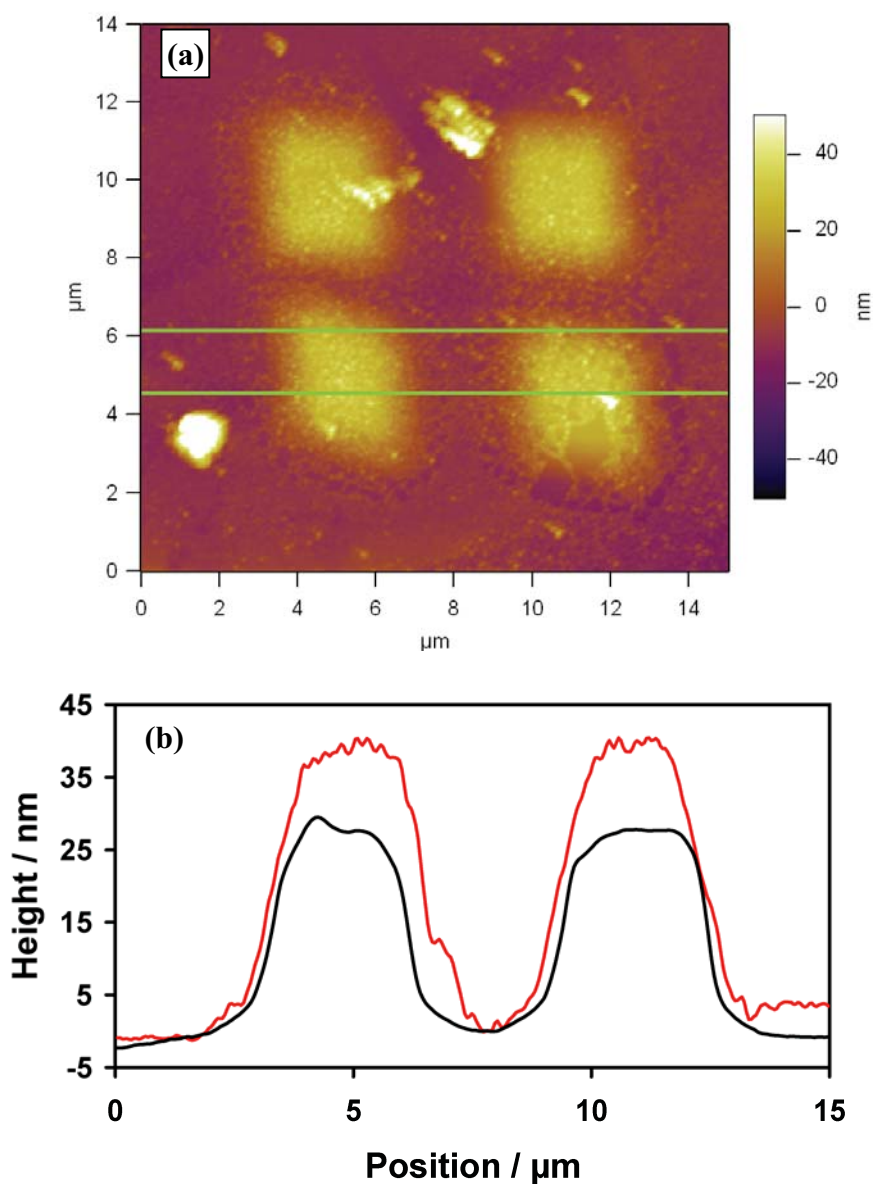


Figure 7-8: AFM micrograph of the $\text{Ru}(\text{bpy})_2(\text{apb})^{2+}$ coated DLC patterned surface (a). The average cross section for two of the DLC squares as defined by the green lines in (a) is shown in (b) with traces representing the surface before (black line) and after deposition of $\text{Ru}(\text{bpy})_2(\text{apb})^{2+}$ (red line). An average height increase of 10 nm in feature size is observed after deposition.

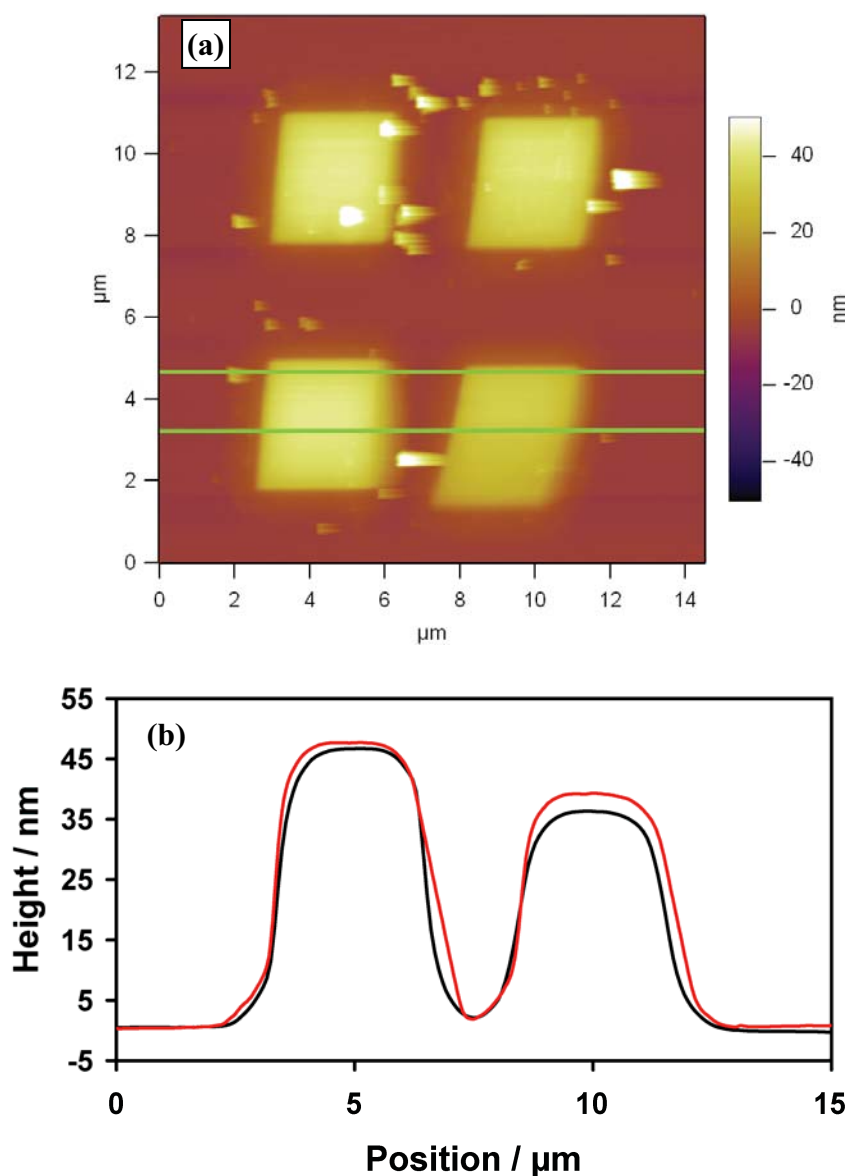


Figure 7-9: AFM micrograph of the DLC patterned surface after immersion in a 0.5 M HCl solution containing NaNO_2 (a). The average cross section for two of the DLC squares as defined by the green lines in (a) is shown in (b) traces representing the surface before (black line) and after immersion (red line) in the solution. After immersion a maximal height increase of 3 nm observed.

The spontaneous deposition of $\text{Ru}(\text{bpy})_2(\text{apb})^{2+}$ onto the DLC patterned surface was undertaken by immersing the pattern in a room temperature solution containing 1.2 mM $\text{Ru}(\text{bpy})_2(\text{apb})^{2+}$, 1.5 mM NaNO_2 and 0.5 M HCl for a period of an hour before rinsing in water and ethanol. Figure 7-8 shows AFM height traces of a surface after immersion in a solution containing $\text{Ru}(\text{bpy})_2(\text{apb})^{2+}$. Cross sections taken before and after deposition of $\text{Ru}(\text{bpy})_2(\text{apb})^{2+}$ show an average height increase of 13 nm. In comparison, control

samples immersed in only HCl and NaNO₂ show an increase in height of no more than 3 nm at the highest point (Figure 7-9). This increase in height suggests that the Ru(bpy)₂(apb)²⁺ preferentially attaches to the surface of the DLC as opposed to the silicon nitride. A small (~4.5 nm) inhomogeneous deposition of material onto the silicon nitride substrate is observed in Figure 7-9a. This deposition is possibly due to residual Ru(bpy)₂(apb)²⁺ precipitating out of solution upon washing of the substrate in aqueous media.

The measured thickness of the film on DLC is larger than expected from surface coverage measurements on glassy carbon (Section 7.2) which indicate a surface coverage equivalent to two monolayers (close packed). From this surface coverage a height increase of 3 nm would be expected. This large difference in film thickness may indicate a more open and porous film morphology with the rate of reaction between diazonium and bound diazonium being faster than that between diazonium and DLC.^{19,20} The roughened surface of the deposited film observed in Figure 7-8 when compared to the control (Figure 7-9) may provide further evidence for this open morphology.

7.4. Conclusions

The spontaneous deposition of the diazonium salt of Ru(bpy)₂(apb)²⁺ from an aqueous solution has been shown to be successful in the formation of an ECL active film at an electrode. The film is sensitive to DBAE, with a limit of detection of 10⁻⁵ M while providing a linear response to DBAE between concentrations of 10⁻⁵ and 10⁻² M. Electrochemical cycling experiments indicate that the film is stable with the peak current of the Ru²⁺/Ru³⁺ redox couple degrading to 35 % of the initial signal before being stable for over 5 hrs.

Surface characterisation of the film by XPS and ToF-SIMS demonstrates that the film is covalently bound to the electrode via both azo and carbon-carbon bonding as is observed with electrodeposited films. However, both XPS and electrochemical evidence suggests less material is deposited via the spontaneous pathway than compared to the electrodeposited attachment, with electrochemical measurements suggesting a surface coverage of $2.7 \times 10^{-10} \pm 9.8 \times 10^{-11} \text{ mol cm}^{-2}$, which is the equivalent of a film that is 1.9 ± 0.7 monolayers thick.

The use of the diazonium attachment for selective deposition onto patterned substrates has also been demonstrated via the spontaneous pathway. AFM measurements reveal that Ru(bpy)₂(apb)²⁺ can be selectively deposited onto DLC structures built onto an insulating silicon nitride substrate, with the produced coating being 13 nm thick. This selective deposition onto electrically isolated substrates may provide simplified control for the creation of both ECL and CL based sensing systems for a variety of online systems including Flow Injection Analysis and lab-on-a-chip applications.

7.5. References

- (1) Lehr, J.; Williamson, B. E.; Flavel, B. S.; Downard, A. J.; *Langmuir* **2009**, *25*, 13503-13509.
- (2) Chamoulaud, G.; Belanger, D.; *J. Phys. Chem. C* **2007**, *111*, 7501-7507.
- (3) Itoh, T.; McCreery, R. L.; *J. Am. Chem. Soc.* **2002**, *124*, 10894-10902.
- (4) Stewart, M. P.; Maya, F.; Kosynkin, D. V.; Dirk, S. M.; Stapleton, J. J.; McGuinness, C. L.; Allara, D. L.; Tour, J. M.; *J. Am. Chem. Soc.* **2004**, *126*, 370-378.
- (5) Price, B. K.; Hudson, J. L.; Tour, J. M.; *J. Am. Chem. Soc.* **2005**, *127*, 14867-14870.
- (6) Adenier, A.; Cabet-Deliry, E.; Chausse, A.; Griveau, S.; Mercier, F.; Pinson, J.; Vautrin-UI, C.; *Chem. Mater.* **2005**, *17*, 491-501.
- (7) Piper, D. J. E.; Barbante, G. J.; Brack, N.; Pigram, P. J.; Hogan, C. F.; *Langmuir* **2011**, *27*, 474-480.
- (8) Susac, D.; Kono, M.; Wong, K. C.; Mitchell, K. A. R.; *App. Surf. Sci.* **2001**, *174*, 43-50.
- (9) Beamson, G.; Briggs, D. *High Resolution XPS of Organic Polymers: The Scienta Database*; John Wiley & Sons: Chichester, 1992.
- (10) Moulder, J. F.; Stickle, W. F.; Sobol, P. E.; Bomben, K. D. *Handbook of X-ray Photoelectron Spectroscopy*; Perkin-Elmer Corporation Physical Electronics Division: Eden Prairie, 1992.
- (11) Lui, G.; Klien, A.; Thissen, A.; Jaegermann, W.; *Surf. Sci.* **2003**, *539*, 37-48.
- (12) Agnes, C.; Arnault, J.-C.; Omnes, F.; Joussetme, B.; Billon, M.; Bidan, G.; Mailley, P.; *Phys. Chem. Chem. Phys.* **2009**, *11*, 11647-11654.
- (13) Laforgue, A.; Addou, T.; Belanger, D.; *Langmuir* **2005**, *21*, 6855-6865.

- (14) Brant, P.; Felthan, R. D.; *J. Organometallic. Chem.* **1976**, *120*, C53-C57.
- (15) Miao, W.; Choi, J.-P. In *Electrogenerated Chemiluminescence*; Bard, A. J., Ed.; Marcel Dekker, Inc.: New York, 2004.
- (16) Shewchuk, D. M.; McDermott, M. T.; *Langmuir* **2009**, *25*, 4556-4563.
- (17) Balaur, E.; Peele, A. G.; *Thin Solid Films* **2009**, *517*, 6520-6526.
- (18) Xia, L. Q.; Chang, M. In *Handbook of Semiconductor Manufacturing Technology*; 2nd ed.; Doering, R., Nishi, Y., Eds.; CRC Press: Boca Raton, Florida, 2008.
- (19) Kariuki, J. K.; McDermott, M. T.; *Langmuir* **1999**, *15*, 6534-6540.
- (20) McCreery, R. L.; *Chem. Rev.* **2008**, *108*, 2646-2687.

Chapter 8: Conclusions and Future work

8.1. Concluding Remarks

The work embodied in this thesis was concerned with the development and evaluation of modified electrode systems. Although a great variety of such systems have been explored in the past, the literature relating to modified electrodes for electrochemiluminescent applications is relatively sparse. The systems which have been described have been plagued by stability issues often related to the high positive potentials required to initiate the luminescence. The development of immobilisation methods for ECL active compounds has often focussed on the improvement of a film's sensitivity, producing useful advances in the field of ECL sensors. In contrast, this thesis provides what is hoped will be valuable insights into the best approaches to achieve stability in solid state ECL sensors. The main findings of the thesis are summarised below.

8.1.1. Nafion/Polypyrrole composites

The use of Nafion/Polypyrrole composites for the immobilisation of $\text{Ru}(\text{bpy})_3^{2+}$ was shown to produce stable films for use in an ECL-based sensor. Surface characterisation of the film correlated strongly with electrochemical measurements and suggested that the PPy is distributed homogeneously within the layer. ToF-SIMS studies demonstrate that the PPy is exclusively doped with the Nafion ionomer.

PPy was found to impede charge transport through the film when compared to a pure Nafion film. However, this impediment to charge transport also appeared to slow the rate of transport of $\text{Ru}(\text{bpy})_3^{2+}$ into the electrochemically inaccessible, hydrophobic regions of the film, improving the stability of the film when compared to pure Nafion films. In

aqueous solution, the Nf/Ru/PPy film was shown to be stable to electrochemical cycling for 7 hours, a significant improvement over the pure Nafion based film. In the presence of acetonitrile, this stability is somewhat reduced; however, the addition of acetonitrile provides an improvement in the ECL sensitivity by an order of magnitude, resulting in the detection of oxalate to a concentration of 1 μM and tripropylamine to a concentration of 10 nM.

8.1.2. Phenyl-bipyridine attachment and complexation

The deposition of thin phenyl-bipyridine films onto gold and glassy carbon substrates from the associated diazonium salt, para-diazonium-4'-phenyl-2,2'-bipyridine tetrafluoroborate, (dpb) was demonstrated. It was shown that the direct electrodeposition of the diazonium salt can be achieved with a reduction potential of -0.65 V. In addition, this deposition can be achieved via the mediated electrolysis of the diazonium by previously bound bipyridine at a potential of -1.4 V.

The deposited film was characterised by both electrochemical and surface analysis techniques. The film is a multilayered structure of approximately 6 nm in thickness (~12 monolayers) and is bound with both carbon-carbon and azo bonds between the individual phenyl-bipyridine moieties. ToF-SIMS shows that both bonding types also bind the film to the underlying substrate. XPS results estimate that approximately 50 % of the dpb within the film is bound through an azo bond.

The complexation of this film with the reagent $\text{Ru}(\text{bpy})_2\text{Cl}_2$ to form an ECL active layer was achieved, XPS and ToF-SIMS analysis confirming the binding of $\text{Ru}(\text{bpy})_2$ to the

surface. However, electrochemical experiments and ToF-SIMS suggest that the complexation reaction may be incomplete with the Ru bound to 5 pyridine groups instead of the desired 6. Cyclic voltammetry demonstrated that the film was electroactive and capable of co-reactant ECL with tripropylamine. However, ECL experiments further show that the film is not highly responsive to the co-reactant, emitting low levels of light compared to other films discussed in this thesis. This low level of light emission is related to the relatively poor oxidising power of the Ru(N)₅ species ($E_{1/2} = 0.9$ V) and to its low quantum yield. Therefore, although the study produced some interesting insights into the behaviour of diazonium species, the results suggest that the film is not well suited to a role as an ECL-based sensor. Despite this, the dpb film may be of potential use in other sensing applications such as the detection of metal ions.

8.1.3. Electrodeposition of Ru(bpy)₂(apb)²⁺ films

The *in-situ* formation of the diazonium salt of Ru(bpy)₂(apb)²⁺ prior to its attachment to an electrode in aqueous media was shown to be effective in producing stable, highly responsive films for ECL-based sensing. This strategy lead to highly stable, covalently-bound layers which will not desorb or degrade at the potentials required to oxidise the ruthenium complexes in the ECL cycle.

The electrochemistry of the system was shown to be consistent with a surface-confined species with a surface coverage equivalent of up to 5 monolayers. Surface characterisation of the film correlates well to electrochemical measurements and suggests that the deposited multilayered film is attached to the surface almost exclusively via azo bonding. The layer provided excellent ECL detection limits for the model analyte DBAE

with a low limit of detection of 10 nM while providing a linear response over 4 orders of magnitude (10^{-8} M to 10^{-4} M). This performance may be related to the multilayer nature of the film with a large proportion of the ruthenium centres effectively isolated from quenching by the electrode surface. The film is also shown to be highly stable with the current response from the layer only decreasing by $< 10\%$ after redox cycling in supporting electrolyte for 5 hrs.

8.1.4. The spontaneous deposition of $Ru(bpy)_2(apb)^{2+}$ films

In contrast to the electroreduced film, the spontaneously deposited film provided a relatively poor sensing performance, although the deposition method was very attractive due to its simplicity. The spontaneously deposited film was sensitive to DBAE, with a limit of detection of 10^{-5} M while providing a linear response to DBAE between concentrations of 10^{-5} and 10^{-2} M. Electrochemical cycling experiments indicated that the film was relatively un-stable with the peak current of the Ru^{2+}/Ru^{3+} redox couple degrading to 35 % of the initial signal before being stable for over 5 hrs. This degradation may be attributed to the binding of a large number of physisorbed species at the electrode surface.

Surface characterisation of the spontaneously deposited film by XPS and ToF-SIMS demonstrated that the film is covalently bound to the electrode via both azo and carbon-carbon bonding, as is observed for the electrodeposited films. However both XPS and electrochemical evidence suggests less material is deposited through the spontaneous pathway when compared to the electrodeposited attachment. Electrochemical

measurements suggested a surface coverage of $2.7 \times 10^{-10} \pm 9.8 \times 10^{-11}$ mol cm⁻², which is the equivalent of a film 1.9 ± 0.7 monolayers thick.

The use of the spontaneous deposition of the diazonium for selective deposition onto substrates has also been demonstrated via the spontaneous pathway. AFM measurements reveal that Ru(bpy)₂(apb)²⁺ can be selectively deposited onto DLC structures built onto an insulating silicon nitride substrate with the produced coating having a thickness of 13 nm. This selective deposition onto electrically isolated substrates may provide simplified control for the creation of both ECL and CL based sensing systems for a variety of online systems including FIA and lab-on-a-chip applications.

8.2. Future Work

There are several areas of research that may from extend from this study. These future interests are varied and are discussed separately below. Briefly, they involve the investigation of new approaches to the immobilisation methods described within the thesis. The proposed approaches may provide further benefits to the immobilised layer including enhanced stability and sensitivity with improved control over the layer deposition.

1) Carbon Nanotube/Conducting Polymer Nafion blends for ECL sensing.

The mechanism of stabilisation for the Nf/Ru/PPy films described in Chapter 4 is thought to be different to those proposed for both sol-gel and carbon-based Nafion composites. In Nafion/polypyrrole composites it is thought that the enhanced stability arises from the occupation of the more hydrophobic regions of the Nafion by polypyrrole preventing the migration of the Ru(bpy)₃²⁺ into these electrochemically inaccessible regions. This is in

contrast to the stability enhancement from sol-gel and carbon based composites where it is thought that the stronger hydrophobic interaction between $\text{Ru}(\text{bpy})_3^{2+}$ and the reinforcement (sol-gel, nanotubes, etc.) discourages the migration of $\text{Ru}(\text{bpy})_3^{2+}$ into the more hydrophobic regions of the Nafion.¹⁻³

A Nafion composite containing both Polypyrrole and sol-gel or nanotubes may provide further enhancements to the stability of the system by inhibiting migration of $\text{Ru}(\text{bpy})_3^{2+}$ by utilising both mechanisms described above. This enhancement in film stability may in turn improve the reliability of the resulting sensor.

2) Investigation of mediated diazonium reductions

The possibility of using an electrochemically mediated reaction to deposit the diazonium to a surface may provide finer control over the deposition. The use of mediated reactions may allow for additional control over both surface chemistry and morphology of the deposited layer. A preliminary investigation of the differences in surface composition and structure between diazonium films formed via direct and mediated reduction is currently being undertaken at La Trobe University.

3) Optimisation of electrochemically and spontaneously deposited films for use in FIA, HPLC and Lab-on-a-Chip applications

The films described in this thesis provide excellent opportunities for further assessment and development as ECL detection systems. For the incorporation of these films into detection systems for devices such as lab-on-a-chip, FIA and HPLC the layers need to be optimised and assessed for the specific application.

4) Investigation of Alkyl Diazonium films

Further advancements in both sensitivity and stability of ECL-active thin films may be achieved via the replacement of aryl diazonium-based films with alkyl diazonium derived films. The use of alkyl diazonium attachment chemistry may provide opportunities to provide finer control of electron transfer to the luminophore and minimise quenching of the excited state by the electrode.

However, alkyl diazoniums are generally considered highly unstable and short lived, readily losing N_2 upon its formation due to the lack of stability typically provided by the aromatic group.⁴ This short lifetime makes alkyl diazoniums unsuitable for many applications, though this instability may not be an issue for the attachment of conjugated metal complexes such as those used in ECL. Alkyl aminated metal complexes may provide enough electron withdrawal to stabilise a diazonium formed *in-situ* for long enough to undergo attachment to the surface by either electrochemical reduction or spontaneous deposition of the diazonium.

8.3. References

- (1) Choi, H. N.; Lee, J.-Y.; Lyu, Y.-K.; Lee, W. Y.; *Anal. Chim. Acta.* **2006**, *565*, 48-55.
- (2) Shi, L. H.; Liu, X. Q.; Li, H. J.; Xu, G. B.; *Anal. Chem.* **2006**, *78*, 7330-7334.
- (3) Song, H.; Zhang, Z.; Wang, F.; *Electroanal.* **2006**, *18*, 1838-1841.
- (4) Patai, S. *The Chemistry of diazonium and diazo groups*; John Wiley and Sons: Chichester, 1978.

Appendix I:

Supporting Information

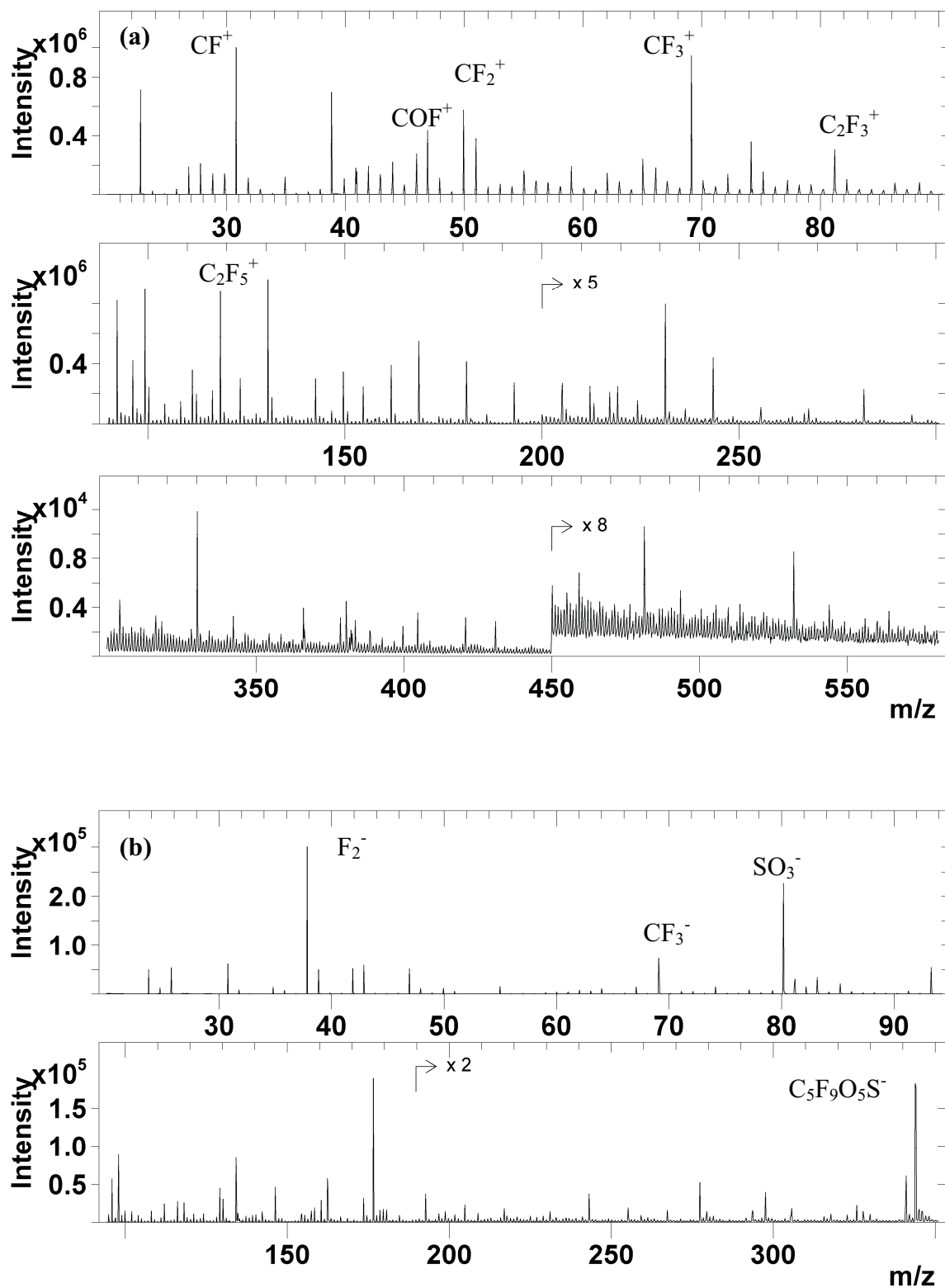


Figure I-1: Positive (a) and negative (b) ion ToF-SIMS spectra of a Nafion layer. Relevant high intensity mass fragments are labelled.

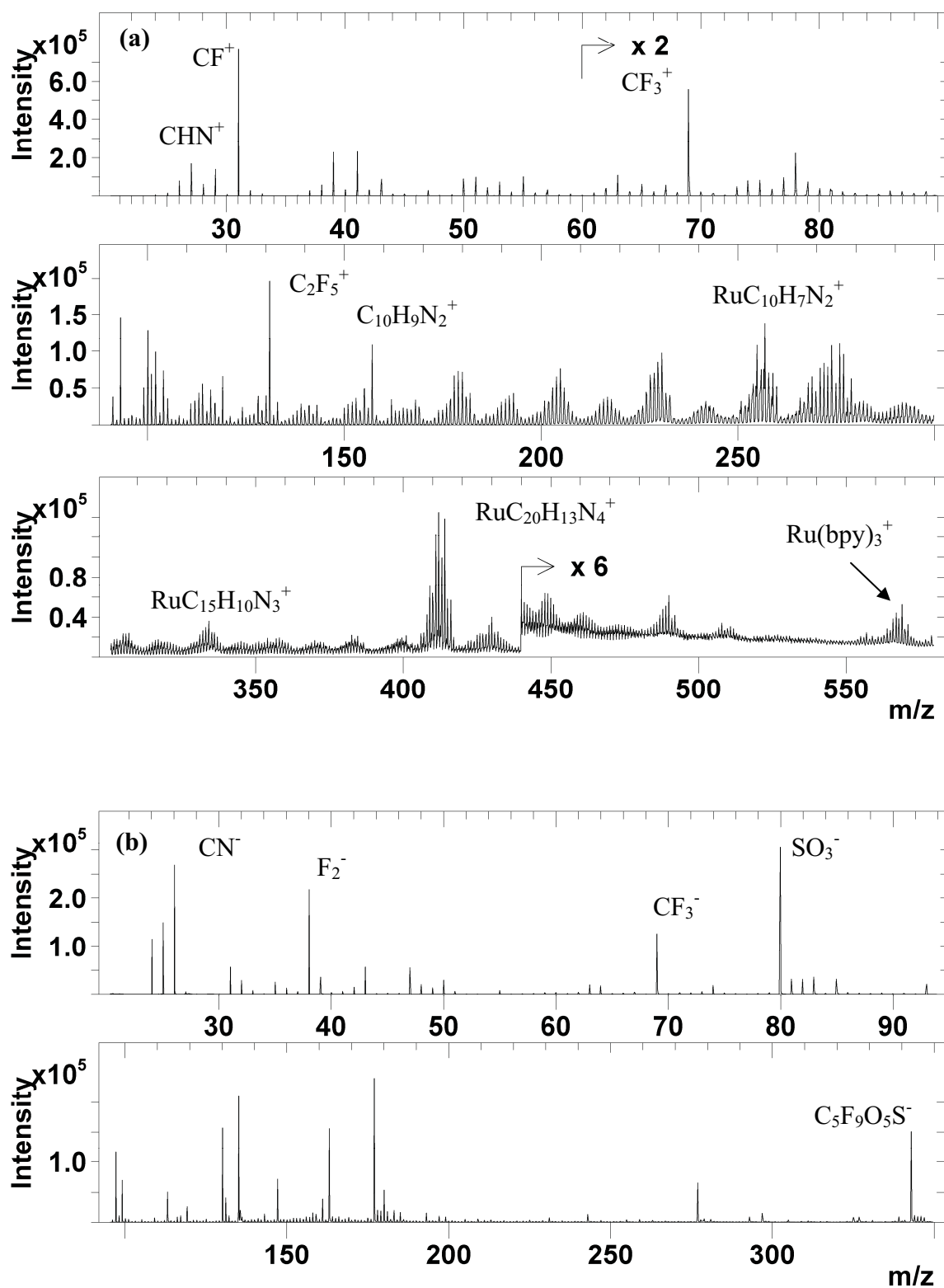


Figure I-2: Positive (a) and negative (b) ion ToF-SIMS spectra for a Ni/Ru layer. Relevant high intensity mass fragments are labelled.

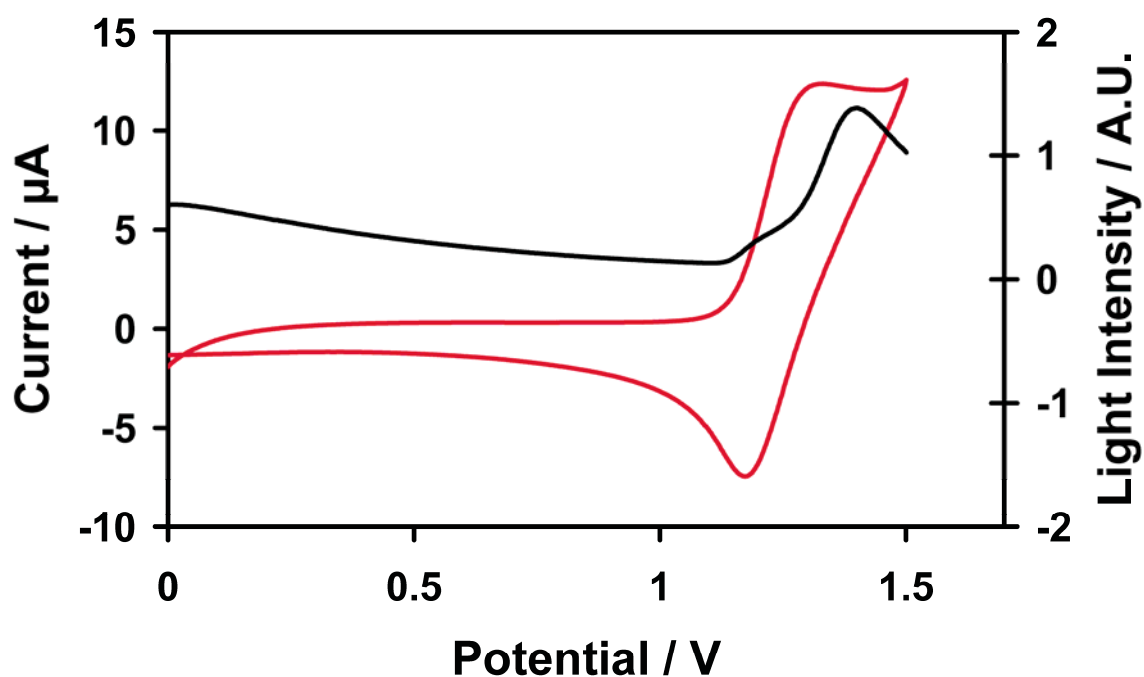


Figure I-3: Typical voltammetric (red) and light emission (black) response of a Nf/Ru/PPy film in aqueous solutions containing 100 μM tripropylamine and 0.2 M Na_2SO_4 electrolyte. The scan rate was 10 mV s^{-1} .

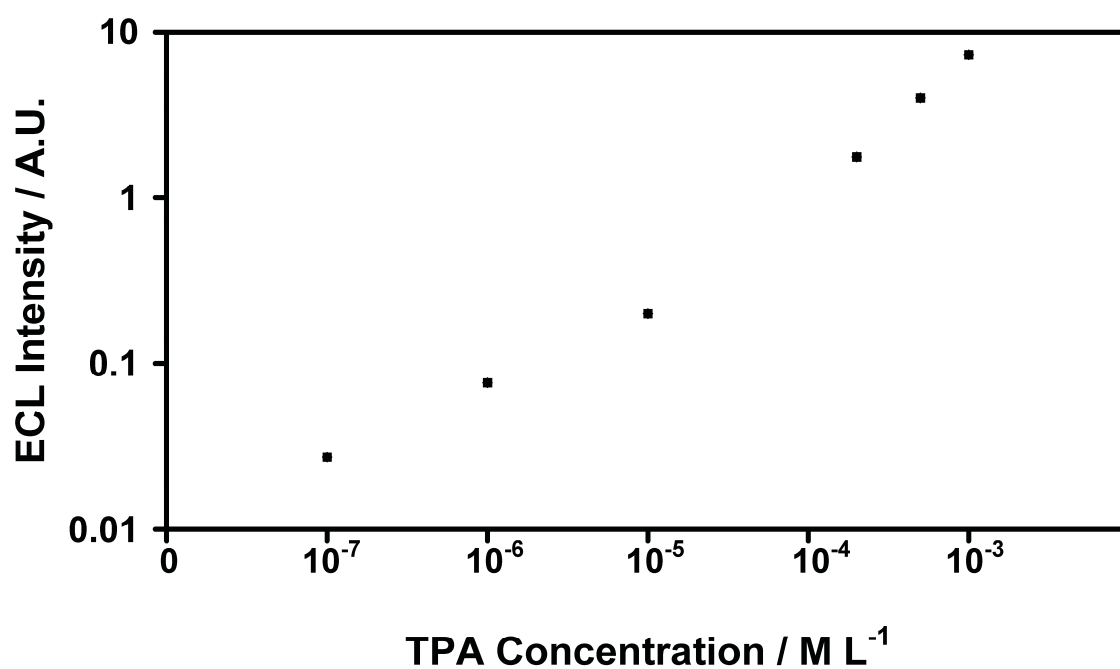


Figure I-4: Dependence of ECL intensity on the concentration of the model analyte tripropylamine for a Nf/Ru/PPy modified electrode.

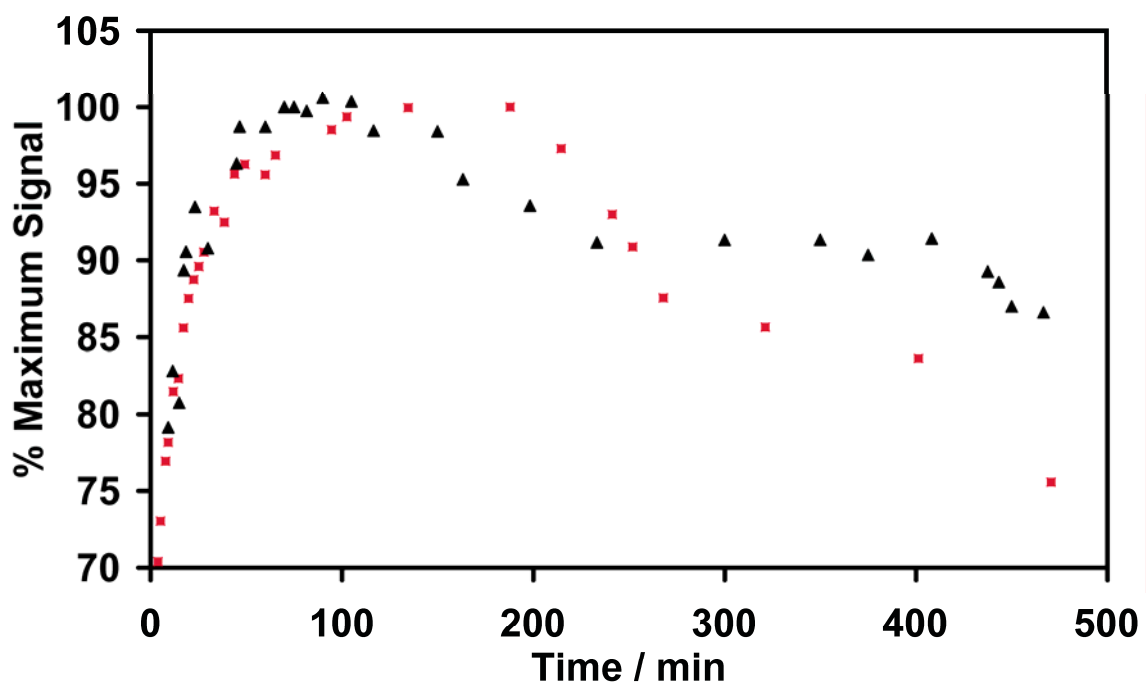


Figure I-5: Comparative response of Nf/Ru (■) and Nf/Ru/PPy (▲) films mean oxidative peak currents over time in 0.2 M Na₂SO₄. Films were continuously scanned at between 0.6 V and 1.5 V at a scan rate of 100 mV s⁻¹.

Appendix II:

Reprints

Highly Stable ECL Active Films Formed by the Electrografting
of a Diazotized Ruthenium Complex Generated *in Situ* from the AmineDavid J. E. Piper,[‡] Gregory J. Barbante,[†] Narelle Brack,[‡] Paul J. Pigram,[‡] and Conor F. Hogan^{*†}[†]Department of Chemistry, La Trobe University, Victoria 3086, Australia, and [‡]Department of Physics, La Trobe University, Victoria 3086, Australia

Received October 13, 2010. Revised Manuscript Received November 11, 2010

The electrodeposition of the electrochemiluminescent (ECL) ruthenium complex, bis(2,2'-bipyridyl)(4'-(4-amino-phenyl)-2,2'-bipyridyl)ruthenium(II), [Ru(bpy)₂(apb)]²⁺, via the *in situ* formation of a diazonium species from aqueous media is reported. Surface characterization undertaken using X-ray photoelectron spectroscopy (XPS) and time-of-flight secondary ion mass spectrometry (ToF-SIMS) determined that the layer is bound to the substrate via azo bonding. The layer displays good ECL activity and is stable over a long period of time. The excellent potential of this system for ECL sensing applications is demonstrated using the well-known ECL coreactant 2-(dibutylamino)ethanol (DBAE) as a model analyte, which can be detected to a level of 10 nM with a linear range between 10⁻⁸ and 10⁻⁴ M.

Introduction

Electrochemiluminescence (ECL), the light emission which occurs when excited state molecules are generated as a consequence of electrochemical reaction, has been shown to be a powerful analytical tool with a wide range of applications.¹⁻⁴ The ECL of tris(2,2'-bipyridyl)ruthenium(II), [Ru(bpy)₃]²⁺, has been used extensively for the sensitive detection of a wide variety of analytes which have the ability to act as coreactants in the ECL reaction. These include oxalate,³ peroxydisulfate,⁵ and a range of species containing secondary and tertiary amine moieties^{3,6} which includes many pharmaceutical compounds.

Although the coreactant is consumed in the ECL reaction, the ECL luminophore is not.⁵ As a result, the luminescent reagent is constantly regenerated in the measurement cycle and can be reused numerous times. This regeneration offers opportunities to immobilize the reagent at the electrode surface, thus providing a simplified experimental design while reducing reagent requirements. A wide range of immobilization techniques have been used to make ECL sensors; for example, the use of self-assembled monolayers^{7,8}

and electrostatic entrapment into Nafion^{9,10} and related polymers¹¹ have been used previously with varying success. Nafion-based films have significant issues with the leaching of the luminescent reagent into electrochemically inaccessible regions of the polymer.^{12,13} Self-assembled monolayers such as alkanethiols suffer from instability at the relatively high potentials required for ECL.^{7,14}

An alternative deposition method is through the use of the reductive electrodeposition of an aryldiazonium salt which can provide a strong covalent bond between the reagent and the electrode that is stable at the high potentials required for ECL. Previously, diazonium-based films have proven useful in a range of electrochemical sensors including pH,¹⁵ gas,¹⁶ inorganic,¹⁷ and biochemical^{18,19} sensing systems. Diazonium-based salts have

*To whom correspondence should be addressed. E-mail: c.hogan@latrobe.edu.au.

(1) Richter, M. M. Electrochemiluminescence (ECL). *Chem. Rev.* **2004**, *104*, 3003-3036.

(2) Wei, H. W.; Wang, E. Solid-state electrochemiluminescence of tris(2,2'-bipyridyl) ruthenium. *Trends Anal. Chem.* **2008**, *27*, 447-459.

(3) Gorman, B. A.; Francis, P. S.; Barnett, N. W. Tris(2,2'-bipyridyl)ruthenium(II) chemiluminescence. *Analyst* **2006**, *131*, 1-24.

(4) Forster, R. J.; Bertonecello, P.; Keyes, T. E. Electrogenerated Chemiluminescence. *Ann. Rev. Anal. Chem.* **2009**, *2*, 1-27.

(5) Miao, W.; Choi, J.-P. In *Electrogenerated Chemiluminescence*; Bard, A. J., Ed.; Marcel Dekker, Inc.: New York, 2004; p 213.

(6) Downey, T. M.; Nieman, T. A. Chemiluminescence detection using regenerable tris(2,2'-bipyridyl)ruthenium(II) immobilized in Nafion. *Anal. Chem.* **1992**, *64*, 261-268.

(7) Zanarini, S.; Rampazzo, E.; Bich, D.; Canteri, R.; Ciana, L. D.; Marcaccio, M.; Marzocchi, E.; Panciatichi, C.; Pederzoli, C.; Paolucci, F.; Prodi, L.; Vanzetti, L. Synthesis and Electrochemiluminescence of a Ru(bpy)₃-Labeled Coupling Adduct Produced on a Self-Assembled Monolayer. *J. Phys. Chem. C* **2008**, *112*, 2949-2957.

(8) Zhang, X.; Bard, A. J. Electrogenerated chemiluminescent emission from an organized (L-B) monolayer of a tris(2,2'-bipyridine)ruthenium(2+)-based surfactant on semiconductor and metal electrodes. *J. Phys. Chem.* **1988**, *92*, 5566-5569.

(9) Rubinstein, I.; Bard, A. J. Polymer films on electrodes. 5. Electrochemistry and chemiluminescence at Nafion-coated electrodes. *J. Am. Chem. Soc.* **1981**, *103*, 5007-5013.

(10) Khranov, A. N.; Collinson, M. M. Electrogenerated Chemiluminescence of Tris(2,2'-bipyridyl)ruthenium(II) Ion-Exchanged in Nafion-Silica Composite Films. *Anal. Chem.* **2000**, *72*, 2943-2948.

(11) Zhang, L.; Guo, Z.; Xu, Z.; Dong, S. Highly sensitive electrogenerated chemiluminescence produced at Ru(bpy)₂+ 3 in Eastman-AQ55D-carbon nanotube composite film electrode. *J. Electroanal. Chem.* **2006**, *592*, 63-67.

(12) Bunker, C. E.; Rollins, H. W.; Ma, B.; Simmons, K. J.; Liu, J.-T.; Ma, J.-J.; Martin, C. W.; DesMarteau, D. D.; Sun, Y.-P. Fluorescence spectroscopic probing of two distinctive microenvironments in perfluorinated ionomer membranes. *J. Photochem. Photobiol. A* **1999**, *126*, 71-76.

(13) Shultz, L. L.; Stoyanoff, J. S.; Nieman, T. A. Temporal and Spatial Analysis of Electrogenerated Ru(bpy)₃³⁺ Chemiluminescent Reactions in Flowing Streams. *Anal. Chem.* **1996**, *68*, 349-354.

(14) Everett, W. R.; Welch, T. L.; Reed, L.; Fritsch-Fauler, I. Potential-Dependent Stability of Self-Assembled Organothiols on Gold Electrodes in Methylene Chloride. *Anal. Chem.* **1995**, *67*, 292-298.

(15) Yang, X. H.; Hall, S. B.; Burrell, A. K.; Officer, D. L. A pH-responsive hydroquinone-functionalised glassy carbon electrode. *Chem. Commun.* **2001**, 2628-2629.

(16) Vaik, K.; Maeorg, U.; Maschion, F. C.; Maia, G.; Schiffrin, D. J.; Tammeveski, K. Electrochemical oxygen reduction on glassy carbon grafted with anthraquinone by anodic oxidation of a carboxylate substituent. *Electrochim. Acta* **2005**, *50*, 5126-5131.

(17) Liu, G.; Nguyen, Q. T.; Chow, E.; Bocking, T.; Hibbert, D. B.; Gooding, J. J. Study of Factors Affecting the Performance of Voltammetric Copper Sensors Based on Gly-Gly-His Modified Glassy Carbon and Gold Electrodes. *Electroanalysis* **2006**, *18*, 1141-1151.

(18) Polsky, R.; Harper, J. C.; Dirk, S. M.; Arango, D. C.; Wheeler, D. R.; Brozik, S. M. Diazonium-Functionalized Horseradish Peroxidase Immobilized via Addressable Electrodeposition: Direct Electron Transfer and Electrochemical Detection. *Langmuir* **2007**, *23*, 364-366.

(19) Corgier, B. P.; Marquette, C. A.; Blum, L. J. Diazonium-Protein Adducts for Graphite Electrode Microarrays Modification: Direct and Addressed Electrochemical Immobilization. *J. Am. Chem. Soc.* **2005**, *127*, 18328-18332.

been reported to react with a variety of conducting and semiconducting substrates^{20,21} and can be deposited via the reductive deposition from a solution of the salt dissolved in organic solvent.^{22,23}

Two significant barriers to the application of this approach to the production of real-world sensing interfaces are (1) the requirement for organic solvent, which precludes the modification of most screen printed electrodes, due to the solubility of the binders used and (2) the instability of diazonium salts, because unstable modification reagents add intolerable variability to the fabrication procedure. Another issue is that most sensing systems based on diazonium attachment rely on a two-step mechanism, where the electrode is first aminated or carboxylated using the diazonium chemistry, with the sensing moiety being attached in a subsequent step using more conventional coupling such as amide bond formation.^{17,24} This two-step approach is undesirable because it complicates and slows the electrode modification process.

Single-step modification is possible if the sensing molecule to be attached contains a diazonium moiety. The synthesis and electrodeposition of metal complexes containing diazonium moieties have been recently described by Joussemle et al., who reported the deposition of the diazonium salt of bis(2,2'-bipyridyl)(*p*-amino-4'-phenyl-2,2'-bipyridyl)ruthenium(II), [Ru(bpy)₂(ph-bpy-N₂⁺)]-[PF₆]₃, as well as its terpyridine analogue, from acetonitrile solution.^{25,26} The stated object of this work was to endow the electrode with properties suitable for optoelectronic applications.

In order to avoid problems associated with the use of organic solvent, an alternative approach is electrodeposition from aqueous solution following the *in situ* formation of a diazonium species from the reaction between a primary arylamine and nitrous acid in the electrochemical cell.^{22,27,28} The *in situ* approach provides for a simple aqueous-based method which is compatible with screen printed electrodes making it ideal for use in many sensing and microfluidic applications. The generation of thin films from *in situ* generated diazoniums has been used previously for the creation of antibody sensors on screen printed electrodes through the coupling of 4-carboxymethaniline to the surface.¹⁹ Metal complexes have also been deposited with the aid of *in situ* diazonium chemistry; Leech et al. reported the *in situ* generation of a diazonium salt to

pre-functionalize electrodes prior to coupling an aminated osmium complex to the surface.^{29,30}

In this work, we report a rapid and facile strategy for depositing stable sensing layers of ECL active metal complexes such as [Ru(bpy)₂(apb)]²⁺, where bpy is 2,2'-bipyridyl and apb is 4'-(4-aminophenyl)-2,2'-bipyridyl. The method relies on the *in situ* formation of the diazonium form of the metal complex shortly before electrochemical attachment to the electrode. Therefore, the sensing interface is formed rapidly in a single step from stable precursors. The resulting covalently bound layer is demonstrated to be electrochemically stable and suitable for ECL sensing providing a wide linear range and low detection limits for several known ECL coreactants. Apart from the case where Ru(bpy)₃²⁺ was electrostatically attached to the electrode via a benzenesulfonic acid monolayer deposited from the diazonium salt,³¹ the use of the diazonium pathway has not previously been used to create stable ECL-based sensing interfaces. The deposition is carried out in aqueous media, and hence it is suitable for use with the types of electrode materials commonly used for sensor applications such as screen printed electrodes. Furthermore, this deposition technique should also allow for the post production modification of electrodes in lab-on-a-chip systems, reducing the possibility of physical damage to the electrode surface and improving reliability.

Experimental Section

Reagents and Synthesis of [Ru(bpy)₂(apb)]²⁺. The ligand *p*-amino-4'-phenyl-2,2'-bipyridine was synthesized by following the procedure described by Johansson.³² Following this, a solution of ruthenium bis(2,2'-bipyridine)dichloride (100 mg, 0.38 mmol) and 4'-aminophenyl-2,2'-bipyridine (94 mg, 0.4 mmol) in a mixture of ethanol and water (20 mL, 1:1) was heated at reflux for 5 h under a nitrogen atmosphere. Once a deep red solution had formed, the solvent was evaporated under reduced pressure. The solid was redissolved in Milli-Q water (20 mL), and the resulting solution filtered through a sintered funnel; the filter cake was rinsed with Milli-Q water (5 mL). The filtrate was treated with a saturated aqueous solution of KPF₆, which gave an orange precipitate. The resulting solid was collected by filtration and washed with Milli-Q water (2 × 5 mL) and diethyl ether (2 × 5 mL). The orange precipitate was recrystallized from an acetone–water mixture to give a dark red powder and then dried under vacuum at 50 °C (0.150 g, 42%). ¹H NMR (300 MHz, DMSO-*d*₆): δ 5.81 (s, 2H), 6.64–6.68 (m, 3H), 7.43–7.61 (m, 8H), 7.68–7.82 (m, 7H), 8.13 (t, 4H, J 7.8 Hz), 8.81 (d, 3H, J 8.4 Hz), 8.91 (s, 1H), 9.1 (d, 1H, J 8.10 Hz); ESI-MS: *m/z* [Ru–PF₆ + H]⁺ 806.0 (calculated: 805.7), [Ru–2PF₆ + 2H]⁺ 663.1 (calculated: 660.74), [Ru–2PF₆]²⁺ 330.6 (calculated: 330.37).

All other chemicals were purchased from Sigma-Aldrich Pty. Ltd., Australia, and were of reagent grade or better and used without further purification. For aqueous solutions and aqueous rinses, Milli-Q water (resistivity ≥ 17.9 MΩ cm) was used.

Electrode Modification. Prior to deposition, all electrodes were polished with alumina abrasives (0.3 μm and then 0.05 μm particle size). Layers were deposited from a cold (0 °C) 0.5 M HCl solution containing 1.2 mM [Ru(bpy)₂(apb)]²⁺ and 1.5 mM NaNO₂ which was allowed to react for at least 2 min prior to electrochemical deposition. The electrochemical cell was kept in ice prior to and during the deposition. Solutions were used for up to 10

(20) Pinson, J.; Podvorica, F. Attachment of organic layers to conductive or semiconductive surfaces by reduction of diazonium salts. *Chem. Soc. Rev.* **2005**, *34*, 429–439.

(21) Allongue, P.; Delmar, M.; Desbat, B.; Fagebaume, O.; Hitmi, R.; Pinson, J.; Savent, J. M. Covalent Modification of Carbon Surfaces by Aryl Radicals Generated from the Electrochemical Reduction of Diazonium Salts. *J. Am. Chem. Soc.* **1997**, *119*, 201–207.

(22) Baranton, S.; Belanger, D. Electrochemical Derivatization of Carbon Surface by Reduction of *In Situ* Generated Diazonium Cations. *J. Phys. Chem. B* **2005**, *109*, 24401–24410.

(23) McCreery, R. L. Advanced Carbon Electrode Materials for Molecular Electrochemistry. *Chem. Rev.* **2008**, *108*, 2646–2687.

(24) Gooding, J. J. Advances on Interfacial Design for Electrochemical Biosensors and Sensors: Aryl Diazonium Salts for Modifying Carbon and Metal Electrodes. *Electroanalysis* **2007**, *20*, 573–582.

(25) Joussemle, B.; Bidan, G.; Billon, M.; Goyer, C.; Kervella, Y.; Guillerez, S.; Hamad, E. A.; Goze-Bac, C.; Mevellec, J.-Y.; Lefrant, S. One-step electrochemical modification of carbon nanotubes by ruthenium complexes via new diazonium salts. *J. Electroanal. Chem.* **2008**, *621*, 277–285.

(26) Agnes, C.; Arnault, J.-C.; Omnes, F.; Joussemle, B.; Billon, M.; Bidan, G.; Mailley, P. XPS study of ruthenium tris-bipyridine electrografted from diazonium salt derivative on microcrystalline boron doped diamond. *Phys. Chem. Chem. Phys.* **2009**, *11*, 11647–11654.

(27) Lyskawa, J.; Belanger, D. Direct Modification of a Gold Electrode with Aminophenyl Groups by Electrochemical Reduction of *In Situ* Generated Aminophenyl Monodiazonium Cations. *Chem. Mater.* **2006**, *18*, 4755–4763.

(28) Lui, G.; Chockalingham, M.; Khor, S. M.; Gui, A. L.; Gooding, J. J. A Comparative Study of the Modification of Gold and Glassy Carbon Surfaces with Mixed Layers of *In Situ* Generated Aryl Diazonium Compounds. *Electroanalysis* **2010**, *22*, 918–926.

(29) Boland, S.; Barriere, F.; Leech, D. Designing Stable Redox-Active Surfaces: Chemical Attachment of an Osmium Complex to Glassy Carbon Electrodes Prefunctionalized by Electrochemical Reduction of an *In Situ*-Generated Aryldiazonium Cation. *Langmuir* **2008**, *24*, 6351–6358.

(30) Boland, S.; Foster, K.; Leech, D. A stability comparison of redox-active layers produced by chemical coupling of an osmium redox complex to pre-functionalized gold and carbon electrodes. *Electrochim. Acta* **2009**, *54*, 1986–1991.

(31) Wang, H.; Xu, G.; Dong, S. Electrochemistry and electrochemiluminescence of stable tris(2,2'-bipyridyl)ruthenium(II) monolayer assembled on benzene sulfonic acid modified glassy carbon electrode. *Talanta* **2001**, *55*, 61–67.

(32) Johansson, O.; Borgstrom, M.; Lomoth, R.; Palmblad, M.; Bergquist, J.; Hammarstrom, L.; Sun, L.; Akemark, B. Electron Donor-Acceptor Dyads Based on Ruthenium(II) Bipyridine and Terpyridine Complexes Bound to Naphthalenediimide. *Inorg. Chem.* **2003**, *42*, 2908–2918.

depositions in succession. Films were deposited by performing six sequential potential scans between 0.5 and -0.7 V vs Ag/AgCl at 100 mV/s.

Apparatus. Electrochemical experiments were carried out using a μ -Autolab Type II (Eco Chemie, The Netherlands) potentiostat/galvanostat. The working electrode was a 3 mm diameter glassy carbon disk electrode embedded in a 6 mm diameter PTFE body (CH Instruments, USA). A platinum wire counter electrode and a Ag/AgCl (3 M KCl) reference electrode were employed. For surface characterization, films were prepared on 15 mm diameter SIGRADUR G glassy carbon disks (HWT, Germany). Unless otherwise stated, all electrochemical experiments on the deposited films were conducted in 0.1 M LiClO₄ solution.

ECL experiments were conducted in a quartz bottomed glass cell and holder, designed for reproducible positioning of the working electrode with respect to the photodetector. Light emission was detected using a photomultiplier tube (PMT) (9828SB, Electron Tubes, UK) biased at +500 V positioned under the cell. The output signal was amplified using a transimpedance amplifier (D7280, Ames Photonics) and acquired using the auxiliary channel of the potentiostat with the GPES software package (Eco Chemie). ECL experiments were conducted in a custom-made light-tight Faraday cage.

X-ray photoelectron spectroscopy (XPS) experiments were conducted using an Axis Ultra DLD spectrometer (Kratos Analytical, UK). A monochromatized Al K α X-ray source ($h\nu = 1486.6$ eV) was operated at 150 W. The analysis area was 700 μ m by 300 μ m. High-resolution region spectra were collected using a 20 eV pass energy. The spectrometer energy scale was calibrated using the Au 4f_{7/2} photoelectron peak at $E_B = 83.98$ eV. Surface charge neutralization was utilized to improve resolution. Spectra were charge corrected using a reference value of 284.6 eV for the aromatic peak in the C 1s spectra.³³ Spectra were quantified using the CasaXPS software program (version 2.3.10, Casa Software Ltd. (UK)). Relative atomic concentrations were determined by applying the associated peak sensitivity factor, after background subtraction (Shirley background shape) and the fitting of Gaussian (70%) / Lorentzian (30%) component peaks.^{34–36} Atomic concentration uncertainties for all fitted spectra were estimated to be $\pm 10\%$ of the measured value.

Time-of-flight secondary ion mass spectrometry (ToF-SIMS) was performed using a ToF-SIMS IV instrument (Ion-ToF GmbH, Germany). A Bi³⁺ ion source was operated at 25 keV with a 150 μ s cycle time, resulting in a current of 0.5 pA at the sample surface. The analysis time was 100 s. The analysis area was 100 μ m \times 100 μ m. The primary ion dose density was at all times below the static SIMS limit of 10^{13} ions cm⁻².

Results

Layer Deposition. Glassy carbon electrodes were modified via the electrochemical reduction of a 1.2 mM Ru(bpy)₂(apb) solution containing 1.5 mM NaNO₂ and 0.5 M HCl. A typical cyclic voltammogram obtained from the deposition is presented in Figure 1. The deposition gives rise to a broad reduction wave, unlike the case with aryl diazonium salts in organic media, where a sharp deposition peak is observed.^{17,37} Similar systems report that the reduction peak for this diazonium occurs at -0.6 V vs Ag/AgCl

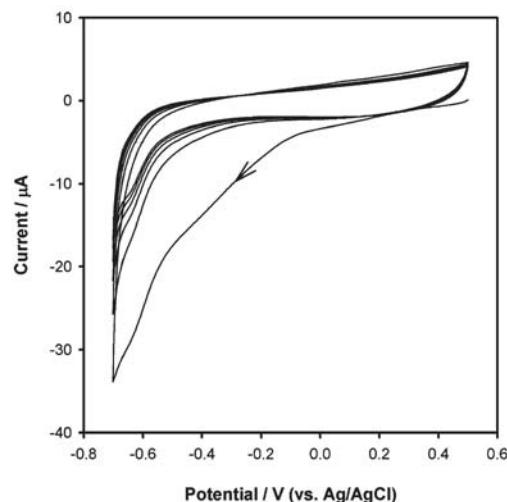


Figure 1. Cyclic voltammetric deposition of [Ru(bpy)₂(apb)]²⁺ onto a 3 mm diameter glassy carbon (GC) electrode from a solution containing 1.5 mM NaNO₂ and 0.5 M HCl. The first six scans are shown. Scan rate was 100 mV/s.

in organic media.²⁶ However, the observed response is consistent with the reduction of the diazonium and subsequent formation of a covalent bond with the substrate through either a carbon–carbon or azo ($-N=N-$) bond as shown previously.²⁶ This cathodic current is only observed if HNO₂ is present. After the initial scan the current drops to background levels in subsequent potential sweeps. The loss of the large cathodic current observed in the first scan indicates that the electrode is largely covered on the time scale of one voltammetric cycle.

Electrochemical Characterization. The cyclic voltammetric response of the electrodeposited layer of the ruthenium complex in blank electrolyte is presented in Figure 2 compared with the response from an electrode treated in exactly the same way with the exception of the addition of NaNO₂. A reversible redox couple centered at 1.15 V is observed which can be attributed to the Ru²⁺/Ru³⁺ couple of the deposited complex. This is consistent with the solution phase voltammetry of the complex and with electrochemistry obtained from immobilized forms of Ru(bpy)₃²⁺.^{7,25,38}

Figure 3 shows the voltammetric responses for a similar layer at a range of scan rates with the inset showing the dependence of peak current on scan rate. After background subtraction is performed on the voltammetric peaks a Gaussian peak shape is observed. The absence of peak tailing and the linear dependence of peak current on scan rate demonstrate that the wave observed for the Ru²⁺/Ru³⁺ redox couple is due to surface confined species bound to the electrode. Integration of the charge under the background corrected voltammetric peaks reveals that the surface coverage (Γ) of the complex on the electrode surface is $(4.8 \pm 2.2) \times 10^{-10}$ mol cm⁻² (average value from 7 electrodes). This value is greater than the estimated theoretical coverage for a close-packed monolayer for the complex (1.4×10^{-10} M cm⁻²), indicating the presence of a multilayered system equivalent to between two and five monolayers.

(33) Moulder, J. F.; Stickle, W. F.; Sobol, P. E.; Bomben, K. D. *Handbook of X-ray Photoelectron Spectroscopy*; Perkin-Elmer Corporation Physical Electronics Division: Eden Prairie, MN, 1992.

(34) *CasaXPS User's Manual: Version 1.0*; Casa Software Ltd.: London, UK, 2000.

(35) CasaXPS, version 2.3.10; Casa Software Ltd., UK; 2005.

(36) Fairley, N.; Carrick, A. *The Casa Cookbook Part 1: Recipes for XPS Data Processing*; Pelican Press: Manchester, 2005.

(37) Delmar, M.; Desarmot, G.; Fagebaume, O.; Hitmi, R.; Pinson, J.; Savent, J. M. Modification of carbon fiber surfaces by electrochemical reduction of aryl diazonium salts: Application to carbon epoxy composites. *Carbon* **1997**, *35*, 801–807.

(38) Obeng, Y. S.; Bard, A. J. Electrogenerated Chemiluminescence. 53. Electrochemistry and Emission from Adsorbed Monolayers of a Tris(bipyridyl)ruthenium(II)-Based Surfactant on Gold and Tin Oxide Electrodes. *Langmuir* **1991**, *7*, 195–201.

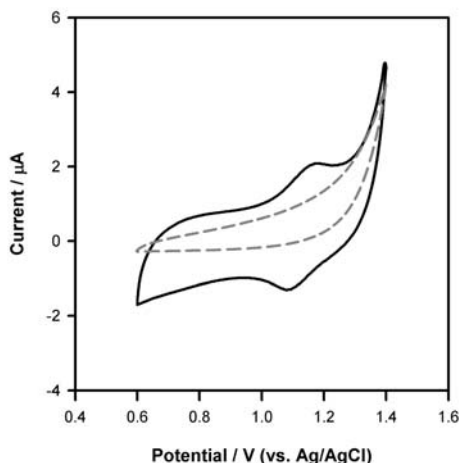


Figure 2. The solid line shows the cyclic voltammetric response for GC electrode in blank 0.1 M LiClO₄ electrolyte after modification with [Ru(bpy)₂(apb)]²⁺, as described in Figure 1. The dashed line represents the response for the control experiment where NaNO₂ was omitted from the deposition solution.

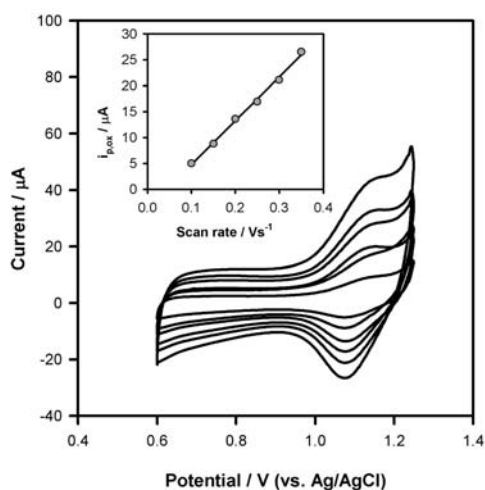


Figure 3. Scan rate dependence of 3 mm diameter GC electrode modified with a layer of [Ru(bpy)₂(apb)]²⁺ in blank electrolyte solution (0.1 M LiClO₄).

Surface Characterization. The nature of the bonding in the layer and the functional groups involved in bonding to the substrate (carbon–carbon or azo–carbon bonding) were examined using XPS and ToF-SIMS. The C 1s and N 1s photoelectron region spectra for the layer are shown in Figure 4. The presence of Ru on the electrode surface is confirmed by the observation of the Ru 3d_{5/2} photoelectron peak at 281.2 eV which corresponds to Ru in the 2+ oxidation state.³⁹ The Ru 3d_{5/2} peak occurs at a binding energy 4.17 eV higher than the Ru 3d_{3/2} peak and lies underneath the aliphatic C 1s component. Other peaks observed in both films include C–N ($E_B = 286.0$ eV), aromatic and aliphatic carbon

(39) Susac, D.; Kono, M.; Wong, K. C.; Mitchell, K. A. R. XPS study of interfaces in a two-layer light-emitting diode made from PPV and Nafion with ionically exchanged Ru(bpy)₂²⁺. *Appl. Surf. Sci.* **2001**, *174*, 43–50.

($E_B = 284.6$ eV and 285.0 respectively), C=O ($E_B = 287.6$ eV), and a $\pi \rightarrow \pi^*$ shake-up ($E_B = 289.6$ eV). These peak assignments are consistent with those previously reported.^{33,40}

Two peaks at 399.0 eV and 400.3 eV are observed in the N 1s region spectrum (Figure 4b). The peak at higher binding energy (400.3 eV) is attributed to the pyridyl nitrogens present in the complex.^{26,41} In previous XPS studies of diazonium-based films the peak at 399.0 eV has often been discounted or ignored as a byproduct of the reaction or possible surface contamination.⁴² However, as first suggested by Belanger,⁴³ this peak is due to the formation of azo (R–N=N–R) bonds in the layer. Recently, it has been shown by Doppelt et al. through the use of ToF-SIMS and IR spectroscopy that this is indeed the case for a range of aryldiazonium systems.⁴⁴ Doppelt suggested that the formation of the azo bonds on a multilayered system is related to the steric crowding of the layer. As such, a large complex like Ru(bpy)₂(apb) would promote their formation in the system under study here. The ratio of Ru to N_{azo} atoms observed via XPS is 1:2, suggesting that through the analysis depth probed by XPS (5–10 nm) the layer is exclusively bound via the azo functionality.

Figure 5 shows a typical positive ion ToF-SIMS mass spectrum for a layer electrodeposited from a Ru(bpy)₂(apb)²⁺ solution, with a selection of relevant mass fragments listed in Table 1. A number of peaks associated with the deposited complex Ru(bpy)₂(ph-bpy), where ph-bpy is 4-phenyl-2,2'-bipyridyl, are present, with the compound fragmenting most typically through the loss of a ligand from the complex, resulting in groups of peaks associated with Ru(bpy)₂(ph-bpy), Ru(bpy)₂, Ru(bpy)(ph-bpy), Ru(ph-bpy), and Ru(bpy) fragments. These broad peak groupings are due to the multiple stable isotopes of Ru present in the sample. Significantly, no peaks exclusively associated with the starting material Ru(bpy)₂(apb) are observed in the spectra. In contrast to the positive ion spectrum, the negative ion mass spectrum for the layer provides little discernible information regarding structure of the layer with the most notable peak present associated with the counterion used (PF₆⁻).

ToF-SIMS provides further evidence for the nature of the bonding of Ru(bpy)₂(apb) within the layer and to the substrate. Peaks associated with the azo functionality are present, including fragment ions such as C₆H₅–N₂⁺ and bpy-ph-N₂⁺ (where ph is the phenyl group), confirming the azo bonding suggested by XPS analysis in this study and the previous work of Doppelt.⁴⁴ Other fragments such as C₆H₅–N=N–C₆H₄⁺ can be associated with the azo binding to both the substrate and other ruthenium complexes within the film. Further investigation of the spectra reveals the presence of peaks that can be attributed to carbon–carbon bonding between complexes and the substrate. These fragments include C₆H₅–C₆H₄⁺, (C₆H₄)₂-bpy⁺, and (ph-bpy)₂⁺, confirming the presence of both modes of bonding in the layer. Because of the aromatic nature of the glassy carbon substrate, it is difficult to discriminate between bonding within the film and to the substrate

(40) Beamson, G.; Briggs, D. *High Resolution XPS of Organic Polymers: The Scienta ESCA300 Database*; John Wiley & Sons: Chichester, 1992.

(41) Lui, G.; Klien, A.; Thissen, A.; Jaegermann, W. Electronic properties and interface characterization of phthalocyanine and Ru-polybipyridine dyes on TiO₂ surface. *Surf. Sci.* **2003**, *539*, 37–48.

(42) Saby, C.; Ortiz, B.; Champagne, G. Y.; Belanger, D. Electrochemical Modification of Glassy Carbon Electrode Using Aromatic Diazonium Salts. I. Blocking Effect of 4-Nitrophenyl and 4-Carboxyphenyl Groups. *Langmuir* **1997**, *13*, 6805–6813.

(43) Laforgue, A.; Addou, T.; Belanger, D. Characterization of the Deposition of Organic Molecules at the Surface of Gold by the Electrochemical Reduction of Aryldiazonium Cations. *Langmuir* **2005**, *21*, 6855–6865.

(44) Doppelt, P.; Hallais, G.; Pinson, J.; Podvorica, F.; Verneyre, S. Surface Modification of Conducting Substrates. Existence of Azo Bonds in the Structure of Organic Layers Obtained from Diazonium Salts. *Chem. Mater.* **2007**, *19*, 4570–4575.

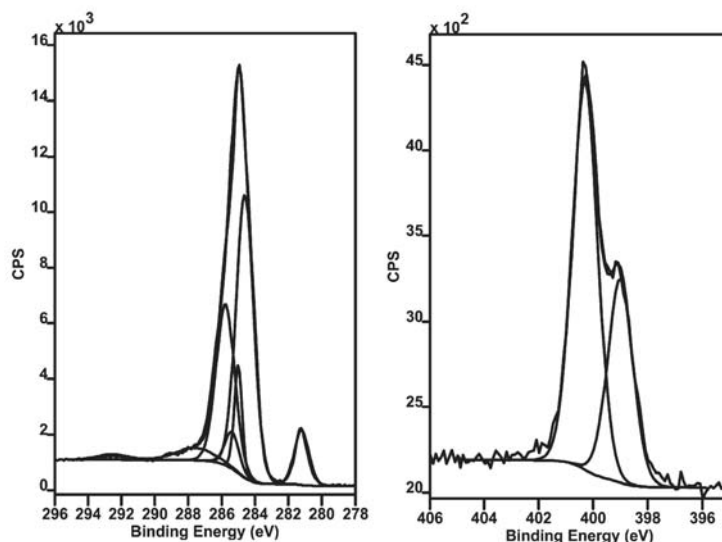


Figure 4. High-resolution C 1s (a) and N 1s (b) XPS photoelectron spectra of $[\text{Ru}(\text{bpy})_2(\text{apb})]^{2+}$ film deposited on a glassy carbon substrate.

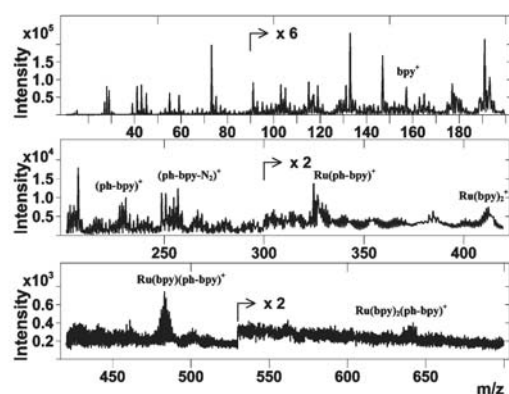


Figure 5. Positive ion ToF-SIMS spectrum of the deposited layer of $[\text{Ru}(\text{bpy})_2(\text{apb})]^{2+}$ on a glassy carbon substrate.

with many of the fragments related to the intermonomer binding also consistent with fragments from either the substrate or the complex.

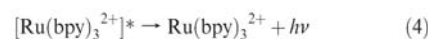
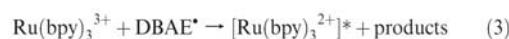
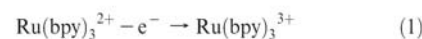
A long ToF-SIMS cycle time (150 μs) was employed to generate mass spectra with a mass range of about 3000 m/z in an attempt to detect oligomers of the complex at the surface. The presence of oligomers can be interpreted as consistent with a multi-layered system. While no oligomers were observed, it is possible that these larger fragments are not produced in sufficient quantities to allow for detection via ToF-SIMS.

Electrochemiluminescence. The ECL activity of the attached $\text{Ru}(\text{bpy})_2(\text{apb})^{2+}$ was investigated using the co-reactant DBAE (2-(dibutylamino)ethanol) as a model analyte. As shown in Figure 6, the electrochemical response shows a broad peak at about 0.8 V due to the direct oxidation of DBAE. The voltammetric response for the $\text{Ru}^{2+/3+}$ redox couple is somewhat ill-defined compared with Figure 2 because of the presence of the coreactant. However, the ECL signal shows a large increase at precisely the potential corresponding to the oxidation of the Ru^{2+} .

Table 1. Relevant Positive Ion Peaks from Figure 6

m/z	ion fragment	m/z	ion fragment
102	$^{102}\text{Ru}^+$	260	$[(\text{ph-bpy})-\text{N}=\text{N}]^+$
105	$\text{C}_6\text{H}_5-\text{N}=\text{N}^+$	308	$[(\text{C}_6\text{H}_4)\text{-bpy}]^+$
153	$\text{C}_6\text{H}_5-\text{C}_6\text{H}_4^+$	333	$\text{Ru}(\text{ph-bpy})^+$
157	$[\text{bpy} + \text{H}]^+$	413	$\text{Ru}(\text{bpy})_2^+$
181	$\text{C}_6\text{H}_5-\text{N}=\text{N}-\text{C}_6\text{H}_4^+$	483	$\text{Ru}(\text{bpy})(\text{ph-bpy})^+$
230	$[\text{ph-bpy-H}]^+$	641	$\text{Ru}(\text{bpy})_2(\text{ph-bpy})^+$
258	$\text{Ru}(\text{bpy})^+$		

This indicates that the ECL mechanisms previously suggested for $\text{Ru}(\text{bpy})_3^{2+}$ in the presence of tertiary amines, as given below, are also applicable in this case.^{5,45}



The very slight increase in ECL signal at ~ 0.7 V prior to the main peak may be due to minute traces of the $\text{Ru}(\text{N}_5)$ complex in the layer produced by photolysis or as a side product during synthesis. The absence of a corresponding peak in the voltammogram (Figure 2) highlights the sensitivity of the ECL signal compared with the electrochemical. The ECL response of the modified electrode to varying concentrations of DBAE is presented in Figure 7. The layer is highly sensitive to the coreactant, achieving a low limit of detection 10 nM, and has a linear response to coreactant between concentrations of 10^{-8} and 10^{-4} M ($R^2 = 0.99$). These

(45) Liu, X.; Shi, L.; Niu, W.; Li, H.; Xu, G. Environmentally Friendly and Highly Sensitive Ruthenium(II) Tris(2,2'-bipyridyl) Electrochemiluminescent System Using 2-(Dibutylamino)ethanol as Co-Reactant. *Angew. Chem., Int. Ed.* **2007**, *46*, 421–424.

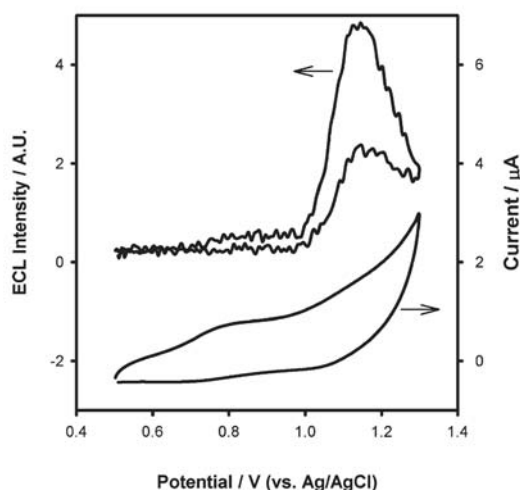


Figure 6. Cyclic voltammogram response with simultaneously detected ECL emission for $[\text{Ru}(\text{bpy})_2(\text{apb})]^{2+}$ layer on glassy carbon in contact with a solution of $10 \mu\text{M}$ DBAE in 0.1 M LiClO_4 . The scan rate was 100 mV s^{-1} .

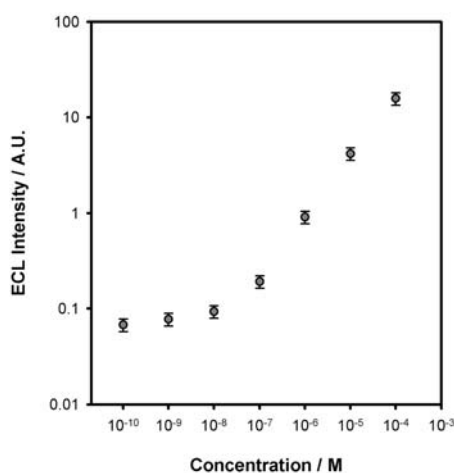


Figure 7. Dependence of ECL intensity on concentration of model analyte DBAE for a $[\text{Ru}(\text{bpy})_2(\text{apb})]^{2+}$ layer deposited on glassy carbon. The error bars represent the maximum difference in response for three measurements.

results show that this system is among the best to be reported to date in terms of sensitivity compared with previous work on ECL from modified electrodes.⁴⁶ The ECL response of the film deposited onto a screen printed carbon electrode was also investigated and was found to be similar to the glassy carbon response presented in Figure 6 with a limit of detection of 10 nM .

Stability is a recurring issue with modified electrodes used for ECL-based sensing, partly because of the strongly oxidizing conditions required to produce light emission. In order to investigate the long-term stability of this layer, a multicycle CV experiment was run over a number of hours (1000 scans at 100 mV s^{-1} between

(46) Li, Y.; Yang, F.; Yang, X. Electrochemiluminescence detection based on Ruthenium(II) tris(bipyridine) immobilised in sulfonic-functionalised titania nanoparticles by ion exchange strategy. *Analyst* **2009**, *134*, 2100–2105.

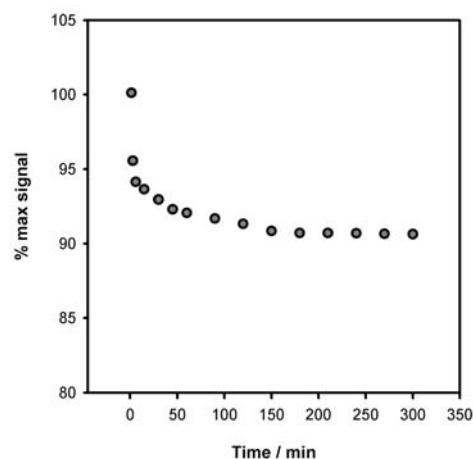


Figure 8. Stability of $[\text{Ru}(\text{bpy})_2(\text{apb})]^{2+}$ film to continuous voltammetric cycling in 0.1 M LiClO_4 between 0.5 and 1.3 V at a scan rate of 100 mV/s . The graph shows the change in the peak oxidation current ($i_{p,\text{ox}}$) over time.

0.5 and 1.25 V) to expose the film to the maximum oxidative stress possible in a period of use, with the resulting $\text{Ru}^{2+}/\text{Ru}^{3+}$ peak current (i_p) shown in Figure 8. As the light emission from the film is dependent on the number of electrochemically active ruthenium centers present, this cycling can be used as a simple measure of the films performance over time. The data in Figure 8 show an initial sharp degradation of the film was followed by only a very gradual decrease in the peak current. Over the analysis period of 1000 scans (5 h) the film degraded to 90% of the initial value. This degradation in performance is most likely due to the removal of any complex that is physisorbed or trapped in the covalently bound film.⁴⁷ The ECL signal from the layer after this period was also within 15% of the initial value, demonstrating that any physisorbed material does not contribute significantly to the light emission. It should be noted that the stringent conditions under which the stability of the layer was tested (5 h of continuous cycling to potentials $> 1 \text{ V}$) were chosen in order to emphasize the high level of stability of the system. The stress imposed on the layer under these conditions significantly exceeds that which would be expected in any normal period of use in a sensing context.

Conclusion

The *in situ* formation of the diazonium salt of $[\text{Ru}(\text{bpy})_2(\text{apb})]^{2+}$ prior to its subsequent attachment to an electrode in aqueous media has been shown to be effective in producing stable highly responsive films for use in an ECL-based sensor. This strategy leads to highly stable, covalently bound layers which will not desorb or degrade at the moderately high positive potentials required to oxidize the ruthenium complexes in the ECL cycle. Instability of, for example, thiol-based monolayers on gold has been an obstacle to the creation of ECL active layers suitable for real-world sensing applications. The electrochemistry of the system is consistent with a surface confined species with a surface coverage equivalent to up to 5 monolayers. Surface characterization of the film correlates well to electrochemical measurements and

(47) Shewchuk, D. M.; McDermott, M. T. Comparison of Diazonium Salt Derived and Thiol Derived Nitrobenzene Layers on Gold. *Langmuir* **2009**, *25*, 4556–4563.

Article

suggests that the deposited multilayered film is attached to the surface almost exclusively via azo bonding. The layer provides excellent ECL detection limits for the model analyte DBAE with a low limit of detection of 10 nM while providing a linear response over 4 orders of magnitude (10^{-8} – 10^{-4} M). This performance may be related to the multilayer nature of the film with a large proportion of the ruthenium centers effectively isolated from

Piper et al.

quenching by the electrode surface. The film is also shown to be highly stable; for example, the current response from the layer only decreases by < 10% after redox cycling to positive potentials in supporting electrolyte for 5 h. This aqueous-based deposition method of an ECL active complex and the resulting film provides an excellent opportunity for the synthesis of sensitive and stable ECL-based sensors.